Baseflow recession Groundwater storage and Rainfall Runoff processes in Inselberg topography in Messica Manica Mozambique

Fieldwork Conveyance and FlexTopo with OCM

J.C.D. van Dijk

Delft University of Technology

TU Delft Delft University of Technology

Challenge the future

BASEFLOW RECESSION GROUNDWATER STORAGE AND RAINFALL RUNOFF PROCESSES IN INSELBERG TOPOGRAPHY IN MESSICA MANICA MOZAMBIQUE

FIELDWORK CONVEYANCE AND FLEXTOPO WITH OCM

by

J.C.D. van Dijk

in partial fulfillment of the requirements for the degree of

Master of Science
in Civil Engineering

at the Delft University of Technology,
to be defended publicly on Thursday May 26th, 2016 at 4:00 PM.

Supervisor:	Prof. dr. ir. H.H.G. Savenije	TU Delft
Thesis committee:	Dr. ir. A.M.J. Coenders -Gerrits,	TU Delft
	W. Beekman Msc,	Resilience BV Mozambique
	Prof. dr. ir. M. Kok,	TU Delft

An electronic version of this thesis is available at http://repository.tudelft.nl/.

TU Delft Delft University of Technology

ABSTRACT

This master thesis investigated the origin of the seemingly perennial (base) flow in a hydrological complex, Inselberg (a type of mountain) dominated catchment in the Municipality of Messica, Manica Province, Mozambique. Smallholders rely on these perennial flows, since they have three growth seasons, two of them during the dry period. This year-round agriculture is of pivotal importance for dwellers' (economical) situation and contributes significantly to Mozambique's food supply.

However, there are many (hydrological) unknowns. How much groundwater is stored where, and how much water can be expected during the growth season. More knowledge will improve plant and irrigation schemes, minimize losses and prevent over-exploitation.

The Messica Irrigation Pilot Project (MIPP) searches for hydrological answers and tries to provide practical and theoretical insights. Therefore, students performed measurements (e.g., precipitation, water levels, discharges, cross-sections) in the 220km2 large Messica Catchment since December 2012 up to August 2014. Most measurements have been performed at Godi Downstream (a headwater from the mountainous ridge). This perennial stream is small and abundantly vegetated. Another important measurement point is a free-flow three-gated bridge downstream in the River Messica. Unfortunately, limited measurements are done here. Overall, the entire Messica Catchment is parsimoniously measured.

Scientists also strive to improve 'Prediction in Ungauged Basins' (PUB). This research took place in recent years. (Parts of) its knowledge and insights are used in this study.

This master thesis continued on earlier theses, together they contribute to MIPP's initiatives on three points. With this insights and practical methods, one might predict headwater baseflow one to two growth seasons ahead.

This study proposes (1) the 'conveyance method' to predict baseflow recession using cross-sectional corrected waterlevels (conveyances). Conveyances are measured continuously and are obtained directly, as opposed to discharge measurements. This method is based on uniform flow and linear (groundwater) reservoir assumptions together with a known cross-section. The conveyances C and discharges Q are linear related. The bottomslope and roughness are combined in one constant $\bar{a}$. From this, we derived groundwater response timescales K_s, and hence, estimated the baseflow recession. Godi's recession timescale is about 550 days. Together with some additional discharge measurements we are able to calculate discharges two growth seasons ahead.

Inselbergs are very steep mountains, ridges or isolated hills in gently sloped areas. They are omnipresent in the Manica province, just as in other parts of East and West Africa. Normally they consist of solid, barely erodible TTG (Tonalite, Trondhjemite, or Granites) materials, as it is the case for the Kalahari Craton, where Messica is located on. Just East of Messica, the Kalahari borders the Barue Complex. Water storage in these solid Inselbergs is not obvious. However, literature study showed that Messica's mountain ridge belongs to the later deposed Gairezi Sedimentary Group on top of the Kalahari Craton. It forms a 220km long belt from Sussendenga in the South to Guru in the North. The Gairezi consists of quartszites and metapelic schists, with internal westward-dipping inclinations. These mountains contain internal cracks and fissures, where water storage can take place.

We developed two Flexible Topography driven, conceptual rainfall runoff (FlexTopo) models (FlexA and FlexC) with an additional output conversion model (OCM) to calibrate on conveyances. FlexA serves as a lumped benchmark model which incorporates all the predefined relevant hydrological processes. FlexC is semi-distributed and distinguishes three different HRUs (hydrological response units), which are entities that show similar hydrological responses. We use two objective parameters to classify the area: Head Above Nearest Drainage (HAND) (as function of the flow accumulation) and hill slope values. FlexC's HRUs are: Wetlands (with saturated overland flow and exfiltration of deeper groundwater), Inselbergs (with perennial baseflow from its large groundwater storages, fast runoff processes due to steep, forested and/or rocky slopes) and Flatlands. The latter covers a wider scope from irrigated areas, grass and shrub lands to rain-fed fields, but contributes also (delayed) to base and peak flows. Every HRU has its own slow groundwater response reservoir. Furthermore, we applied altitude corrected precipitation to correct for orographic effects. Both FlexA and FlexC are calibrated on the River Godi and validated on the River Messica.

FlexC showed that (2) Messica's Inselberg ridge most likely contains an over-year storage. It predicted a groundwater storage of about 800mm in 2013-2014. This led to a specific discharge q of 1.45 mm/s at the beginning of the dry period. In general, this storage guarantees a continuous streamflow during the dry season and makes the area more resilient for dry years.

Moreover, we showed with FlexA and FlexC that (3) conveyances can be used to calibrate year-round discharge variations (both base and peak flows). It also proved that FlexModels are transferable, i.e. discharge variations for the (ungauged) downstream locations (Messica Downstream Station) can be predicted based on calibration on a (gauged) subcatchment (Godi Downstream Station). Where FlexA showed better peak flow predictions according to objective functions, FlexC narrowed down uncertainty intervals around predictions on other locations and gave a more consistent model performance. Given the smaller uncertainty intervals, the landscape dependent FlexC is better transferable than the lumped FlexA. However, FlexC seemed to overestimate peak flows, for which several explanations and improvements are given.

In general, the conveyance method appeared accurate to predict baseflow recession and to calibrate on low flows. It performed less well during peak flows, since the uniform flow assumption was violated. This was mostly due to the abundant (water) vegetation. The vegetation was even denser above the average water level. Additional work is needed in order to make the method fully functional for the whole flow regime.

ACKNOWLEDGEMENTS

Very enthusiastic, over-ambitious and extremely motivated I started with my final act in March 2014: my master thesis research. Willing to contribute to societies in non-Western countries, learning from other cultures, getting to know myself, experiencing adventures, challenging myself to the max, planning a future path, developing tools to 'conquer' the work field ànd, unfortunately, proving myself. I achieved most of it, but proving myself cost me a lot. However, I am feeling blessed to have had the opportunity to make my own mistakes and to learn my lessons. Therefore, I am looking forward to future challenges with just a slightly lower ambition level.

Within this period, many people supported me on various ways. Unfortunately, I cannot name them all here, since I would forget people. Thank you all for your love and comforts, friendship and laughters, trust and pep talks. Without you, I would not have been able to finish this work. A few people I would like to thank personally: Mum, Dad, Lianne, Grandpa, Grannies, Liesbeth, Arthur, Pieter, Peter, Kees-Jan, Elza and Tasmara. Thank you for being there.

I am also grateful for the opportunities, advices and patience given by Huub Savenije and Wouter Beekman. David Muchena, mister Piloto and Anja Mann who – together with Wouter – guided, supported and nurtured me in Mozambique. Arman Middendorp who helped me out with calibrating the EC-meter at TU's laboratory. Anke, Juval and René who red my thesis and, last but certainly not least, Miriam Coenders, who put lot of effort in reading and helping me to finish my thesis.

Above all, I admit that I would not have been able to overcome the last 10 years without God's love, guidance and blessings, which makes me grateful.

J.C.D. van Dijk
Delft, May 2016

CONTENTS

1

INTRODUCTION

Gently sloped areas with very steep mountains, ridges or isolated hills are omnipresent in the Manica province in Mozambique, just as in other parts of East [1, 2] and West Africa [3]. These mountains are also called Inselbergs (German for 'Island Hills'). Base flow recession, (over year) groundwater availability and rainfall runoff processes in Inselberg dominated catchments are vaguely understood and poorly investigated. This study, therefore, provides both practical and theoretical new insights on these topics.

There is a strong incentive to understand the hydrological processes in these solitary mountains. Besides the fact that some large river systems (e.g., Pungwe, Buzi, Revue) spring in these mountains and artificial lakes like lake Chicamba rely on their water sources, many smallholders also profit from Inselberg's appeared perennial headwaters. Being so, they are of 'pivotal importance' in 'combating rural poverty' and 'present contribution to irrigated food production' [4], which is widely acknowledged and therefore highly ranked on national and international policy agendas. However, Beekman *et al.* [5], who surveyed the increasing smallholder exploitation over the last years, states that the importance of smallholder irrigation is still broadly underestimated. Since they estimate already 115,000 ha of irrigated smallholder fields in Mozambique excluding large productional irrigation fields. Whereas FAO identify 118,000 ha equipped for irrigation in entire Mozambique [6]. Beekman *et al.* [5] base their estimations upon extrapolation of field surveys in seven districts in Manica province, including the Messica catchment. They believe that other studies (highly) underestimate the small scale irrigation efforts.

Irrigated agriculture is very profitable in Manica Province, due to the fertile soils, favorable climate and perennial Inselberg flows. On the hill slopes, two to three growing seasons are possible. From this, the first season consists predominantly of non-irrigated, catchment wide, rain fed maize production. The second and third irrigation-induced growing seasons deliver vegetables and production crops like red chili peppers and baby corns, during the dry season [5]. Although the headwaters are called perennial with little inter-seasonal variation, they do, however, experience baseflow recession. Some streams even (locally) dry up, restricting the irrigation potential for the second and third growth season [7]. More insight in water availability is needed to avoid investment losses due to water shortage or over-exploitation of the available water resources.

Oord and Beekman [4] therefore strive for a widely applicable implementation framework, including a standardized cost-effective hydrological survey to support sustainable irrigation development. They implemented this within the Messica Irrigation Pilot Project (MIPP) (2012-2014) [5]. MIPP combines a hydrological and irrigation development study. It aims proper hydrological understanding to successfully quantifying water availability and avoiding land degradation going hand in hand with irrigation development including a good understanding of the (local) driving forces for farmer-led irrigation development [5].

Several research studies including field campaign are conducted within the MIPP Framework. Among other things, water levels, discharges and precipitation are measured [e.g., Beekman *et al.* [5], Weemstra *et al.* [7], de Boer [8, 9], Holsteijn [10], Reumkens [11], Krüger [12]]. Beekman *et al.* [5] investigated the extent of farmer-led irrigation development and the underlying driving forces. One of these drivers concerns water availability and knowledge thereof. de Boer [9] and Reumkens [11] mapped the very extent of the irrigation canals, the course of the headwaters and the trajectory of the River Messica using hand held GPS. Weemstra *et al.* [7] and de Boer [8] focused on the hydrological functioning of the area. They proposed a baseflow prediction method based on a few selective discharge measurements during the dry season in combination with the linear reservoir assumption. This is supported with field observations and a HBV-light conceptual

model [13, 14]. This method resulted in a estimated baseflow recession value (K_s) for the River Godi of 1666 up to 2500 days. Furthermore, the HBV model scenarios suggest that total precipitation volumes and timing (early or late in the wet season) outweigh the effects of individual rainfall events and intensities on baseflow recession. Weemstra *et al.* [7] concluded that the headwater tributaries (e.g., Godi and Chirodzo) gain seepage over the reach length.

Besides the MIPP project, this case study also fits into a broader research called (flow-) "predictions in ungauged basins" (PUB) [15]. One of the objectives of PUB was to achieve better understanding of hydrology in general by combining multiple data sources and developing physical based distributed conceptual model approaches. These approaches have observable parameters and introduce smart techniques to extract information from data.

The study area exists of an unique, not often researched landscape element: Inselbergs. There are only parsimonious observations and short/ incomplete time series available at limited locations, whereas there are many (sub-) catchments.

A promising model concept which fits within the PUB-research is FlexTopo [16, 17]. Nature's self-organizing principle is the main philosophy of the FLEXible TOPOgraphy driven distributed conceptual rainfall runoff model [16]. Hence, landscape unfolds certain information about its govern hydrological processes. Once the right processes at the right scales are extracted, the model can be successfully transferred to other ungauged (or sparsely gauged) catchments. Within a given catchment, this framework distinguishes hydrological response units (HRU's) which are defined by certain dominant hydrological processes (like fast subsurface flow, percolation, seepage, saturated overland flow etc). The HRU's are typically distinguished by general observable landscape properties like topography and/or landuse, e.g.,slopes, head above nearest drainage level (HAND [18]), grass/crops, forests etc. For each HRU its perceived key processes are represented by means of a conceptual model. The linear superposition of all these models form the final semi-distributed conceptual model, for which both processes and input forcings can be spatially distributed.

In recent years, much research has been done to estimate model parameters based on physical observable properties. Although, the above sketched FlexTopo framework incorporates a lot of different processes, it is less prone to equifinality or physically impossible parametrization than ordinary lumped conceptual rainfall run-off models. The physical traceability of model parameters, parameter constraints and process constraints confine feasible parameter sets [e.g.,Gharari *et al.* [19], Gao *et al.* [20], Euser *et al.* [21], Hrachowitz *et al.* [22]]. Being so, the FlexTopo framework is already successfully applied in other study areas like Central Europe [17, 19, 21, 23, 24], Asia [20, 25], Africa [26–28], all with their own unique climatological zones, landscape elements, anthropological influences or calibration methods. Inselberg topography is not earlier applied in the FlexTopo framework, which makes this study unique.

This report's objective is to test whether (1) base flow recession can be estimated on cross-sectional corrected water level (conveyance) measurements only, (2) Availability and location of water storage can be further determined using a semi-distributed conceptual FlexTopo model and (3) Streamflow dynamics in both gauged and ungauged catchments can be predicted using semi-distributed transferable FlexTopo models calibrated on conveyances. In order to do so, we continued extensive field and model studies, keeping in mind both the practical framework of the MIPP project and the more sophisticated PUB-research. In this study, we combined the obtained knowledge and techniques from both MIPP and PUB studies, suggested some improvements and indicated new elements. Therefore we:

1. Extended the field survey and paid extra attention to the cross-sections and hydrological characterization of the area.

2. Proposed a method to derive baseflow recession values (K_s) directly from cross-section corrected water level changes, here called conveyances. Therefore, we applied the quasi-static uniform flow assumption (Manning-Strickler) and an altered method to correct for the no-flow zone. In this way, the K_s can already be derived without knowing any discharge figures. It also resulted in Q-conveyance rating curves, which solve parts of the high-flow extrapolation dilemmas [8] of currently used polynomial non-physical based Q-h rating curves [7, 8].

3. Compared Q-conveyance rating curve with a Q-h rating curve based on Steven's method as earlier applied by Piet et al. [25]. Though the latter method is primarily based on wide rivers and not small, vegetated streams as presented here.

4. Estimated roughly the over-year water storage based on baseflow measurements in combination with conveyances and the linear reservoir assumption. Since perennial flows are a hydrological key element [4, 7] and Weemstra *et al.* [7] already indicated high baseflow recession times (K_s), hence over-year storage has to be true. Therefore, a quick estimate based on simple analyses would be very useful.

5. Dived into the mountain's geology to investigate its origin, to test if they can be typed as Inselbergs and to indicate similar areas with equal (geo-) hydrological properties, to which the outcomes of this study might eventually hold [4].

6. Replaced the earlier applied HBV-light model concept by FlexTopo, since the latter showed good results in earlier studies. We tested whether a semi-distributed FlexTopo model - consisting of three HRUs - performs equally good or better than a lumped FlexTopo model. To test whether it is able to capture the typical hydrological behavior of this topography correctly, we applied it on two different catchments (validation by transferability) [16, 20, 29]. To do so, we developed a first edition to a generic applicable, open source model code within the free open source Python 2 environment, since current codes are only available in Matlab (which is restricted to licenses).

7. Extended the 'regular' discharge calibrated FlexTopo model with an Output Conversion Model (OCM) to convert calculated discharges to conveyances and water levels to calibrate on. This is in continuation of earlier work from Piet et al. [25]. Discharge information is only parsimoniously available and traditional Q-h rating curves are hold only reliable for low flows.

8. Used the semi-distributed FlexTopo model to test whether the majority of water is stored within the mountain ridge.

9. Applied elevation corrected precipitation. Since we indicate a strong orographic gradient in the precipitation and applied this to the input forcings using a simple linear altitude dependent precipitation relation.

Finally, we added a chapter with practical implementation of this and previous studies together with suggested improvements for future studies in this (types of) area.

2

METHODOLOGY

2.1. GENERAL APPROACH

This research study investigates the baseflow recession, water storage availability and rainfall runoff processes in Messica's Inselbergs. In order to do so, we followed a five-stage approach, see Fig. 2.1. Firstly, we extended the field measurements [5, 7–9] with a field campaign from March to August 2014. These measurements are worked out and stored into databases for further application. Our field observations gave input to our hydrological perception, and therefore to our model structure. The fieldwork is summarized in Section 2.2.

Secondly, we applied the FlexTopo rainfall runoff model framework [16]. Where we designed a lumped model FlexA (which is the basic FlexTopo model) which serves as a benchmark model for the more sophisticated semi-distributed models FlexB, -C and -D (see Section 2.3).

Thirdly, since we lack(ed) discharge time series at most locations, but we did have water level time series in combination with cross-sectional information, we proposed a method to calibrate the hydrological model on conveyances (cross-sectional corrected water levels) and waterdepths. These conveyances reveal hydrological information of the system. In order to calibrate FlexTopo on conveyances, we developed an Output Conversion Model (OCM), which is described in Section 2.4. This model converts FlexTopo's specific discharges q[mm/s] to Conveyances $C[m^{8/3}/s]$ and waterdepths d[m]. These model simulations are compared with the field observations. This OCM is a continuation of earlier work from Piet [25].

Fourthly, in Section 2.5 we derived parameters from measurements and literature to feed into the model.

Fifthly and lastly, we calibrated and validated the model stepwise (see Section 2.6).

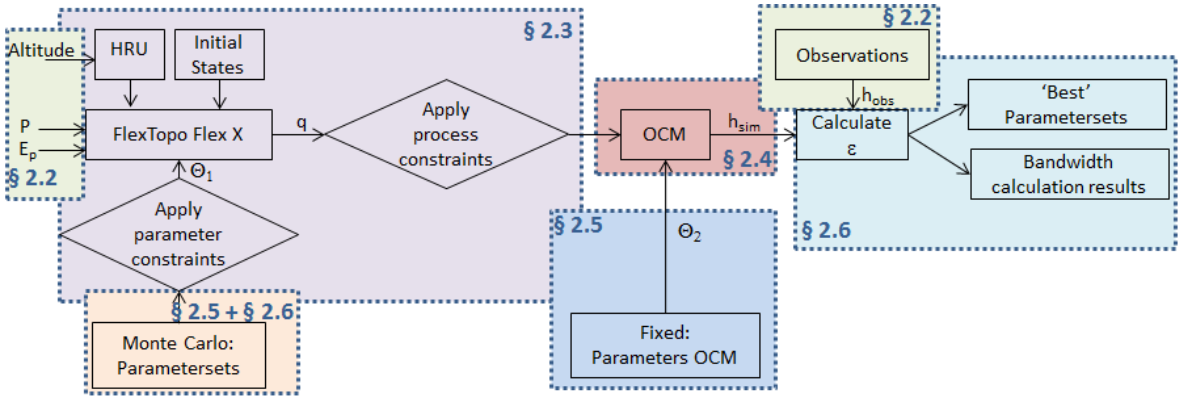

Figure 2.1: General set-up model composition and calculation flow scheme including reading guide.

2.2. BACKGROUND AND DATA

2.2.1. SITE DESCRIPTION AND LOCATION

The area of interest is located in the Zimbabwean bordering province Manica in Mozambique in the municipality of Messica, see Fig. 2.2. The total catchment area is approximately 220km2, with a total river length of 31km and an approximated catchment width of 10km. The catchment is drained by the north -south flowing River Messica. From the east side, small perennial tributaries from the mountain ridge feed into the River Messica, e.g.,river Godi, Chirodzo and Ruaga. The western catchment border is formed by a gently sloped ridge with a maximum height above river level of 50m. West of this boundary, the River Revue drains the adjacent catchment. We assume that the River Revue do not influence the Messica hydrology. The northern, upstream boundary is formed by a small hill ridge and a solitary Inselberg. In the south, the River Messica ends up in lake Chicamba. The latter is an artificial lake bordered by a north-south oriented mountain formation, called Gairezi Metasedimentary Group [2], from which our mountains of interest are part of.

2.2.2. GEOLOGY AND ELEVATION

Inselbergs are generally steep-sided mountains, ridges or isolated hills that rise abruptly from adjoining plains or gently sloping areas [4], see Fig. A.1. The Messica plains have an averaged altitude of 617m+AD, whereas the highest points at the eastern catchment border rise up to 1478m+AD (see Fig. I.5), intermediate hill slopes have inclinations up to 40% (Fig. I.6).

Messica's Gairezi Inselberg ridge is located on top of the Archaean Zimbabwe Craton (ca. 2300Ma [30]), also known as Kalahari Craton or at this place as Messica Granite. The whole Gairezi Sedimentary Group (or Frontier Formation according to Manhica *et al.* [30]) extend from the village of Sussundenga in the south to the village of Guro ca. 220 km northwards. Fig. 2.2 shows the surrounding geology around the Messica Catchment (the extends of Gairezi Sedimentary is showed in Fig. B.4). The entire Gairezi is located on the very eastern edge of the Kalahari Craton, truncated by the sinistral (left sided) movement of the Mozambique Belt (or Barue complex) in the east (see map) and the Zambezi Belt (not on the map) in the north. The last two stems both from the Paleoproterozoic eon. Manhica *et al.* [30], who identified the Messica ridge as Frontier Formation, estimated its age between $ca.$ < 2300Ma and > $ca.$465M, which is also during the same eon.

However, there are some small mountains circumventing the Messica ridge, which most likely are part of the Kalahari Craton, e.g., southwards in the city of Messica and within Lake Chicamba (Fig A.36), but also within the catchment other Inselbergs can be found. For example the typical mountains in Ruaga's subcatchment (see Fig. A.5), the waterfall at Godi downstream measurement station (GodiDS) (Fig. A.34), Messica downstream measurement station (MessDS) (Fig. A.35) and a waterfall in Ruaga catchment (see Fig. A.33). Hence, the ridge consists of the Gareize Sedimentary Group, whereas the remainder of the catchment might be located on top of the Kalahari Craton.

The River Revue, which also drains the Messica Basin, crosses the Gairezi Group at Lake Chicamba at a large hydropower dam (Figs. A.37, A.38 and A.39). This dam is the first out of two hydropower dams [1]. Lake Chicamba therefore also serves as a buffer to ensure a constant hydropower generation.

The Gairezi Group's origin is unknown, possibly it is formed out of metasedimentary deposits, but tectonically transport cannot be excluded, since this is both found north of Manica province and at the southern border of the Kalahari Craton. North of our catchment and east of the city Manica, a silent witness of this tectonically possibility is found in the presence of isoclinal folds within the Gairezi mica schist, in a limb of an open, upright syncline, close to the underlying Archaean bedrock surface. Literature which in- or exclude similar layering in the Messica catchment is not found, but we assume its existence. Talking about meta layering, the whole Kalahari Craton is gently east dipping [30]. So, if deep groundwater flows exist, possibly the flow direction is eastwards, understreaming our mountainous catchment's border.

On smaller scale, the preferential layer inclination (schistology) of the schist is presumably west-dipping, according to the geological map of Mozambique [31] (see Fig. B.1). This implies that the catchment's replenishment area is possibly larger than expected based on the surface elevation map, and, being so, that percolation water from the eastern ridge might feed into the Messica catchment at the western side. In Fig. A.10 is a rock outcrop pictured where the layers are clearly visible and possibly some traces of outflow are found.

Unfortunately, we lack knowledge about the exact layer inclination in the underlying mountain ridge, and therefore about preferential, intragranular flow paths. It is plausible that it might happen, since we found

[1] The second, more downstream dam, is located at the edge of the Barue Complex, where a sudden land drop causes a natural elevation difference of 80m.

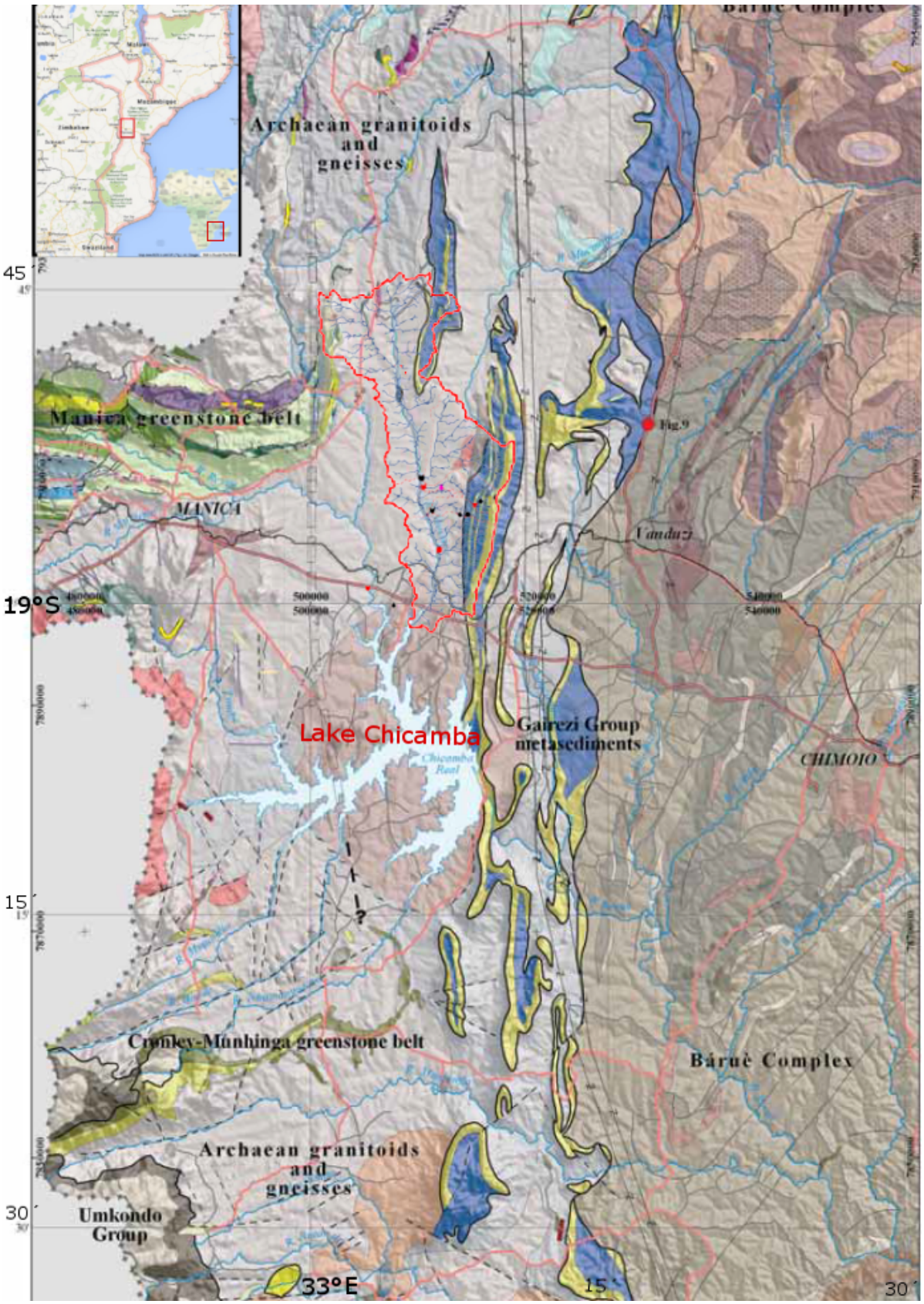

Figure 2.2: Location Messica Catchment (red) in Mozambique, Africa (see inlay [Google maps ©]) between Manica and Chimoio, north of Lake Chicamba, with our research area located on the Gairezi Sedimentary Group's eastern slope. The Figure is compiled from Koistinen *et al.* [2]. Spots in catchment indicates measurement locations, see Fig. 2.6

both large vertical inclinations on top (Fig. A.22) and (perennial) wells and wetlands along the slopes (Figs. A.8, A.26, A.23, A.27, A.10) during our field work campaign.

Messica's Inselbergs are described as 'quartzite and mica schist outliers in the area' which form 'highly compressed, upright, narrow sub continuous and interlocking synclines with horizontal north-south axes' [2], [31]. We found a more sandstone like material on top of the inselberg (Fig. A.21). In contrast to other TTG (Tonalite, Trondhjemite, Granite) gneisses more westwards, the core of our Inselbergs mainly consists of mica [2] (or metapelitic [30]) schist, but is seldom exposed. The gneisses, on the other hand, consist of the basement materials like leucocratic (low content of ferromagnesium minerals) granite and originate from the Archaean [2, 30]. Furthermore TTG's fabric structure is more random and lacks uniform stratification. Therefore, we might suggest that the Inselbergs found in the Messica catchment are not the typically exposed TTG's which are more common in e.g., between Messica and beyond the border of Zimbabwe, Malawi and in the North of Mozambique (around the city Nampula).

Koistinen *et al.* [2] describes a color-based soil determination; he distinguishes dark-red soils to have a mica schist origin. We found these typical soils on the Inselberg hill slope (e.g., Figs. A.23 A.25 A.4 A.15). This strengthens the idea that the mountain ridge consists of quartzite and Mica schist and therefore is not a typical granite gneiss. The more pale greyish / whitish soils belong to weathered materials originating from granitoids, i.e. the Messica Granite or Kalahari Craton. We found these soils in the valley, near River Messica, see for example Fig. A.3 . All in all, we expect that the mountain itself is formed of quartzite and mica schists with a internal west-dipping inclination, and that around the foothills the older Kalahari Craton is found, with deep regoliths and a sandy bottom.

Due to mechanical and biochemical weathering, the top layers of massive cratons erode to small rocks and course sand. This layer is generally called a regolith [e.g., Chilton and Foster [1]](see App. B). Note again that we have two different geological formations, since the materials differ, also the existence and depths of regoliths differs. Concerning the depth of Messica's regolith, we did not found any specific figures in literature, though Chilton and Foster [1] mentions in a conceptual hydrogeolical model of the weathered crystalline-basement aquifer in Africa that depths go up to 50m (see Figs. B.2 and B.3). So we might deduct that, assuming the climate to be more or less similar and given the fact that this part is also Africa, the Messica regoliths also have a depth of 20 to 50m . Assuming the existence of such a regolith, there might be an aquifer with a low permeability [1], which possibly heads to lake Chicamba (this deduction does not necessarily conflict with our earlier statement that, due to the light east dipping orientation of the Craton, groundwater, if occurring, possibly flow eastwards. It is rather a logical conclusion given the location of Lake Chicamba in the mountainous ridge and the fact that no other large rivers spring in this area, then purely in this lake).

About the regolith at the mountains of the Gairezi Group, presumably the regoliths on the hill slopes are rather shallow, witnesses to the bare cap rock layers, outcrops at the ridges, and possibly they can also be deduced by the type of trees on some parts of the hill slopes (e.g.,Figs. A.10, A.11 and A.12). The regolith layer on the peak might be thicker, since pristine deciduous forests cover these peaks (Figs. A.9, A.20, A.18 and A.19). Both assumptions, the shallow on the slopes and deeper regoliths on the peak, are in line with Parmentier [3] who investigated vegetation composition on three Inselbergs in West Africa.

At the caprocks (bare hard rocks) we observed ongoing processes of mechanical and biochemical weathering. Mechanical weathering, caused by sun, temperature and wind is visible by the desquamation (flaking) of the rocks (Fig. A.32) and falling apart of rock pieces (Fig. A.31). Biochemical weathering as for example induced by organisms is visible in the grass vegetation on the rocks (Fig. A.30, A.29).

A noteworthy phenomenon is the existence of a gully in the Ruaga catchment, which confirms part of our above deductions. According to Beekman (interview), this gully is quickly increasing every rain season . During the rain season of 2013-2014 the gully extended approximately 30m upstreams (from the tree to the end of the gully, see Fig. A.46). The very interesting part of this gully is two fold. The first and most important observation is the pale grayish soils at the north-west side of the gully and the red tropical soils at the south-east side. This indicates that we found here the border between the two geological entities and confirms our earlier assumption that the Messica mountains are formed out of other material (Gairezi Sedimentary Group) than the Messica Valley (Kalahari Craton). This also proofs that the smaller gneisses found within the catchment possibly can origin from the Kalahari Craton (Fig. A.44). Secondly, we could deduce the regolith depth (>3m), the rootzone depth (observe roots in valley) and the existence of preferential flow paths (observe the large holes in the walls), see Figs. A.47, A.46, A.45 and A.43. Furthermore observe that the layering from Kalahari Craton (grayish soils) are similar to the description as given by Chilton and Foster [1], see also Fig. B.3.

2.2.3. LANDUSE

The catchment's land cover roughly consists of deciduous sub-tropic forests on the hill slopes above an altitude of *c*.800m+AD, the lower hill slopes are mainly covered with (irrigated) cropland, grassland and small residual forests. The lower located, flatter areas consists of large shrublands, (moistures) grasslands or rainfed maize plots (which are only cropped during the first rain season). FAO mapped landuse in their GlobCover map [32], see Fig. 2.3. The figures shown in Appendix A give more insight in land use and local circumstances.

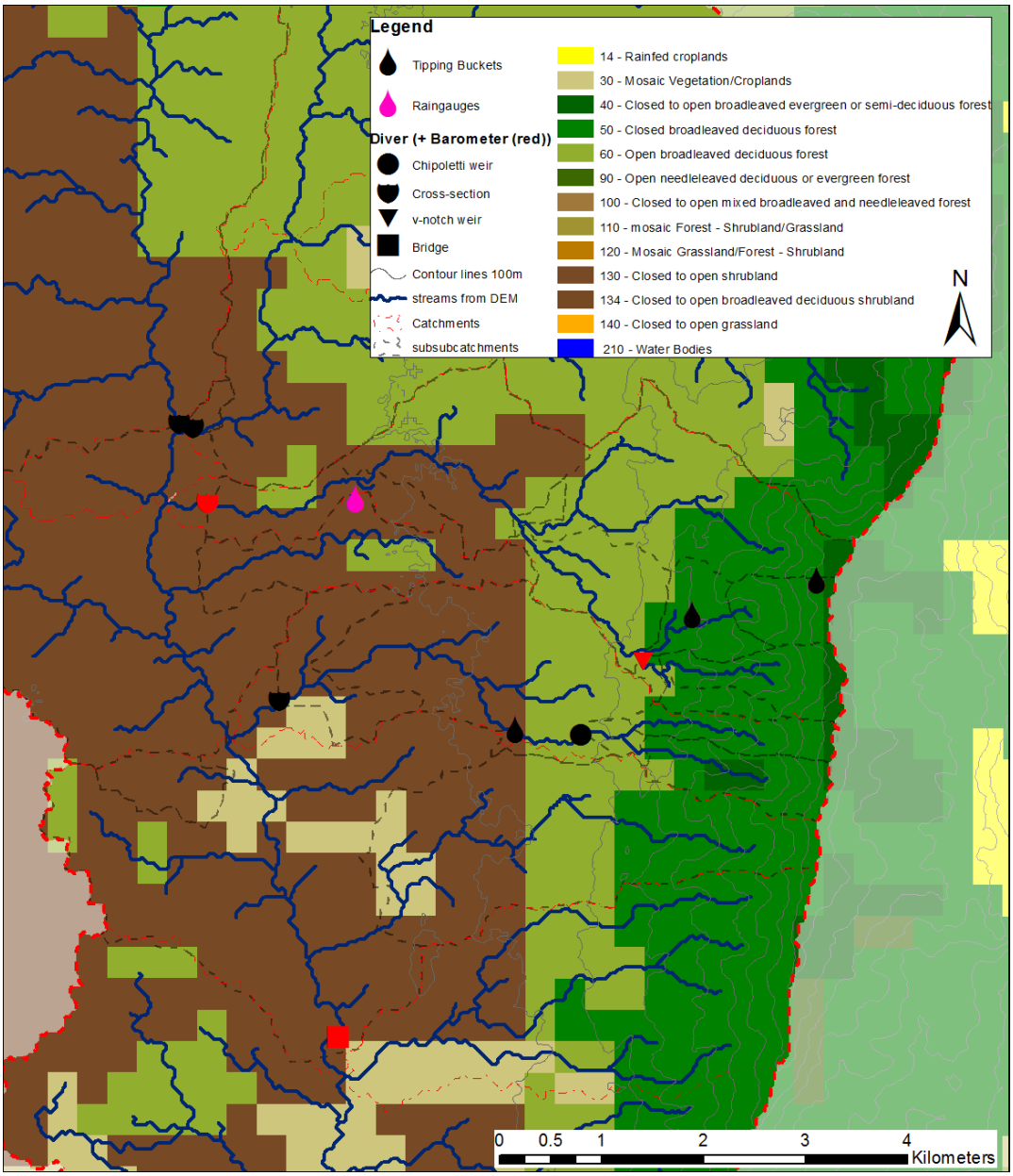

Figure 2.3: Globcover landuse map [32]

2.2.4. CLIMATE

The study area has a warm, temperate climate with a hot, wet summer together with intense rain events (December to March). During the autumn (March - June) generally some heavy rain events take place and the daily maximum temperatures slowly decrease from 35 degrees Celcius to 20- 25 degrees Celcius. The winter and spring are usually dry (June - November). Officially the climate is characterized as Köppen-Geiger type Cwa [33].

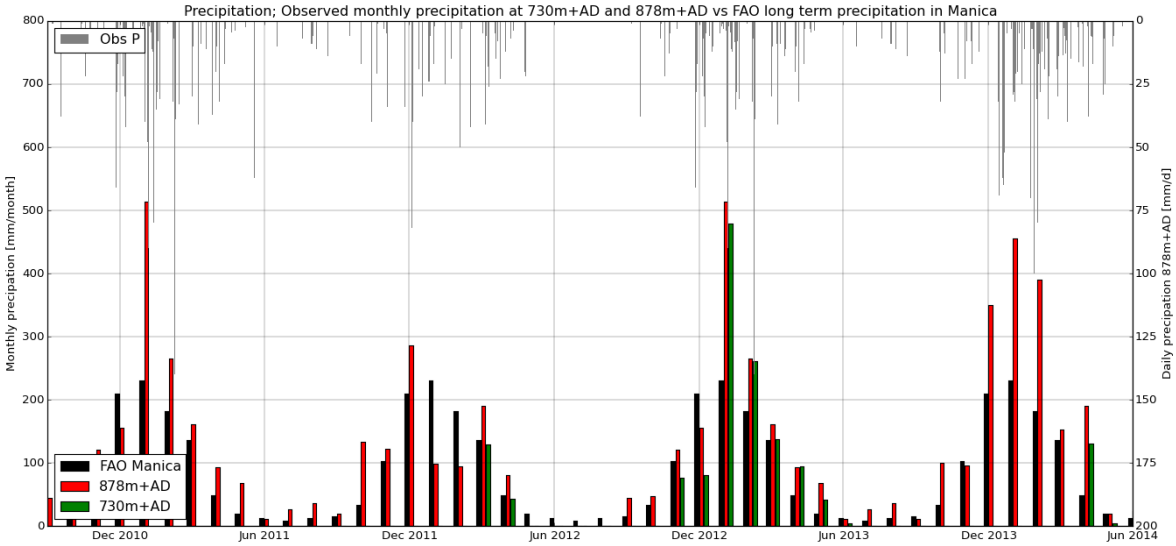

Figure 2.4: Measured daily and monthly precipitation amounts at two stations within the catchment, where 878m+AD concerns P_{David} and 730m+AD $P_{Chimoio}$ (not to be confused with the city of Chimoio) compared with FAO long term best estimated precipitation series at Manica [33].

2.2.5. PRECIPITATION

The long term averaged yearly precipitation (1961 -1990) is 1014mm/a in Manica [2] (30km westwards from the catchment) [33], see Fig. 2.4 and App. C.1.

During the dry season, rainfall events are typically short and intense. There is barely no wind so the rainfall is nearly vertical. Interviews during field inspections point out that the wet season contains both the intense events and the long drizzling periods. We observed that the mountain peaks are often covered by clouds. Trees, grass and other surface objects most likely intercept moisture from these clouds, while this interception is not measured in raingauges. At the peaks, grass and trees remain green, whereas at lower altitudes grass turns yellow during the dry period. This indicates cloud forest interception processes. However, the contribution of this cloud interception relative to the total precipitation is unknown.

Local smallholders performed daily precipitation measurement using manual raingauges, in total at 5 different locations, see Table 2.1. Some of them are also equipped with a tipping bucket. The longest and most complete time sequence is obtained by David at an altitude of 878m+AD, see Figs. 2.4 and 2.6. He started his measurements in October 2011. The (red) measurements in Fig. 2.4 between October 2010 and October 2011 are not observed, but are measurements from October 2012 to October 2013. The extra year is needed as warming-up period for our rainfall runoff models. The other manual raingauge measurements as for example perfomed by Chimoio (green bars), show (large) gaps and are therefore only partially useful.

Question is whether recorded precipitation amounts from last year are representative or have to be considered 'dry'. For the catchment 2012-2013 is considered dry, 2013-2014 normal and 2014-July 2015 wet. We came up with this classification by interviews and mutually comparing these years. However, we only can compare this to other years in the same catchment or to long term averaged data by FAO[33] at Manica. For the latter, all years are normal to (extremely) wet. We included statistics in App. C.

Increased precipitation volumes are measured at higher altitudes [see also Weemstra *et al.* [7]], most likely this is caused by orographic effects, since mutual distance between raingauges are such small, spatial precipitation variations are not a plausible explanation for the structural differences. In this study, we assumed a linear relation to correct David's precipitation measurements P[mm/d] for the altitude h[m]+AD, Eq. 2.1, in order to derive semi-distributed precipitation input for the FlexTopo models. For more information, see Fig. 2.5 and Appendix C.2.

$$P(h,t) = \left(1 - \frac{878-h}{878-730} * 0.16\right) P(t) \tag{2.1}$$

[2] Manica weather station long 32.86, lat -18.93

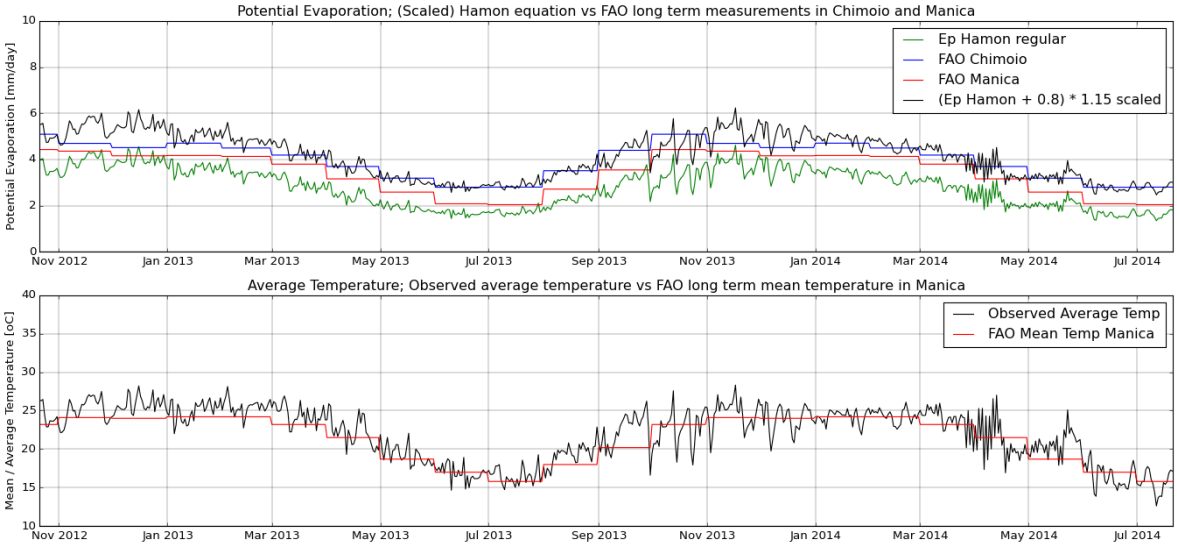

Figure 2.5: Calculated and scaled potential evaporation with Hamon [34] compared with long term observed potential evaporation at Manica and Chimoio. The black line is used applied in this study.
Observed daily averaged temperatures measured at barometers in the catchment compared with mean temperature measured at Manica. [33]

2.2.6. EVAPORATION

Long term potential evaporation at Manica's Weather station concern $1252 mm/a$, and monthly average temperatures ranges between 16 and 24 ^oC [33].

During this fieldwork campaign, no evaporation measurements are performed. The daily potential evaporation is estimated with the Hamon Equation [34] based on the daily average temperatures, obtained from in-situ barometers. The outcome of Hamon (green line in Fig. 2.5) is visually scaled to the long term monthly evaporation flux from FAO[33] at Manica / Chimoio (red and blue lines). The potential evaporation from FAO is based on the Penman Montheith equation. The used potential evaporation (black line) is found by adding 0.8 to Hamon and multiplying this with 1.15. For more information see Appendix C.4.

2.2.7. STREAM MEASUREMENTS AND SUBCATCHMENTS

From the Inselberg several headwaters originate, to wit Ruaga, Godi, Chirodzo, Nyamasongo and others. These perennial tributaries feed into the River Messica (which itself spring at another Inselberg). In this study 7 'permanent' measurement locations have been used, see Table 2.1. Three of them - Godi downstream, Chirodzo down- and upstream - have been installed during previous field campaigns [7, 8] and had been measuring until the beginning of this field campaign. Therefore these measurements were continued. New locations are chosen for Godi upstream, Messica upstream and Messica downstream, since the locations were already dismantled. Ruaga downstream is newly introduced, see Fig. 2.6.

We distinguish three types of 'permanent' measurement locations. All of them concern water pressure measurements with divers which are corrected for barometric pressures (see Appendix E). Between the three types, only the setting differs, we have:

- (vegetated) Cross-sections with quasi-static uniform flow assumption (see Appendix F.1).
- Gauging weirs for which discharge relations are known (see Appendix F.2.2).
- A three-gated bridge with (super-) critical flow which is therefore considered as a free-flow structure (see Appendix F.2.5).

Code Map Fig. 2.6	Name measurementpoint	Type measurementpoint	Period* from	to	Resolution	Area [ha]	Source
David	Precipitation David	Manual raingauge + partly tipping bucket	01/10/2011	01/08/2014	daily		[1] [2] [3]
Chimoio	Precipitation Chimoio	Manual raingauge	01/03/2012	01/10/2012	daily		[1] [2]
Chimoio	Precipitation Chimoio	Manual raingauge	01/12/2012	01/06/2013	daily		[1] [2]
Chimoio	Precipitation Chimoio	Manual raingauge + partly tipping bucket	01/04/2014	01/08/2014	daily		[3]
Alberto	Precipitation Alberto	Manual raingauge	01/03/2012	01/10/2012	daily		[1] [2]
Alberto	Precipitation Alberto	Manual raingauge	01/12/2012	01/06/2013	daily		[1] [2]
Alberto	Precipitation Alberto	Manual raingauge	01/04/2014	01/08/2014	daily		[3]
-	Precipitation Caritas	Manual raingauge + tipping bucket	01/04/2013	01/06/2013	daily		[1] [2]
-	Precipitation Caritas	Manual raingauge + tipping bucket	01/04/2014	01/08/2014	daily		[3]
Inselberg	Precipitation Inselberg peak	Manual raingauge + tipping bucket	01/04/2014	01/08/2014	daily		[3]
Godi DS	Godi downstream	Water levels in cross-section	12/12/2012	22/07/2014	60 minutes	1012	[1] [2] [3]
Godi IS	Godi intermediate	Discharges with v-notch weir	26/03/2014	21/07/2014	30 minutes	248	[3]
Chir DS	Chirodzo downstream	Water levels in cross-section	11/12/2012	22/07/2014	60 minutes	659	[1] [3]
Chir IS	Chirodzo intermediate	Discharges with Chipoletti weir	** 18/07/2011	18/07/2014	7 days	172	[1] [3]
Ruaga DS	Ruaga downstream	Water levels in cross-section	07/04/2014	22/07/2014	30 minutes	3586	[3]
Mess IS	Messica intermediate	Water levels in cross-section	26/03/2014	22/07/2014	30 minutes	10130	[3]
Mess DS	Messica downstream	Water levels behind 3 gate bridge	26/03/2014	23/07/2014	30 minutes	17684	[3]

Table 2.1: Overview most important measurement points
$*$ from 12-8-2013 to 26-3-2014 barometric pressure partly available
$**$ real weekly interval started at 11-5-2012
[1] [7]; [2] [8]; [3] This study

During the period from March 18th up to July 23th 2014, salt dilution measurements are performed all over the catchment. They contribute to multiple longitudinal routings in order to obtain better insight of the origin of the water, the stream flow variance at different locations and the baseflow recession curves, see Fig. I.1 for an overview of all locations.

Additional calibration and timestep correction appeared necessary in order to derive proper discharges from these salt dilutions, see Appendix D. Notwithstanding these uncertainties, also for earlier performed salt dilution measurements, we do use them in this study as a measure / reference for calibrating the channel roughness for the conveyance method. Since one can argue whether the relative impact of current improvements outweigh the general uncertainties going along with salt dilution measurements, like applied salt mass, the well-mixed assumption and background salt concentrations. Therefore it is only used as a 'best we got' for reference purposes.

For all these measurement locations, subcatchments and streams are derived using a Digital Elevation Map (DEM, Aster2 $30 * 30 m^2$ [35]) together with the ESRI Arcmap 10.1 toolbox Hydrology ©, see Figure 2.6. All (sub-)subcatchments are presented in Appendix I Fig. I.1.

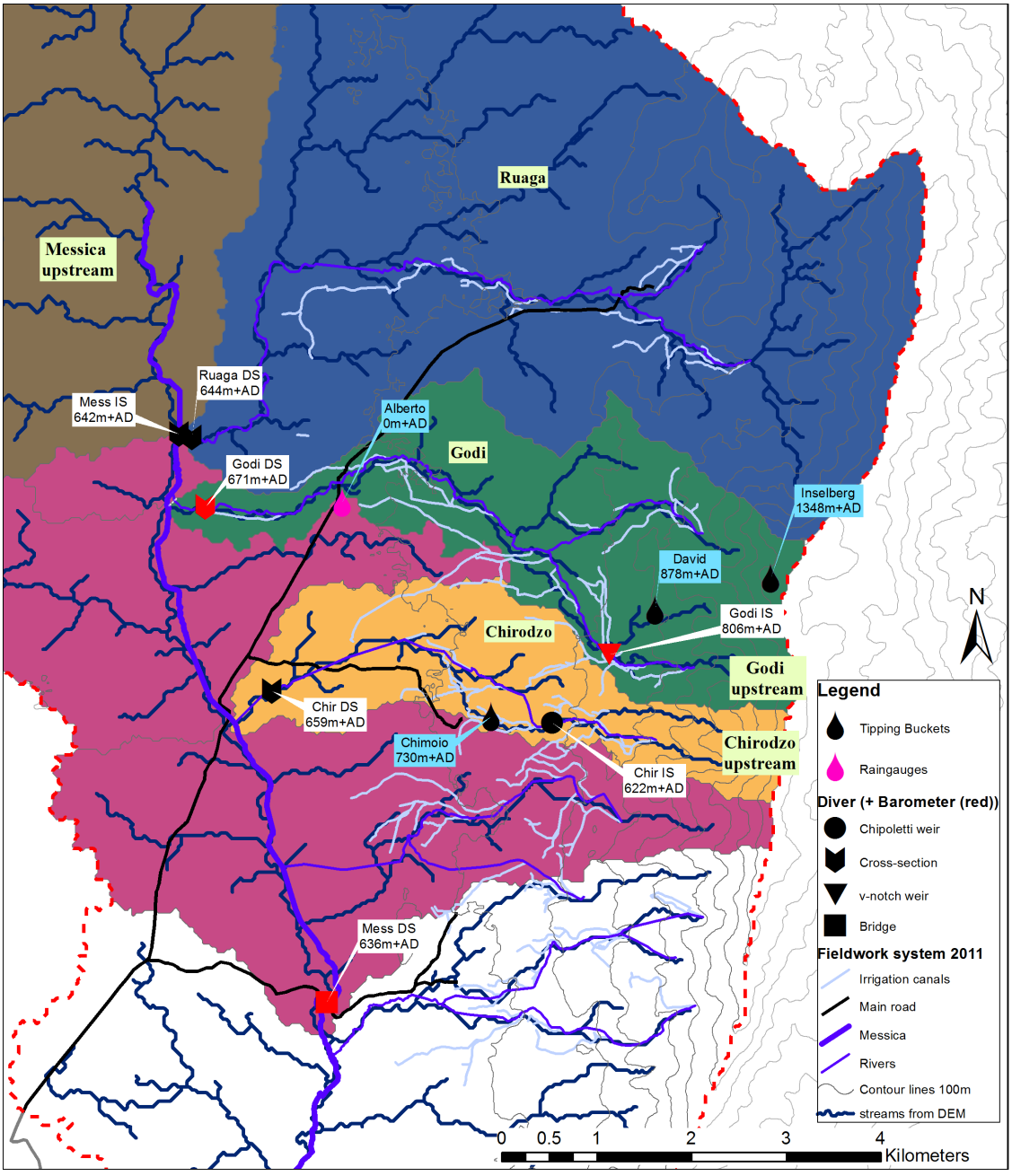

Figure 2.6: Area focus containing the main catchments. The model area is corrected for the exact location of the measurement stations, Appendix I.
Measurement stations: DS = downstream outlet station; IS = intermediate outlet station. The red colored points were (temporarily) equipped with an additional barometer. Black manual raingauges were temporarily fitted out with a Tipping Bucket. Mapped irrigation canals in light blue and streams in turquoise. [9, 11]. Where the DEM derived streams are shown in dark blue

2.3. RAINFALL RUNOFF MODEL

2.3.1. MAIN ASSUMPTIONS

For the rainfall runoff modeling several assumptions are made. Here we shortly discuss the main assumptions (while some assumptions are already tested during the study). The most important tests are further explained during this report.

MODEL CHOICE

Starting point for the hydrological model is the FlexTopo framework [e.g.,Savenije [16]]. For this study the model is coded in the programming language Python 2.7.9 win32 ©[3] in combination with Microsoft Access©Databases containing the preprocessed and validated fieldwork data, see App. G. The FlexTopo model is loosely based on previous work [19]. We chose the FlexTopo framework, because the framework strives to connect hydrological processes to objectively observable land characteristics like head above nearest drainage levels (HAND), slopes and landuse. This data is extracted into a distributed model structure (which is a linear superposition of lumped models). This enhances the physical foundation and verifiability of our model perception. If true, the model's transferability will be improved. A lumped FlexTopo model is used to test whether the distributed model structure lead to better results.

In earlier studies [7, 8] HBV-light[4] [14] is applied. We chose to replace this model concept for physical reasons. A correct comparison between HBV-light and FlexTopo is therefore not performed in this study. We assume that our lumped FlexTopo model (FlexA) will be able to reproduce similar results.

OCM MODEL TO CALIBRATE ON CONVEYANCES

The FlexTopo model is calibrated on cross-sectional corrected waterdepths, so called conveyances, using a here proposed Output Conversion Model (OCM). Normally hydrological models are calibrated on observed discharges, unfortunately, we lacked long discharge series and only had salt dilution discharge measurements during the low flows. However, we gained water level time series for these points as well as cross-section dimensions. To calibrate on conveyances (and waterdepths), we used the Output Conversion Model (OCM) to convert calculated specific discharges q[mm/d] to calculated waterdepths h[m] and cross-sectional corrected waterdepths (conveyances) C[m$^{8/3}$]. This approach is chosen since:

1. Discharge time series were not available or had a lot of uncertainties.

2. Conveyances also reveal useful information about the catchment dynamics and retention times, since they prove to be linear related to the discharges.

3. A comparable study [25] successfully applied calibration on water levels for large (wide) rivers.

4. Water levels in small rivers/ streams may not be re-sampled (by normal averaging) from hourly to daily values without correcting for its cross-sectional influence.

TEMPORAL TIMESTEPS

The models are calibrated on a daily time scale resolution, because this is the highest measured time resolution. For the precipitation measurements are performed every once a day at 8am in the morning. Smaller time resolutions will therefore not lead to more physical *observed* refinement[5] of timescale dependent processes. Courser time scales are not tested in this study, since we expected response times in the order of hours rather than days for the fastest runoff processes.

[3] This platform is freeware and open source, and therefore accessible for everyone, independent of software licences.

[4] *"HBV Light corresponds in principle to the version described by Bergström [13, 36] with only slight changes. In order to keep the software as simple as possible several functions available in the SMHI (Swedish Meteorological and Hydrological Institute) version have not been implemented into HBV-light.The newest version of HBV-light was reprogrammed in collaboration with M. Vis (2010) to migrate the software from the programming language VB6 to VB.NET [Seibert and Vis [37]]".* Text quoted from website [38].

[5] Impose measured daily rainfall in shorter periods and downscale outcomes to daily timesteps might improve the calculations, however, we do not observe nor test this in current study

RESAMPLING OF MEASUREMENTS

To match timescales of waterdepth, discharge [6], and conveyance measurements to the model input timestep resolution, we averaged these measurements between 8am previous day to 7am current day in our model [7]. This is exactly the same time interval as where the precipitation measurements are performed on. This avoids incorrect travel time delay due to different time scales and/or averaging windows. Note that 'normal' averaging of waterdepths is theoretically not allowed (as explained later in this thesis), so they are only used for visual inspection.

RAINFALL ALTITUDE CORRECTION

For the final calculations, the precipitation volumes are linear corrected for the altitude effect conform Eq. 2.1. The corrections are applied on the rainfall measurements at David's place, see Table 2.1, and applied to HRU (Hydrological Response Unit) scale.

CALIBRATION AND VALIDATION AREA

The calibration is performed on Godi Dowstream Station(GodiDS) for two reasons. Firstly, this point entails the longest time series and, secondly, the measurement point is located at the mountain's foot and therefore the influence of the Kalahari Craton (if available) is limited.

Messica Downstream Station (MessDS) serves as validation point [8]. This point is located at a bridge in the River Messica downstream from GodiDS's inflow point. Points for consideration are the limited available measurements, they are restricted to some baseflow recession after the wet season. Furthermore that the catchment is not purely Inselberg dominated, but contains also large gently sloped areas, most likely not connected to the Inselbergs (see slopes in Fig. I.6). Finally, the fact that the catchment covers two different geological entities, the Gairezi Sedimentery Group (from which the majority of Godi Catchment is formed of) and the Kalahari Craton. For the latter no calibration station is available[9].

IRRIGATION INFLUENCE

We did not incorporate a correction for widely available irrigation activities in the (Godi) catchment. Smallholders extract water from headwaters and irrigate their croplands. In general irrigation activities only take place within the catchment. Only near the spring, irrigation canals connect separate catchments. The canals are very leak, most water flow back to the mainstream immediately. Irrigation excess water will infiltrate and drain to the streams via subsurface processes. The large measurement points (e.g., GodiDS and MessDS) are not circumvented by irrigation canals, so all surface water leaving the catchment should pass these stations. Other (intermediate) measurement points (Appendix I) are sometimes circumvented, so special attention is needed when transferring information to these points.

Irrigation is in this catchment is hard to conceptualize in a conceptual model. Since man-induced irrigation is very sensitive for human unpredictability, since we lack precise information of location and size of irrigated fields and, lastly, we lack knowledge about seasonality of transpiration. Besides, there is also diurnal streamflow variation due to riparian vegetation [e.g., Bren [39]]. Therefore, we did not incorporate irrigation fluxes into the model concept, not in the least since overall hydrological uncertainties will outnumber the irrigation uncertainties. As a result, the model will compensate the transpiration in the calibrated Transpiration coefficient and rootzone depth and therefore might overestimate the baseflow. Hence, we take this into account when judging the model performance.

CALIBRATION PROCEDURE

This is elaborated in the chapter 2.6.

2.3.2. FLEXTOPO MODELS

This study proposes four different FlexTopo models: FlexA, FlexB, FlexC and FlexD. For which two models are actively tested; FlexA and FlexC. FlexB and FlexD are only implemented and form a possible extension of this study. They are described in Appendix K. FlexA is a lumped benchmark model involving all considered hydrological processes of the whole catchment. Section FlexA describes the components and processes of

[6] Discharges are available at a v-notch weir at Godi Intermediate Station, see Appendix F.2.4, a chipoletti weir in Chirodzo Intermediate Station on weekly scale, see Appendix F.2.2 and salt dilution measurements, Appendix D

[7] Using Microsoft Access' model specific scripting language SQL

[8] Other measurementpoints (see App. F) are not tested during this study, but observations and model instrumentation are ready to do so.

[9] Note that MessIS covers mainly the Kalahari Craton, however time series are rather short and the observations' quality is poor.

this benchmark model. The distributed model concepts FlexB, -C and -D distinguish two to four different units. Each unit encapsulate distinct hydrological responses. These are called Hydrological Response Units (HRU's). Each HRU on its own, is described using the FlexA lumped model, with some alterations, such as removed processes or different input forcings. So FlexC is a tailor-made linear superposition of three FlexA models, however, the slow response reservoir is somehow connected. Same hold for FlexB with two and FlexD incorporating four different reservoirs.

FLEXA

As said, FlexA is our lumped benchmark model, the building stone for the more complex semi-distributed models FlexB, FlexC and FlexD. This benchmark model consists of four buckets which are mutually connected by predefined flow paths and (state dependent) dividers. Together they represent all incorporated hydrological processes as taken into account in this study, see Fig. 2.7. The remainder of this paragraph will describe the model bucket-wise, the analytical code is presented in Table 2.2 and the numerical in Appendix L.2.

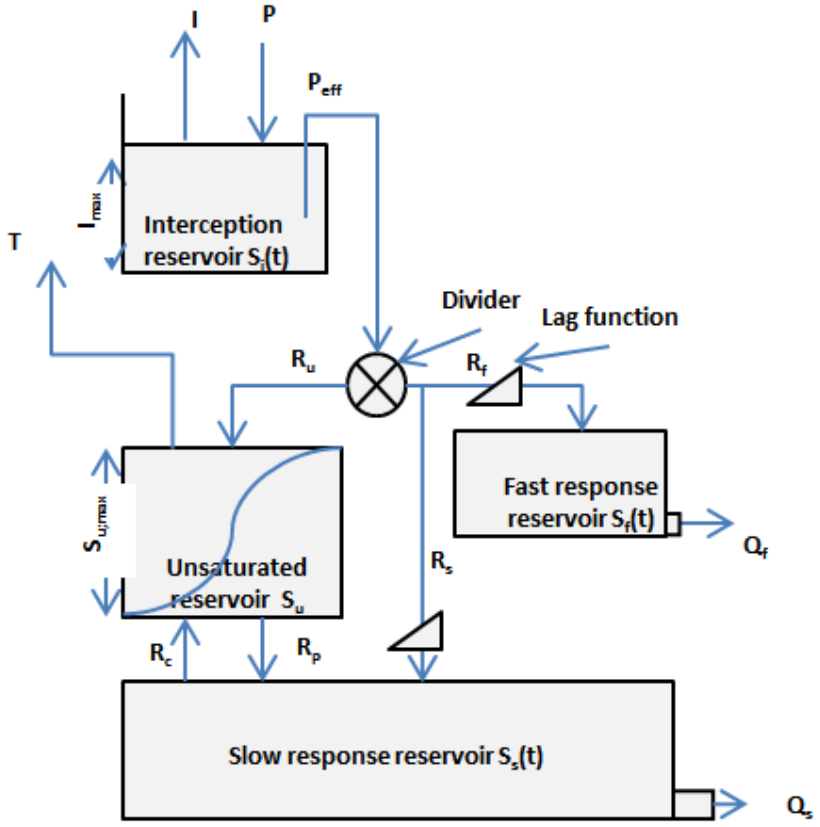

Figure 2.7: Model code FlexA; lumped benchmark model

Interception bucket Interception is a form of evaporation, it represents evaporation from the wet surface area. The very first rain never enters the soil, but stays on the surface and evaporates directly. We call this interception evaporation E_I[mm/d]. The interception bucket is maximized to a certain fixed value I_{max}[mm], this is the maximum capacity that can be stored in the interception bucket. The surplus precipitation enters the soil as effective precipitation (P_e[mm/d]). The interception bucket is emptied through evaporation. We assume, firstly, no evaporation resistance and, secondly, that interception is preferred over other evaporation types (e.g.,transpiration and soil evaporation). If the potential evaporation capacity is too low, the surface stays wet. The remaining water will be stored in the interception bucket. If, on the other hand, extra potential evaporation capacity is available, then transpiration by plants will take place.

Reservoir	Water balance equation	Constitutive relations
Interception	$\frac{\Delta S_I}{\Delta t} = P - P_e - I$	$P_e = \begin{cases} 0 & S_I < I_{max} \\ (S_I - I_{max})/\Delta t & S_I = I_{max} \end{cases}$ $I = \begin{cases} E_p & E_p \Delta t < S_I \\ S_I/\Delta t & E_p \Delta t \geq S_I \end{cases}$
Unsaturated	$\frac{\Delta S_u}{\Delta t} = R_u - T - R_p + R_c$	$R_u = C_r P_e$ $T = K_T(E_p - I)$ $R_p = \left(\frac{S_u}{S_{u;max}}\right) P_{per}$ $R_c = \left(1 - \frac{S_u}{S_{u;max}}\right) C$ $C_r = \begin{cases} 1 - \left(\frac{S_u - S_{u;max}F_c}{S_{u;max} - S_{u;max}F_c}\right)^B & S_u \geq S_{u;max}F_c \\ 1 & S_u < S_{u;max}F_c \end{cases}$ $K_T = \begin{cases} \frac{S_u}{S_{u;max}L_p} & S_u < S_{u;max}L_p \\ 1 & S_u \geq S_{u;max}L_p \end{cases}$
Fast	$\frac{\Delta S_f}{\Delta t} = R_{f;lag} - Q_f$	$R_f = (1-D)(1-C_r)P_e$ $R_{f;lag} = R_f * N_{f;lag}$ $Q_f = S_f/K_f$
Slow	$\frac{\Delta S_s}{\Delta t} = R_{s;lag} - Q_s + R_p - R_c$	$R_s = D(1-C_r)P_e$ $R_{s;lag} = R_s * N_{s;lag}$ $Q_s = S_s/K_s$

Table 2.2: Water balance equations and constitutive functions used in FlexA [19]. Meaning units also listed in Table 2.4
$*$ is the convolution parameter

Divider and Lag function The effective precipitation (P_e[mm/d]) is divided over three fluxes in two steps. The first division is made between the unsaturated reservoir and the recharge of the fast and slow response reservoir. The division is steered by the timestep dependent C_r[-] coefficient. This is calculated with a power law relation based on the current unsaturated zone storage (S_u[mm]), the maximum rootzone storage ($S_{u;max}$[mm]), the relative field capacity threshold (F_c[-]) and a power B[-] that accounts for the spatial variance in the catchment. When the relative field capacity is exceeded, groundwater flow is activated. Depending on C_r part of the water is divided to the fast and slow response reservoirs.

The second division divides the preferential recharge over the fast (R_f[mm/d]) and slow (R_s[mm/d]) response reservoir. The model implicitly assumes a fixed division between these two states, so it is not state-dependent.

Physically, both the R_f and R_s fluxes travel from the entering point until it reaches the storage of the corresponding reservoir. Once reaching the storage of the corresponding reservoir, the system response is described with the linear reservoir assumption. The model concept describes the travel time with a delay function (a convolution integral), where a predefined conversion shape (for example a triangular, rectangle or irregular shape) can be stretched with one parameter such that the average travel time is described. The area of the conversion shape is one by definition, since it only mathematically maps the shape. The shape parameter is called a delay coefficient $N_{f;lag}$[d] and $N_{s;lag}$[d] [10].

Unsaturated reservoir The unsaturated reservoir actually represents the effective root zone storage S_u[mm] ranging between $[0, S_{u;max}]$ [40].

Plants withdraw water only from the rootzone storage for which we now call the unsaturated zone, but, theoretically speaking it is not the same. When plants are unrestrained in up-taking water (S_u[mm]$> L_p$[$-$]$*$ $S_{u;max}$ [mm]), the transpiration (E_T[mm/d]) equals the potential evaporation diminished by the interception evaporation. The uptake resistance (or better uptake smoothness) (K_T[-]) linearly increases when less soil water is available (water stress) until plants cannot uptake any water anymore. The transpiration flux also implicitly accounts for open ground evaporation. L_p is a transpiration coefficient.

Within the unsaturated zone, water slowly percolates (R_p[mm/d]) to the deeper groundwater under gravitational influence. The percolation flux depends on the actual rootzone storage and the maximum percolation rate (which is a soil parameter). The other way around, due to suction forces of roots, capillary rise draws groundwater from deeper layers into the rootzone (R_c[mm]). This flux is also linear dependent on the actual

[10] These delay functions are not used in the model and the parameters are set to 1, which implies that there is this process is schematized as instantaneous, under assumption that this will be solved in the general K-parameter due to equifinallity.

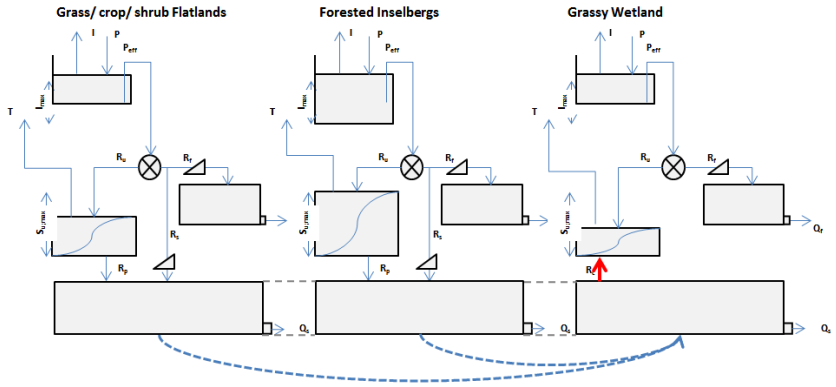

Figure 2.8: Modelcode FlexC; landuse based

rootzone storage (S_u[mm]) and the maximum capillary flux C (which is a soil property also).

Irrigation subtracts water from the river (so the outflow of the fast and slow reservoir) and recharges the unsaturated zone. This process can be either schematized by adding it to the effective precipitation flux or by direct injection into the unsatured zone reservoir [11].

Fast response reservoir The fast (response) reservoir reflects the catchments fast runoff response after rainfall events. Generally, fast subsurface runoff (through the rootzone) and saturated overland flow processes are captured with this process. By absence of hortonian or flash surface runoff, these very fast processes are also included in this reservoir. Notice that this reservoir simulates system responses caused by the active participating fraction of water, and not the total available amount of water, which is stored in the unsaturated reservoir. Furthermore, this reservoir represents response times (Eulerian) and not actual travel times (Lagrangian). The process is conceptualized using the linear reservoir assumption, where the response time K_f is calibrated. Interactions with other hydrological processes (like horizontal flow, percolation or evaporation) is excluded from this process by definition.

Slow response reservoir The slow (response) reservoir typically represents the (active) deep groundwater flows, this reservoir is also designed as a linear reservoir. The recharge of the reservoir consists of two fluxes, the direct groundwater percolation through preferential flow paths (R_s) and the matrix percolation from the rootzone storage (S_u). Also two fluxes leave the reservoir, to wit the capillary rise R_c to unsaturated soil and the (groundwater) baseflow discharge Q_s. The latter is dependent on the system response time K_s. Note that this reservoir also only evaluates the active contributing part of the groundwater and not the total groundwater storage (since not all availabe water is contributing to the process).

FLEXC

FlexC (Fig. 2.8) divides the area in three different units: Inselbergs, Wetlands and Flatlands.

Construct HRUs We combined three data sources to objectively distinguish between the three HRUs; the head above nearest drainage level (HAND) as function of the FlowAccumulation: HAND(FlowAcc), the hill slope and our Field observations.
The HAND-Slope method is generally applied in FlexTopo models [e.g.,[16, 29]] and stems from Rennó *et al.* [18]. He defines the HAND-Level - or short HAND - as a measure to use the elevation of the receiving stream as a reference level to calculate for every piece of land the elevation (head) above its drainage point (in stead of using a fixed plane like Sea Level). Gharari *et al.* [29] proved for a catchment in Luxembourg that the method indeed is able to separate (the dominant hydrological processes of) Wetlands, Hill slopes and Plateaus. He found that HAND $\leq$ 5.9m serves as a good indicator to separate wetlands from hill slopes and plateaus. Furthermore, he tuned the Slope treshold to 12.9% to divide hill slopes $\geq$ 12.9% from Plateaus. These values are in combination with a DEM resolution of 30*30m2 and a flow accumulation value of 20, which implies that when 20 gridcells drains to one cell, at this point a stream start, and therefore, from this point the HAND value

[11] This irrigation flux is not implemented in this model, since we cannot clearly distinguish irrigated lands form other landscapes.

is calculated. Indeed the methodology is grid resolution dependent and the flow accumulation threshold is of large importance.

In this study we used our field observations together with our hydrological perceptions to tune the HAND, Slope and FlowAccumulation thresholds. A script judges for every single gridcell (30x30m2) to which HRU it belongs:

Wetland:	HAND(FlowAcc=50) ≤ 2m	
Forest:	HAND(FlowAcc=50) > 2m	AND Slope ≥ 11%
GrassCrop:	HAND(FlowAcc=50) > 2m	AND Slope < 11%

The methodology is further explained in Appendix I. The used ASTER grid has its anomalies, especially around water surfaces and flat areas, where suddenly large non-existing mountains arise. Also there are deviations with reality cause of vegetation. For this study however, the uncertainties of the ASTER grid are considered in line with other uncertainties.

Forests or Forested Inselbergs We recognize the very steep mountainous ridge which has slopes up to 25 deg. The slopes are vegetated with pristine subtropical forests, show spots with massive caprocks and deep carved streams running down from the top. Along the slopes and on the top cracks are visible. At some locations water is flowing out of the mountain. Indicating preferential flow paths. We expect that most water is stored within these mountains, since the perennial streams spring at the mountain. So the water storages here have to very large and also recharged locally via preferential recharge and matrix percolation, since recharge cannot take place from outside the mountain. Furthermore, since the slopes are very steep and the rootzones of the sub-tropical forests are well developed, we expect fast runoff processes, which are even faster than further downhill. The rootzones of the forests are most likely larger than those of the grass and croplands. Though, some parts of the mountain are really shallow, since caprock is at or very near the surface. We neglect this phenomenon. We expect the forest to have higher interception capacity than other parts of the area. Therefore, we use field observations and the HAND method to separate these mountains from other parts of the catchment. We combine this to one hydrological response unit (HRU), called *Forested Inselbergs* or simply abbreviated to *Forests* or *Inselbergs*.

Wetlands or Grassy Wetlands At the inclination of the hill slope, seepage water leaving the mountains, feeding into new streams. Also, along the rivers downstreams wet zones are available. Grass is the dominant vegetation of these zones. Since these areas are always wet, saturated overland flow will be the dominant flow process. Meanwhile seepage water will continuously refill the unsaturated zone, maximizing the transpiration and open water evaporation. Since groundwater is leaving the system in these areas, it will not infiltrate into the soil here. So we neglect all infiltration fluxes to the deeper groundwater system. We used our field knowledge and HAND to separate these lands from the rest of the area. We grouped these areas into one HRU called *Grassy Wetlands* or short *Wetlands*.

Grass_crops or Grass, Crop, Shrub gently sloped Flatlands The remaining areas stretch from irrigated croplands at the Inselbergs to shrublands in the Messica Valley. The area contains rainfed maizefields, grasslands with small plots of pristine forests and irrigated croplands. We grouped this area within one HRU called *Grass, Crop, Shrub gently sloped Flatlands*, *Grass_Crops* or *Flatlands*. Since the area is very broad, the soil moisture capacity, interception capacity and response time of the fast runoff processes will be an average of this system. In general we expect them to form the middle between Forested Inselbergs on the one hand and Grassy Wetlands on the other. Since the area dry up in the dry season, seepage is not taken into account in these areas. Irrigation activities of the smallholders is not taken into account explicitly. Irrigation will maximize transpiration because of the wetter soil, fast subsurface runoff and deep groundwater recharge will be underestimated.

Connection slow reservoir responses In this study we try to determine the amount and location of groundwater that feeds the so profitable perennial streams. To do so, we define for each HRU an own slow groundwater reservoir, so each HRU is actually the FlexA-model with some processes turned off, being so we can apply linear superposition of the different HRUs to come up with the actual situation.

We allow the wetlands to have negative slow groundwater storages, these occur since we state that there is no groundwater recharge only subtraction due to capillary rise. The groundwater originates from other HRUs. The outgoing groundwater flow of wetlands becomes negative, and should be interpreted as a recharge of the slow reservoir of the wetland. The total outflows of the other HRUs are thus reduced with the extraction to the wetland. This method, however physically not totally correct but numerical far more efficient, works since there is no feedback between the slow reservoir and the other processes for the Flatlands and Inselbergs. We proved mass conservation in Appendix L.3.1.

To make sure that it all works fine we restraint the process. The physic-numerical constraint ensures that the cumulative of the slow response reservoir outcome (Q_s) for the three HRUs is larger or equal than zero for every single timestep ($\forall t$). Since otherwise the model would (physically speaking) introduce passive groundwater into the model, which is conceptually impossible, since we only take the active slow groundwater storage into account (that part that actually participate into the rainfall runoff process). This constraint read (Eq. 2.2)

$$\sum_{HRU=1}^{3} Q_{s;HRU} \geq 0 \forall t \tag{2.2}$$

Since we now have the slow groundwater dynamics for every HRU, we also might draw conclusions about the locations and amounts of groundwater storage.

Parameter bandwidths and constraints The hydrological responses from the different HRUs are different. This is taken into account in the parameterization of the processes. On forehand we define parameter bandwidths based on literature (see Paragraph 2.5). Next to this, we also know that some processes have a mutual dependency, for which we can test our parameter sets on physical reliability. For example we know that the fast response processes from forests (on hill slopes) are faster than those of grass/crops and wetlands. The following parameter constraints are applied. All the parameter sets that do not fulfill these constraints are rejected beforehand.

$$\begin{cases} I_{max;forest} \leq I_{max;grass\_crop} \\ I_{max;forest} \leq I_{max;wetland} \\ K_{f;grass\_crop} \leq K_{f;wetland} \\ K_{f;forest} \leq K_{f;wetland} \\ S_{u;max;forest} \leq S_{u;max;grass\_crop} \\ S_{u;max;forest} \leq S_{u;max;wetland} \end{cases} \tag{2.3}$$

Process constraints We applied for FlexC two process constraints. All the calculations which do not fulfill these constraints are rejected afterwards.
The first process constraint is an evaporation constraint. The total actual evaporation in the dry seasons (from April up to November) should be smaller than the total actual evaporation in the wet seasons for the calculated period. This constraint is not very firm, see Eq. 2.4.

$$\sum E_{a;dry} \leq \sum E_{a;wet} \tag{2.4}$$

The second process constraint concerns the discharge coefficient. This is again a very soft constraint, since we set the boundaries very weak, Eq. 2.5.

$$0.1 \leq \frac{\sum Q_m}{\sum P} \leq 0.9 \tag{2.5}$$

2.4. OUTPUT CONVERSION MODEL

The Output Conversion Model (OCM) is an extension of the FlexTopo rainfall runoff model and converts FlexTopo's outcome - specific discharge q[mm/d] - to the observed variables to calibrate on - daily averaged waterdepths d[m] and/or daily averaged cross-section corrected waterdepths, called Conveyance C[$m^{8/3}$/s]. In this study we calibrate some measurement points (See Table 2.1) on conveyances. Discharges are never

observed directly, but always indirectly and are a result of discharge relations (weirs), rating curves(cross-sections) or mass balances (salt dilution measurements). Since every method has its own (rough) assumptions, we introduce in this section an other way to derive discharges directly from water levels. To do so, we start with the general approach.

2.4.1. ASSUMPTIONS

This study assumes a quasi-static uniform flow assumption. Note that the waterdepths and/or conveyances - called here θ - under this assumption are directly related to the discharge q[mm/d], i.e. $\theta(t) = f(q(t))$, since the rates of discharge changes $\mathrm{d}Q/\mathrm{d}t$ are negligible. Also hysteresis effects due to peak flows are negligible. For uniform flow we assume that the water level slope equals the bottom slope with absence of backwater curves, so $\mathrm{d}z/\mathrm{d}x = \mathrm{d}d/\mathrm{d}x = I$. Finally, we consider the bottom roughness due to bedrock and vegetation constant over the year, and neglect roughness change due to water depth change (which might be not true, since streams are abundantly overwhelmed by water plants, this can introduce depth-dependent back water curves). We assume that the errors introduced by the last assumption to be only significant during higher discharges.

Discharges under quasi-static uniform flow conditions can be described by the Manning-Strickler formula (Eq. 2.6).

$$Q(t) = \frac{AR^{2/3} * \sqrt{I}}{k} \tag{2.6}$$

In which Q[m^3/s] is the discharge, A[m^2] the wet cross-sectional area, R[m] the hydraulic radius where $R = A/P$ with P[m] the wet perimeter, all as function of the depth $d(t)$. I[-] the bottom/ water level slope and k[s/m$^{1/3}$] the smoothness coefficient of the reach, see Chow [44].

2.4.2. NORMAL PRACTICE

In order to translate waterdepths to discharges (under the uniform flow assumption) often a rating curve is used (Eq. 2.7). Most common practice is to extrapolate the parsimonious observed discharge measurements to find a discharge-waterdepth ($Q-d$) relation for high flows. Note that this general equation is often expressed in h rather than d.

$$Q = a(d(t) - d_0)^b \tag{2.7}$$

For which Q[m^3/s] the discharge, d[m] the observed water level relative to a reference level, d_0 [m] the bottom level relative to a reference point. a [m^{3-b}/s] and b [-] are free calibration parameters to fit a line through the discharge measurements, this is often done in ln-scale.

$$\ln Q = \ln\left(a(d(t) - d_0)^b\right)$$

$$\ln Q = \ln a + b \ln\left(d(t) - d_0\right) \tag{2.8}$$

Main objection for this approach is the high flow extrapolation problem, since high flows are rarely measured, just a few points are available to derive the curve for, resulting in a wide bandwidth of possible $Q-d$ relations.

A way to circumvent the high flow problem is to apply the Stevens method. Therefore, we measured the cross-section, and derived the wet perimeter R and cross-sectional area A as function of the waterdepth d. With Steven's method we can calibrate a and b[-] in Eq. 2.7 from the cross-section's shape, see Fig. 2.9b. However, a[m^{3-b}/s] is also accounting for the roughness and bottomslope. For this we compare Eqs. 2.6 and 2.7 and observe

$$\frac{\sqrt{I}}{k} A(d) R(d)^{2/3} = \tilde{a}\tilde{a}(d - d_0)^b \tag{2.9}$$

if we define

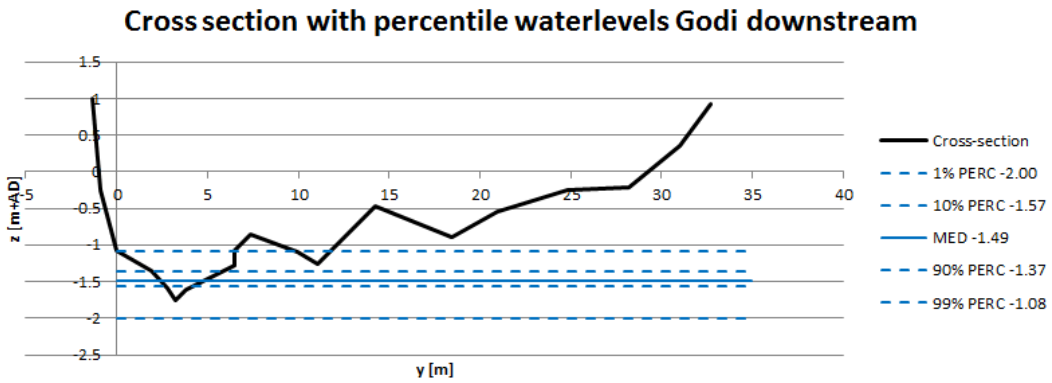

(a) Cross-section of Godi Downstream Station (GodiDS) with percentile values of measured waterdepths. Note that the graph is expressed in z in stead of d

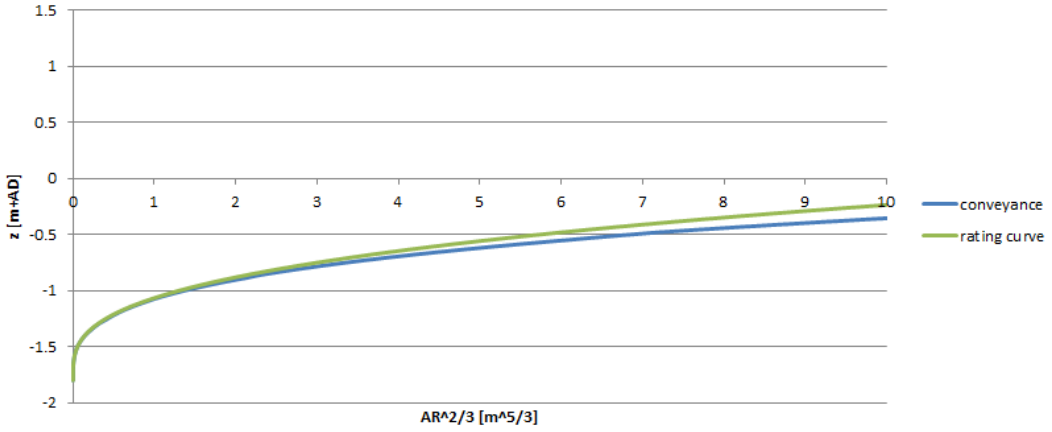

(b) Real $AR^{2/3}$ or Conveyance of GodiDS in blue and the calibrated rating curve in green. with $\bar{a} = 3.5$, $b = 2.9$ and $d_0 = z_0 = -1.75$. The latter is only done to vertically shift the to $z = 0$ if $AR^{2/3} = 0$.

Figure 2.9: Calibrating Stevens method on GodiDS

$$\bar{a} = \frac{\sqrt{I}}{k} \tag{2.10}$$

then

$$\tilde{a}(d - d_0)^b = A(d)R(d)^{2/3} \tag{2.11}$$

Note that $a = \bar{a}\tilde{a}$ where $\tilde{a}$ is a result of fitting b to the cross-section and $\bar{a}$ incorporates the roughness and bottom slope. So in Fig. 2.9b we actually fit $\tilde{a}$ as shown in Eq. 2.11. This is done (visually) for all measurement locations (see App. F), for which we choose to fit the low depths best [12]

Please note that we assume here that the whole cross section contributes to the flow, i.e. there is no no-flow zone $d_0 = 0$. In reality $d_0 \neq 0$, so we have to compensate for the no-flow zone d_0[m], i.e. the maximum depth for which $Q = 0\text{m}^3/\text{s}$. In normal practice this depth is subtracted from the total depth d[m] in the argument, see Fig. 2.10a, so $Q(h(t) - z_0 - d_0)$ (for which $h(t)$ is the water level and z_0 the bottom level both relative to a reference point). In this way, Eq. 2.7 actually introduces vertical bottom level shift, reducing the whole cross-sectional area and therefore restricting the flow more than physically possible[13]. So this method is only applicable for a special case; a rectangular cross-section.

Therefore we introduce a new concept to correct for the no-flow zone. We state that a better approximation would be to superpose both solutions. So $Q(t) = Q(d(t)) - Q(d_0)$, see Fig. 2.10a. This method simply

[12] Step functions can be introduced to achieve a better approximation, but the inverse of step functions not always exist.
[13] Note that flow velocity $v = 0$ at the bottom is already incorporated in the roughness assumption of the Manning-Strickler equation

subtracts the no-flow zone from the total wet cross-sectional area. Notice that, doing so, the friction between the no-flow zone and the flow zone is zero, which is actually physically more reliable than when it is taking into account, though this is just of minor influence.

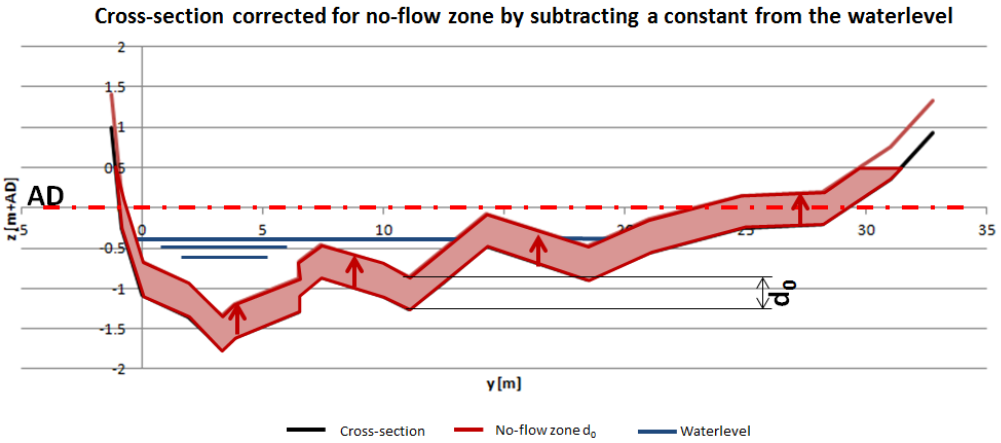

(a) Constant subtraction of no-flow depth d_0 from the total depth d resulting in a cross-section shift

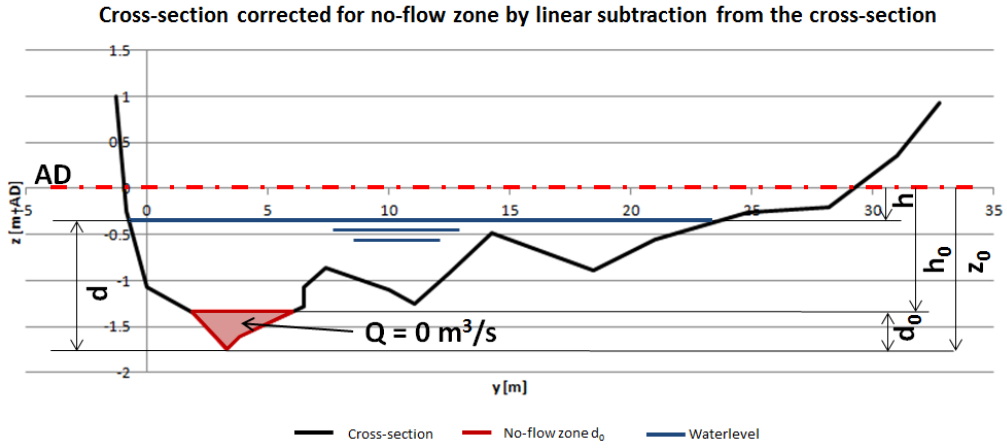

(b) Subtraction of no-flow area from the total cross-section

Figure 2.10: Two different methods to correct for d_0: the maximum no-flow waterdepth

2.4.3. CROSS-SECTIONAL CORRECTED RATING CURVE

With the cross-sectional corrected rating curve the non-linear influence of the cross-section on the mapping from $Q \rightarrow d$ is removed. This can be best understood from the Manning-Strickler formula Eq. 2.6. Within the quasi-static uniform flow assumption, the influence of the cross-section is described by the term $AR^{2/3} = C(t)[\mathrm{m}^{8/3}/\mathrm{s}]$, which we call the cross-sectional corrected waterdepths or conveyance. The conveyance $C(t)$ is known, since for every $d(t)$ the A, R can be derived from the cross-section measurements (see Appendix F.1 for the derivation of A, R). Leaving a very simple linear relation between conveyance $C(t)$ and discharge $Q(t)$. The only remaining term $\bar{a}$ accounts for the bottom slope and the roughness, see Eq. 2.10.

Now also applying the principal of linear subtraction of the no-flow zone (Eq. 2.12), we end up with Eq. 2.13

$$Q(t) = \bar{a}C(t) - \bar{a}C_0 \tag{2.12}$$

With $Q = 0$ if $(C(t) - C_0) \leq 0$

$$C(t) = \frac{Q(t)}{\bar{a}} + C(d_0) \tag{2.13}$$

For the roughness and bottomslope term $\bar{a}$ we tried both automatic calibration and derivation from the parsimonious salt dilution measurements. The latter is shown in the next section.

2.4.4. OVERVIEW RATING CURVES

Table 2.3 gives an overview of the applied $Q-d$ and $Q-C$ rating curves

Description	Equation
Ordinary rating curve: For which a and b are derived with Steven's method and a constant correction for no-flow zone in the argument.	$Q = a(d(t) - d_0)^b$ $d(t) = \sqrt[b]{\frac{Q}{a}} + d_0$
Linear rating curve: Linear subtract the no-flow zone from the wet cross-sectional area.	$Q(t) = a(d(t) - z_0)^b - a(d_0)^p$ With $Q = 0$ if $(d(t) - z_0) \leq d_0$ $d(t) = \sqrt[b]{\frac{Q(t) + a(d_0)^b}{a}} + z_0$
Cross-sectional corrected linear rating curve: Maps cross-sectional influence on waterdepths to the conveyance and linear subtract the no-flow zone from the wet cross-sectional area.	$Q(t) = \bar{a}C(t) - \bar{a}C_0$ With $Q = 0$ if $(C(t) - C_0) \leq 0$; $C(t) = A(d)R(d)^{2/3}$; $C_0 = A(d_0)R(d_0)^{2/3}$ $C(t) = \frac{Q(t)}{\bar{a}} + C_0$

Table 2.3: Overview $Q-d$ and $Q-C$ rating curves and OCM equations

2.4.5. (IM)POSSIBILITY TO AVERAGE d AND C

Although we provided for both waterdepths (using the Stevens method) and conveyances a mathematical correct concept, they are exchangeable if and only if all the observed waterdepths are unaggregated applied in waterdepths method, i.e. daily linear averaged waterdepths do not incorporate the non-linear cross-sectional influence[14]:

$$\overline{Q(n\Delta t)} = \overline{\bar{a}\theta(n\Delta t)} \tag{2.14}$$

for which n is the number of time steps. and θ is a non-linear term

$$\theta(t) = \tilde{a}(d(t) - d_0)^b$$

$$\overline{\theta(n\Delta t)} \neq \frac{\tilde{a}\sum_{i=1}^{n}(d(t_i) - d_0)^b}{n}$$

So linear averaging of waterdepths is not correct. We discussed the effects in Chapter 4, the effects of wrong averaging are in particular plotted in Fig. 4.2. Whereas conveyances are linear dependent to discharges and can therefore be averaged:

[14] Circumventing this by calculating $\tilde{a}(d(t) - d_0)^b \forall t$ is actually calculating the conveyances

$$\overline{Q(n\Delta t)} = \overline{\bar{a}C(n\Delta t)}$$

$$\overline{Q(n\Delta t)} = Q(\Delta t) = \bar{a}\frac{\sum_{i=1}^{n} C(t_i)}{n} \tag{2.15}$$

Since conveyance is linear related to discharge, we can average high frequent observations to less frequent observations. This gives the method flexibility which is not possible for water levels.

2.5. DERIVATION PARAMETERS FLEXTOPO AND OCM

After introducting the FlexTopo with accompanying OCM-model, we try to pinpoint or to restraint parameters as much as possible. This section will cover the parameter bandwidths as known from literature and/or estimate parameters based on mathematical derivation or physical reasoning.

2.5.1. PARAMETER BANDWIDTHS FOR FLEXTOPO MODEL

Table 2.4 presents the parameter bandwidths for the different FlexTopo model codes (for FlexB and FlexD are presented in Appendix K). These bandwidths are derived from earlier studies [19, 20, 40].

		FlexA	FlexC		
			Grassy Wetlands	Grass/Crops Flatlands	Forested Inselbergs
I_{max}	Interception storage [mm]	1-5	2-3	2-3	3-5
$S_{u;max}$	Maximum rootzone capacity [mm]	50-500	50-100	150-300	300-500
B	Soil moisture distribution coefficient [-]	1-5	1-5	1-5	1-5
L_p	Transpiration coefficient [-]	0.5	0.5	0.5	0.5
F_c	Relative soil moisture at field capacity [-]	0	0	0	0
D	Divider fast - slow reservoir [-]	0-1	0-1	0-1	0-1
C	Maximum capillary rise rate [mm/day]	0-0.3	0-0.3	0	0
P_{per}	Maximum matrix percolation rate [mm/day]	0-0.5	0	0-0.5	0-0.5
K_f	Fast reservoir delay time [day]	0-20	0-5	0-10	0-20
K_s	Slow reservoir delay time [day]	400-600	300-700	300-700	300-700

Table 2.4: Predefined parameter bandwidths for FlexA and FlexC

The bandwidths of K_f are already further refined for FlexC, since we believe the wetlands with instantaneous runoff (Rainfall on the water surface) and saturated overland flow (SOF) as dominant fast processes to be faster responding than any other process, actually in order faster than 1 day. We stretched up the bandwidth a little to account for other processes. The rocky and very steep (forested) hill slopes are suspected to respond faster flat grasslands or irrigated hill slopes, though we do not force this within our parameter constraints. We admit that there will be faster processes like Hortonian Overland Flow (HOF) and flash floods, though we miss the rainfall intensity to find these processes. Mostly they are considered non-dominant, therefore they are leaved out (for now).

The reservoir constant of the slow responding reservoir K_s can be derived from the conveyance as proved in Paragraph 2.5.2. For GodiDS we derived a K_s value, however since we lacked long time series in general, we decided to leave a bandwidth, so the model could fit to the optimal K_s value itself, which then ultimately might also be better transferable, since we lack the information to replace the K_s values for other catchments. Note that the K_f and K_s values only act as a filter, and do not alter the internal waterbalance of the model. We can therefore change these values as more information is available, without disturbing the model. Since we lack all the necessary information for other stations, we decided to leave a larger bandwidth.

2.5.2. PARAMETERS FOR OCM-MODEL

Table 2.5 shows the parameters of the OCM per measurement point. Not all values are derived in this study, since not all points are used for calibration or validation. For the measurement weirs GodiIS and ChirIS, these parameters are not necessary since the $Q-d$ relation is already know from the discharge relations. In the next subsubsections more attention is paid to the derivation of these parameters.

NO-FLOW DEPTH d_0 AND C_0

The no-flow zone depth d_0 is lower than the lowest observed waterdepth (d_{obs}), since water was still flowing. We assume that the true value holds between $d_0 \in [0, \min d_{obs}]$. This value can be derived by calibration, here

	d_0[m]	C_0[m$^{8/3}$/s]	z_0[m+AD]	$\bar{a}$[m$^{1/3}$/s]	$\tilde{a}$	b	K_s[days]
ChirDS	0.01	0.0001	-0.62	??	4.0	2.5	??
ChirIS	-	-	-	-	-	-	??
GodiDS	0.03	0.00017	-1.75	0.75	3.5	2.9	??
GodiIS	-	-	-0.28	-	-	-	??
MessDS	0	0	-1.04	1.75	1.3	2.0	??
MessIS	0.05	0.0087	-1.43	0.2	5.0	2.1	??
RuagaDS	0.15	0.0052	-0.935	0.3	3.2	3.5	??

Table 2.5: Parameters OCM per measurement point. Not for all measurement points the values are derived in this study, since we did not use them all.

we try to choose the right value based on our field observations. The C_0 is then calculated based on the cross sectional Area (A) and hydraulic radius (R). See equations in Table 2.3.

STEVENS METHOD $\tilde{a}$ AND b

The derivation from the parameters for the Stevens method is already explained in Section 2.4.2. This is applied to all measurement stations, see Appendix F.

ROUGHNESS COEFFICIENT $\bar{a}$

The roughness coefficient $\bar{a}$ accounts for bottom slope I and bottom roughness k. And is equal but unknown for both the Stevens method and the Conveyance method. The roughness parameter $a, \bar{a}$ differ a factor $\tilde{a}$ from each other, resulting from the shape factor (Eqs. 2.9 and 2.11). Since the fit of the shape function in the low region is very precise, $\bar{a}$ does not compensate for a possible misfit.

In general the longitudinal bottom slope around the measurement points is approximately $I = 0.01$, based on some longitudinal measurements of the river bed and the (relatively) course scaled DEM. We fix this value, however incorporating local conditions I can range between $[0.1, 0.001]$. These uncertainties will be solved by the roughness term k

The Strickler roughness k from Eq. 2.6 generally ranges between $[20, 50]$ [15], where 20 is a mountain stream with rocky bed and river with variable sections and some vegetation along banks and 50 a straight unlined earth canal in good condition [Chow [44]]. In this case the channels are heavily vegetated, even lacking a free flowing zone (see e.g.,Figs. F.28 and F.30), that k-values are likely to be lower $[2, 15]$. Estimating the lower and upper bounds: $\bar{a} = \sqrt{I}/k$ so

$$\frac{\sqrt{I_{min}}}{k_{max}} \leq \bar{a} \leq \frac{\sqrt{I_{max}}}{k_{min}} \tag{2.16}$$

$$\frac{\sqrt{0.001}}{15} \leq \bar{a} \leq \frac{\sqrt{0.1}}{2}$$

$$2.1e^{-3} \leq \bar{a} \leq 0.16$$

In this study we eventually calibrated $\bar{a}$ based on the parsimonious discharge measurements. Using the properties of logarithmic functions we should be able to calibrate the $\bar{a}$ using some discharge measurements. (salt dilution measurements). Note that depth dependent roughness (due to increased vegetation density by larger water depths) is not taken into account. The calibration is shown in Fig. 2.11 and proved in below equations. The final outcomes are presented in Table 2.5. Though the derived values for $\bar{a}$ are outside our predefined expectations.

$$C = \frac{Q}{\bar{a}} + C_0 \tag{2.17}$$

[15] Note Strickler is the inverse of Manning

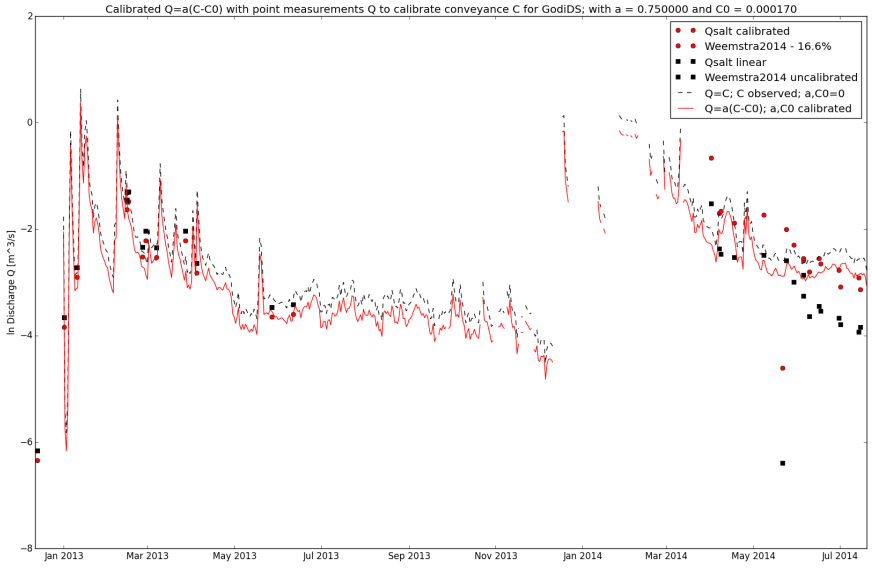

Figure 2.11: Observed Conveyance Godi DS calibrated with point observations discharge Q; calibrating the a and C_0. Parameter tuning is performed visually.

$$\ln(C - C_0) = \ln(\frac{Q}{\bar{a}}) \tag{2.18}$$

$$\ln(C - C_0) = \ln(Q) - \ln(a) \tag{2.19}$$

on the right axis

$$Q = aC - aC_0 \tag{2.20}$$

$$\ln Q = ln(a) + ln(C - C_0) \tag{2.21}$$

DERIVING K FROM WATER LEVELS IN KNOWN CROSS-SECTIONS

For the FlexTopo model estimates for the recession curves, or delay constants K can be derived from the cross-sectional corrected waterdepths, conveyances $C(t)$. Again making use of the quasi-static uniform flow assumption (Eq. 2.6), substituting $AR^{2/3} = C$, $\sqrt{I}/k = \bar{a}$ and applying the linear reservoir assumption (Eq. 2.22) [43],

$$Q(t) = \frac{S(t)}{K} \tag{2.22}$$

where Q represents the discharge $[m^3/s]$, S the storage $[m^3]$ and K the delay time $[s]$, together with the simplified water balance (Eq. 2.23), assuming all other processes (P, I, E, T, Q_{gw}) to minor influence the deep groundwater storage:

$$\frac{\mathrm{d}S(t)}{\mathrm{d}t} = -Q(t) \tag{2.23}$$

we have

$$\begin{cases} Q(C(t)) = \bar{a}C(t) \\ Q(t) = Q_0 e^{-t/K} \end{cases} \tag{2.24}$$

Since the cross-sectional corrected waterdepths $C(t)$ are known, Q can be substituted with $\bar{a}C$, where $C_0 = Q_0/\bar{a}$

$$C(t) = C_0 e^{-t/K} \tag{2.25}$$

$$K = \frac{t}{\ln(C_0) - \ln(C(t))} \tag{2.26}$$

The residence time K follows from the tangent line through the semi- logarithmic plot of $[t, \ln(C(t))]$, notice that the unknown term C_0 drops out of the equation.

$$K = \frac{\Delta t}{\Delta \ln(C_0/C(t))} = \frac{t_2 - t_1}{\ln(C_0) + \ln(C(t_2)) - \ln(C_0) - \ln(C(t_1))} \tag{2.27}$$

$$K = \frac{t_2 - -t_1}{\ln(C(t_2)) - \ln(C(t_1))} \tag{2.28}$$

With this equation, residence times K can be derived for the measurement points Godi downstream, Chirodzo downstream, Messica intermediate and Ruaga downstream station.

DERIVING K FROM WATER LEVELS FOR BRIDGE WITH 3 GATES

Similar approach can be followed for the 3 gates bridge at Messica downstream. The bridge is made and aligned with concrete, and has a angle of 27 degrees perpendicular to the bridge normal line (Fig. 2.12b). Each gate has different dimensions and sill levels (see Appendix F.2.5). During the whole year the bridge acts as a free flow construction.

(a) Gates Messica bridge

(b) 27^o orientation of the gates

Figure 2.12: Bridge over the River Messica, acts as a free flow construction. This is the most downstream measurement point

The general equation for a free flow construction reads

$$Q(h) = mB\,(h(t) - h_{sill})^{3/2} \tag{2.29}$$

Where $Q[m3/s]$ is the discharge, m a roughness coefficient, $B[m]$ the sill width, $h(t)[m] + AD$ the water levels and $h_{sill}[m] + AD$ the the sill level. We assume that:

- the gates act independent of each other, that is, streamlines do not influence inflow in gates;
- the roughness coefficient m is constant and equal for all gates;
- the total bridge flow is a linear superposition of the three individual gates;
- the catchment responds as a linear superposition of several independent linear reservoirs.

$$\begin{cases} Q(h) = \sum_{i=1}^{3} m_i B_i \left(h(t) - h_{sill;i}\right)^{3/2} \\ Q(t) = Q_0 e^{-t/K} \\ Q(h) = Q(t) \\ m_i = m \end{cases} \tag{2.30}$$

$$Q(h) = m \sum_{i=1}^{3} B_i \left(h(t) - h_{sill;i}\right)^{3/2} \tag{2.31}$$

with $C(t)$ the cross sectional corrected waterdepths which can be determined for every water level $h(t)$.

$$C(t) = f(h(t)) = \sum_{i=1}^{3} B_i \left(h(t) - h_{sill;i}\right)^{3/2} \tag{2.32}$$

After substituting Eq. 2.32 into Eq. 2.31 into Eq. 2.30 one find again Eq. 2.28.

2.6. CALIBRATING MODELS

In order to calibrate the models, a number of assumptions and choices are made. They lead to the final results as presented in the next chapter. In chapter Discussion we elaborate further on the impacts of these decisions.

The steps below summarize the calibration approach bullet wise, where the letters reflect choices and the numbers results:

a. The calibration is performed on Godi Dowstream Station(GodiDS), since it entails the longest time series and the measurement point is close to its spring at the Inselberg.

b. Messica Downstream Station (MessDS) serves as validation point [16]. This point is located at a bridge in the Messica downstream from GodiDS's inflow point. Points for consideration are

   - The available measurements are restricted to some baseflow recession after the wet season.
   - The catchment is not purely Inselberg dominated, but also contain large gently sloped areas, most likely not connected to the Inselbergs (see slopes in Fig. I.6).

c. The precipitation amount is linear corrected for the altitude effect conform Eq. 2.1. The corrections are applied on the rainfall measurements at David's place, see Table 2.1.

d. The observed Conveyances and Waterdepths are daily averaged from 8am the previous day to 7am current day, to match with the precipitation observations.

e. The conveyances are only used to objectively judge the model performance, since water levels are affected by the linear average problem.

f. Division FlexC buckets based on Flow Accumulation of 50 cells on a 30*30m2 grid with an accompanying HAND value of 2m and a hill slope threshold of 11% to split the area over *Grassy Wetlands, Grass, Crop vegetated and/or irrigated Flatlands* and *Forested Hillslopes*.

g. The groundwater recharge area is restricted to the catchment area as derived from the DEM. The final results do not extend the groundwater recharge area to the western hill slope to correct for internal fracture inclination.

1. Calibrate the OCM parameters for each measurement point. These paramaters are tuned such that the observed daily averaged conveyances match the observed salt dilution discharge measurements. These parameters are fixed, since they are location specific and considered time-invariant.

2. Apply the Monte Carlo method[17] to generate 10,000 parameter sets to feed into the FlexTopo model. Before calculation, the parameter sets are tested on physical feasibility with so called parameter constraints to filter out physical impossible (or unlikely) parameterizations.

[16] Other measurementpoints (see App. F) are not tested during this study, but observations and model instrumentation are ready to do so.

[17] A method to select parameters from a uniform distribution with prefixed boundaries.

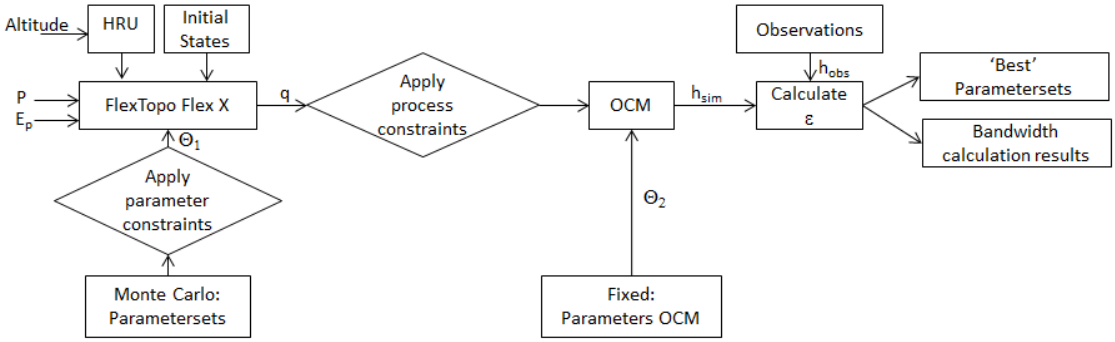

(a) Calibration process
Calibrate FlexTopo FlexX model including OCM on GodiDS with additional process and parameter constraints

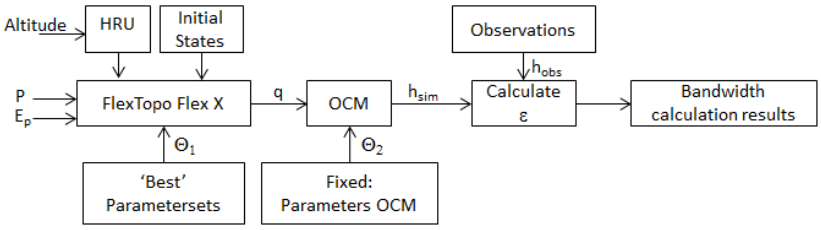

(b) Validation process
Validate FlexTopo FlexX model on other measurement points

Figure 2.13: Calibration and validation steps

3. Calculate the different FlexTopo models FlexA, -B, -C and -D for the calibration point GodiDS. Models that not fulfill physical processes (process constraints) are rejected, just as models with objective scores for Log Nash-Suthcliffe for the Conveyances (LogNS_C) below zero.

4. Calculate for every timestep the median, 10 and 90 percentile values of calculated discharge, water levels and conveyances of all accepted calculations. This gives a measure of the reliability of the model ensemble.

5. Calculate the discharges Q [m^3/s] for the validation point and compare the median, 10 and 90 percentile values with the (discharge) observation[18].

6. Select the 2% best performing models (highest LogNS_C) and determine the bandwidth of water storage development in time for the slow response reservoirs (which is a measure for the active participating groundwater storage in (parts of) the catchment).

We tested the effectiveness of all above choices (letter bullets) and came up with this set of choices for the best results for now, given the available time and assumptions.

In this study we did not apply automatic calibration routines[19] yet. To calculate larger ensembles of parameter sets this would be an improvement.

We calculated the median and percentile values for every timestep for the total set of accepted calculations. This is a subjective choice, and meant to reflect on an easy way the effectiveness of the model ensemble on both calibration and validation points. Another method would be to apply the GLUE method (Generalized Likelihood Uncertainty Method) which weights the calculations to their objective scores and being so makes another bandwidth.

Figures 2.13a and 2.13b illustrate the subsequent steps taken in this process. Figure 2.13b shows how the accepted parameter sets are applied on validation points. If information is available, the model effectiveness is calculated with the objective functions.

[18] In case of Messica DS more information is available, so this is also used to judge the validation performance
[19] For example MOSCEM-UA [Vrugt *et al.* [45]] or one of the latest methods designed for hydrologic purposes AMALGAM [Vrugt [46]].

With objective functions we compare the model outcome with the observed measurements. These functions evaluate the accuracy and correctness of the model and are a measure for model feasibility. The objectives are applied on conveyances, waterdepths and discharge time series (if available). The functions objectively [20] rate the goodness of fit, see Table 2.6. All parameter sets that do not fulfill acceptation bandwidths are rejected. In this study the only restriction reads $\text{LogNS}_C \leq 0$. For other objectives no additional penalties are applied, since to much models point out to be rejected.

A small remark about the (Log) Nash-Sutcliffe functions. A score of (Log)NS= 1 represents a perfect match, whereas (Log)NS< 0 the average of the observations would be a better estimation of the system response than the underlying calculation.

Description	Equation	Optimal value	Accepted band widths
Nash Suthcliffe: Function generally applied to compare peak - medium observed values to modelled ones.	$\text{NS} = 1 - \frac{\sum_{i=1}^{N}(O_i - S_i)^2}{\sum_{i=1}^{N}(O_i - \bar{O})^2}$	1	[0,1]
Log Nash Suthcliffe $\log_{10}$ of NS commonly used to judge the low (baseflow) values[a]	$\text{LogNS} = 1 - \frac{\sum_{i=1}^{N}(\log_{10} O_i - \log_{10} S_i)^2}{\sum_{i=1}^{N}(\log_{10} O_i - \log_{10} \bar{O})^2}$	1	[0,1]
RMSE: Root Mean Square Error	$\text{RMSE} = \sqrt{\frac{1}{n}\sum_{i=0}^{n}(O_i - S_i)^2}$		N.R.
NRMSE: The Normalized Root Mean Square Error. The RMSE is unbounded. Normalizing the RMSE is done by dividing the outcome by the observation's average.	$\text{NRMSE} = \frac{\sqrt{\frac{1}{n}\sum_{i=0}^{n}(O_i - S_i)^2}}{\overline{O}}$	1	N.R.
NRMSE_FDC: Calculates the Normalized RMSE of Flow Duration Curve, i.e. the ascended sorted observed and ascended sorted simulated values.		1	N.R.
WBalance: Balance equation, this objective function evaluates how accurate the total observed flow / water level is approximated by the simulated one, with $B \in (-\infty, 1]$ [Hartmann *et al.* [47]]	$B = 1 - \frac{\left\lVert\sum_{i=0}^{N} O_i - S_i\right\rVert}{\sum_{i=0}^{N} O_i}$	1	[0.25,1]

[a] Note that the Log10 and Natural Logarithm LN will end up in the outcome space and only differs a constant from each other, since the base numbers of the Log functions can be changed. This therefore will not lead to an extra objective score.

Table 2.6: Objective functions applied in this model
N.R.: Not restricted

Finally to calculate the groundwater storage in the buckets, we chose to narrow down the bandwidth of accepted models to 2% in order of the best performing models, that is the cumulative score of LogNS_C + NS_C of every model simulation. Narrowing the bandwidth was necessary, since otherwise the bandwidths are too large, and no clear patterns are visible. We believe, that although this choice is a little subjective, it is justified because of the fact that we did not apply automatic calibration routines and/ or the GLUE method. Nor did we manual calibration to come to subjective optimal solutions.

[20] that is, the algorithm do not include subjective evaluation

3

RESULTS

This chapter presents FlexA and FlexC model's calibration and validation results for Godi Downstream Station (GodiDS) and Messica Downstream Station (MessDS) respectively. The results show that the baseflow recession can be estimated based on conveyances only. Furthermore FlexC seems capable to pinpoint and estimate the waterstorage. Both FlexModels incorporate altitude corrected precipitation. Only the final calculations are shown here, more outcomes are given in the appendices.

3.1. MEASUREMENTS

This section discusses first the measurements as plotted in Figures 3.1 and 3.2 for GodiDS and 3.11 and 3.12 for MessDS. The figures consist of 4 subfigures a to d.

Subfigure a shows the unadjusted precipitation measurements at David's place, which is located halfway the Inselberg Ridge at an altitude of 878m+AD[1]. For the spin-up time of the model we duplicated the observations between October 2012 to October 2013 to October 2010 to October 2011 (See App. C). Note that the wet period 2011-2012 have been quite dry compared to the subsequent years. Furthermore that no precipitation events are recorded between April and September 2012.

The observed discharges are plotted in subfigure b. The green and black dots are obtained with salt dilution measurements (see Appendix D). The black dots represent the corrected and/or calibrated measurements and the green dots the uncorrected or uncalibrated measurements. Weemstra *et al.* [7] conducted measurements in 2012 to 2013. His measurements most likely include a structural overestimation of 19% due to a device error [2]. He applied a different method to determine sample's initial salt concentration, then we did. Therefore we calibrated measurements afterwards (see D). We performed the salt dilution measurements in 2014. The black dots show the discharges after calibrating the EC-salt concentration relation, whereas the green dots assume a linear relation between the EC and salt concentration (which is not true).

Subfigure c plots the daily, linearly averaged waterdepths relative to the bottom level (red line) [3]. The black dots represent the manually observed waterdepths. These observations are done independently of each other, so the overlap between these data increases the reliability of the measurements. Unfortunately, the barometer was not working well during the wet period of 2013-2014, therefore this data is excluded from the calibration and only serves for visual validation of the results. To do so, we have to keep in mind that the red peaks during this period do not represent the maximum water levels, but only tells us that there was a peak event at that moment[4].

Finally, the conveyance is presented in the semi-Log scaled subfigure d. By conveyance's very nature, the differences between peak and baseflow values are already very pronounced, but are even more amplified because of the large differences between peak and baseflow. This is a result of semi-tropical convective storms in rain season versus no rain and therefore small baseflows during the dry period.

[1] Note that the applied precipitation is about 2% less than presented here, since the overall elevation of the Godi catchment is 861m+AD. The reduction of the precipitation due to the altitude dependency is calculated according to Eq. 2.1, see Appendix C.

[2] A wrong internal recording time interval of 3.5s instead of 3.0s(see Appendix D)

[3] More background information about the derivation of the waterdepths is given in Appendices F2.3 and E

[4] The value is actually the vertical distance between the barometer and the diver. So it only indicate at which moments the barometer was flooded too and therefore presents us a time indication for the peak flow events

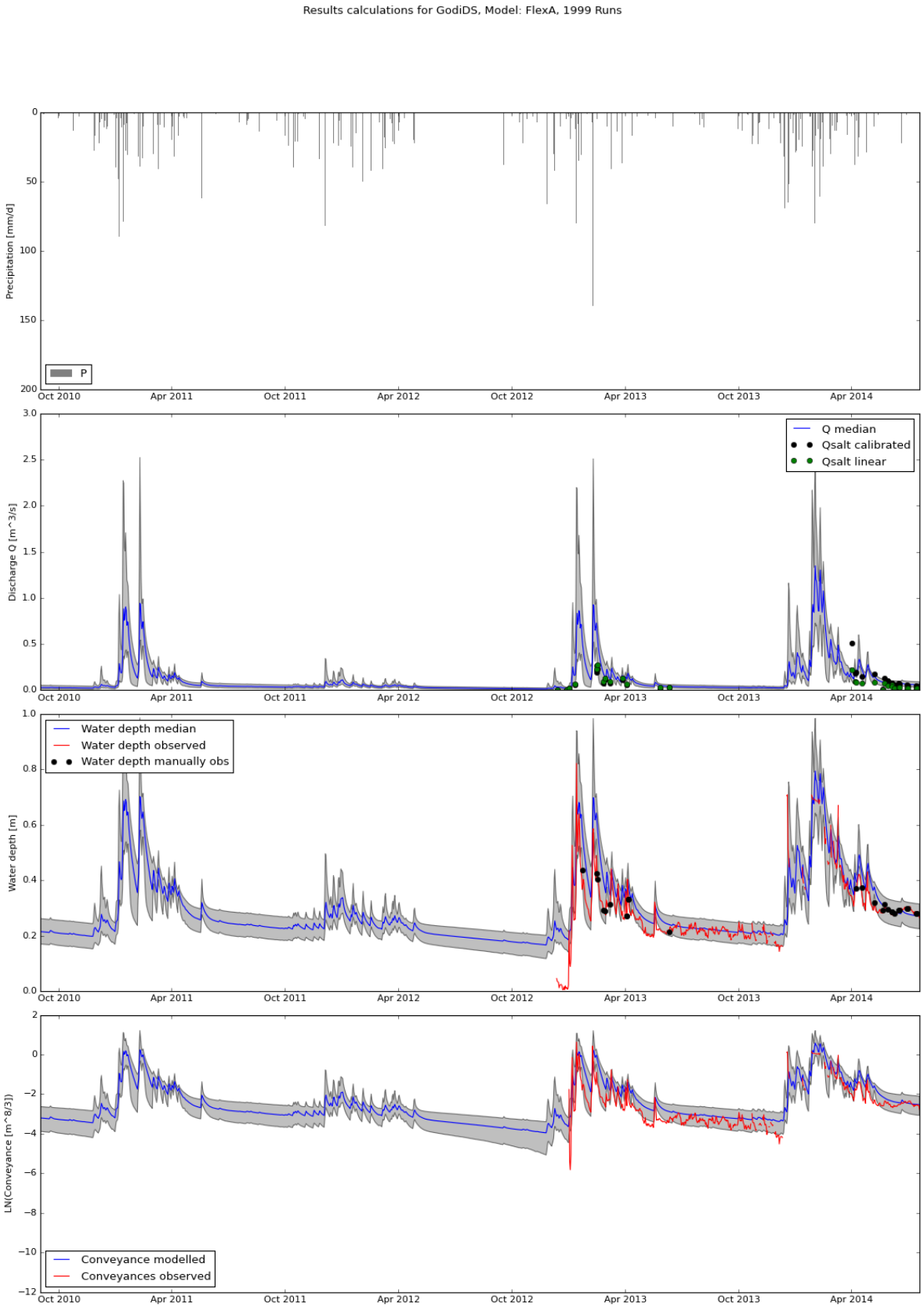

Figure 3.1: 10 to 90 percentile bandwidths of all accepted model simulations for Godi Downstream Station with FlexA. The blue median simulates the observed values as good as NS Waterdepths = -0.08, LogNS Waterdepths = 0.02, NS Conveyance = -0.07 and LogNS Conveyance = 0.14.

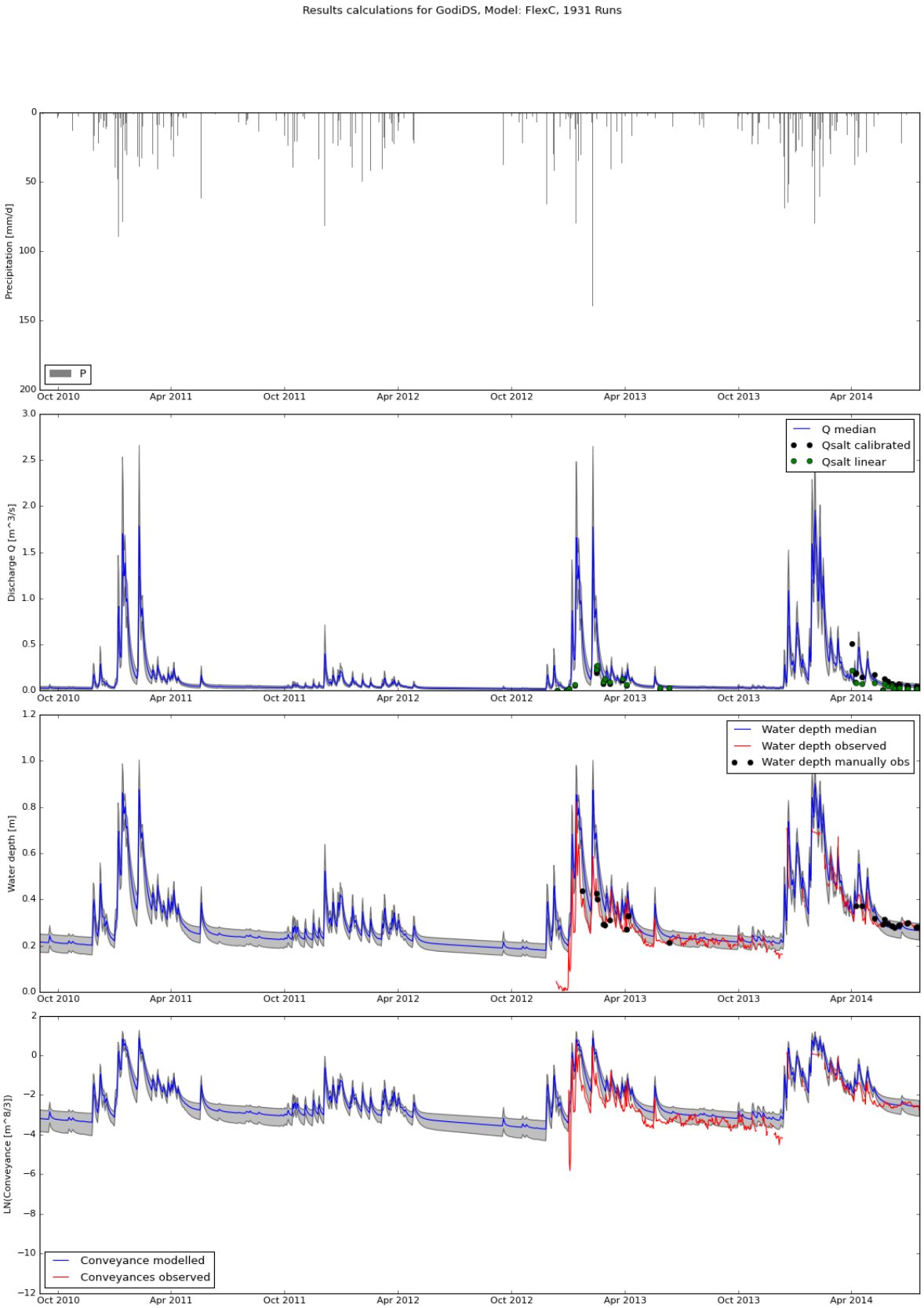

Figure 3.2: 10 to 90 percentile bandwidths of all accepted model simulations for Godi Downstream Station with FlexC with altitude corrected precipitation amounts on HRU scale. The blue median simulates the observed values as good as NS Waterdepths = -0.04, LogNS Waterdepths = 0.01, NS Conveyance = -0.05 and LogNS Conveyance = 0.15

3.2. CALIBRATION

The calibration is performed on GodiDS. We drew 10,000 uniform distributed Monte Carlo Sample parameter sets for the calibration. This resulted in 1999 accepted simulations for FlexA and 1931 accepted ones for FlexC.

A parameter set is accepted when the LogNS Conveyance value is equal to or larger than zero (i.e. LogNS_C ≥ 0). We only apply one constraint, since constraints on waterdepths are theoretically incorrect (because of the linearization problem). Furthermore, we also did not constraint the NS_C value, since the ratio between peak and low conveyances is very large, because of conveyance very nature and because of the pronounced wet and dry season. Peak flows appear to be hard to predict by FlexA and FlexC. Moreover, the baseflows are less influenced by backwaters than peak flows, which supports the use of LogNS_C over NS_C.

All accepted parameter sets are combined in a sample of parameter sets, the calculations of all different sets are combined and we calculated the 10th, 50th (i.e. median) and 90th percentile values for every time step. The 10th and 90th percentiles are shown in the gray bandwidths, whereas the blue line illustrates the median calculated value. See Figs. 3.1 and 3.2. The model outcomes are visually validated on temporability at GodiDS in the period October 2013 to July 2014 and (automatically) validated on transferability at Messica Downstream Station, as will be discussed later.

GodiDS's calibration results show a large degree of similarity between FlexA and FlexC. The overall performance of the model judged on the median value of the outcomes is comparable. For both models calculated discharges, water levels and conveyances line up with the baseflow recession observations. Next to this, the resulting 10 and 90% uncertainty intervals from FlexA and C are in the same order. The extremes, however, have different magnitudes. If we compare FlexA with FlexC, we observe that peaks in 2012-2013 runs up to 1.0m3/s for FlexA versus 1.7m3/s for FlexC and for 2013-2014 1.5m3/s for FlexA versus 2.0m3/s for FlexC. Judging the water level and conveyance dynamics, it is more likely that FlexC overpredict the discharge, since the calculated conveyances are higher than the observed ones. Whereas we would expect an underestimation of the conveyances, since positive backwater curves[5]. FlexA, on the other hand, underpredicts the maximum conveyances and, being so, might predict the discharges better. However, discharge measurements during peak events lack, so final conclusions cannot be drawn here.

During the dry period, the medians of water depths and conveyances nicely cut through the observed (maximum) water depths and conveyances[6]. We expected the baseflow to slightly overpredict (i.e. cutting through the maximum observed values), since daily and weekly discharge variations due to riparian transpiration and irrigation activities are not explicitly taken into account in the model conceptualization. Hence, the model returns non-corrected daily maximum catchment outflow, which occurs around 4am according to de Boer [8], Meyboom [48]. Please note that FlexC shows more dynamics than FlexA in the last months of the dry season. This indicates that rainfall events in this period are captured better with the FlexC's semi-distributed model concept.

Boxplots Figs. 3.3 and 3.4 present the outcomes of the objective functions. All model realizations with a LogNS Conveyance value lower than zero are rejected, which explains the skewed boxplots for LogNS_C for both FlexA and FlexC. There are no additional penalties for the other objectives. About 25% of FlexA realizations return a NS conveyance (NS_C) value higher than zero, whereas the score for FlexC is much lower. This is most likely the result of FlexC's overpredicting behaviour. The waterdepth duration curve (similar to the flow duration curve) (CVRSMEFDC_WDepth) is pretty good simulated as well as the waterbalance of the waterdepths (WBalance_WDepth), which is the cumulative of all observed waterdepths compared to the cumulative of all calculated waterdepths[7]. For both objective functions hold that one is the optimal value.

Overall, FlexA denotes higher objective scores than FlexC. Possibly this is due to the fact that a parsimonious-constraint flexible lumped model can mimic observations better than a more complex, higher-constraint distributed model concept like FlexC. On the other hand, note that all FlexC's interquartile ranges are smaller than FlexA's. There is however one exception, the NS_C perform worse for FlexC than FlexA. Probably this is due to the earlier mentioned peak overestimation. All in all, FlexC shows a more consistent model performance than FlexA.

[5] Partially due to peak flows, partially to denser vegetation above 'average' water level. Therefore water levels will rise even more, since the cross-section is partially blocked

[6] Keep in mind that due to daily linear averaging the plotted water levels are not totally representive, whereas conveyances are

[7] these values are not calculated for Conveyances.

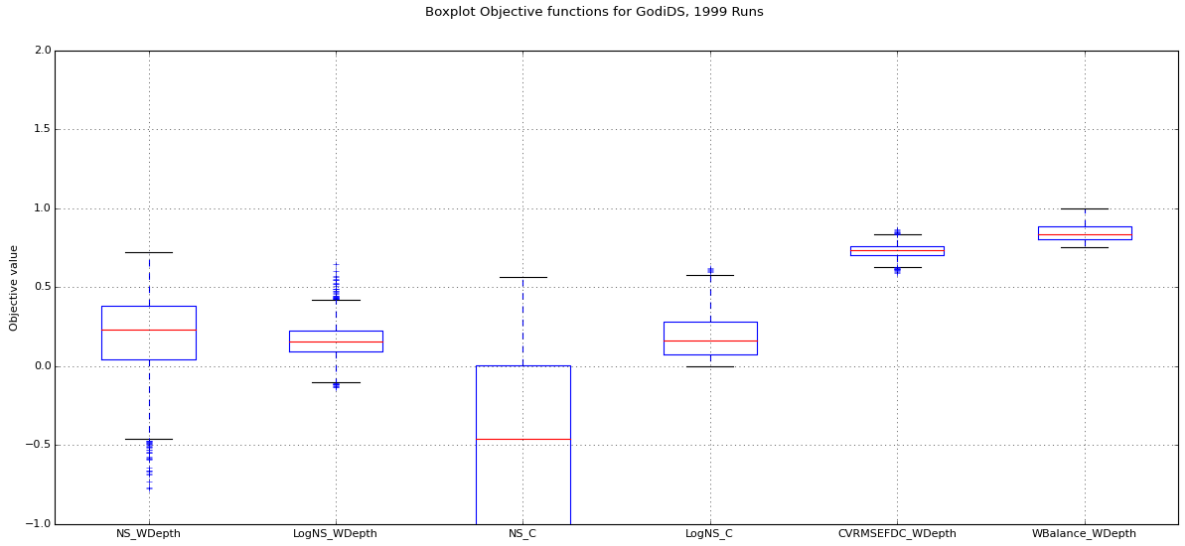

Figure 3.3: Boxplots outcomes objective functions Godi Downstream Station for FlexA
* **CV**RMSEFDC_WDepth = **N**RMSEFDC_WDepth

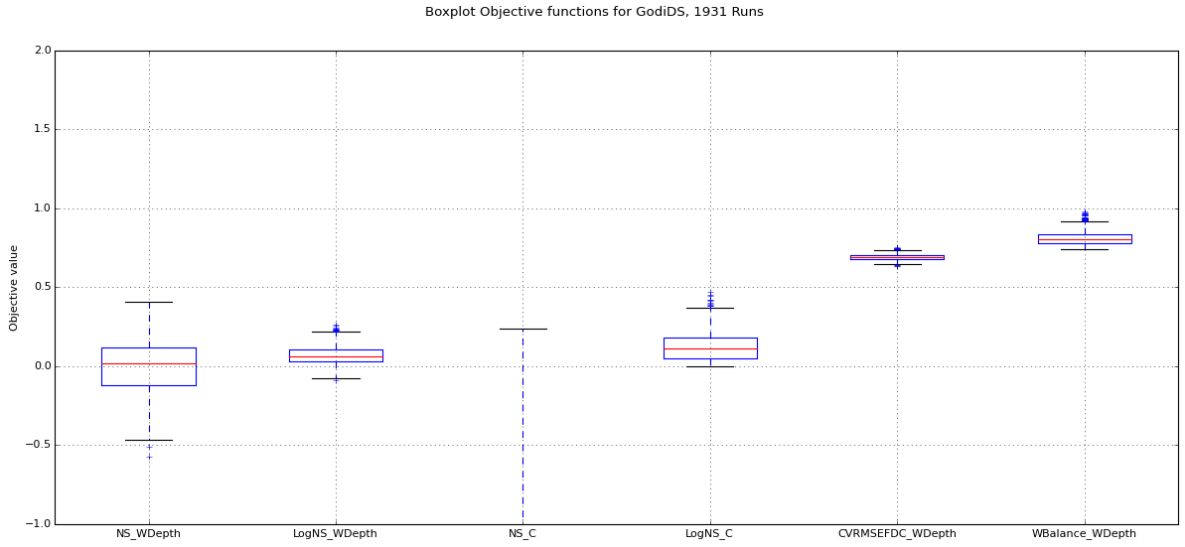

Figure 3.4: Boxplots outcomes objective functions Godi Downstream Station for FlexC
* **CV**RMSEFDC_WDepth = **N**RMSEFDC_WDepth

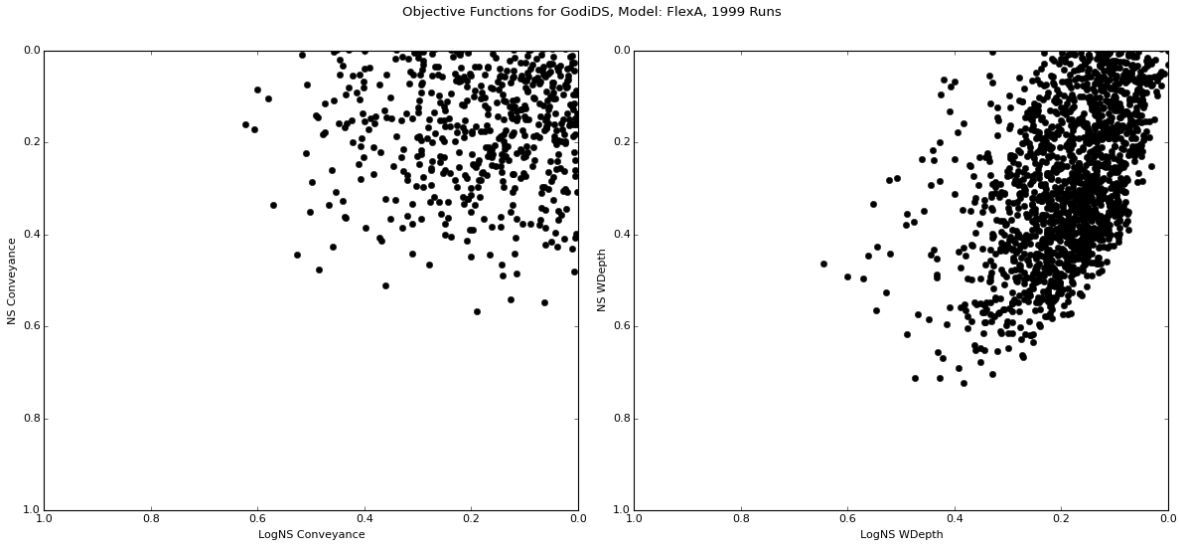

Figure 3.5: Pareto fronts Conveyance (left) and Waterdepths (right) for Godi Downstream Station FlexA

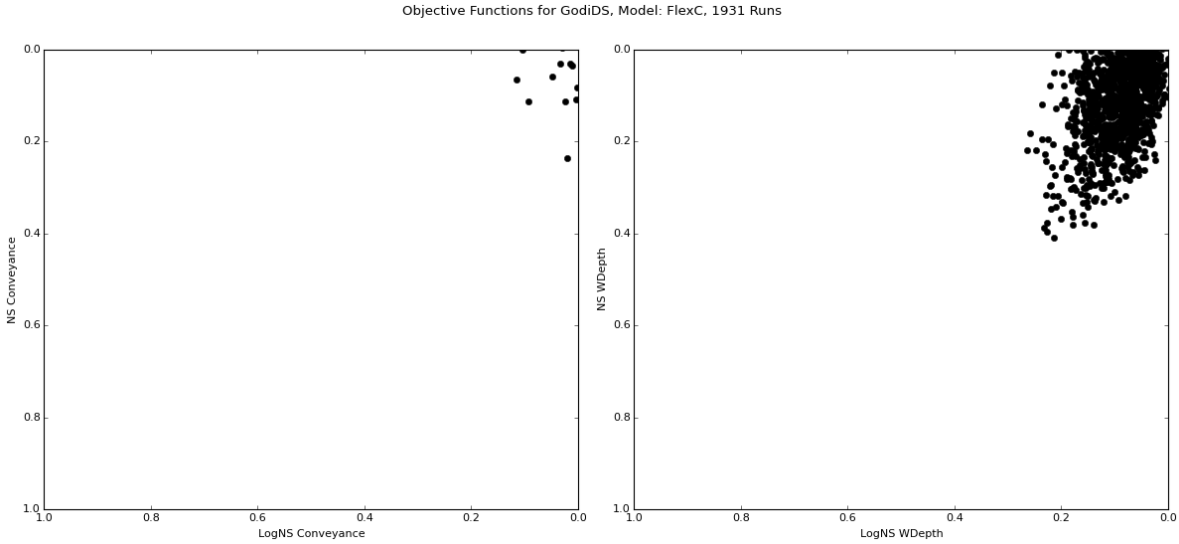

Figure 3.6: Pareto fronts Conveyance (left) and Waterdepths (right) for Godi Downstream Station FlexC

Next to the boxplots, the pareto fronts (Figs. 3.5 and 3.6) emphasize the NS versus the LogNS scores[8]. Every dot indicates one model realization, the closer the dot is placed to the origin (1,1) the closer the outcome overlaps the measurements. The left graph presents the pareto fronts for the NS and LogNS Conveyance Objective, its waterdepths equivalent is shown in the right graph.

As mentioned, about 25% of FlexA calculations score a NS Conveyance higher than zero (see Fig. 3.3, NS_C). Being so, this explains the low dot density of the left chart compared to the right since this one hold more than 75% of all accepted model realizations. Furthermore, the left plot lacks a very sharp pareto front, this is because automatic calibration routines like MOSCEM-UA [**?**] or AMALGAM [46] are not applied and therefore model performance are not tweaked to find (local and global) optima.

Concerning the right graph, we recognize a pareto front at the right hand side (towards (0,1)) in stead of on the expected left hand (towards (1,1)). The skewness of the pareto front, however is caused by 2 facts.

If we zoom in to the peak levels in winter 2012-2013 (which is part of the calibration period) (Fig. 3.1**c**), we observe that the measured (red) peak observations nicely fall within the gray bandwidths, whereas the

[8] Note that the Pareto plot is just a 2D representation of the Boxplots (Figs. 3.3 and 3.2, boxes NS_C, LogNS_C, NS_WDepth and LogNS_WDepth)

observations during recessions are closer to the lower band (10-percentile). This causes that the NS in this period will be higher than the LogNS. While during the low flow period, the median approximately averages the observations, therefore NS and LogNS will stay close to 0[9]. Firstly, note that the water level extremes range between 0.2 and 1.0m. Whereas the minimum and maximum values for conveyances are more pronounced. This effects the mutual relation between the objective functions NS_WDepth and LogNS_WDepth[10].

Secondly and most significantly, the daily averaging problem causes a biasness in the outcomes, especially for the high flows, since the cross-section is strongly non-linear. Therefore the LogNS_WDepth and NS_WDepth are not fully objective scores anymore[11].

For the Paretoplots belonging to FlexC (Fig. 3.6) we simply observe that only a very small amount of model realizations score higher than zero for NS_C (see Fig. 3.4). This explains the absence of a pareto front. For the waterdepths plot, also here the results are biased due to the averaging problem and the scores are more confined with a lower average. Also for FlexC, more extensive calibration (for example using automatic routines) would result in better scores and pareto fronts.

[9] Please note that NS and LogNS returns 0 for the average value by definition

[10] In general high NS_WDepth scores are easier achieved than high NS_Conveyance values

[11] This can be understood as follows: on the one hand the water level measurements are daily averaged, whilst they are obtained on (half) hourly base. On the other hand, the model calculates daily averaged discharges, mapping these to water levels take the cross-sectional influence implicitly into account. Whereas from the measurements to the discharges, the cross-sectional non-linearity was not taken into account. The result is that the measured discharge is underpredicted, in reality the discharge is higher. This explains why low flows are overpredicted (observe that measurements in low flow periods are close to lower bandwidth) and calculated high flows are not underpredicted (calculations are close to median).

Figure 3.7 presents FlexA's parameter samples. Every dot belongs to a parameter set. The value of the dot is randomly selected from a uniform distribution between upper and lower limits (Monte Carlo). The closer the dot comes to one, the better that simulation performed. There is some structure in the parameter plots notable. However, since no automatic calibration is applied, the parameter plots are not very pronounced. Please note that due to parameter equifinality, hydrological processes will compensate for each other, which lead to greater difficulty in observing parameter values.

The maximum interception (I_{max}) does not show a clear optimum. Most likely there will be one within the domain $I_{max} \in [3, 4.5]$ mm/day. This value ranges between Forest interception ([3,5] mm/day) and Grassland interception ([2,3] mm/day). This is in line with our field experiences.

The maximum soil moisture capacity of the unsaturated zone's ($S_{u;max}$) optimum approaches [450,500] mm. Model sensitivity tests with maximum $S_{u;max}$ values up to 1000mm does not result in optima larger than 500 mm (see Appendix N.2). Since 500mm is rather large storage (it is the total volume of soil moisture available for the plant roots) it might indicate that the influence of forests is rather large in this catchments.

Same holds for the B parameter, which steers the division C_r of water between the unsaturated zone and the preferential flow via the fast and slow response reservoir. In general, the larger the B the more threshold like behaviour will occur. That means, all water is directed to the unsaturated zone, until the S_u equals the field capacity threshold $F_c * S_{u;max}$. Then almost all effective precipitation P_e will be directed to the preferential processes. Here we find a optimum value $B \in [4.5, 5][-]$, stretching the maximum B to 10 does not lead to optima higher than 5 (see Appendix N.2).

The capillary rise C interfere with matrix percolation P_{per}, since both occur in the same model with the same units. They counteract with each other and therefore can be subtracted from each other. We observe from the graph that optima for capillary rise is $C \in [0.2, 0.25]$ where the matrix percolation P_{per} shows a optima between [0.1,0.2]. In general capillary rise is a dominant process for this lumped catchment. This seems a little unrealistic, since capillary rise is restricted to wetlands and riparian zones, whereas matrix percolation occurs at the remaining part of the catchment.

The divider D between the fast and slow response reservoir has a clear optimum around 0.4. This indicates that about 40% of the preferential flow enters the slow response reservoir and the remaining 60% the fast one. It is in line with our expectations that there will be a clear optimum for a lumped conceptual model. The answer the question around which value the optimum will occur, is less clear to answer.

For the response time K_f of the fast response reservoir, we observe an optimum between [2,4] days. The response time K_s for the slow response reservoir is less obvious and ranges between [500,550] days. One can argue that the K_s value can be derived from the hydrograph, or in our case from the conveyance graph (as proven in section 2.5.2), however, due to lack of longer time series for other measurement points we maintain a bandwidth around the expected value. Both the fast and slow response reservoir acts as signal filter. They do not influence the water balance [12]. It is therefore possible to change these values (based on derivations from the hydrograph) without disturbing the calibration. Unfortunately, since we lack these values for other catchments, like our validation station Messica Downstream, and we do not know for sure that MessDS's K_s value equals the Godi's one, we choose to maintain a bandwidth to prevent pre-exclusion of the optimal response time.

We chose not to alter the $N_{s;lag}$ and $N_{f;lag}$. These are shape parameters of the delay function which steers the rate and shape of inflow from the unsaturated / root zone to the slow and fast flow. By setting these parameters equal to 1, we model an instantaneous recharge process. We justified this assumption by the problem of equifinality. This will solve our simplification by (slight) adjustment of the K-values. The assumption seems to be justified for now, Since we do not clearly observe that the baseflow recession of the model starts earlier than that of the measurements, it is rather the other way around.

The model lacks a flow routing function (for the combined discharge of Q_s and Q_f). This would increase the transferability of model structures to other catchments with different reach lengths.

[12] Since there is no internal feedback within the model to precedent processes, the K-values only steer the response or delay time of the signal

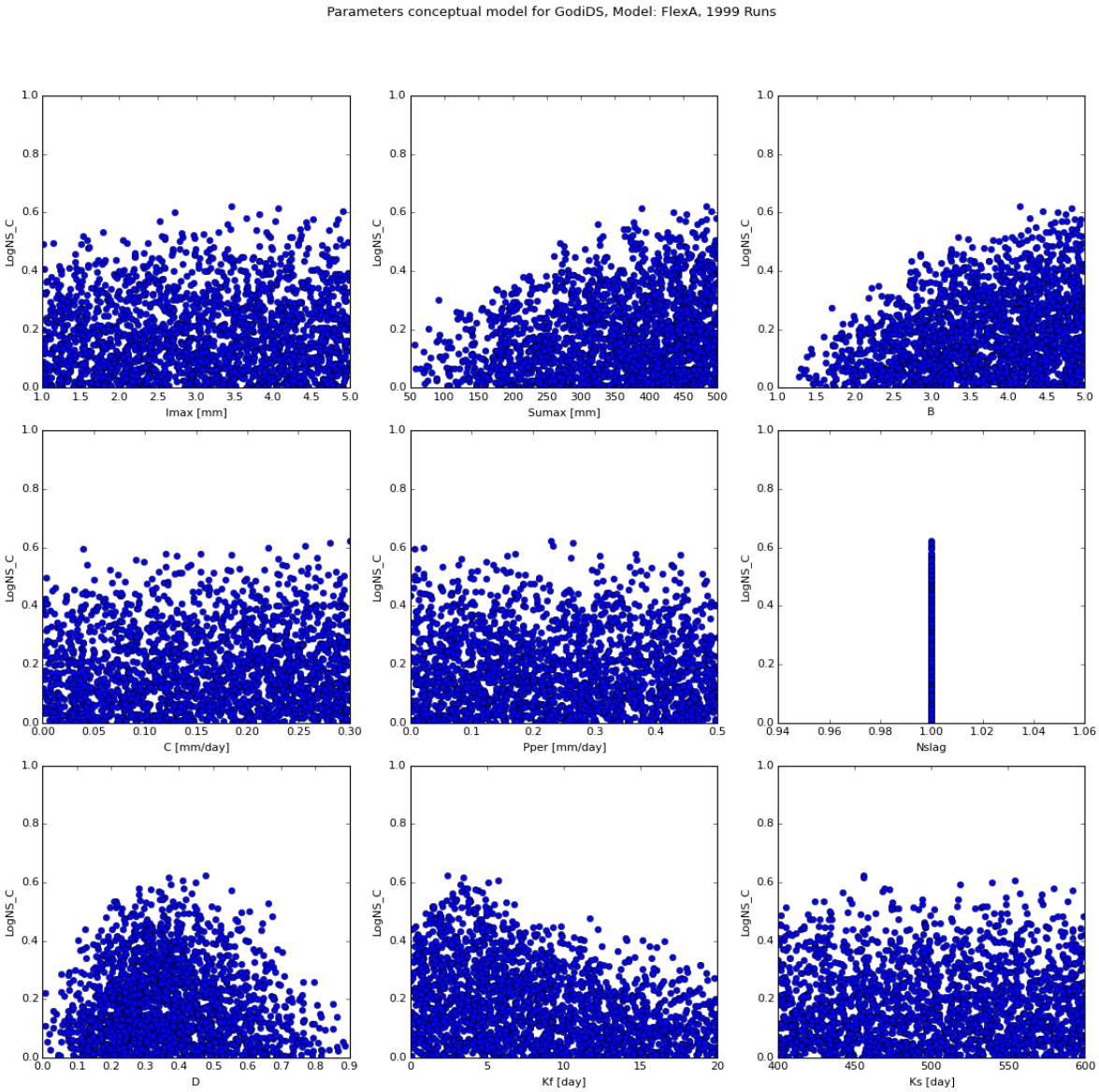

Figure 3.7: FlexA Conceptual model parameters. The objective LogNS Conveyance score (y-axis) of a model realization (a dot) plotted against its specific parameter value (x-axis)

Since FlexC is a distributed lumped model, the parameters are split up to the different HRUs. First of all, again we lack sharp contours in these scatterplots[13], though, some structure can be observed. We will discuss them here row wise.

For I_{max}, a clear deviation between the HRUs is already predefined in the parameter bandwidth. For the red dots a real optimum is not observed, for the forest (green) an optimum value concentrates around 4.3, lastly for the wetlands (blue) 2.4 appears to be an optimum value.

For the B more structure is visible. The B steers the shape of recharge of the rootzone. The larger the exponential B, the larger model's sensitivity and the more water is routed towards the fast and slow runoff processes. The smaller B the larger the fraction that stays within the rootzone. For forest (green), optimum pops up around 4, for wetlands, blue, optimum shows around 4.5 and for irrigated croplands, possibly the optimum value is around 5 of even higher (see Appendix N.4. It is hard to give a qualitative judgment, since this parameter also compensates for the spatial drainage deviation, rootzone depth and matrix percolation in the catchment. Though, we would expect a lower B value for grasslands than for forests. Possibly this deviation is caused by interdependency with rootzone depth.

Matrix percolation is only taken into account for Flatlands and Inselbergs. Where Flatlands show optima values around 0.3, Inselbergs around 0.1. We do not have a predefined expectation.

Capillary rise is only considered as an important process in the wetlands. An optimal value might be 0.4mm/day.

The bandwidth for the D parameter is for both the flatlands as the Inselbergs very wide. Though a parabolic shape could be recognized. Note for the flatlands (red dots) that values $D = 0$ (all water goes to the slow groundwater) result in pretty high objective scores, but the real peak appears around 0.4. Same holds for D, although, their might also be an parabolic front between 0 and 0.2. For both graphs hold that a dominance of fast processes does not lead to good results. Note that we neglect the slow groundwater recharge in wetlands, so $D = 1$ by definition (all flow goes to the fast groundwater response reservoir).

About the maximum rootzone storage $S_{u;max}$. Clearly visible are the predefined bandwidths between the different HRUs. For flatlands an optimum value appears around 225mm. Whereas the forest at the Inselbergs and hill slopes have values around 475mm and wetland around 80mm. But again, more extensive calibration might lead to sharper fronts.

For K_f we constraint the parameter spaces. We assume the fast processes of wetlands faster than those of forests and crop, grasslands. Whilst, the very fast processes like hortonian overland flow and flash flows are not taken explicitly into account (since the input is on daily and not hourly base), the outcomes suggest that a very fast process bucket should be included. Since K_f for grasslands and forests both show relatively high objective scores for the very fast processes. A second optimum in K_f values can be recognized between [7,13] for the grasslands and [6,8] for the forests, This is in line with our hypothesis that hill sloped forests respond faster than flatter grass-/croplands, though not included in our parameter constraints, to avoid biasness in the outcomes.

Finally the K_s value shows an optimum between [550,650] days. Those values are a little higher compared to K_s of FlexA. Possibly we have equifinality issues around here.

[13] This is mainly caused by the absence of automatic calibration routines, but partly also to the amount of calculations

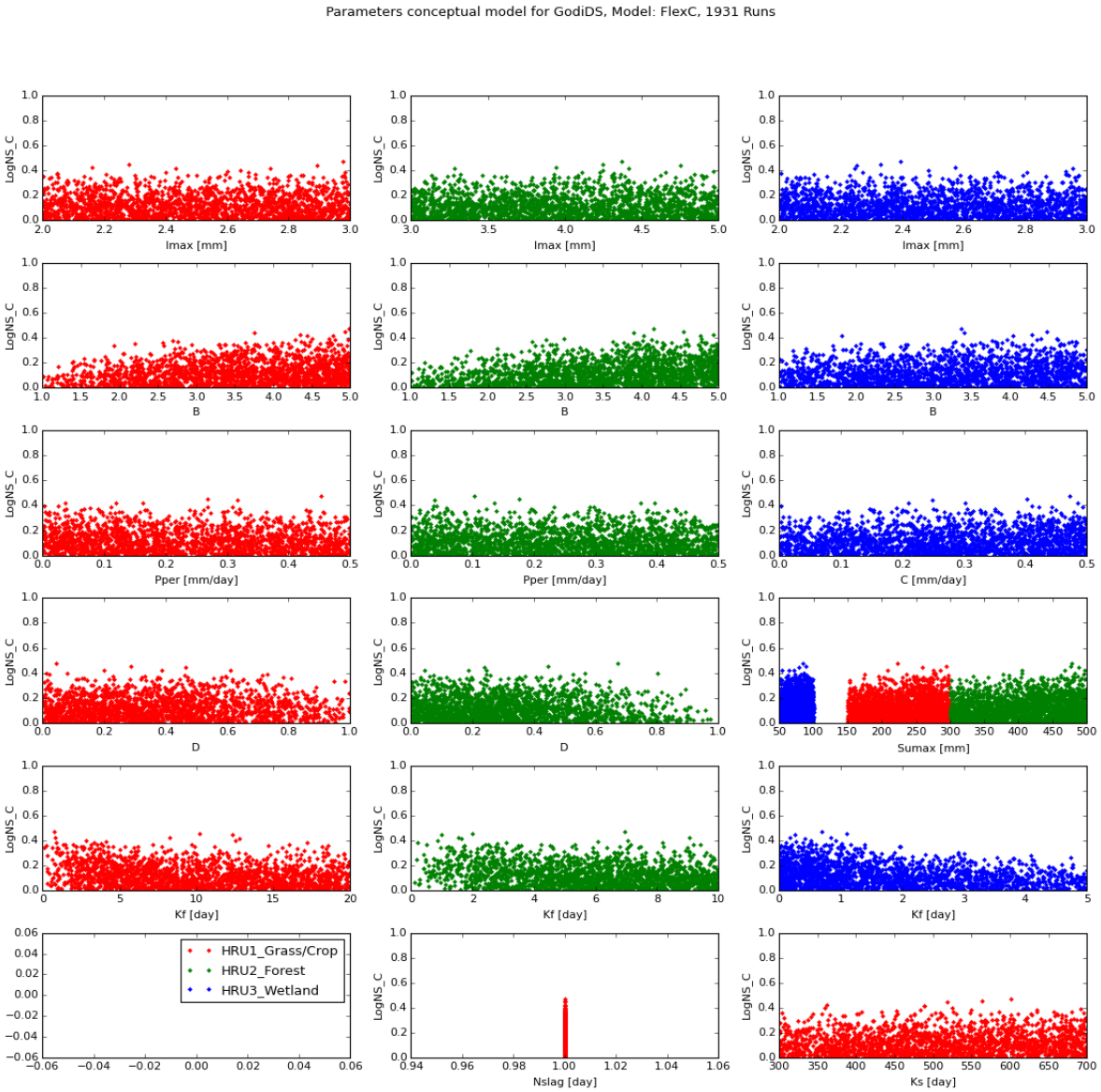

Figure 3.8: FlexC Conceptual model parameters. The objective LogNS Conveyance score (y-axis) of a model realization (a dot) plotted against its specific parameter value (x-axis), where the left columns (red dots) represents the irrigated and grass shrubland dominated, gently sloped flatlands, the green dots in the middle column the predominantly forested Inselbergs and the blue dots in the right column the grassy wetlands

3.3. VALIDATION

The validation of FlexA and FlexC is performed at Messica Downstream Station (MessDS), see Fig. 2.6. MessDS is the most downstream located measurement station, see App. F.2.5. Measurements are performed at a three gated bridge with a free flow regime. Because of the very high flow velocities and jet-like streams, salt dilution measurements where hard to perform over here, however, other spots around the bridge prove worse, since up- and downstream the river was quite wide, very low flow velocity and even not always single channeled, not to speak about inapproachability. Therefore the measurements at the bridge offer a best estimate, see Fig. 3.11. The water levels and conveyances are measured relatively to the bridge cross-section. In the pool just upstream of the bridge, we assume the water level horizontal and the flow velocity negligible ($v \rightarrow 0$m/s).

Above a water level of 0.95m all gates are fully filled, from 1.15m onwards the bridge is flooded. This is not included in our OCM model, so conveyance and discharges at higher levels concerns overestimations. From cross-section measurements, we estimate a total effective flow width increase from 10m just above the bridge up to 30m[14]. We found flood marks upstream of the bridge, and by memory we would estimate these marks approximately 0.5m above bridge deck. What would increase the total wetted area from 2.2m2 at waterdepth $h = 0.95$m (full gates) to 7.5 up to 17.5m2. Assuming an average flow velocity of 1m/s, we expect peak flows in the order of 7.5 to 17.5m3/s. We neglect the fact that flood marks can be deposed by the maximum flows, so possibly daily averaged peak flows might be lower. Though, this depends on diurnal discharge variation.

The parameter sets with a NS_C ≥ 0 for GodiDS and re-ran them for MessDS[15]. The results are presented in Figs. 3.11 and 3.12. Note that we calculate the total discharge Q and convert this to waterdepths and conveyance with the OCM model. Therefore, the absence of correct cross-sectional information above 1m is not affecting the model simulations.

From both FlexA and FlexC we observe that the median values simulate the baseflow recession in April to June 2014 pretty well. This is remarkable result, since this is purely based on the model. Though, we have some critical notes. First, the waterdepths are better predicted with FlexA, whereas the conveyances are slightly underpredicted. Whilst, this was not the case for the calibration. This give rise to the idea that FlexA little underpredicts the (base) flow discharges. On the other hand, FlexC overestimates the water levels and predicts the conveyances quite accurate. This feeds the suggestion that FlexC predicts baseflow better. Overall, FlexC's bandwidths are much smaller than FlexA's.

Since most baseflow measurements in 2013 [7] fall within the uncertainty boundary, this indicates that the total model ensemble is capable to capture these flows[16]. The plotted observed discharge (red line) is obtained using a polynomial rating curve [7] at a measurement location upstream of the bridge. Unfortunately, the high flow extrapolation is not reliable, since this rating curve lack peak flow measurements, cross-sectional information and additional flood plain inundation thresholds.

FlexA's median estimate a peak flow of 10 to 12.5m3/s for 2012-2013 and approx. 17.5m3/s for 2013-2014. Whereas FlexC returns peak flows around 30m3/s for both years. Since we lack accurate discharge information in the peaks, it is hard to judge which model performs better. The total discharges from FlexA however are closer to our rough discharge estimates than FlexC's.

The perceived overpredictive behavior of FlexC compared to FlexA is most likely a result of overestimation of Q at GodiDS. There might be three reasons. First, FlexC consists of 3 different HRUs, each with their own response times e.g., travel times, drainage times. This is not explicitly calibrated. Therefore, transferring the calibrated model to other catchments with different compositions, will not compensate for travel times etc. This might increase calculated peak flows significantly[17]. Secondly, we applied altitude corrected precipitation volumes. Overestimation at the peaks will give more discharge from especially the Inselbergs. This will increase the contribution. Thirdly, the Godi Catchment mainly consist of the Gaizeri Sedimentary Group, and therefore deep groundwater infiltration is negligible, but will occur in the lower parts of the catchment since this part is also located on top of the Kalahari Craton. The Messica catchment on the other hand, is mainly located on top of the Kalahari Craton. So here deep groundwater infiltration cannot be neglected and will lead to less water at MessDS, especially in the dry season.

Lastly, a general explanation for overpredictive behavior at MessDS (which also holds for FlexA as FlexC) is that we neglect all streamflow hydraulics in especially the River Messica. Limited discharge obstruction due

[14] The total flow width is hard to estimate, since the bridge length 60m, but a little curved, sloped and obstructed

[15] We recalculated the initial state of the slow response reservoir, based on its total recharge during the first year in order to simulate a very long time sequence full of average years. We changed this initial state because the total precipitation amount for the HRU units differs from the calibration area.

[16] Unfortunately, this graph does not give insight into the Objective scores of the individual models.

[17] This is less the case for FlexA, since here we purely calibrate on a catchment response and not a unit response.

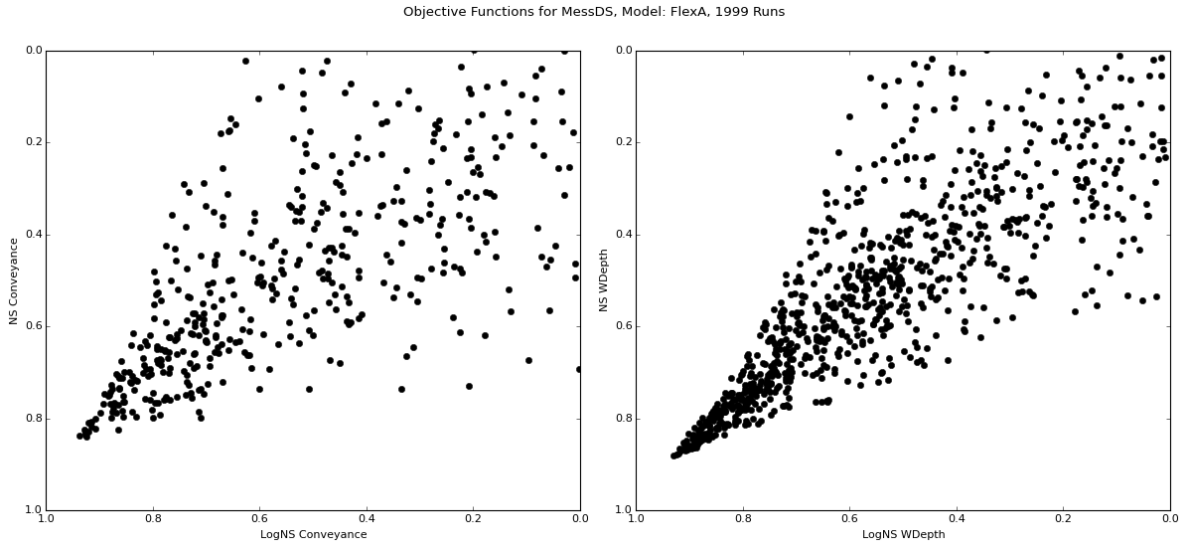

Figure 3.9: Pareto plots Validation FlexA on Messica Downstream Station

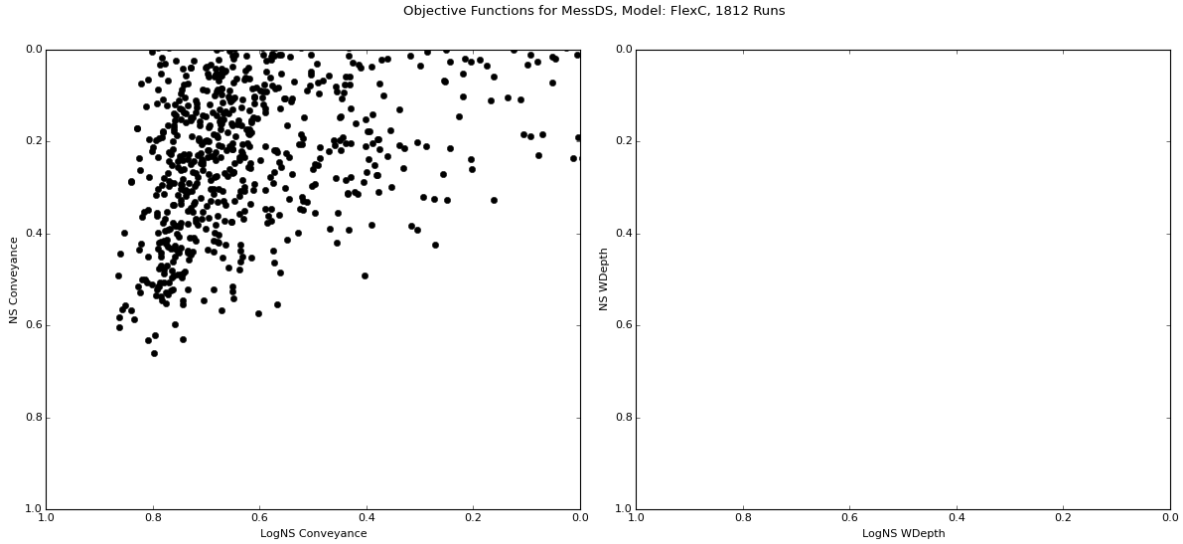

Figure 3.10: Pareto plots Validation FlexC on Messica Downstream Station

to construction and inundations are not taken into account, which also will affect the observed discharges.

The Pareto plots(Figs. 3.9 and 3.10) present the objective scores (Log-)NS_Conveyance and (Log-)NS_WDepth based on the parsimonious *baseflow* measurements between March and August 2014. Therefore all plots are biased.

For FlexA, the Pareto front (wrongly) suggest that there is even an optimal model (Fig. 3.9), because of the very sharp edge and one dot closest to (1,1). However, this is caused by the absence of peakflow measurements. Since only baseflows are measured, the model basically fits a baseflow recession curve.

Also the results for FlexC are influenced by the absence of peakflow dynamics (Fig. 3.10). The Pareto plot at the left hand side show generally good results for the LogNS_Conveyance (because of the baseflow recession) and less good for NS_Conveyance. This explains the leftoriented front. The right Pareto plot is empty, this is due to the fact that all water levels are overestimated. Therefore the objective scores are rather poor, once again, since water levels may not be daily linear averaged, the model outcomes and measurements are not directly comparable.

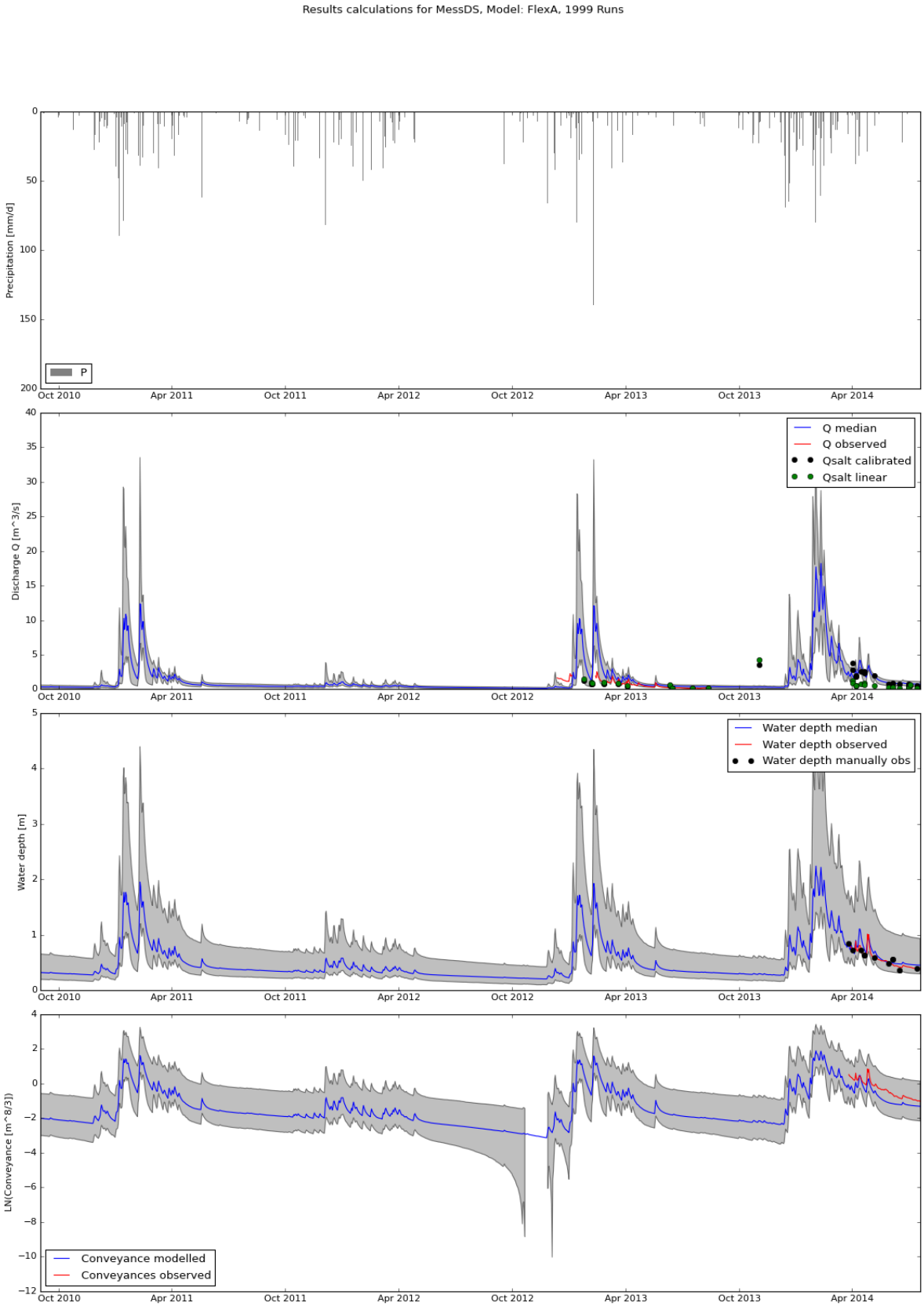

Figure 3.11: Bandwidths Discharge, Water levels and Conveyance for Messica Downstream Station for FlexA.

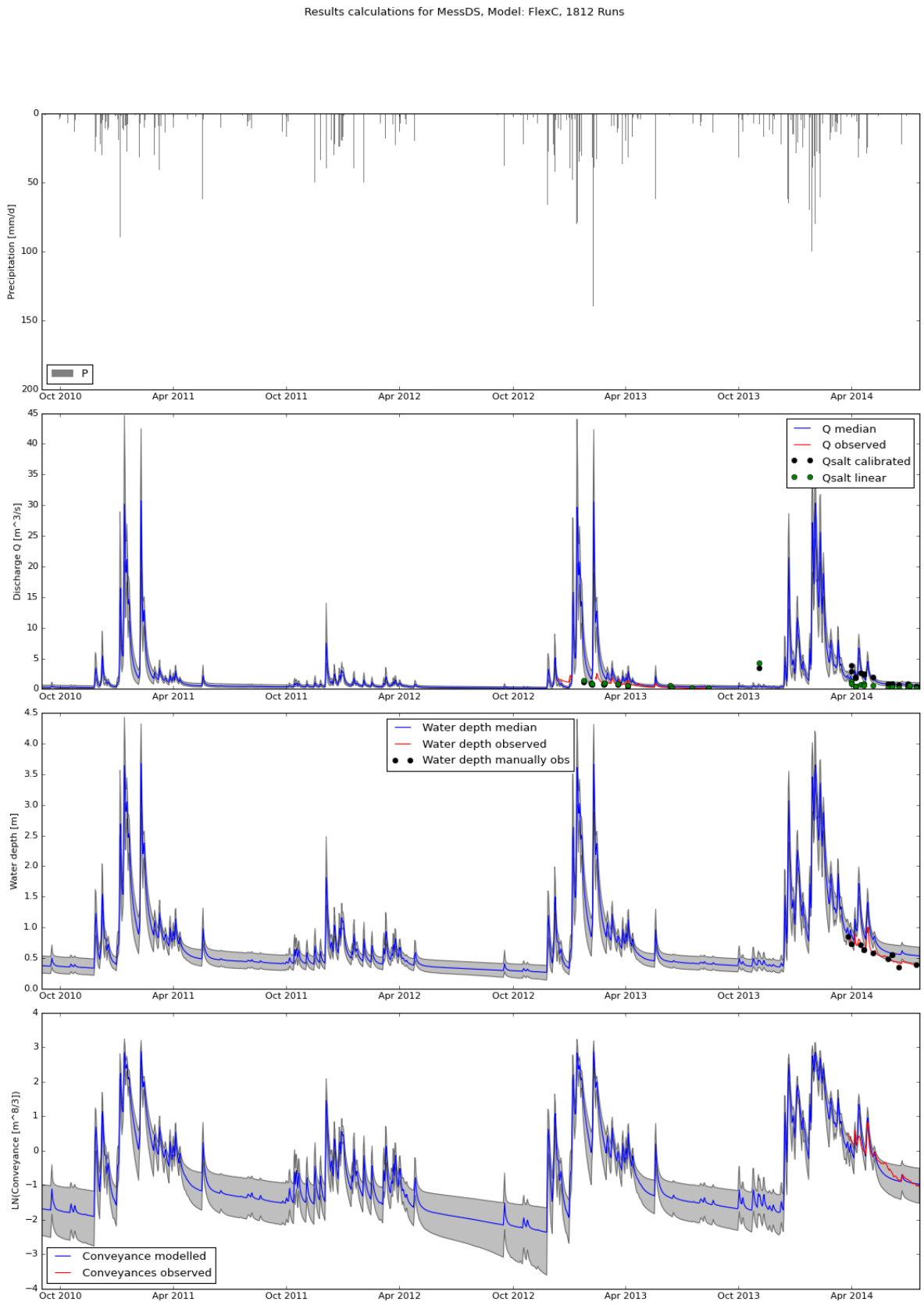

Figure 3.12: Bandwidths Discharge, Water levels and Conveyance for Messica Downstream Station for FlexC.

3.4. WATER STORAGE

It point out that we can actually estimate the total storage from the model's slow response reservoir(s). The groundwater storage in this reservoir is that amount of water that participate in the rainfall-runoff processes and what possibly leave the system in dry years[18]. Please remember that these groundwater storages are not (directly) reachable by vegetation or soil evaporation, so the area can dry-up during the dry season while there is still groundwater available, this is in line with the observed situation.

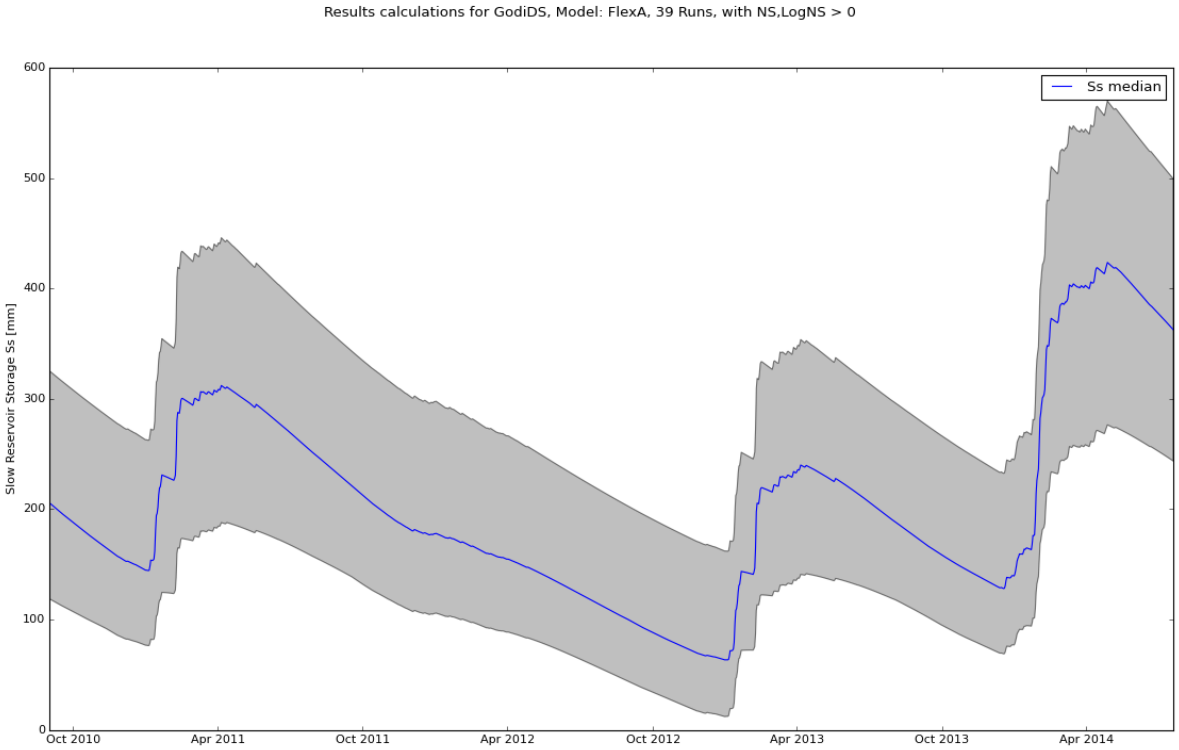

Figure 3.13: FlexA Slow Reservoir Storage Dynamics, Filter: model realization fulfill the 98% quantile of NS_C + LogNS_C

Fig. 3.13 shows the groundwater storage from FlexA's slow response reservoir. The gray bandwidth presents the minimum and maximum state for subset of the total model ensemble[19]. We selected those models that exceed the 98-percentile of the (NS_Conveyance + LogNS_Conveyance) objective[20], so the 2% 'best' performing models. The blue line represents the median value of this subset.

From Fig. 3.13 we recognize the dry rain season of 2011-2012. The groundwater reservoir is drained in this period, whereas the subsequent wet seasons recharged the slow reservoir. In 2013-2014, which is considered as a wet year, the maximum storages run up to 400mm for the whole catchment[21]. Assuming an overall soil porosity of 30%, the active groundwater storage variation of 300mm which equals to 1.0m all over the catchment.

However, the catchment's groundwater storages and recharges differs over the catchment. Therefore FlexC distinguishes the three landscapes *grass_crop dominated gently sloped Flatlands*, *forested Inselbergs* and *grassy Wetlands*, see Fig. 3.14.

Most water is stored within the Inselbergs, where we find a total groundwater storage of 800mm on average. If we assume that the groundwater is only stored within cracks and fissures - which approximately takes 1 to 5% of the total volume - the total groundwater depth within those cracks and fissures would be 16 to 80m. Since the mean HAND value for this HRU is 75m, this is theoretically possible.

[18] Note that passive groundwater storage therefore is not represented, this is implicitly taken into account as an unchangeable status quo.
[19] The bandwidth for all the accepted models was too broad for this solution. Again automatic calibration or GLUE might improve this.
[20] Note that doing so we select ca. 40 models (with highest combined objective scores, whereas the other plots include all results with LogNS_Conveyance equal to or higher than 0[−].
[21] Without discriminating between wetlands, flatland and Inselbergs

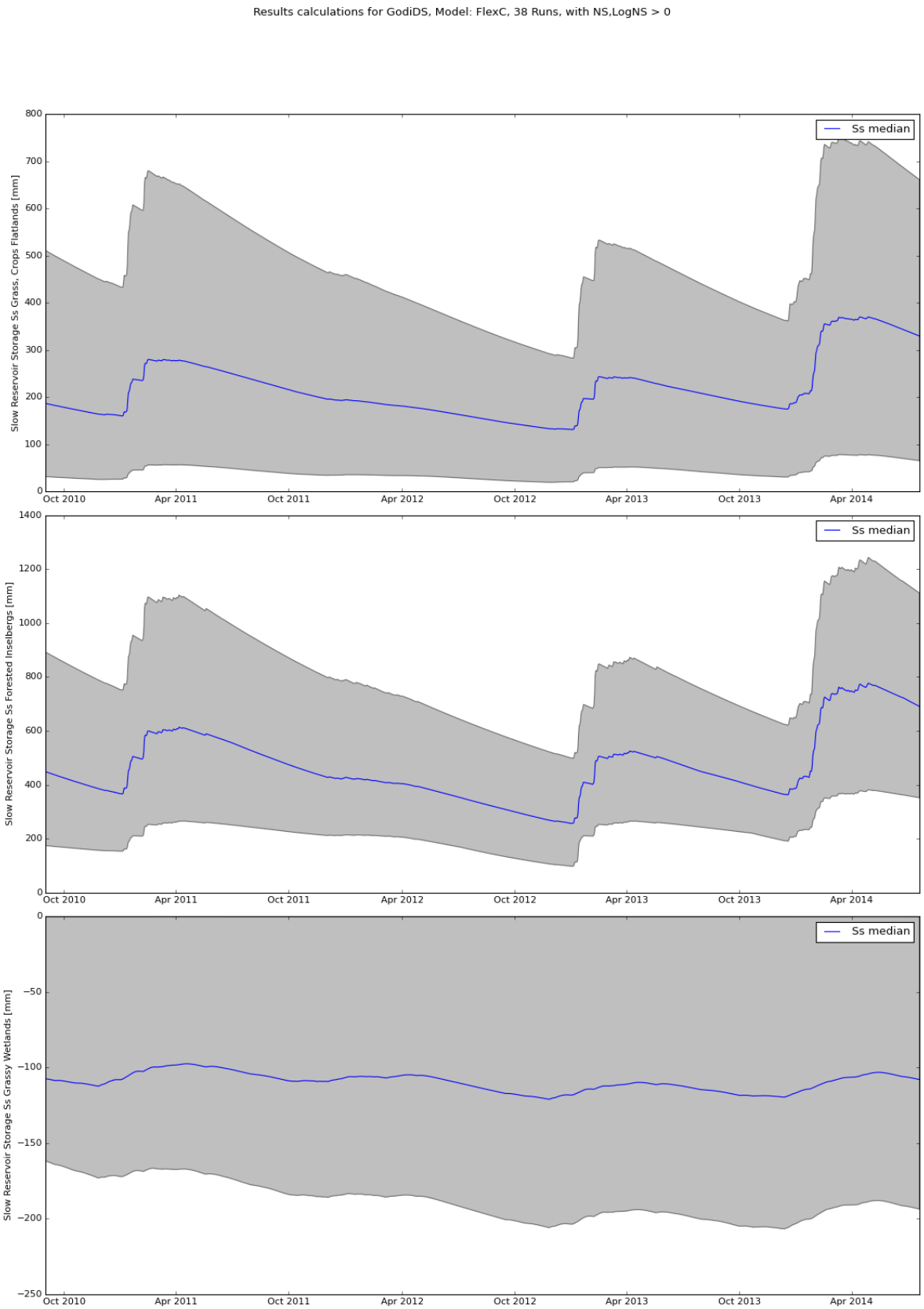

Figure 3.14: FlexC Slow Reservoir Storage Dynamics, Filter: model realization fulfill the 98% quantile of NS_C + LogNS_C

Less water storage is available in the Flatlands, where we observe a maximum storage of 400mm. Within the Flatlands we assume deeper regoliths. We assume therefore the soil porosity between 20 to 30%. A maximum of 400mm storage would then result in an active groundwater variation of 1.3 to 2.0m. This does not sound unreasonable to us.

Please note that (by definition) the Wetlands have only seepage water and do not recharge groundwater itself, it receives groundwater from Flatlands and Inselbergs. This is conceptualized with a negative storage (and negative groundwater fluxes). On average the groundwater is 100mm short in the wetland, representing a flux (or specific discharge) of $Q = S/K = 0.1$[m] /550[days] = 0.18mm/day. All (total) fluxes can be calculated by multiplying the specific discharge with the HRU area.

4

DISCUSSION

4.1. SET UP DISCUSSION

This chapter discusses the choices made considering (model) forcings, conveyance, waterdepth and flow measurements, FlexTopo - OCM conceptualization and calibration.

4.2. FORCINGS

4.2.1. INCLUDE INSELBERG INCLINATION IN WATERSHEDS

The active contributing groundwater reservoir is probably larger than expected based on the DEM derived (surface water) catchments. Due to the east dipping inclination, groundwater from the west ridge will flow to the investigated east side and contribute to the baseflow.

We propose therefore the following work routine. From the outflow location on the mountain ridge, independent of its altitude, an inclination line can be drawn from as far as the outflow to the westside through the mountain. The inclination angle is undefined, a rough estimate could be the rock inclination. The zone that falls between the mountain peak and the intersection of the mountain slope and the inclination line, will contribute to the Messica catchment. However, note that only (part of) the slow groundwater reservoir will contribute, whereas the fast reservoir will participate to the discharge at the west side of the mountain.

This concept is already built into the models and data structure[1], but is still to be tested. Possibly the K_s value will become even larger.

4.2.2. ALTITUDE CORRECTED PRECIPITATION

We have a good indication that the precipitation amount is effected by the Inselberg, a so called orographic effect. At an altitude of 878m+AD around 16% more rainfall is measured over a longer period than at lower locations (730m+AD and ca. 650m+AD). These differences are not caused by human forgetfulness, since they are structurally registered at rainy days.

This study tested the effect of this observation by linear correcting the rainfall amount as function at lower altitude. The corrected rainfall amounts is applied on the HRUs. Wet- and flatlands are generally lower located, and therefore receives less rain, whereas the forested Inselbergs receive more rain. This leads to lower peakflows and a more reliable distribution of groundwater storage (FlexC), compared to none distributed rainfall amounts. Overall the calibration and validation results improved. (See appendix N)

However, the proposed linear relation is only dependent on two stations with altitude as the only parameter, whereas the horizontal distance to the peak might also be a reliable parameter. Since rainfall measurements performed on the top, show smaller rainfall amounts than at Davids place (878m+AD), half way the mountain. Also, the lower located raingauges (at 730m+AD and 650m+AD) do not show a large mutual cumulative deviation. Unfortunately measurement periods of other locations were too short to draw conclusions from this. Further research to the precipitation distribution is to correct for the orographic effects is recommended. Which probably will lead to a non-linear distribution (e.g., parabolic, bell shaped or a superposition). This possibly will lead to less rainfall on the top of the mountain. On the other hand, though

[1] See appendix clsHRU and clsFlexC

rainfall volumes on the very peaks may be overestimated, it does compensate for cloud forests effects. These mountains are often covered by clouds, but the moisture contribution to the hydrological cycle is generally not measured. It might, however, have a significant contribution to the total water balance. So when refining the altitude corrected precipitation, cloud forest effects should also be explicitly taken into account.

4.3. CONVEYANCE AND WATER LEVELS

The reservoir response times (K-values) of the baseflow recession can be successfully derived from the cross-section corrected water level dynamics or conveyances. This is mathematically proofed in chapter 2 and application in the model showed that the K-value bandwidths could be easily restrained, which directly leads to good baseflow estimates.

For the K-values, discharge information is not necessary, and together with the (quasi-) uniform flow assumption and cross sectional information, this could be successfully derived from the water level measurements.

There are however some drawbacks for this method, on which we elaborate in this section.

4.3.1. RIGHT CORRECTION OF WATERDEPTHS

Reconstructing[2] the right (occured) waterdepths appears from significant importance for the correct outcomes of this study. It points out that incorrect waterdepths affects most significantly the division between fast and slow runoff processes, which results in a different recharge ratio between fast and slow reservoirs, and therefore to another predicted (slow) storage amount, which is/ is not available in the dry periods.

4.3.2. UNIFORM FLOW ASSUMPTION

The main assumption for the conveyance method is quasi-static uniform flow. However, the flow is not uniform. Especially due to the abundant water plant vegetation, backwaters will occur. The Manning-Strickler formula is not designed for this flow regime. Still, under baseflow circumstances the assumptions appear to hold.

Possibly the assumption holds since the formula corrects for the backwaters in its roughness and bottom slope parameter $\bar{a}$. This explains the fact that the optimal $\bar{a}$ falls outside the predefined bandwidths, see Eq. 2.16

4.3.3. CALIBRATION ROUGHNESS COEFFICIENTS NECESSARY

Automatically calibrating the roughness parameter $\bar{a}$ (that is applying Monte Carlo Analysis to find optimal parameters) did not lead to better overall results. One explanation is that the OCM-model implicitly corrects for backwaters, as mentioned in above section. Therefore, manual (or separate) calibration of the roughness parameter appeared necessary in this study (see Appendix N.2 for results of free calibration of $\bar{a}$.
Another note, $\bar{a}$ is calibrated on daily averaged conveyances. This is done, since calibration is performed on daily time scales. However, the effects of not calibrating the $\bar{a}$ on the highest available time resolution is not further investigated. Possibly the values will change.

4.3.4. INCREASED RESISTANCE VEGETATION BY HIGHER WATER LEVELS

As mentioned, the streams are strongly vegetated with reeds and waterplants. During baseflow periods, the water flows between the stems of the reeds. In the high flow period however, the streams swell and water also flows between the denser reed tops. Often also (old) debris is sticked between the plant tops. This causes extra resistance and being so, extra water level set-up. This overrules the linear relation between conveyances and discharges. The conveyance method does not correct for this depth-dependent roughness. This is something which can be added in the model in next studies.

The results of this phenomenon is that water levels rise faster than discharges increases. Being so, peak water levels and peak conveyances will be higher in reality than expected based on the uniform flow assumption. So, if the FlexModel calculates the right peak discharges, the conveyances will be under-predicted, as observed in calibration and validation.

[2] Since multiple students read out diver information and replaced divers, moreover, we have to cope with bottom erosion processes and a broken barometer, this was a hard job. We reported our final water levels in Appendix F.2.3.

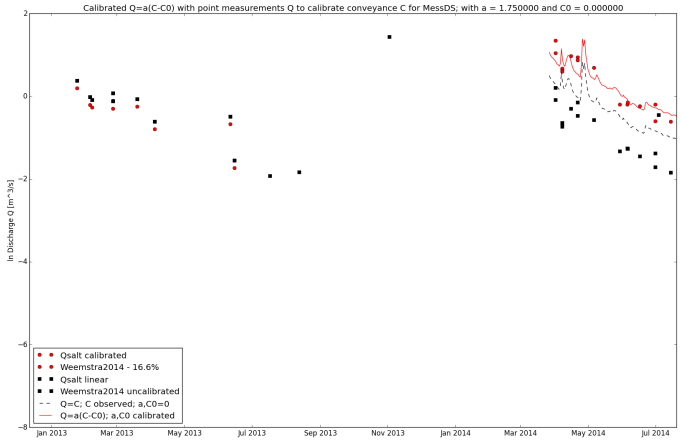

(a) roughness parameter $\bar{a} = 1.75$ calibrated *on conveyances* for MessDS

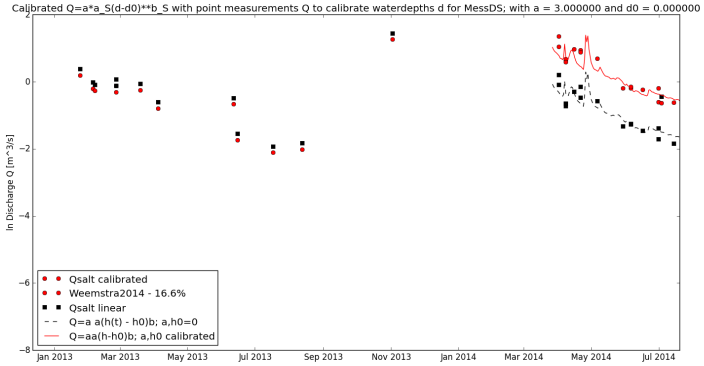

(b) roughness parameter $\bar{a} = 3.00$ calibrated *on water levels* for MessDS

Figure 4.1: Calibration roughness parameter $\bar{a}$ for water levels and conveyances for MessDS

4.3.5. RESAMPLING OF WATER DEPTHS

Hourly observed waterdepths cannot be scaled to daily averaged waterdepths, contrary to conveyances and discharges. This is because waterdepths are not linear dependent to discharges, whereas conveyances (cross sectional corrected waterdepths) are. The effects of averaging are shown in Fig. 4.2, a few notes:

- Timing errors between rain events and observed peak events, e.g.,see 5-1-2013, where waterdepth peak is earlier than registered rainfall amount. This is because precipitation is reported the day after.
- Linear averaging waterdepths over 24 hours without taking cross-sectional influences into account consequently underestimates peak discharges and peak waterdepths, compare red to blue lines in Figs. 4.2a and 4.2b.
- In case of minor daily water level variations, normal (linear) averaging and cross-sectional-corrected averaging give the same results, so the latter is especially relevant in case of very sharp and short water level rises and declines.
- The peak water levels are partly caused by extra vegetation resistance and backwaters. This overestimates discharges. However, for physical reasons it would be wrong to apply linear averaging to mitigate these effects.

In the presented model we did not calibrate on these daily averaged waterdepths, they are purely indicative. We did however tested it. It appeared that we had to recalibrate the roughness and bottomslope

parameter $\bar{a}$ also, see Fig. 4.1. Most likely this is necessary in order to compensate for the mathematically incorrect daily averaging.

Applying cross-sectional averaged waterdepths is a solution, since the water depth bandwidth is quite narrow (compared to these of the discharges/ conveyances), applying objective functions on waterdepth simulation might be helpfull during calibration, since the scores differs, see for example Fig. 3.5.

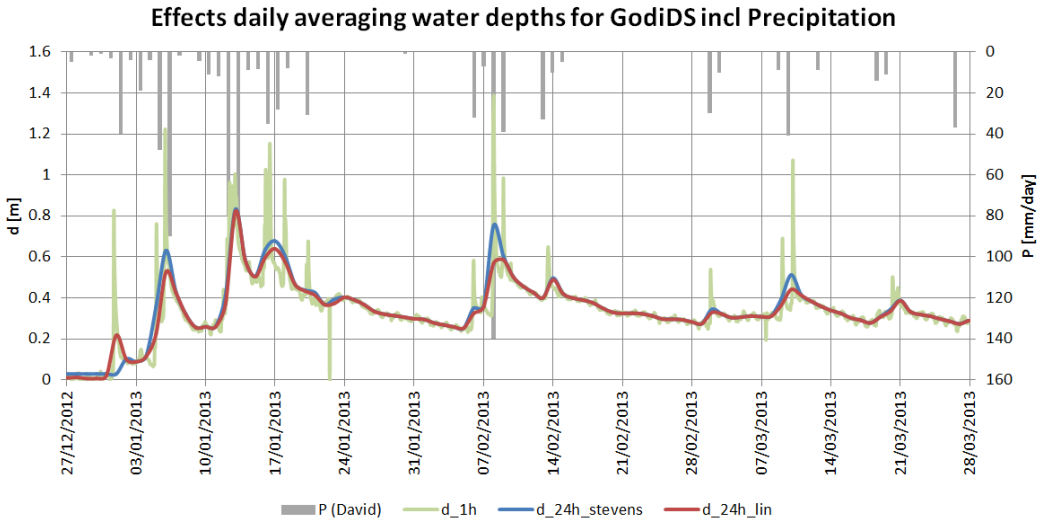

(a) Waterdepths high water period 2012-2013 GodiDS; in green the hourly observed water depths, in red the linear daily averaged water depths (which underpredicts the peaks) and in blue the daily averaged water depths where cross-sectional influences are taken into account

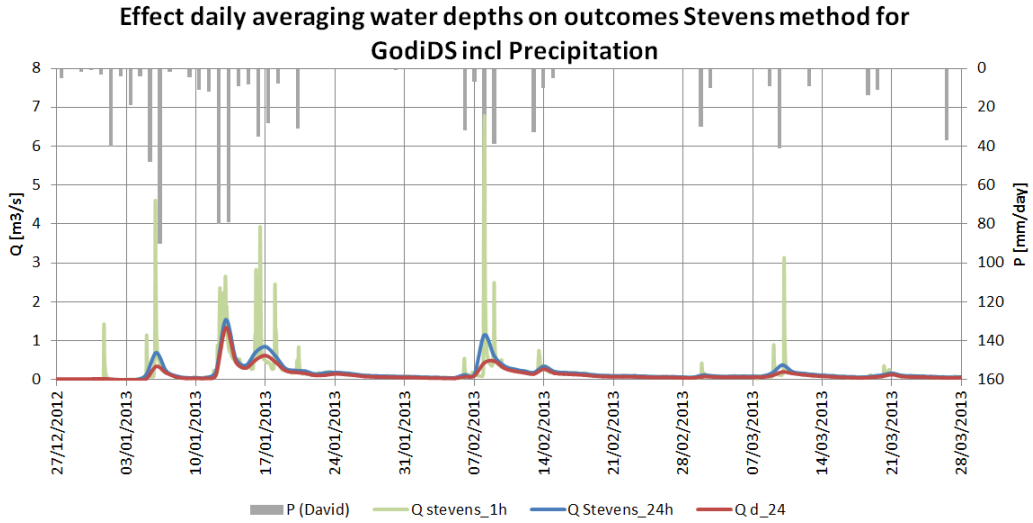

(b) Derived discharges high water period 2012-2013 GodiDS using Stevens method; in green the discharges based hourly observed water depths, in red discharges based linear daily averaged water depths (which under-predicts the peaks) and in blue the discharges derived from daily averaged water depths where cross-sectional influences are taken into account

Figure 4.2: Effects non-linear influence cross-section on calculated daily averaged discharges and water depths

4.4. MODEL CONCEPTUALIZATION

Some remarks about the conceptualization of the area.

4.4.1. 3 HOURLY TIMESTEPS PREFERRED ABOVE DAILY TIMESCALING

In this research all measurements (rainfall, water levels, discharges) are aggregated to daily timesteps from 8am the previous day to 8am current day. Since this resample period covers raingauges measurement interval. Incorrect system delays are avoided by taking 8am instead of 12pm as starting point. Calibrating on daily averaged values seems to work, since the hydrograph can be simulated by the models. However, question is whether the models return the right output due to the right processes. We believe that the very fast runoff processes (those that respond within 1 day) are integrated within the K_f-values of the fast runoff processes, leading to an altered process division within the model. This can cause an overestimation of rainfall entering the soil (deep groundwater or root zone) which in reality directly runoff to the streams. So possibly, a larger percentage of precipitation directly leaves the system.

A quick evaluation of resampling time intervals shows that a three hour averaged time interval represents the stream flow dynamics correctly, see Fig. 4.3 (for transparency 6h and 12h resampling is left out of the figure). We acknowledge the trade off between computational costs and physical accuracy, therefore we suggest a three hour interval, since we expect that smaller timesteps will not introduce more faster runoff processes. See Fig. 4.3. However, since we lack information about precipitation timing and intensities, we suggest to apply daily rainfall in a 3hour timestep and compute the system on a 3hour time resolution[3], but we recommend to judge the model performance on daily averaged (24hour) outputs to mitigate timing problems for the rainfall.

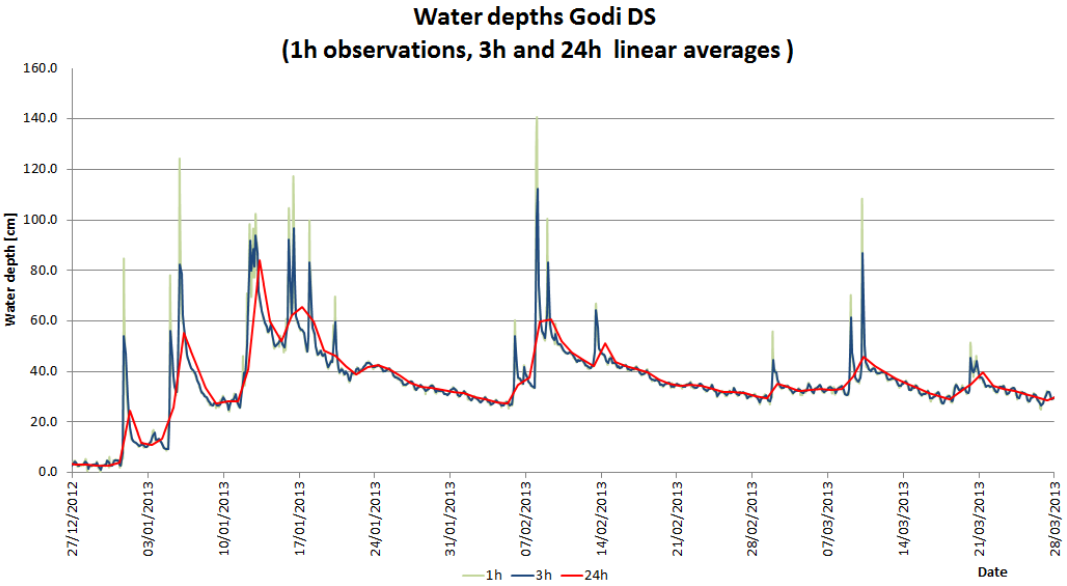

Figure 4.3: Effect daily averaging water depths (or discharges or conveyances). The hourly observations show much higher peak values, which point to very fast runoff processes. Three hourly averaging shows the timing to be quite right, compared to 6h (not shown in graph) or even 24h.

4.4.2. TIMING AND VOLUMES PRECIPITATION

Weemstra *et al.* [7] suggested that timing and volumes of precipitation events in the wet period outweights the rainfall intensity for the base flow recession. We did not test this conclusion in this study. However, a critical footnote would be that since high intensities will lead to more runoff than long drizzling rains, neglecting this will effect the recharge of the groundwater reservoirs. This effect is both in their and our model not taken into account. Therefore we suggested in Section 4.4.1 to calibrate on smaller timescales and upscale rainfall intensity for this places.

[3] To do so, we should also change our input values to hourly input values and change our model to hourly based in stead of daily based

4.4.3. INFILTRATION IN KALAHARI CRATON

The River Messica is located on top of the Kalahari Craton. We suspect a deep and permeable regolith in this area. Therefore it is very well possible that the River Messica infiltrates over the flow length of the river and drains to Lake Chicamba, especially in the dry season. Local people and governments believe the River Messica to be infiltrative, which sounds as an extra argument.

In our model concept we can add infiltration in the slow response reservoir and base this on the craton basins. Possible also the most downstream part of the Godi catchment falls within the Kalahari Craton.

We performed longitudinal flow routings around the River Messica, with MessIS as upstream and MessDS as downstream border. The inflow from headwaters is taken into account, see App. J. From this measurements we might conclude a subtraction / leak of water over teh length of the River Messica, especially in April and May, but unambiguous evidence to support infiltration lacks.

4.4.4. HRU CLASSIFICATION

FlexC's three different HRUs are composed using objective data sources. Though, some data aggregation and assumptions will affect the HRU composition and therefore the model outcomes:

- The Digital Elevation Map (DEM) in m+AD [35] is rounded to integer values. Therefore, calibration of HAND was bounded, and will affect size of wetlands. Possibly rounding to multiples of .25 will improve the calibration sensibility.
- The model is sensitive for the flow accumulation or drainage area. After a certain area, a stream starts. The HAND and flow accumulation value are biased.
- In this study we found a HAND value of 2m in combination with a flow accumulation drainage area of 50*30m2 = 1500m2. Therefore we combined own perceptions of HRU classification (wetland, flatland, inselberg) and flow maps. This is still rather subjective and need a further evaluation for this area.
- Flatlands covers a wide scope of irrigated fields at hillslopes to rainfed maize fields and shrublands between the River Messica and the River Revue (this land is not influenced by the Inselbergs). We believe that the areas around the River Messica are prone for deep groundwater infiltration (since they are located on top of the Kalahari Craton with deep permeable regoliths). Therefore, we overpredict the streamflow.

4.4.5. HEADWATERS IN- AND EXFILTRATE

We did not take into account the observed dryfall of headwaters. At some places, for example just upstream of Chirodzo IS, the headwater completely infiltrates and a little downstream the stream gains water from drainage water.

Also the surplus of stream water (after irrigation water is withdrawn) infiltrates into the soil and exfiltrate further downhill. This gives thought to the idea of very permeable soils or cracks.

It is important to notice that on catchment scale these local effects average out disappear, but on very local scale these effects significantly influence the result, and are not modelled.

4.4.6. FLOW ROUTING

In the FlexTopo model FlexA and FlexC no flow routing to model the flow delay is applied[4]. Therefore, transferring models to other area (compositions) is more difficult, especially in case of very elongated areas or small time resolutions. This can lead to incorrect timing of peakflows and/or overestimation of them.

A first estimate for surface flow routing is for example to determine the peak delay and damping of observed peaks in two different measurement stations. For the River Messica such a peak delay can be observed, see Fig. 4.4b. In this figure the peak event is first observed at MessIS and GodiDS and after a while also at

[4] Though the flow routing concept is almost fully implemented in the models, but need further optimization for computational efficiency

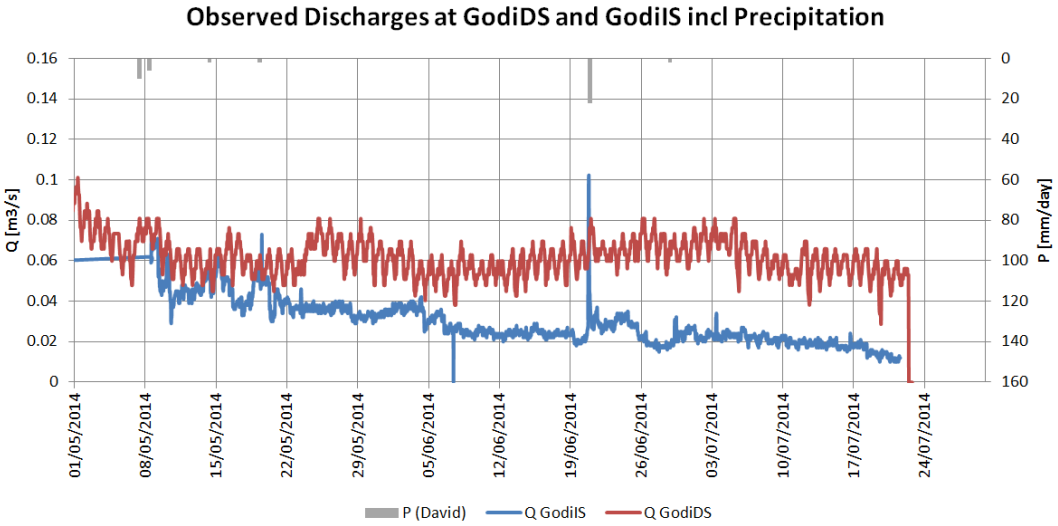

(a) A peak observed at Godi Intermediate Station is not observed at Godi Downstream Station. Observations are too short to calibrate flow routing function on.

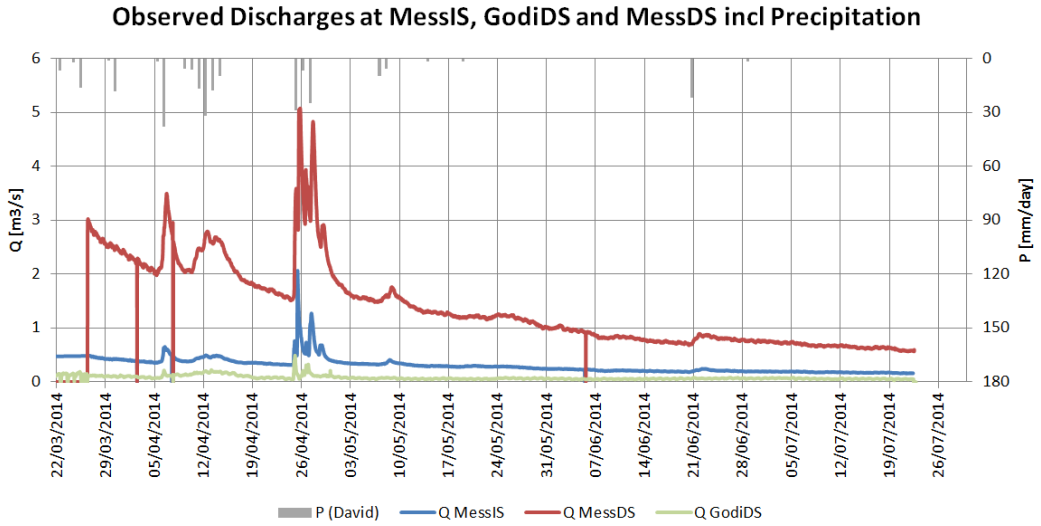

(b) Peaks observed at MessIS and GodiDS are also, but later, observed at MessDS. Flow routing could possibly be calibrated on this information.

Figure 4.4: Calibrate flow routing function on observed peak delays and flattening

MessDS. Using the distance[5] and the observed time delay, coefficients for diffusion and advection could be calibrated (i.e. under some special assumptions like constant discharge).

In case of River Godi such a time delay is not yet observed, see Fig. 4.4a. However, possibly this is due to the short observation period.

4.4.7. GROUNDWATER VOLUME OVERESTIMATION

The volume S_s of the groundwater reservoirs for HRU Inselberg and Flatlands are overestimated, since they are not corrected for the groundwater flow to the HRU Wetland. The effect on the total outcomes is presumably not very large, but should be improved in future studies.

[5] This already available in the HRU class of the model

4.5. MODEL CALIBRATION AND PRESENTATION

In order to improve model performance large sample calculations, we offer some improvements. In this study we choose for automatic calibration in combination with manual calculation. The latter is necessary to get insight in the system and model, the first gives insight in parameter and uncertainty bandwidths of the predictions.

4.5.1. (AUTOMATIC) CALIBRATION

In this case we derived parameters from measurements, literature or draw them from a uniform distribution (Monte Carlo). The resulting parametersets are calculated, without looking for an (global or local) optimal parameter set. This can be done with an automatic calibration routing like MOSCEM-UA Gharari *et al.* [29], Vrugt *et al.* [45] or AMALGAM Vrugt [46], which are designed for hydrological modelling. Applying these algorithms certainly will improve model performance, i.e. will result in higher objective scores and, being so, will also narrow uncertainty bandwidths, giving more pronounced pareto fronts and parameter plots.

4.5.2. OBJECTIVE FUNCTIONS AND SIGNATURES

This study clarifies that the selection of objective functions impacts the final result. A well performing set of objective functions is not yet found. Objective functions and signatures serve as an indicator for model performance[6]. More attention to this subject should be paid to so, possibly also hydrological signatures can be added, like flash flow, peak timing, fraction analysis etc..

The research study shows that calibrating on baseflow indicators (LogNS_C), leads to better predictions of the baseflow and result in larger groundwater storages for Forested Inselbergs than for grass_crops Flatlands, which is in line with our field expectations. A LogNS downside however, is its low focus on peaks, and therefore it can easily lead to over or under-prediction of peak waterdepts and flows.

The NS_C has a stronger focus on peaks than the LogNS. However, adding penalties for NS_C does not lead to a better set of behavioral models; moreover, all FlexC's parameter sets are rejected. Most likely this is caused by the large peak - base ratio, which is greater than order 10. Same holds for calibrating on discharges Q, since Q is linear related to C. This large ratio is the result of convective storms with very high flows and very low baseflows.

The max-min water level ratio is only a factor 3. Therefore, we applied objective functions for the waterdepths and remove the penalties for the conveyances. Unfortunately, this does not lead to better calibration results (see App. N). This is because, NS_WDepth penalty limits the peakflow, but overpredicts baseflow. Apart from this, groundwater storages 'behavioral' models pointed out to be larger for the grass_crop flatlands than for forested inselbergs, which contradicts our expectations. This calibration issue is most likely caused by the linearisation problem of the waterdepths. Solving this problem, might result in an extra objective function to test on.

4.5.3. BANDWIDTHS OR GLUE

In this study we choose to equally accept all 'good' behavioral parameter sets, these are all parameter sets resulting in model outcome with a objective score higher than LogNS_C > 0. From this set of model outcomes, for every timestep the 10th, 50th (median) and 90th-percentile values are calculated. The model is calibrated on the median of these outcomes. The idea is that the ensemble of good performing parameter sets which is able to reproduce the discharge at the calibration point, also would be able to predict discharge for other catchments. The choice to use the Median value to calibrate on is rather arbitrary.
Another choice would be to apply GLUE (Generalized Likelihood Uncertainty Estimation). This method weighs the outcomes with the objective scores to obtain a weighed averaged including uncertainty bandwidths. Possibly automatic calibration in combination with GLUE will further improve the model performance. Note, however, that the weighing factor of GLUE also introduce a new calibration parameter. So neither this method is perfect.

[6] Note, we that expert judgment should go hand in hand with standardized computational modelling. Without the right knowledge, computer models will not be able to understand the hydrology. Hence manual calibration stays necessary in order to judge models represents the right hydrological behavior

5

CONCLUSIONS

In this study we investigated the origin of the seemingly perennial (base) flow in a hydrological complex Inselberg (a type of mountain) dominated catchments in the Messica Catchment in the Province of Manica, Mozambique. Only limited measurement data was available in the period from December 2012 to August 2014, so this catchment is classified as poorly gauged. Due to the perennial baseflow property, the area is very suitable for year-round smallholder irrigation and contributes significantly to Mozambique's total food production. However, the base flow recession, (over year) groundwater availability and rainfall runoff processes in these type of catchments are vaguely understood and poorly investigated. This research study, therefore, provided both practical and theoretical new insights on these topics.

We showed that (1) base flow recession can be estimated on cross-sectional corrected water level (conveyance) measurements, but do need some additional discharge information to calculate discharge. (2) Availability and location of water storage can be further determined using a semi-distributed conceptual FlexTopo model and (3) Streamflow dynamics in both gauged and ungauged catchments can be predicted using semi-distributed transferable FlexTopo models calibrated on conveyances.

Previous research studies showed that baseflow recession can be estimated based on parsimonious discharge measurements [7]. We showed that baseflow recession values (i.e. representative (groundwater) response time scales; K-values) can also be estimated with cross-sectional corrected water levels (conveyances), under the quasi-static uniform flow ànd linear reservoir assumption. These time scales follow from the slope of the $t - C$ graph (time-Conveyance) on LN-scale. We came up with this method, since discharge measurements during this field research at first appeared to be failed - which we solved later in the study. And since discharge measurements in general are always obtained indirectly, mostly non-continuous and often lack during peak discharges, we searched for a method to obtain more information from directly measured water levels (dynamics). In the study area, divers have recorded every 30 to 60 minutes barometric and water pressures at several locations.

From measurements at Godi Downstream Station, which has been equipped with pressure divers and barometers for about 1.5 year, we derived a recession timescale of about 550 days. This implies that a certain amount of storage reduces to 50% in about 380 days and to 10% in about 3 years. So we can speak of over-year groundwater storage.

Furthermore, we can estimate the discharge development during base flow periods and therefore we can predict the streamflow at the end of the second and third growth season, which is very useful for smallholders. It proved that the method can be used independently from computer models if some discharge measurements are available. So we can actually derive a discharge relation based on water level (i.e. conveyance) measurements. This is possible, since the concept of conveyances is based on the Manning-Strickler formula. Therefore it can be simplified to a linear dependency with discharge Q, multiplied with a constant $\bar{a}$ to account for bottom roughness and bottomslope. This constant can theoretically be estimated based on literature and field inspections, but in this study calibration on the available parsimonious discharge measurements significantly improved the performance. We applied the conveyance method on both small, very vegetated headwaters and on a three-gated bridge that acted as a free-flow construction. For both applications the results during low flows are rather good, however, during peak flows the uniform flow assumption is violated mostly due to the abundant (water) vegetation, which becomes even denser at larger water depths.

Additional work is needed in order to make the method fully functional for the flow regime.

On forehand, we suspected the groundwater storage to be in the mountains. In this study we showed that this is likely the case. However, since Inselbergs often consist of solid Tonalite, Trondhjemite, or Granites (TTGs), which are considered almost unerodible and impermeable, this was not very obvious in advance. Literature study showed however, that despite similar visual appearance, the mountains do no originate from the Kalahari Craton like most Inselbergs do in Zimbabwe and between the Zimbabwean border and Messica. The mountains are formed from a later deposed sedimentary rock, called the Gairezi Sedimentary Group (or Frontier Formation). This group does not consist of TTG-materials, but of quartszites and metapelic schists, which are not very unerodible and impermeable as TTGs. In field surveys we found evidence to confirm our literature sources. The Gairezi stretches from Sussendenga in the South to Guru in the North over a length of 220km along the geological fault.

We developed two rainfall runoff models (FlexA and FlexC) based on the FlexTopo concept with an additional output conversion model (OCM) (a) to prove that baseflow can be estimated based on conveyances with some additional discharge measurements, (b) to confirm or reject the mountain as groundwater storage 'reservoir' and to estimate its volume and (c) to test whether year round discharge variations (both base and peak flows) can be predicted for a catchment (Messica Downstream Station) based on calibration on a subcatchment (Godi Downstream Station).

FlexA serves as a lumped conceptual rainfall runoff benchmark model which incorporates all the predetermined relevant hydrological processes. Based on FlexA, we developed a software package to easily compose and test semi-distributed conceptual rainfall runoff models based on our field observations and hypothesis, of which FlexC is one of them. FlexC distinguishes three different HRUs (hydrological response units) (an entity that show similar hydrological responses), namely wetlands (with saturated overland flow and exfiltration of deeper groundwater), inselbergs (with perennial baseflow from its large groundwater storages, fast runoff processes due to steep, forested and/or rocky slopes) and flatlands - which covers a wider scope from irrigated areas, grass and shrub lands to rain-fed fields - which will contribute (delayed and minimized) to both base and peak flows. In our latest hypothesis we believe that flatlands on top of the Kalahari Craton might infiltrate to a deeper groundwater aquifer and, being so, leave the system unmeasured. This is however to be tested in future studies. FlexC's HRUs are objectively distinguished on HAND (head above nearest drainage level) and hill slope values [18, 29]. Every HRU has its own slow groundwater response reservoir, in order to pinpoint the location and amount of groundwater storage. In FlexC these reservoirs are connected. In the final model calibration we applied altitude adjusted precipitation, such that every HRU receives different volumes (based on its average altitude).

From this study we conclude that (a) one can succesfully calibrate both FlexA and FlexC for baseflows using the conveyance method. Being so, we also prove that the supposed method works independently of the Flexmodel under mentioned assumptions and that one can derive parameters to feed into the Flex model in order to minimize (free) calibration.

(b) Model calibration shows that (slow) groundwater storages are largest in this HRU and that most perennial flow indeed originates from the mountain. This follows from FlexC's hydrological response unit "Inselberg" which represents the majority of the mountain ridge. The model predicts for Godi catchment an active storage of 800mm in 2013-2014, which implies a specific discharge Q of 1.45 [mm/s] at the beginning of the baseflow recession. Assuming an average depth above nearest drainage level (HAND) of approximately 75m with a pore volume of 1% this is also physically possible.

Moreover, (c) both FlexA and FlexC can predict year round discharges at a downstream station of the River Messica (MessDS) for a calibration performed on conveyances at a different measurement station (GodiDS). Both models performed already quite well. Where FlexA shows better peak flow predictions according to objective functions, FlexC narrow down uncertainty intervals around predictions on other locations. However, it seems to overestimate peak flows.

Finally, although FlexC incorporates more degrees of freedom (calibration parameters) than FlexA, the calibration is restricted due to predefined parameter and process constraints. Moreover, the smaller uncertainty bandwidths also pleads for a more consistent model performance by FlexC than FlexA. Both models however, can be optimized; computationally by using a different method to calibrate and predict uncertainty bandwidths, and hydrologically to incorporate extra processes like infiltration to deeper groundwater, higher rainfall resolution (3hours in stead of 24hours timestep) resulting in very fast runoff and flow routing.

6

APPLICATION AND RECOMMENDATIONS

One of the goals for MIPP-project is to obtain a widely applicable implementation framework, including a standardized cost-effective hydrological survey to support sustainable irrigation development for Messica Catchment specifically and Mozambique in general. Amongst others, Weemstra *et al.* [7] and underlying study contribute to this ultimate goal.

6.1. ACHIEVEMENTS

Weemstra *et al.* [7] investigated that the baseflow recession can be estimated with single discharge measurements performed at selective moments in time. With the linear reservoir assumption, a first base flow recession estimate can be made. This study confirms that finding, although we estimate lower recession values: around 400-600 days instead of 1700 days[1]. A possible explanation for this deviation is the inaccuracy of single observation salt dilution discharge measurements. This method relies on the accuracy of fitting a recession line through those individual observations, without explicitly taking its hydrological history into account (e.g., discharge variations due to rainfall events, irrigation activities or daily variation), and not to mention measurements errors. Altogether the recession time scale as found with this method can easily deviate from reality.

This study proceeds the quest for an easy determinable method to predict the recession time scales. It appears possible to derive these time scales directly from water level dynamics. By taking the uniform flow assumption and measuring the cross-section, water levels can be converted to conveyance scale. Subsequently, the slope of the conveyance on semi-logscale present these timescales, since the conveyance is linear dependent on the discharge. Hence, recording the water levels and cross section next to the discharge measurements gives an extra possibility to successfully estimate the (base) flow recession.

This study even proves the possibility to calibrate and validate hydrological model on these conveyances (cross-sectional corrected water levels).

Weemstra *et al.* [7] also discovered that headwaters gain water while running down from the Inselberg, and that the River Messica seems to infiltrate water over its length. This is in line with the findings of our model, where the mountainous area is mostly indicated as Inselberg, which is actively contributing to the stream. The validation calculations at Messica downstream appear to overestimate peak discharges, which might also be caused by the negligence of infiltration processes. The discharge measurements done in this study do not provide a conclusive evidence for infiltration, see water balances in App. J. Future studies should answer whether the River Messica is prone to infiltration.

Furthermore, Weemstra *et al.* [7] suggested that total precipitation volumes and timing outweighing the effect of rainfall intensity for the baseflow recession in the dry season. We did not further investigate this in this study, but we suggest a second opinion after implementation of hourly or 3hourly rainfall amounts. This, to take into account the altered hydrological response of high intensive rainfall events. Since aggregated precipitation intensities to daily time steps underestimates the peak events will lead to a different deviation

[1] At the beginning of the dry season Weemstra *et al.* [7] suggested 250 days

between infiltration and (very) fast surface runoff.

Finally, Weemstra *et al.* [7] noticed the occurrence of a strong rainfall gradient as function of the altitude. We proposed a linear relation to account for the rainfall amount as function of the altitude. This indeed leads to better calibration and validation results, where more rainfall is applied at higher altitudes and less to lower. However, we have indications that this linear relation is a too simple approximation of the rainfall deviation as a result of orographic effects. For precipitation measurements on the peak of the mountains are equal or smaller compared to those halfway the mountain ridge (at David's place), whereas the linear relation predicts the largest rainfall volumes on the top of the mountain. Therefore, we suggest to also take the horizontal distance to the peak into account. We were not able to investigate this due to the absence of long rainfall measurements on top of the mountain.

de Boer [8] dived into influences of irrigation activities on diurnal streamflow variation. Applying Meyboom [48], and an assumption of 1 L/s.ha irrigated cropland, she proved being able to estimate the irrigation areal in unmapped area. She also corrected measured discharges for irrigational influences, which is, as explained earlier, not implemented in this study.

Weemstra *et al.* [7], de Boer [8] made a first hydrological rainfall runoff model using the HBV light model [13, 37]. This already gave insight in baseflow recession in the Messica Basin. We replaced the HBV model for a semi-distributed flexible, topography driven conceptual rainfall runoff model FlexTopo. This improves insight in location and amounts of groundwater storage.

6.2. APPLICATION MODEL

The developed methodology using the conveyance method and FlexTopo model can already be applied in this area:

- To predict current discharges and groundwater storages. For example due to the effects of El Ninõ (2016)[2].
- To analyze irrigation potential for ungauged catchments in the Gairezi Sedimentary Group.

We suggest for future irrigation projects the following steps to predict water availability in ungauged areas within the Gairezi sedimentary group:

- Install divers and barometers at locations with uniform flow conditions and known cross section, or install weirs (e.g. v-notch weirs). Conduct discharge measurements at regular time interval at these locations (for example with the Salt Dilution Method). Derive the conveyance from these measurements. Together with the discharge measurements baseflow recession and streamflow evolution can be predicted at these locations (even without using FlexTopo).
- Install a network of rainfall gauges (on daily frequency) and tipping buckets for rainfall intensities. Make sure that the gauges are equally spread over the valley, the ridge and the peak in order to derive a multi variable rainfall amount function, with altitude and horizontal distance to the peak as variables.

6.3. IMPROVEMENTS MODEL

In order to improve current model concept for this (type of) area(s), we recommend to:

- Test the model concept in other regions within the Gairezi Sedimentary Group. To see whether the proposed conceptualization is indeed general applicable.
- Combine geological, elevation and land use information to come up with Hydrological Response Units. This information is needed to feed the FlexTopo Model concept.
- Improve the classification of Wetlands by drilling holes to monitor groundwater levels at the edge of expected Wetland boundaries. This will improve insight in the location of wetlands [29].

[2] Though extreme situations push the model beyond its calibration limits, which have to been kept in mind when interpreting the results.

- Try to use remote sensing data (like LANDSAT) to enhance HRU classification in order to make the method even wider applicable.
- Place piezometers to monitor the groundwater levels in the Kalahari Craton, in order to gain more insight in possible infiltrative behavior in this area.
- Add an extra process to account for infiltration around the Messica basin, since this is located on top of the Kalahari Craton, and consists of other material.
- Install measurement stations in Messica Upstream area, to learn more about runoff from areas which are mainly located on the Kalahari Craton.
- Use sequential measurement stations to calibrate wave routing through the reaches.
- Conceptualize River Messica as open gutters/reaches, from where infiltration and wave damping due to travel time and flooding can take place.
- Investigate effects of internal mountain inclination, which can positively contribute to groundwater availability at the western Messica side of the mountain. However, at the same time negatively influence baseflow at the eastern Vanduzi slope.
- Improve precipitation altitude correction. The current applied linear altitude relation might be to simplified.
- Resample daily precipitation volumes to take place within 3h. This will increase rainfall intensity and will therefore introduce faster hydrological runoff processes.
- Calibrate the model on smaller time step resolutions, but not larger than the rainfall time resolution (so max 3hr). If necessary, compare daily averaged modeloutcomes with daily averaged observations to mitigate timing errors, which are introduced by artificial rainfall resampling.
- Implement automatic calibration routines like AMALGAM[46] or MOSCEM-UA[45]. Investigate the calibration improvement by taking more hydrological signatures [e.g., [21, 24]] into account. Optionally apply GLUE to obtain a better weighted result.

6.4. THREATS FOR THIS FRAGILE ENVIRONMENT

From field experience we observe some on-going (national) threats that possibly significantly effect the current hydrological system. We leave these here as mental notes for the reader, without providing further scientific or historical evidence.

- Global climate change, or climatic effects like El Ninõ. Unfortunately there is no local solution possible for this threat.
- Cutting forests. This changes the hydrological system (root zone development, preferential flow paths, (cloud forest) interception, hydrological cycle). There are some examples in comparable areas like in the Tete Province, where interviews with local people sketched the deterioration of the area's local water sources after cutting the forest on the mountains.
- Exploiting passive groundwater storage, due to deep groundwater extraction. This is not happening yet, but it will effects the recession time. Most likely the storages will become smaller and thus emptying faster. Secondly, longer recovery times will be needed, because more precipitation is necessary to refill the storages to the original levels.
- Too neat field and irrigation management can lead to loss of biodiversity. Leaking canals and diverge vegetation lead eventually to a more sustainable ecosystem, which on the long run is more beneficial to the (local) society.

6.5. CONTINUATION RESEARCH BESIDES THIS STUDY

Apart from the side-specific recommendations, also some topics passed the scene and might lead to interesting insights as well:

- Make the conveyance method wider applicable by deriving it from Saint-Venants equation, such that the method incorporates a depth-dependent roughness model and is not restricted to (quasi-) steady-state uniform flows.
- A possible different method to quantify discharge-water level ($Q-h$) relations is the advection-diffusion equation (which is a simplification of the the saint-venants equation). The diffusion and advection properties as well as discharges can be measured with the salt dilution method using two or more EC-meters at different distances from the entry point. The progression of the salt wave shape is caused by the stream properties (e.g., turbulence due to roughness and transport capacity), since discharge is assumed constant during the measurement. We tried to measure this effect in Mozambique, unfortunately, we lacked the right equipment.
- Set-up a vast network of smallholders to measure daily rainfall volumes and water level variations at fixed points. This contributes to measurements, we can use to train our models and extend (hydrological) knowledge. This might reduce costs of laborious field campaigns and at the same time enhance local knowledge and insight. A good example is David Muchena, who proved a proficient student and co-worker. Of course, training, regular visitation and supervision is inevitable.
- We believe that more information can be extracted from conveyance dynamics, such as smaller response timescales K-values and periods (and possibly even amounts) of groundwater recharge. Since, baseflow dynamics are a result of the groundwater storage. However, since the observed conveyance is a result of complex non-linear rainfall-runoff processes ànd flow routing, this is rather challenging. A first step might be to identify recharge periods, a second step to correct for flow routing (therefore longitudinal flow measurements are needed).

BIBLIOGRAPHY

[1] P. J. Chilton and S. S. D. Foster, *Hydrogeological characterisation and water-supply potential of basement aquifers in tropical africa,* Hydrogeology Journal **3 no. 1** (1995).

[2] T. Koistinen, M. I. Lehtonen, S. Fernando, and R. Matola, *Contribution to the structure at the eastern margin of the archaean zimbabwe craton, mozambique,* Geological Survey of Finland **Special Paper 48**, 121 (2008).

[3] I. Parmentier, *Study of the vegetation composition in three inselbergs from continental equatorial guinea (western central africa): effects of site, soil factors and position relative to the lower or upper forest fringe.* Belgian Journal of Botany **136(1)**, 63 (2003).

[4] A. L. Oord and P. W. Beekman, *Hydro(geo)logical Study Messica Catchment, Manica Province, Mozambique*, Tech. Rep. OWS2012-002-0905 (Oord Water Services Resilience BV, 2012).

[5] W. Beekman, G. J. Veldwisch, and A. Bolding, *Identifying the potential for irrigation development in mozambique: Capitalizing on the drivers behind farmer-led irrigation expansion,* Physics and Chemistry of the Earth, Parts A/B/C **76–78**, 54 (2014).

[6] FAO, *Fao's information system on water and agriculture,* http://www.fao.org/nr/water/aquastat/main/index.stm (2012).

[7] H. Weemstra, A. L. Oord, F. S. de Boer, and P. W. Beekman, *Baseflow prediction in a data-scarce catchment with inselberg topography, central mozambique,* Physics and Chemistry of the Earth, Parts A/B/C **76–78**, 16 (2014).

[8] F. S. de Boer, *Hydrological response of the Messica catchment in Manica Province, Mozambique; A case study of the Rio Godi*, Internship, Wageningen University (2013).

[9] J. P. de Boer, *Irrigation Development in mozambique*, Bachelor internship, Wageningen University (2012).

[10] S. D. Holsteijn, *Improvement of discharge data collection methods in the Messica Catchment, Mozambiqe; The development of rating curves for the rivers Chirodzo and Ruaca*, Bsc internship, University of applied sciences Van Hall Larenstein (2013).

[11] D. A. Reumkens, *Irrigation Development along Africa's Rift Valley*, Bachelor, Wageningen University (2012).

[12] A.-L. Krüger, *Farmers Portrait, Small holder irrigation - Irrigation efficiency of furrow systems - Messica, Manica Province, Mozambique*, Ph.D. thesis, Wageningen UR (2011).

[13] S. Bergström, *The hbv model,* in *Computer models of watershed hydrology, The Oxford Handbook of Innovation*, edited by V. P. Singh (Water Resources Publications, Highlands Ranch, Colorado, USA, 1995) Chap. 13, p. 443–476.

[14] J. Seibert, *Estimation of parameter uncertainty in the hbv model,* Nordic Hydrology **28 no 4-5**, 247 (1997).

[15] M. Hrachowitz, H. H. G. Savenije, G. Blöschl, J. J. McDonnell, M. Sivapalan, J. W. Pomeroy, B. Arheimer, T. Blume, M. P. Clark, U. Ehret, F. Fenicia, J. E. Freer, A. Gelfan, H. V. Gupta, D. A. Hughes, R. W. Hut, A. Montanari, S. Pande, D. Tetzlaff, P. A. Troch, S. Uhlenbrook, T. Wagener, H. C. Winsemius, R. A. Woods, E. Zehe, and C. Cudennec, *A decade of predictions in ungauged basins (pub)—a review,* Hydrological Sciences Journal **58**, 1198 (2013).

[16] H. H. G. Savenije, *Hess opinions "topography driven conceptual modelling (flex-topo)",* Hydrol. Earth Syst. Sci. **14**, 2681 (2010).

[17] F. Fenicia, J. J. McDonnell, and H. H. G. Savenije, *Learning from model improvement: On the contribution of complementary data to process understanding,* Water Resources Research **44**, n/a (2008).

[18] C. D. Rennó, A. D. Nobre, L. A. Cuartas, J. V. Soares, M. G. Hodnett, J. Tomasella, and M. J. Waterloo, *Hand, a new terrain descriptor using srtm-dem: Mapping terra-firme rainforest environments in amazonia,* Remote Sensing of Environment **112**, 3469 (2008).

[19] S. Gharari, M. Hrachowitz, F. Fenicia, H. Gao, and H. H. G. Savenije, *Using expert knowledge to increase realism in environmental system models can dramatically reduce the need for calibration,* Hydrol. Earth Syst. Sci. **18**, 4839 (2014).

[20] H. Gao, M. Hrachowitz, F. Fenicia, S. Gharari, and H. H. G. Savenije, *Testing the realism of a topography-driven model (flex-topo) in the nested catchments of the upper heihe, china,* Hydrol. Earth Syst. Sci. **18**, 1895 (2014).

[21] T. Euser, H. C. Winsemius, M. Hrachowitz, F. Fenicia, S. Uhlenbrook, and H. H. G. Savenije, *A framework to assess the realism of model structures using hydrological signatures,* Hydrol. Earth Syst. Sci. **17**, 1893 (2013).

[22] M. Hrachowitz, H. H. G. Savenije, T. A. Bogaard, D. Tetzlaff, and C. Soulsby, *What can flux tracking teach us about water age distribution patterns and their temporal dynamics?* Hydrol. Earth Syst. Sci. **17**, 533 (2013).

[23] M. G. P. de Weerd, *Modelling ungauged lowland basins; Does complementary groundwater data add value to topography driven conceptual modelling?*, Master thesis, Delft University of Technology (2014).

[24] S. J. H. Rikkert, *Improving model consistency and process realism in conceptual rainfall-runoff models; by increasing model complexity and making use of expert-knowledge*, Master thesis, Delft University of Technology (2015).

[25] M. M. Piet, *Dropping the rating curve: calibrating a rainfall-runoff model on stage to reduce discharge uncertainty*, Master thesis, Delft University of Technology (2014).

[26] A. de Kloe, *Calibrating a rainfall-runoff model in a data scarce catchment in Mozambique*, Master thesis, Delft University of Technology (2014).

[27] S. F. M. Gijsbers, *Thinking inside the box: Using reservoir levels to improve a conceptual rainfall-runoff model in the Umbeluzi River Basin*, Master thesis, Delft University of Technology (2015).

[28] P. Hulsman, *Sediment transport modelling: Determination of the main areas contributing to the suspended sediment load in the Mara River, Kenya*, Master thesis, Delft University of Technology (2015).

[29] S. Gharari, M. Hrachowitz, F. Fenicia, and H. H. G. Savenije, *Hydrological landscape classification: investigating the performance of hand based landscape classifications in a central european meso-scale catchment,* Hydrol. Earth Syst. Sci. **15**, 3275 (2011).

[30] A. D. S. T. Manhica, G. H. Grantham, R. A. Armstrong, P. G. Guise, and F. J. Kruger, *Polyphase deformation and metamorphism at the kalahari craton — mozambique belt boundary,* Geological Society, London, Special Publications **184**, 303 (2001).

[31] Ministério Dos Recursos Minerais and Instituto Nacional De Geologia, *Geological map of mozambique 1:1,000,000 rep ública popular de moçambique,* (1987).

[32] FAO, *Land cover of mozambique - globcover regional,* http://www.fao.org/geonetwork/srv/en/main.home?uuid=e58eada2-046a-4277-a812-5c11762ed902 (2009), accessed: June 23th, 2014.

[33] FAO, ed., *Local Climate Estimator*, new_locclim 1.10 ed. (Food and Agriculture Organization of the United Nations, 2005).

[34] H. W. Russell, *Estimating potential evapotranspiration*, Bachelor thesis, Massachusetts Institute of Technology (1960).

[35] Ministery of Economy Trade Industry (METI) Japan and United States National Aeronautics and Space Administration (NASA), *Advanced spaceborne thermal emission and reflection radiometer (aster) global digital elevation model version 2 (gdem v2),* (2011).

[36] S. Bergström, *The hbv model: Its structure and applications,* (Swedish Meteorological and Hydrological Institute (SMHI), Norrkoping, Sweden, 1992) p. 35.

[37] J. Seibert and M. J. P. Vis, *Teaching hydrological modeling with a user-friendly catchment-runoff-model software package,* Hydrology and Earth System Sciences **16**, 3315 (2012).

[38] *HBV-light introduction, tutorial and downloads from university of zurich department of geography,* http://www.geo.uzh.ch/en/units/h2k/services/hbv-model, accessed: 2016-05-11.

[39] L. J. Bren, *Effects of slope vegetation removal on the diurnal variations of a small mountain stream,* Water Resources Research **33**, 321 (1997).

[40] H. Gao, M. Hrachowitz, S. J. Schymanski, F. Fenicia, N. Sriwongsitanon, and H. H. G. Savenije, *Climate controls how ecosystems size the root zone storage capacity at catchment scale,* Geophysical Research Letters **41**, 7916 (2014), 2014GL061668.

[41] F. Fenicia, H. H. G. Savenije, P. Matgen, and L. Pfister, *Is the groundwater reservoir linear? learning from data in hydrological modelling,* Hydrology and Earth System Sciences **10**, 139 (2006).

[42] H. H. G. Savenije, *Equifinality, a blessing in disguise?* Hydrological Processes **15**, 2835 (2001).

[43] P. Purcell, *Physical analog of the linear reservoir,* Journal of Hydrologic Engineering **11**, 184 (2006).

[44] V. T. Chow, ed., *Handbook of Applied Hydrology, A Compendium of Water-resources Technology* (McGraw-Hill Book Company, 1965).

[45] J. A. Vrugt, H. V. Gupta, L. A. Bastidas, W. Bouten, and S. Sorooshian, *Effective and efficient algorithm for multiobjective optimization of hydrologic models,* Water Resources Research **39**, n/a (2003), 1214.

[46] J. A. Vrugt, *Multi-criteria Optimization Using the AMALGAM Software Package: Theory, Concepts and MATLAB Implementation*, Tech. Rep. (2016).

[47] A. Hartmann, T. Wagener, A. Rimmer, J. Lange, H. Brielmann, and M. Weiler, *Testing the realism of model structures to identify karst system processes using water quality and quantity signatures,* Water Resources Research **49**, 3345 (2013).

[48] P. Meyboom, *Three observations on streamflow depletion by phreatophytes,* Journal of Hydrology **2**, 248 (1965).

[49] N. R. G. Walton, *Electrical conductivity and total dissolved solids—what is their precise relationship?* Desalination **72**, 275 (1989).

[50] R. C. Weal, *CRC Handbook of Chemistry and Physiscs*, 56th ed. (CRC press, Cleveland, Ohio, 1975-1976) pp. D252–253.

[51] C. E. Kindsvater and R. W. Carter, *Discharge characteristics of rectangular thin plate weirs,* Journal of Hydraulics Division **83**, 1 (1957).

[52] M. I. Budyko, *The Heat Balance of Earth's Surface,* Tech. Rep. (US Department of Commerce, Washington, DC, 1958).

A

PICTURES OF FIELD OBSERVATIONS

This Appendix provide extra site specific background information in the form of photos.

A.1. VIEW OF MESSICA INSELBERG RIDGE

Figure A.1: Gently sloped landscape with very steep Inselberg ridge. The red shaped triangle on the ridge is a gully in the ruage catchment. This gully arose during the wet season of 2013-2014. Just below this gully one observe grasslands. The upper boundary of the grasslands are more on the same altitude (horizontal oriented). This is approximately on an altitude of 800 to 900m+AD. According to villagers, the local chief of the village of Chirodzo does not allow to cut forests and/or built houses at higher altitudes. One of the reasons would to protect the vulnerable environment [source: Interview]. In every very toe a small stream start, cutting through the landscape. Picture taken from the mainroad Messica - Godi Market. In front the wet grasslands (compare Fig. A.2). (April 2016)

Figure A.2: Wetlands/ grasslands near the River Messica. These fields are very wet in the wet and early dry season, however, tend to become dry in the late dry season. Note also the clouds around the mountain peaks, most likely vegetation will intercept moisture from the clouds (cloud forests), which is not observed by raingauges. Possibly this precipitation source is larger than expected. (March 2014)

Figure A.3: Grassland in Godi catchment on gently sloped terrain. no irrigation possible. Terrain only used for rainfed maize during wet season. Note whitish soil color, indicating weathering material from granitoids [2]. We pose that this most likely originates from the Kalahari Craton / Messica Granite [30] (June 2014)

Figure A.4: View to Inselberg from 800m+AD zone. Hill slopes are predominantly forested. Observe areas with caprock; the very steep hill slope inclination; the red soils in front. David Muchenga (who operates the daily raingauge station) lives at the beginning of the slope forest at the left hand side, in the very dark green grove just at the edge of the slope forest. Note a small house at the right hand side. This is one of the highest located households in this area. (March 2014)

Figure A.5: Inselberg seen from the Ruaga Catchment. The small mountains in front possibly originate from the Kalahari Craton and consist of TTG materials. We did not further investigate this. Observe also the bare caprocks at the very left of the picture. (March 2014)

Figure A.6: Godi Catchment, Scene right from Fig. A.4. Observe the small house on the hill slope at the very left end of the picture. We note here a small valley between the large Inselbergs on the left and small 'baby' Inselbergs on the right hand side. Very fertile area and moistures area, year round, streams find their ways between these small mountains. (March 2014)

A.2. INSPECTING INSELBERG RIDGE

Figure A.7: Godi upstream close to location Godi_1. Sub-tropic forests along the headwaters, very pristine landscape. Only riperian to the stream are banana trees planted. (May 2014)

Figure A.8: Spring like groundwater exfiltration over a very short reach on the very top of Inselberg at the Vanduzi side. The stream can only drain the groundwater in the very top layer of the mountain, judged by its relative position to the mountain peak. (April 2014)

Figure A.9: Giant hardwood trees in riperian zones along Godi stream (near location Godi_1), more than 1m in diameter. These trees are also found on the very top of the mountain, compare e.g.,Fig. A.20 (April 2014)

Figure A.10: On the mountain edge there are rock outcrops everywhere. Note again the red soil, indicating mica together with the clear layers or schistology of the stones and the (east) dipping inclination [2]. Traces of groundwater exfiltration are not very clear (April 2014)

Figure A.11: Forests on the foothills of the Inselberg. Small, tough trees with rocks very close to the surface, suggesting thin soil layer. (July 2014)

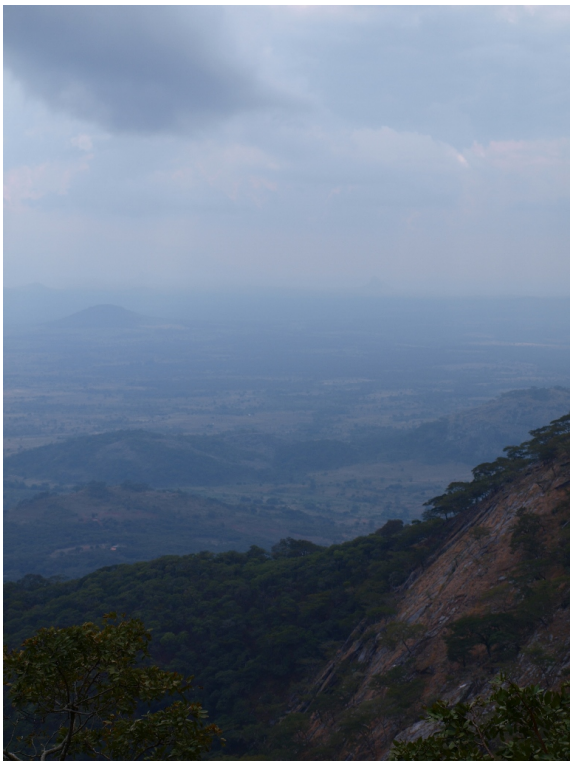

Figure A.12: Very steep rocky slopes, with caprocks visible at the surface. Also note the unclear sky due to smallholders burning their fields (July 2014)

Figure A.13: Clearly visible the foothills of the Inselberg with in between the headwaters Chirodzo and Godi. Vegetation consists of small, tough trees (July 2014)

Figure A.14: View from Inselberg to the Messica catchment. Pastures crop land, only small forested plots. Observe the clear view, only in this period it is possible to look this far. Later in the year people start burning their fields [source: interviews] (March 2014)

Figure A.15: View on Ruaga Catchment, Fig. A.44 views from down the valley to this location and mountain ridge in front (March 2014)

Figure A.16: View from highest point (at 1472m+AD) on Chirodzo and Godi headwaters. Observe forested, steep hill slopes, quite flat grass lands on top due to deforestation (see Fig A.20) and pastures land below in the wide and seemingly flat Messica valley. Note the large orange / red colored gully in the Ruaga Catchment, the color could indicate mica [2], which strength the idea of the Gairezi Group Metasediments. (April 2014)

Figure A.17: Top inselberg: Villagers from the east side of the ridge, deforestate the mountain peaks and plant rainfed maize. Grassland is result of earlier deforestation, the total grass area increase yearly according to local villagers [Interview David Muchenga]. On the slopes grow pristine forests. On the very end of the grass land, a tipping bucket and manual raingauge is located (not visible) (March 2014)

Figure A.18: On the edge of the forest, as depicted in Fig. A.20. It appears to us as a tuff penetrable, pristine forest, with hard wood trees, lianas and baboons. David is about 1.60m tall (April 2014).

Figure A.19: Description see Fig. A.18 (April 2014)

Figure A.20: Deforestation peaks by Vaduzi's villagers east from the Inselberg ridge, making room for rainfed maize fields. Leaving trees burned and unused and destroying the unique and humid ecosystem. (April 2014)

Figure A.21: Rocks on top of Inselberg ridge. Gairezi Group Sediments [2]. (March 2014)

Figure A.22: Large vertical fractures in rocks. many of these large fissures can be observed on top of mountain. Possibly rainwater infiltrates here into the mountain and leaves the mountain at Godi / Chirodzo side via preferential flowpaths through slight east dipping schistology [2]. The stick placed in the crack is about 1.5m tall and thick as a brick. (March 2014)

A.3. EXAMPLES OF GROUNDWATER SOURCES

Figure A.23: Chirodzo catchment. Small pool containing groundwater (location **Chir_4**). The pool is used as drinking water source. Discharge from this pool was about 2 - 2.5 L/s (with bucket method). See also Fig. A.24. The receiving stream is a continuous stream springing far upstream, though during winter (dry period) the stream disappear in the ground (due to irrigation take of and infiltration). From this point onwards the stream drains the groundwater and continuous flowing. (April 2014)

Figure A.24: Chirodzo catchment. A close up from Fig. A.23. Standing water originating from groundwater. There is some inflow at the sides and bottom. No clear iron deposits. The greyish soils are possibly sediments from 'piping'. (April 2014)

Figure A.25: Groundwater exfiltration in plot with bananas near Davids place. Source most likely groundwater from upper areas. This hand dugged canal become one of the small tributaries to the Godi (April 2014).

Figure A.26: Groundwater outflow in Godi catchment (measurement location Godi_3). This concerns groundwater. pH, EC and Temperature values also indicate that this water is not similar to the water flowing on top of it (small irrigation canal). The pipe is only placed to guide the water. (March 2014)

Figure A.27: Wetland near place Chirodzo in the Chirodzo catchment. According to villagers this is always wet, and forms a source for streams. No clear hill slopes circumventing this stream, which is different from other wetlands which are located just at hill slope toe. Point coordinate for landuse investigation Lu_Chir_22 (June 2014)

A.4. CAPROCKS

Figure A.28: Downstream in Godi Catchment. Massive plates of caprock at surface. Note the treelike grass vegetation on the rocks, indicating biochemical weathering processes. Note the red gully on at the mountain ridge in the back of the picture and the small hill at the left hand side. This caprock and the adjacent hill at the left side origin possibly from the Kalahari Craton, and are therefore of a different structure than the ridge in the back of the back of the picture (June 2016)

Figure A.29: Note the vegetation on the caprock, which are no trees, but grass polls which grows on top of each other. The stems are formed out of roots. (June 2014)

Figure A.30: Close up of similar grass polls as shown in Fig. A.29 (May 2014)

Figure A.31: Rock material from caprock Fig. A.28. Course sand-stone like material. Note the difference in structure with Fig. A.21 as found on top of the Inselberg (June 2016)

Figure A.32: Close up of Fig. A.28. Note the mechanical weathering. Flaking of rocks due to temperature differences. (June 2014)

Figure A.33: Waterfall in Ruaga Catchment. The lithology of the rocks is not clear. Possibly it are TTG gneisses from the Kalahari Craton. (March 2014)

Figure A.34: Waterfall in Godi Catchment just upstream of measurement point GodiDS (located between the reeds in the right lower corner of the picture). The lithology of the rocks is not clear. Possibly it are TTG gneisses from the Kalahari Craton. (March 2014)

Figure A.35: Rapid in the River Messica, just downstreams of the bridge at MessDS. The lithology of the rocks is not clear. Possibly it are TTG gneisses from the Kalahari Craton. (May 2014)

A.5. LAKE CHICAMBA

Figure A.36: View on Lake Chicamba. Note the gneisses and steep mountains within the lake. These are presumably not part of Gairezi Sedimentary Group (compare Fig. 2.2) and therefore originates possibly from Messica Granite. This stretches the uniqueness of the Messica mountains (March 2014)

Figure A.37: Chicamba dam. (March 2014)

Figure A.38: Chicamba Dam (March 2014)

Figure A.39: Chicamba Dam (March 2014)

Figure A.40: Lake Chicamba seen from the mountains at the west side. Note the rocks which are clearly from another material than Messica's mountains. (with thanks to an anonymous backpacker April 2014)

Figure A.41: Lake Chicamba seen from the mountains at the west side. If right, the mountains at the other side are Messica's mountains, i.e. the Gairezi Sedimentary Group (with thanks to an anonymous backpacker April 2014)

Figure A.42: Lake Chicamba seen from the mountains at the west side. If right, the mountains at the other side are Messica's mountains, i.e. the Gairezi Sedimentary Group (with thanks to an anonymous backpacker April 2014)

A.6. GULLY IN RUAGA CATCHMENT

Figure A.43: Gully in Ruaga Catchment. Observe greyish soil, indicating Kalahari Craton. Depth of Gully 4-5m, for reference the length of the tallest person is about 1.95m. Observe the continuous, but very small stream. Observe the holes in the walls caused by piping due to preferential flow paths (March 2014)

Figure A.44: In the bottom one observes the gully in Ruaga Catchment, just below the tree. The mountain ridge in the back of the picture is the continuation of the Gairezi Sedimentary Group. The small solitary mountains in front possibly are TTGs from the Kalahari Craton. Fig. A.15 is made on top of the left mountain and looks over the mountain ridge on the left and this valley. (March 2014)

Figure A.45: Gully in Ruaga Catchment. Observe greyish soil on the left and bottom part of the gully, whereas the right wall consists of red soil, refering to the Gairezi Sedimentary Group. The gully forms around the border of both cratons. (March 2014)

Figure A.46: Gully in Ruaga Catchment. Observe greyish soil, at the left side and red coloured soil at the left side of the gully. The gully increases during rainseason 2013-2014 from the tree at to the end, a length of about 30m. (March 2014)

Figure A.47: Gully in Ruaga Catchment. Observe greyish soil at the left and red soil at the right side. This is the end of one stretch of the gully. Note the large holes at the ends caused by preferential flow paths. (March 2014)

A.7. AGRICULTURE AND IRRIGATION

Figure A.48: Irrigated babycorn field in dry season. David is measuring the soil moisture content in top layer (June 2014)

Figure A.49: Irrigated cropland, babycorns (June 2014)

Figure A.50: Rainfed crops red chili peppers for the agricultural Vandouzi company (June 2014)

Figure A.51: Villagers start (under supervision of Resilience BV) with concrete lining of their irrigation canals to minimize leakage (June 2014)

Figure A.52: Common practise in lined and unlined irrigation canals; leakage of water along the length. Most of the water already flows back to the original stream within the first meters (June 2014)

Figure A.53: Downstream outflow at Chirodzo from Fig. A.55 (wheretion the valve is completely closed) (June 2014)

Figure A.54: Start of a irrigation canal in the Godi Catchment (Location Godi_1_1_us_in). At the right side, the Godi stream continuous, at the left side the irrigation canal, which ends up in a pipe to bridge a steep slope Fig. A.56. (April 2014)

Figure A.55: One of the headwaters of Chirodzo (location Chir_1_1_us_in), the stream is regulated with a (leak) valve (bottom of the picture), from which water continuous in the Chirodzo stream. The side spill flows into an irrigation canal. Holsteijn [10] took here his measurements (June 2014)

Figure A.56: A pipe is used to bridge the water in the irrigation canal over the slope (April 2014)

Figure A.57: Irrigated croplands of smallholder Chimoio, who also performs daily rainfall measurements (location in the cattle coral left of house below the large tree). note the red soils. The mountains in the back of the picture are part of the Greenstone Belt. At the very right some houses of the community of Chirodzo are visible (June 2014)

Figure A.58: Rainfed maize with in the far end the mountains in the Greenstone belt (see Fig **??**). Picture is token from the main road to Godi Market which is on the catchment border between Messica en River Revue. This part is draining towards River Revue. There is no possibility for irrigation here during the dry season (March 2014)

B

GEOLOGY

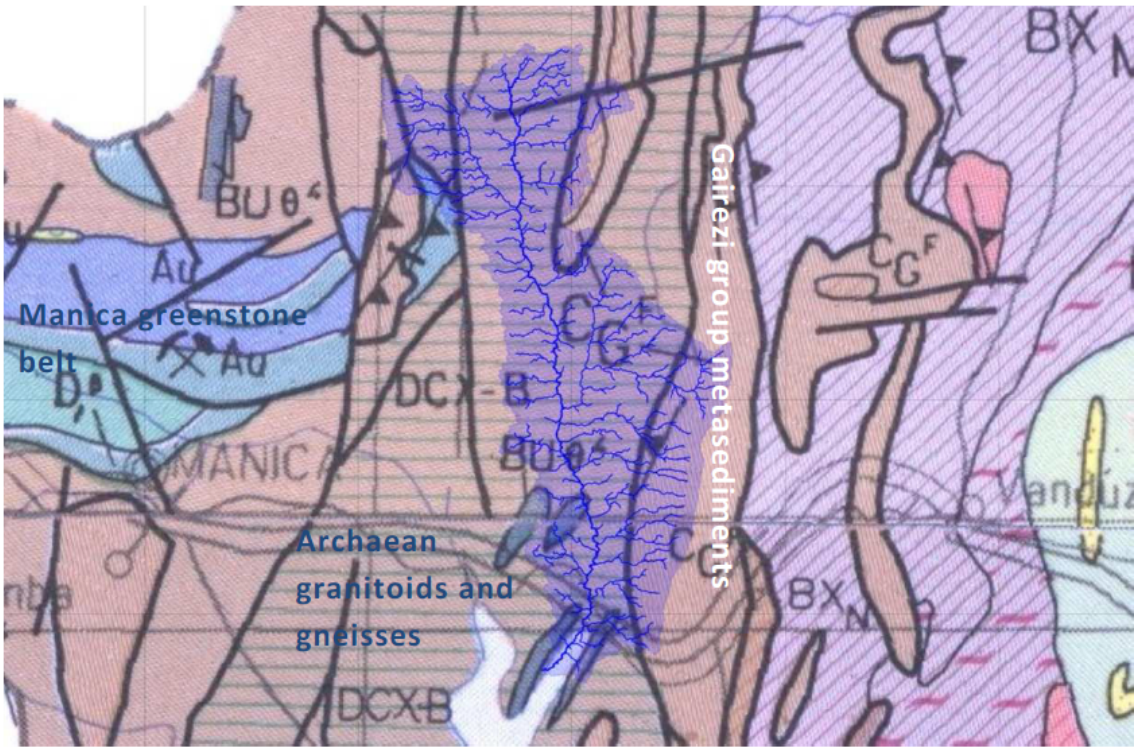

Figure B.1: An excerpt of the Geological Map of Mozambique 1987 [31] retrieved from [4]

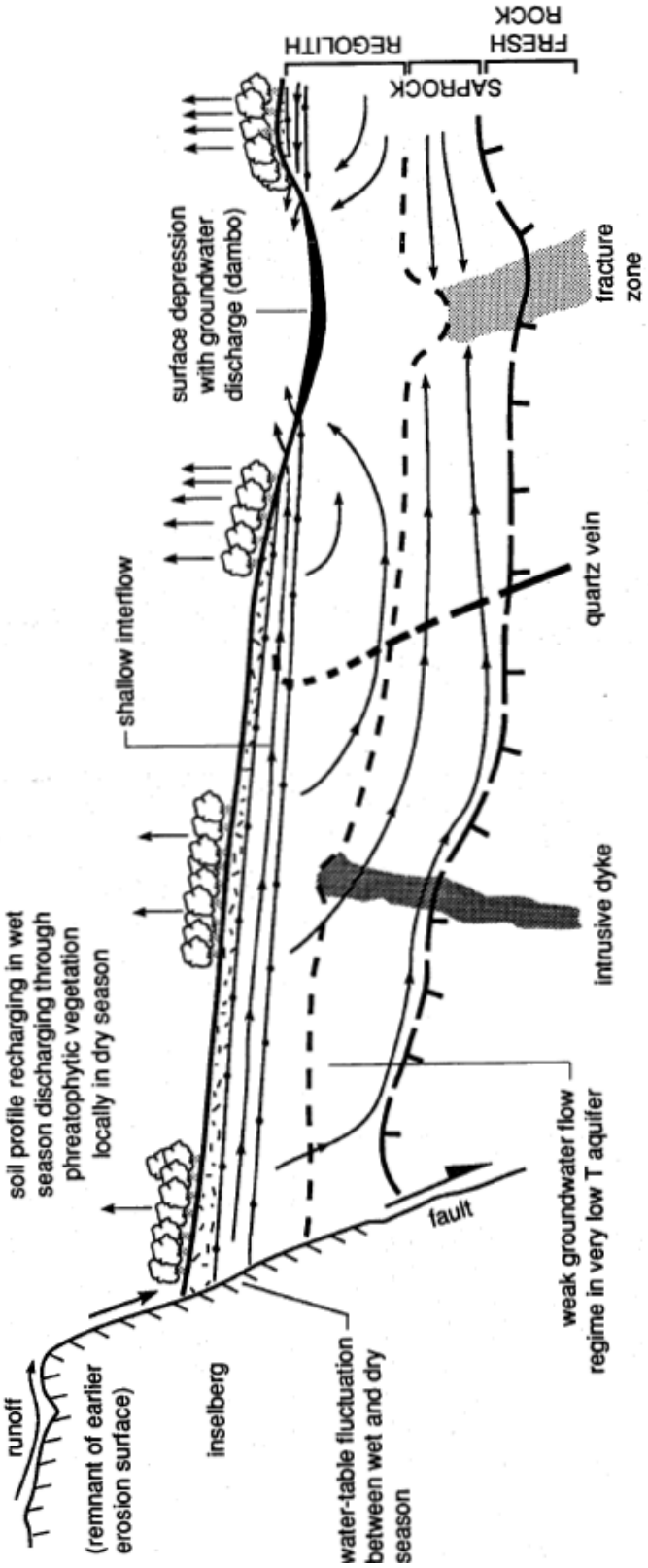

Figure B.2: Generalized section of the groundwater flow system in the weathered crystalline-basement aquifer in Malawi [1]

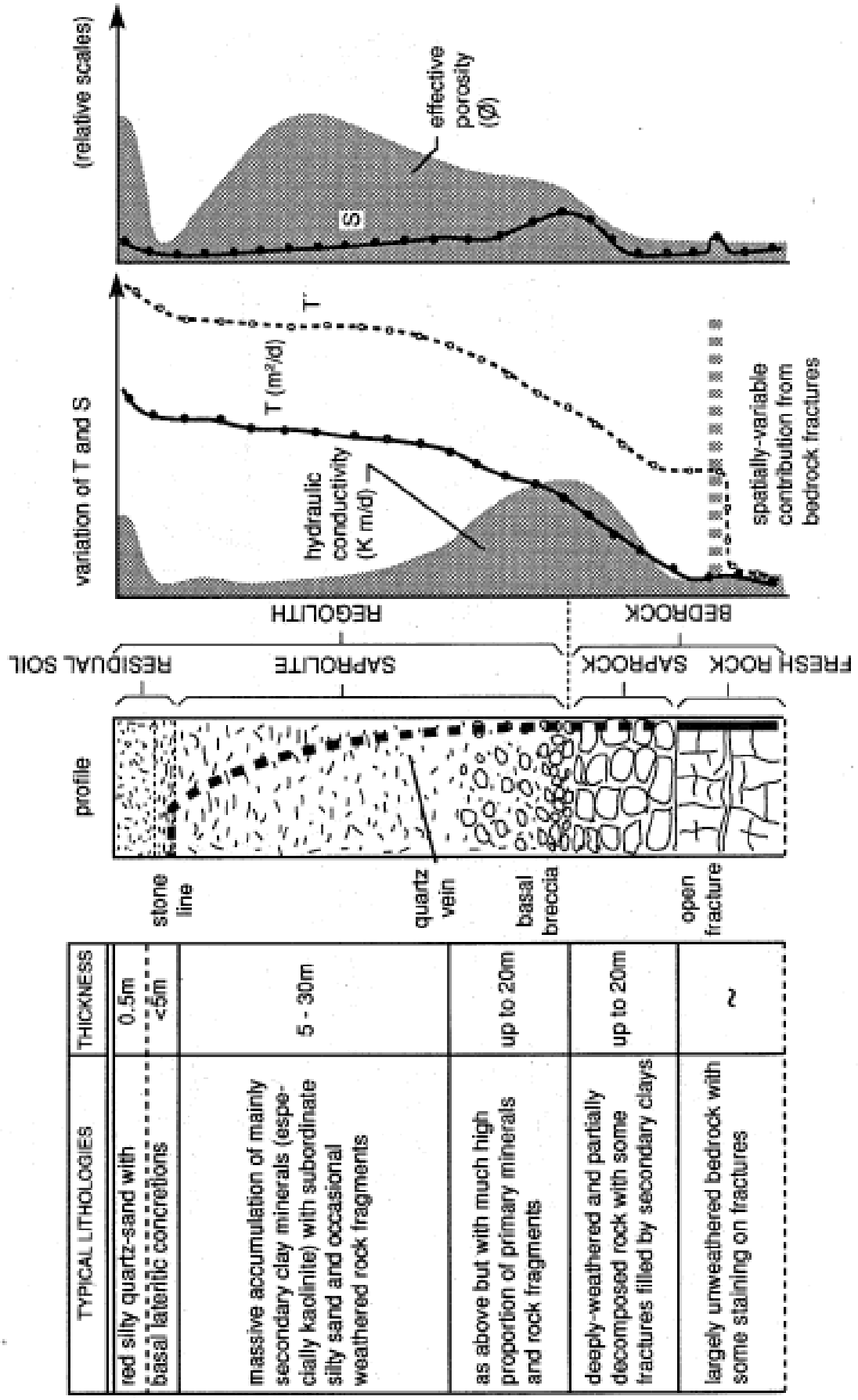

Figure B.3: Conceptual hydrogeological model of the weathered crystalline-basement aquifer in Africa [1]

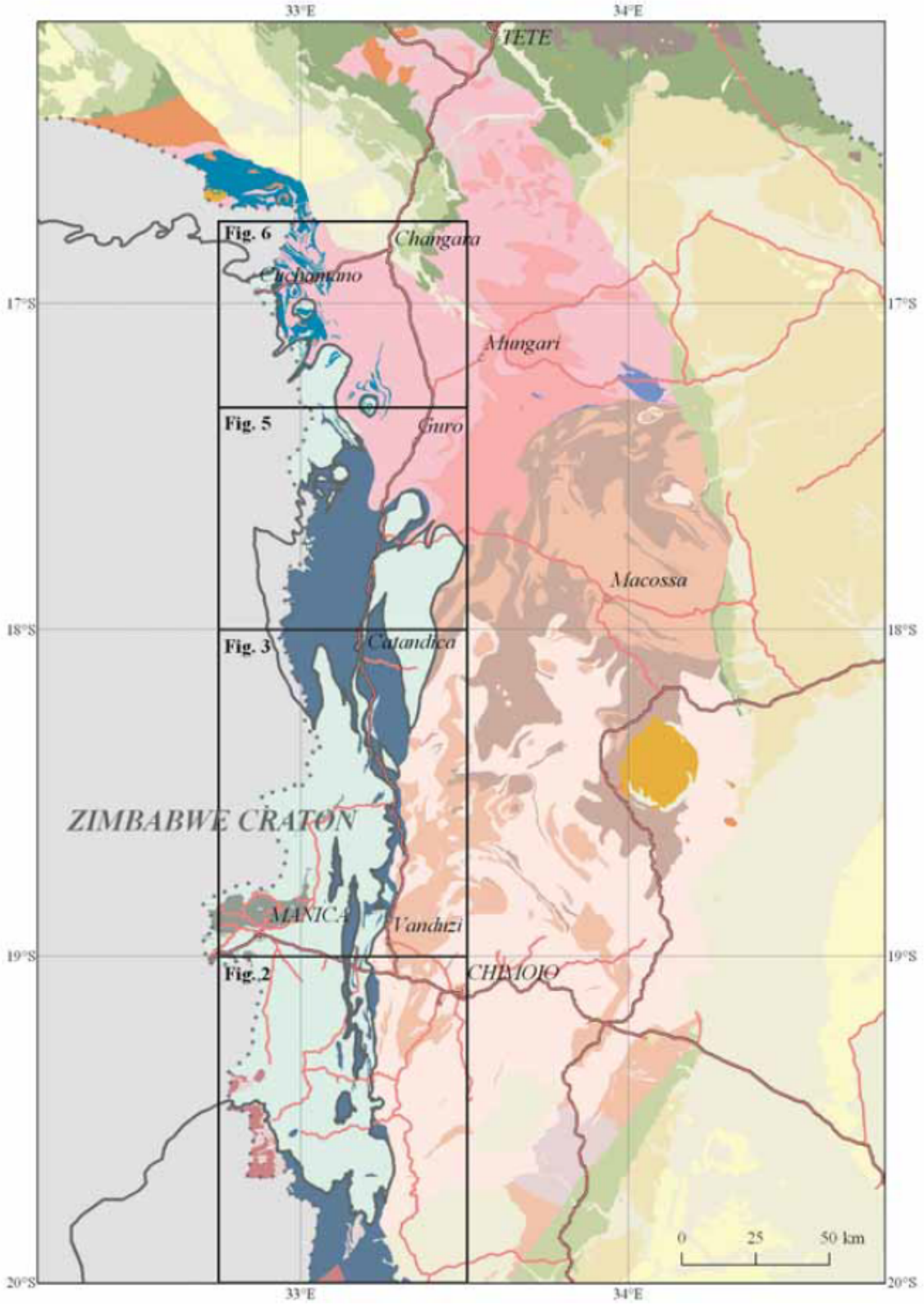

Figure B.4: The eastern margin of the Archaean Zimbabwe Craton with in blue the extends of the Gairezi Sedimentary Group (as plotted in the boxes of Figs 2,3 and 5). The heavy line, partly in Zimbabwe (Geological map of Zimbabwe 1: 1000 000, 1985) marks the boundary of the exposed Archaean. Right of the boundary the Barue Compex is located. Inlays refers to Figs 2, 3, 5 and 6 in the original paper [2], from which Figs 2 and 3 are used as background for Fig. 2.2

C

Precipitation, Evaporation and Temperature

C.1. Climatological data from FAO

This data is derived from the free online available databases of FAO New_LocClim 1.10 [33]. The tables are consulted at July 30th, 2015. The measurements originate from Manica's weather station. This city is situated about 30km west from the catchment. It is unclear if there are any orographic effects available in this station. Therefore, this data should only be considered as reference data.

Data presented in Tables C.1, C.6, C.3, C.4 and C.5 are also stored in the database "Measurements.accdb" table "FAO_new_LocClim" as monthly timeseries from January 1st, 2009 to December 1th, 2014. For P and E_p the 'best estimates' are selected.

C.2. Precipitation

Measurements are performed at different locations during different periods, see Table 2.1 and C.2. Some additional observations are made:

- There is a clear distinction between dry and wet seasons (Fig. C.3a)
- de Boer [8] mentions that the winter in 2012 was 'exceptionally dry' with no rain events between. However, between April 27th to September 6th, 2012 not one event is recorded. Hence, we believe that during this period no precipitation measurements have been performed, since normally about 54mm is expected. This results in a underestimation of the water balance. However, the total effect is unclear.
- There seems to be an altitude effect in the precipitation, cumulatives from David's place at a elevation of 878m+AD show higher rain totals than other lower located measurements points (Fig. C.3b and Eq. C.3).
- Rainfall is measured on daily basis. Every morning at 8 am, covering the total precipitation of the last 24 hours. However, it is very likely that the bulk of rain occur within 3 hours.

C.2.1. Measurements

Figure C.3a shows the integrated precipitation as measured at the individual raingauges. These daily rain depth observations are extended over different periods. Sometimes the measurements stopped for a (short) period. Table 2.1 gives an overview of the measurement locations, the periods and altitude of the locations.

Since the raingauge at David's place is the longest ánd most complete one, we compared the integrated precipitation amount with the other raingauges. See Figure C.3b. Some observations:

- Double mass curves gives a decent insight in mutual biases. Observe a structural deviation between the mass curve of David's raingauge compared to the one of Chimoio and Alberto. This could be caused by an orographic or altitude effect.

Figure C.1: Raingauge installed at Chimoio' place

Figure C.2: Raingauge and tipping bucket installed at the top of the Inselberg

Prec	**Best Estimate** [mm]	**Low Estimate** [mm]	**High Estimate** [mm]	**Standard Error** [mm]	**Bias** [mm]
January	230	168.04	291.96	61.96	-6
February	182	138.17	225.83	43.83	0.33
March	136	92.12	179.88	43.88	-3.11
April	49	32.62	65.38	16.38	-2
May	19	8.65	29.35	10.35	-0.78
June	13	2.35	23.65	10.65	-0.67
July	9	0.69	17.31	8.31	-0.67
August	13	3.21	22.79	9.79	-1.11
September	16	9.17	22.83	6.83	1
October	34	19.37	48.63	14.63	-1.56
November	103	74.29	131.71	28.71	-4.11
December	210	165.26	254.74	44.74	-2.11
Total	**1014**	**713.94**	**1314.06**		
Mean	**84.5**	**59.5**	**109.5**	**25**	**-1.73**

Table C.1: FAO Long term precipitation averages measured at Manica's weather station FAO [33]

- Chimoio and Alberto stopped measuring for a certain period.
- There are several gaps in the data, these are represented by horizontal lines in the graph. These unmeasured periods can be found by comparing Figure C.3a and Figure C.3b. Roughly the x-axis can be divided in 6 domains representing 6 periods.

1. $P_{David} \in [0,750]$: Oct 2011 – Mar 2012. Only measured by David
2. $P_{David} \in [750,1000]$: Mar 2012 - May 2012. Measured by David, Chimoio and Alberto.

   From May 2012 until Sept 2012. Nobody measured rainfall.
3. $P_{David} \in [1000,1150]$: Sept 2012 – Dec 2012. Only measured by David
4. $P_{David} \in [1150,2500]$: Dec 2012 – Jun 2013. Measured by David, Chimoio and Alberto. And the last months at Caritas also.
5. $P_{David} \in [2500,4100]$: Jun 2013 – Apr 2014. Only Measured by David.
6. $P_{David} \in [4100,4350]$: Apr 2014 – Jul 2014. Measured at 5 locations.

Year Month	Alberto ca.650m+AD	Caritas Messica ca 650m+AD	Chimoio 730m+AD	David 878m+AD	Inselberg 1348m+AD
2010					
Sep				44	
Oct				48	
Nov				121	
Dec				156	
Total 2010				**369**	
2011					
Jan				514	
Feb				266	
Mar				161	
Apr				93.5	
May				68.5	
Jun				11.2	
Jul				26	
Aug				36	
Sep				19	
Oct				133	
Nov				123	
Dec				286	
Total 2011				**1737.2**	
2012					
Jan				99	
Feb				95	
Mar	146		129	191	
Apr	54		43	81	
May				0 *	
Jun				0 *	
Jul				0 *	
Aug				0 *	
Sep				44	
Oct				48	
Nov	75		77	121	
Dec	99		81	156	
Total 2012	**374**		**330**	**835**	
2013					
Jan	459		479	514	**
Feb	252		261	266	**
Mar	134		137	161	**
Apr	83	17	94	93.5	**
May	45	66.6	42	68.5	**
Jun	7	1.6	5	11.2	**
Jul		20.3		26	**
Aug		5.4		36	**
Sep				12	
Oct				100.1	
Nov				96	
Dec				350	
Total 2013	**980**	**110.9**	**1018**	**1734.3**	
2014					
Jan				456	
Feb				390	
Mar		8		152.5	
Apr		66.3	130.2	189.9	
May	4	4.5	5	20	19
Jun	12	0	14	24	18
Jul	0	0	0	0	0
Total 2014	**16**	**78.8**	**149.2**	**1232.4**	**37**

Table C.2: Monthly precipitation volumes obtained at the different stations.
* We believe that this period no rainfall measurements are performed at Davids place
** Measurements done by Weemstra *et al.* [7] are not used in this study

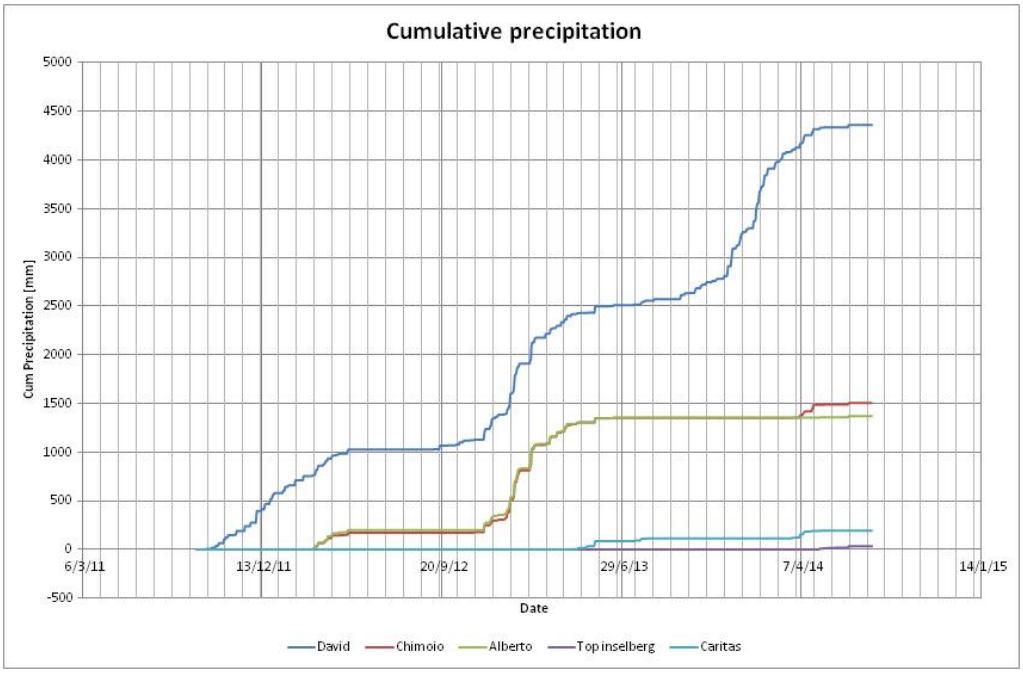

(a) Integrated precipitation over the whole measurement period for several rain gauges

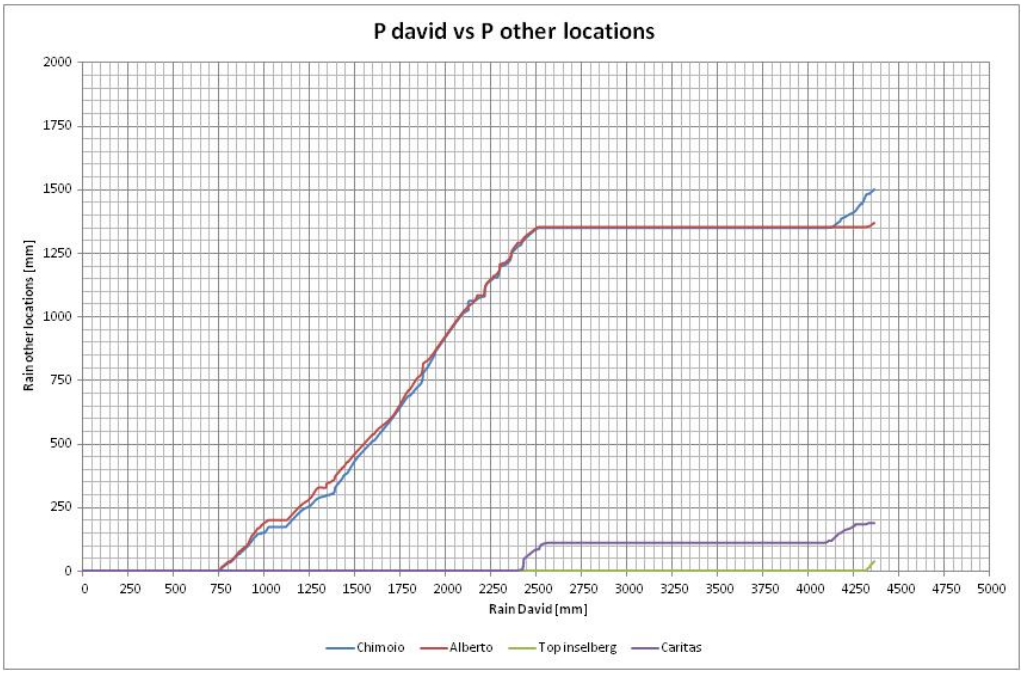

(b) Double mass curve plotting David's raingauge 848 m+AD (x-axis) versus the other raingauges

Figure C.3: Integrated plots of precipitation over the whole period

C.2.2. ALTITUDE EFFECT

One can also observe from Figure C.3b a elevation precipitation gradient. Between the stations Alberto, Chimoio and David. From this chart, a first estimation is made based on the direction coefficient of the line from coordinate (750,0) to coordinate (2500,1350):

$$\frac{\Delta P_{Chimoio}}{\Delta P_{David}} \approx \frac{\Delta P_{Alberto}}{\Delta P_{David}} \approx \frac{1350-0}{2500-750} = \frac{1350}{1750} = 0.77 \tag{C.1}$$

Taking into account that between points (1000,225) and (1150,225) measurements only occurred at David's place, we find:

$$\frac{\Delta P_{Chimoio}}{\Delta P_{David}} \approx \frac{\Delta P_{Alberto}}{\Delta P_{David}} \approx \frac{1350-0}{2500-750-150} = \frac{1350}{1600} = 0.84 \tag{C.2}$$

Meaning that there is structurally 16%(= 1−0.84) more rain at David's place then at Chimoio's and Alberto's place. We can generalize this deviation. Assuming that (at least) at daily scale precipitation events occurs catchment wide and that this relation applies on every single precipitation event. Plus that the increase and decrease of the volumes is linear with the elevation change, we come up with this simple relation:

$$P(h,t) = \left(1 - \frac{h_{David} - h}{h_{David} - h_{Chimoio}} * 0.16\right) P_{David}(t) = \left(1 - \frac{878-h}{878-730} * 0.16\right) P_{David}(t) \tag{C.3}$$

There are too few measurements available from Caritas and the inselberg to derive a similar relation for these points.

Two important notes to make. First, we used the elevation of $P_{Chimoio}$ to correct for the alititude effect, whereas we state that $P_{Alberto} \approx P_{Chimoio}$, however its elevation is ca. 650m+AD[1], taking the average between both locations, will alter 730 in $\frac{730+650}{2} = 690$ and therefore make the altitude correction less pronounced.

Secondly, it is possible that the increased precipitation amount is more dependent on the distance away from the ridge of the mountain, than the altitude, which might imply that there is not such a strong altitude relation, but more a horizontal distance relation. However, we do not have enough points to support or reject this assumption.

C.2.3. EXTEND PRECIPITATION TIME SERIES

The first rainfall measurements in the Messica catchment are performed by David and start in October 2011. For the rainfall runoff model, we need a warming-up period. Therefore we extend the precipitation time series by pasting measured precipitation between October 2012 until October 2013 before October 2011, in order to achieve a serie from October 2010 to August 2014.

C.3. TEMPERATURE

Within the catchment we recorded temperatures with barometric pressure divers. The daily averages are applied to calculate the potential evaporation with Hamon [34]. The long term observations done by FAO[33] are presented in Tables C.4 to C.5.

C.4. EVAPORATION

Table C.6 show the long term potential evaporation for the city of Manica as estimated by FAO using the Penman-Monteith equation.

Within this study no (potential) evaporation measurements have been performed. Weemstra *et al.* [7] did, but due to the very short character of these measurements, we have not implied this in this study.

We chose to use the potential evaporation as calculated with the Hamon equation [34]. This simple equation only need the latitudinal position of the catchment and daily averaged (air) temperatures. Since the result underestimates the potential evaporation according to FAO [33], we (visually) scaled[2] Hamons equation to match the FAO, see Eq. C.4.

$$E_{p;scaled} = 1.15 * (E_{Hamon} + 0.8) \tag{C.4}$$

[1] We do not have an exact altitude of Alberto's house. Only a estimate from the DEM [35], whereas other altitude information is derived with a hand held GPS.

[2] python script used: "Climate comparison, Hargreaves, Hamon, FAO.py"

T_Mean	Best Estimate [°C]	Low Estimate [°C]	High Estimate [°C]	Standard Error [°C]	Bias [°C]
January	24.2	21.74	26.66	2.46	-0.17
February	24.2	21.74	26.66	2.46	-0.23
March	23.2	20.92	25.48	2.28	-0.22
April	21.5	19.13	23.87	2.37	-0.1
May	18.7	16.59	20.81	2.11	-0.1
June	17	14.71	19.29	2.29	-0.19
July	15.8	13.63	17.97	2.17	-0.07
August	18	15.57	20.43	2.43	-0.16
September	20.2	17.97	22.43	2.23	-0.06
October	23.2	20.91	25.49	2.29	-0.12
November	24.1	21.49	26.71	2.61	-0.21
December	24	21.45	26.55	2.55	-0.16
Mean	21.18	18.82	23.53	2.36	-0.15

Table C.3: FAO Long term mean temperature measured at Manica's weather station FAO [33]

T_Max	Best Estimate [°C]	Low Estimate [°C]	High Estimate [°C]	Standard Error [°C]	Bias [°C]
January	30	27.62	32.38	2.38	-0.11
February	30	27.85	32.15	2.15	-0.18
March	29.2	27	31.4	2.2	-0.38
April	28.2	25.89	30.51	2.31	-0.02
May	26.6	24.19	29.01	2.41	-0.28
June	24.6	22.18	27.02	2.42	-0.48
July	24.3	21.87	26.73	2.43	-0.53
August	26.7	24.26	29.14	2.44	-0.38
September	28.6	26.04	31.16	2.56	-0.63
October	30.8	28.59	33.01	2.21	-0.09
November	30.7	28.13	33.27	2.57	-0.13
December	30.2	27.74	32.66	2.46	0.1
Mean	28.33	25.95	30.7	2.38	-0.26

Table C.4: FAO Long term maximum temperature averages measured at Manica's weather station FAO [33]

T_Min	Best Estimate [°C]	Low Estimate [°C]	High Estimate [°C]	Standard Error [°C]	Bias [°C]
January	18.3	16.92	19.68	1.38	-0.27
February	18.5	17.09	19.91	1.41	-0.18
March	17.1	15.73	18.47	1.37	-0.09
April	14.6	13.29	15.91	1.31	0.19
May	11	10.09	11.91	0.91	0.13
June	9.5	8.29	10.71	1.21	0.2
July	7.3	5.89	8.71	1.41	0.47
August	9.1	7.73	10.47	1.37	0.39
September	12	10.47	13.53	1.53	0.18
October	15.6	14.46	16.74	1.14	-0.02
November	17.3	15.98	18.62	1.32	-0.14
December	17.7	16.4	19	1.3	-0.18
Mean	14	12.69	15.31	1.31	0.06

Table C.5: FAO Long term minimum temperature averages measured at Manica's weather station FAO [33]

Other methods to calculate potential evaporation asked more information which was not available. Therefore we did eventually not apply these methods.

PET	Best Estimate [mm]	Low Estimate [mm]	High Estimate [mm]	Standard Error [mm]	Bias [mm]
January	129.4	114.67	144.13	14.73	-1.06
February	115.8	99.46	132.14	16.34	-1.41
March	117.8	104.91	130.69	12.89	-2.82
April	94.9	84.54	105.26	10.36	-2.67
May	80.3	74.51	86.09	5.79	-2.04
June	62.5	58.46	66.54	4.04	-1.67
July	63.4	58.31	68.49	5.09	-1.92
August	84.3	76.64	91.96	7.66	-3.14
September	106.5	93.55	119.45	12.95	-4.09
October	137.4	120.47	154.33	16.93	-3.38
November	130.9	117.34	144.46	13.56	-1.84
December	129	116.03	141.97	12.97	-0.22
Total	**1252.2**	**1118.89**	**1385.51**		
Mean	**104.35**	**93.24**	**115.46**	**11.11**	**-2.19**

Table C.6: FAO Long term potential evaporation averages measured at Manica's weather station FAO [33]

C.4.1. EXTEND EVAPORATION TIME SERIES

The potential evaporation time serie runs from October 23th, 2012 to July 21th, 2014, since in this period barometric pressure divers with internal temperature sensors have been installed. In order to extend the period to January 1th, 2008 (to at least cover the same period as precipitation) we used observed data in later years:

- from 1-1-2010 to 22-10-2012 is filled with data derived between 1-1-2013 and 1-1-2014.
- from 1-1-2009 to 1-3-2009 is filled with data derived between 1-1-2013 and 1-3-2013.
- from 1-3-3009 to 1-1-2010 is filled with data from 1-3-2012 to 1-1-2013.
- from 1-1-2008 to 1-10-2008 is filled with data from 1-1-2012 and 1-10-2012.
- from 1-10-2008 to 1-1-2009 is filled with data derived between 1-10-2013 to 1-1-2014.

Year month	Hamon_+08_x1.15	Hargreaves*	Hamon [34]	FAO [33]
2008	1512.219193			1467.709677
2009	1527.114047			1448.290323
2010	1507.08211			1463
2011	1507.08211			1463
2012				
Jan	156.9229672			146
Feb	140.7443227			116
Mar	133.6949803			130
Apr	110.0150179			111
May	95.93074656			99
Jun	85.24335876			84
Jul	90.53562367			87
Aug	109.2583289			109
Sep	129.8360944			132
Oct	148.3385123	18.23633257	39.95132365	158
Nov	160.8472102	54.30332382	115.8671393	141
Dec	170.8839678	177.2433792	123.7947546	140
Total 2012	**1532.251131**	**249.7830356**	**279.6132175**	**1453**
2013				
Jan	156.9229672	164.8496515	111.6547541	146
Feb	136.0876369	170.6413741	95.93707557	126
Mar	134.3215931	182.7799124	92.00138526	130
Apr	110.5303529	161.2615743	72.11335031	111
May	96.56454121	151.5479071	59.16916627	99
Jun	85.20139065	115.7638806	50.08816578	84
Jul	90.30902232	130.3331652	53.72958462	87
Aug	108.5266425	196.8508282	69.57099349	109
Sep	129.8267196	219.1924401	88.89279968	132
Oct	143.8707289	217.9997364	100.3049816	158
Nov	157.7718595	215.3193839	113.1929213	141
Dec	157.1486552	187.3127508	111.8510045	140
Total 2013	**1507.08211**	**2113.852605**	**1018.506183**	**1463**
2014				
Jan	151.3311739	154.0875097	106.7923251	146
Feb	128.8921499	102.6996063	89.68013034	126
Mar	130.7736634	129.6054276	88.91622904	130
Apr	105.7872871	89.89620798	67.98894528	111
May	102.4039122	67.03415957	64.24688017	99
Jun	84.0152526	77.60107645	49.0567414	84
Jul	58.55461331	61.77129753	34.11705505	87
Aug				109
Sep				132
Oct				158
Nov				141
Dec				140
Total 2014	**761.7580524**	**682.6952851**	**500.7983064**	**1463**

Table C.7: Derived monthly potential evaporation volumes [mm/area] for period October 23th, 2012 to July 21th, 2014. The Hamon_+08_x1.15 is applied in the models

* The potential evaporation calculated with Hargreaves is not further applied in this study, since daily min and max temperature values proved to significantly influence the outcomes and the min max observations were not very reliable.

D

SALT DILUTION MEASUREMENTS

D.1. INTRODUCTION

This appendix elaborates on the calibration of the EC-meter (electrical conductivity meter) **type ...** as conducted at the Water Laboratory of Delft University of Technology. Goal was to find a proper relation between TDS (Total Dissolved Solids) and EC values. The EC-meter has a non-linear relation between the EC value and TDS. We experienced this already in the field, and the phenomenon is also described by Walton [49]. Furthermore, the internal clock / timer of the meter has a strong deviation, the recording timestep appeared to be 3.5s instead of 3.0s as suggested by the manual.

This appendix shows that the following formulas should be applied to derive the river discharge from the performed bucket salt dilution measurements.

$$Q = \frac{\left(\phi_s - \phi_0\right) V_s}{\Delta t \sum_{n=1}^{N} \phi_n - \phi_0} \tag{D.1}$$

$$\phi(t) = \begin{cases} 0.5EC(t) & ,EC \in [0.015, 1.5] \\ 0.0096EC(t)^2 + 0.4969EC(t) + 3.4228 & ,EC \in (1.5, 167.] \end{cases} \tag{D.2}$$

Where $\phi(t)$ is the salt concentration in kg/m^3, ϕ_n measured at time step n, ϕ_0 the background and ϕ_s the salt concentration of the sample. Δt the length of the time step $[s]$, Q the river discharge in m^3/s, V_s the volume of the sample in m^3 and EC the measured electrical conductivity obtained by the EC-meter in $[mS/cm]$.

D.1.1. APPLICATION OF THE EC METER

This meter is used during the fieldwork campaign in Mozambique. More specific, it is used to measure the breakthrough curve of salt dilution measurements in order to determine the discharge of the river at a certain point. The measurements are performed by dissolving an unknown mass of salt (NaCl) into a bucket of river water with a known volume. After measuring the EC value of this sample, it is thrown into the water. We made sure it mixes over the entire cross-section and measure the electrical conductivity more than 10 river widths downstream of the input point. Next to this, we used the meter to measure the background conductivity as one single point measurement.

D.2. DERIVATION OF EQUATIONS

The discharge of the river can be measured with the salt dilution measurements. In general, a mass balance is conservative, meaning that no mass will disappear nor appear. In order to calculate the discharge here, we do the following assumptions:

- river discharge is constant during the measurements and so is the background EC caused by dissolved minerals/ solids concentration (TDS);
- the relation between the measured EC value and the salt concentration is unique and can be derived;

- the measured breakthrough curve, the surplus over the background conductivity, is caused by the added salt concentration, and so an unique relation between salt concentration and background conductivity can be applied on the measurements;
- the salt dilution is completely mixed over the whole cross sectional area (meaning there is no preferential flow path conveying all the salt nor stagnant pools where salt is trapped and, being so, disturbing the measurement). To ensure a proper mixing, we maintain a minimum distance of 10 times the river width between the input and measurement place.

The change of salt mass in the system can be described as follows

$$\begin{cases} \frac{\mathrm{d}M(t)}{\mathrm{d}t} = -Q(t)\phi(t) + Q(t)\phi_0(t) \\ M(t_0) = V_s(\phi_s - \phi_0) \end{cases} \tag{D.3}$$

Where $\phi(t)$ is the salt concentration in kg/m^3, $\phi(t)_0$ the background concentration and ϕ_s the salt concentration of the sample. $Q(t)$ the river discharge in m^3/s leaving the system. V_s the volume of the sample in m^3 and $\frac{\mathrm{d}M(t)}{\mathrm{d}t}$ the change of total salt mass in the system.
Multiplying the system D.3 with -1 to change the coördinate system in order to calculate the change of salt mass passing the measurement place and integrating the system leads to

$$-\mathrm{d}M = Q(t)\left(\phi(t) - \phi_0(t)\right)\mathrm{d}t \tag{D.4}$$

$$\int_{t_0}^{t} -\mathrm{d}M = \int_{t_0}^{t} Q(\tau)\left(\phi(\tau) - \phi_0(\tau)\right)\mathrm{d}\tau \tag{D.5}$$

if M is continuous and smooth and Q and ϕ_0 are constant, we can simplify. After using the boundary condition of eq D.3

$$V_s(\phi_s - \phi_0) = Q\int_{t_0}^{t}\left(\phi(\tau) - \phi_0\right)\mathrm{d}\tau \tag{D.6}$$

Taking into account that the measurements are not continuous but discrete with a timestep Δt we replace the integral with an approximation by a summation over the number of measured timesteps N. So, only from the mass balance we can derive Q

$$Q = \frac{\left(\phi_s - \phi_0\right)V_s}{\Delta t\sum_{n=1}^{N}\phi_n - \phi_0} \tag{D.7}$$

In order to calculate Q we need to know the consecutive relation for ϕ. We assume that there is an unique relation between the measured electrical conductivity EC and the salt concentration ϕ, so $\phi = f(EC)$ with $EC \in [0, \rightarrow)$.

In earlier studies [i.e. Weemstra *et al.* [7]] this relation is hold to be linear [1] over the whole domain without making difference between EC of salt and EC of TDS in water, if so, we can write $EC = f^{-1}(\phi)$ and solve the discharge Q by solving the EC balance. Note that the linear properties of the function: $f(ax + bx) = af(x) + bf(x)$ and that a sum over N steps is linear as well. So (only) in this case, we do not need to know the exact relation between EC and ϕ.

$$f^{-1}(Q) = f^{-1}\left(\frac{\left(\phi_s - \phi_0\right)V_s}{\Delta t\sum_{n=1}^{N}\phi_n - \phi_0}\right) \tag{D.8}$$

$$Q = \frac{\left(EC_s - EC_0\right)V_s}{\Delta t\sum_{n=1}^{N}EC_n - EC_0} \tag{D.9}$$

However, once the relation $\phi = f(EC)$ is not linear, one cannot solve a EC balance anymore, but need to calculate the salt / TDS concentration. In the field we already observed non-linearity in this $EC - \phi$ relation. This is further investigated in laboratory.

[1] which might be assumed, since he diluted the original sample 10 times with untreated river water, and doing so, entered the linear domain. By taking the river's background EC into account, and assuming a linear relation between sodium chloride and EC values, the original EC value can be determined.

Another short remark about eq D.7 involves the timestep Δt. The device measures an instantaneous value $3s$ according to the manual. However in practice this Δt value appears to be approximately $3.5s$, which causes an underestimation of 17% to the final result.

D.3. LABORATORY CALIBRATION EC METER

Since the used EC meter in the field responded strongly non-linear when doubling the salt mass in mineral water (with $EC \approx 30-35\mu S$) multiple times up to maximum concentrations we used for the salt dilution samples, the urge for calibration was demonstrated. This paragraph therefore describes the laboratory results.

D.3.1. CALIBRATING ON SALT CONCENTRATION SAMPLES

For the calibration 7 samples are used, see TableD.1. Sample #1 concerns de-mineralized water, for which we assume that $EC = 0\mu S/cm$ by definition, while #2 is a standard sample of $1413\mu S/cm$ at 25^oC. Samples #3 to #7 are made in laboratory for this calibration specifically. Therefore, pure NatriumChloride (NaCl) (also called SodiumChloride) is dissolved into de-mineralized water. The concentrations and related EC values at a temperature of 20^oC are based on CRC Handbook of Chemistry and Physics, Section D252-253 Table 71 SodiumChloride, Weal et al (1975-1976) [50].
The EC values are temperature dependent. The higher the temperature the higher the electrical conductivity. EC-meters correct for temperature dependency and express EC values at a temperature T of 25^oC according to Eq. D.10. This is a linear approximation of temperature dependency and is rather accurate for at least the domain $T \in [20,26]$. The device's k factor is unknown, but we assume the device's correction to be accurate enough within normal water temperature ranges. That is, not introducing significant deviations from the 'truth'.
Since the CRC Handbook of Chemistry [50] expresses the EC values at a temperature of 20^oC and the EC-meters convert the measured EC values to EC_{25^oC}, an inequality is introduced. Therefore, we derived the k-factor of eq. D.10 based on the standard sample of $EC = 1413\mu S/cm$. The EC values at given temperatures are tabulated, see Table D.2. To calculate EC_{25^oC} based on EC_{20^oC} we apply eq D.11 on this data, resulting in $\tilde{k} = 2.113$. This relation is used to calculate the EC_{25^oC} of the samples in Table D.1. For this we assume that the relation is independent of the salt concentration.

$$EC_{25^oC} = EC(T)k(T - 25^oC) \tag{D.10}$$

$$EC_{25^oC} = EC_{20^oC}(1 + \tilde{k}(T - 20^oC) \tag{D.11}$$

Sample #	Theoretical NaCl concentration [g/L]	EC_{20^oC} theoretical [mS/cm]	Volume sample [L]	Added Mass NaCl [g/200ml]	Real NaCl concentration [g/L]	EC_{25^oC} calculated [mS/cm]	Ratio conc / EC_{25^oC} [−]	Remarks
1	0	0	0.200	0	0	0.000		de-mineralised water
2			0.200			1.413		standard sample
3	1.0	1.7	0.200	0.2061	1.0	1.880	0.53	sample made in laboratory
4	11.1	17.5	0.200	2.233	11.2	19.349	0.57	sample made in laboratory
5	41.1	57.3	0.200	8.223	41.1	63.354	0.65	sample made in laboratory
6	80.0	101.	0.200	16.04	80.2	111.671	0.72	sample made in laboratory
7	160.2	167.	0.200	32.06	160.3	184.644	0.87	sample made in laboratory

Table D.1: Salt concentration Samples for calibration EC-meters
EC_{20^oC} based on CRC Handbook of Chemistry [50], EC_{25^oC} calculated on theoretical concentration NaCl and the sample volume includes NaCl

Note that the non-linearity of the relation $\phi = f(EC)$ is already proven when dividing theoretical salt concentration by the calculated EC_{25^oC} in Table D.1.

D.3.2. EC METERS USED

The samples in Table D.1 have been measured with three different EC-meters, in order to exclude errors in the samples.

- ECM_{Field}: This meter is used for field measurements before laboratorium calibration
- ECM_{WB}: This is ECM_{Field} the after calibration. This meter is not further applied in this thesis

Temperature [^oC]	EC standard sample [$\mu S/cm$]	EC approximated [$\mu S/cm$]
20	1278	1278
21	1305	1305.004
22	1332	1332.008
23	1359	1359.012
24	1386	1386.017
25	1413	1413.021
26	1440	1440.025

Table D.2: Temperature dependency of EC-values standard sample $1413 \mu S/cm$

- ECM_{TUD}: EC-meter of Technical University of Delft. This meter is used only for the River Revue, which is excluded in the scope of this research.
- ECM_{Lab}: EC meter TetraCon©325 from WTW owned by Technical University of Delft. This is a laboratory EC meter which was just calibrated.

D.3.3. RESULTS EC METERS

Table D.3 presents the measured EC values per meter per sample. The fact that ECM_{Lab}'s measurements are very close to the calculated EC values of the samples, gives extra support for the reliability of the observations. Sample #3 is approximated badly by all EC-meters, this might indicate a faulty sample.
From Table D.3 we also observe that ECM_{TUD} approximates the sample EC's rather well. More interesting is ECM_{Field}'s large underestimation, even after calibration (ECM_{WB}).

	EC_{Sample}		ECM_{Lab}		ECM_{TUD}		ECM_{Field}		ECM_{WB}	
Sample #	[NaCl] [g/l]	EC_{25^oC} [mS/cm]	T [^oC]	EC_{25^oC} [mS/cm]	T [^oC]	EC_{25^oC} [mS/cm]	T [^oC]	EC_{25^oC} [mS/cm]	T [^oC]	EC_{25^oC} [mS/cm]
1	0	0.000		0		0.0076		0		0.0056
2		1.413	25.6	1.416	25.1	1.388	24.7	1.382	25	1.413
3	1.0	1.880	25.9	2.5	25.5	2.190	25.6	2.249	24.7	2.032
4	11.1	19.349	26.0	19.86	25.9	18.44	25.8	14.46	25	14.23
5	41.1	63.354	25.8	64.60	25.8	59.20	25.8	32.46	25	35.27
6	80.0	111.671	25.7	113.9	25.3	104.6	25.6	73.17	25	76.60
7	160.2	184.644	25.8	190.6	25.7	174.9	25.4	102.9	24.8	111.6

Table D.3: Temperature corrected EC Values and real temperatures measured by different EC-meters for samples #1 to #7 of Table D.1

For each EC-meter we derived a linear $\phi(EC) = aEC + b$ and a second order polynomial relation $\phi(EC) = aEC^2 + bEC + c$ with EC in $[mS/cm]$. The coefficients are determined with Microsoft Excel 2013, which most likely applies a least square error approximation. Furthermore we (only) force the linear trend line to fulfill $EC = 0 \rightarrow \phi = 0$. The latter is necessary since, because if a linear approximation holds for $\phi = f(EC)$ then the order of magnitude of the coefficient should be similar to coefficients found in literature.

The found formulas read

$$\text{ECM}_{Field} \begin{cases} \phi = 1.3865EC & R^2 = 0.9484 \\ \phi = 0.0096EC^2 + 0.4969EC + 3.4228 & R^2 = 0.983 \end{cases} \tag{D.12}$$

$$\text{ECM}_{WB} \begin{cases} \phi = 1.2969EC & R^2 = 0.9589 \\ \phi = 0.0074EC^2 + 0.5597EC + 2.7425 & R^2 = 0.9889 \end{cases} \tag{D.13}$$

$$\text{ECM}_{Lab} \begin{cases} \phi = 0.7901EC & R^2 = 0.9814 \\ \phi = 0.0017EC^2 + 0.5169EC + 0.0677 & R^2 = 0.9999 \end{cases} \tag{D.14}$$

$$\text{ECM}_{TUD} \begin{cases} \phi = 0.8609EC & R^2 = 0.9813 \\ \phi = 0.002EC^2 + 0.561EC + 0.0638 & R^2 = 0.9999 \end{cases} \tag{D.15}$$

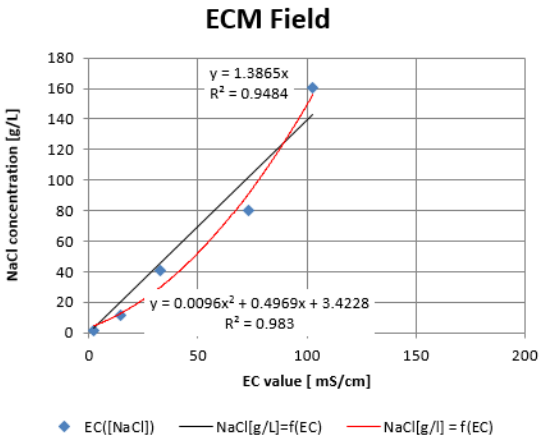

Figure D.1: Calibration $\phi = f(\text{ECM}_{Field})$

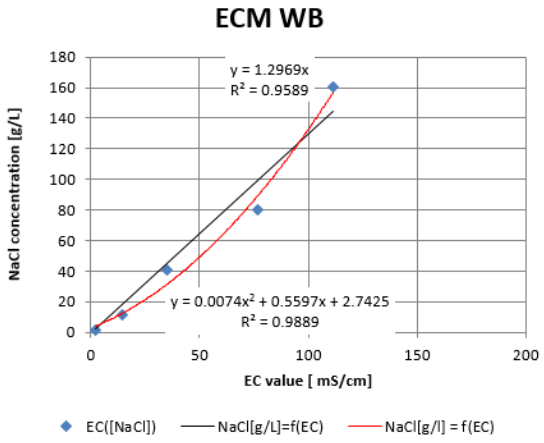

Figure D.2: Calibration $\phi = f(\text{ECM}_{WB})$

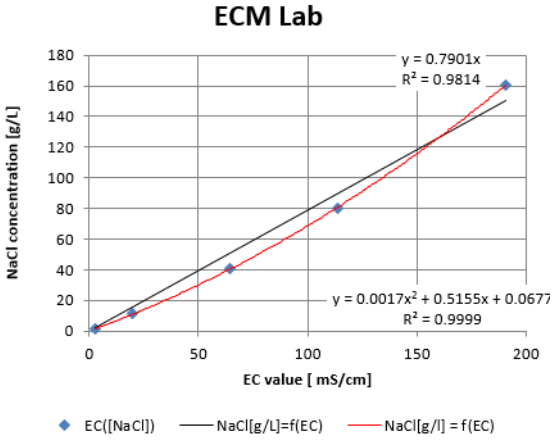

Figure D.3: Calibration $\phi = f(\text{ECM}_{Lab})$

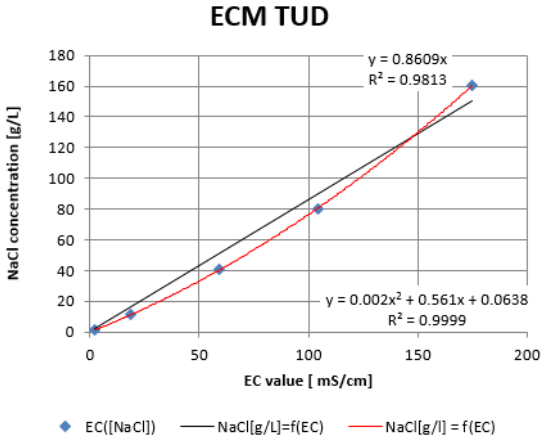

Figure D.4: Calibration $\phi = f(\text{ECM}_{TUD})$

D.3.4. COEFFICIENTS LITERATURE

Walton [49] researched the relationship between electrical conductivity and total dissolved solids. He concludes that there is no one linear approximation for $\phi = f(EC)\ \forall\ EC[mS/cm] \in [0.015, 150.]$, rather a piecewise linear approximation should be applied. Being so, the linearity assumption in Eq. D.9 in order to solve the EC balance instead of the salt mass balance, does not hold for piecewise linear functions.

Furthermore, Walton [49] give rise to the linear approximation

$$\phi = 0.5EC \quad \forall \quad EC[mS/cm] \in [0.015, 1.5] \tag{D.16}$$

This assumption is applied for the measurements.

D.3.5. LINEARITY EC METER

The EC meter ECM_{WB} shows a linear relation between ϕ and $EC\ \forall\ EC[mS/cm] \in [0.022, 1.402]$, according to a simple experiment. Therefore Eq. D.16 can be applied. Unfortunately, this test is not performed on every EC meter. However, it gives an indication for the most important meter's behavior.

For this experiment a standard sample of $1413\mu S/cm$ at 25^oC is used. We diluted the sample with demineralized water, and calculated and measured the conductivity for every step (Table D.4). For the calculated EC-values a linear behavior is assumed. Note that the influence of small volume errors increase for the higher sample numbers.

Sample [−]	Total volume [ml]	Volume standard sample [%]	Volume demi water [%]	Temperature sample [^oC]	EC_{25^oC} ECM_{WB} [$\mu S/cm$]	EC_{25^oC} calculated [$\mu S/cm$]	Ratio EC meas/calc [−]
1	19	100	0	21.8	1402	1413	0.99
2	38	50	50	22.0	689.7	706.5	0.98
3	21	25	75	22.3	368.2	353.3	1.04
4	42	12.5	87.5	22.5	165.3	176.6	0.94
5	28	6.25	93.75	22.6	82.65	88.3	0.94
6	56	3.125	96.875	22.5	46.01	44.2	1.04
7	32	1.5625	98.4375	22.3	23.22	22.1	1.05
8	40	0.78125	99.21875	22.2	13.89	11.0	1.26
9	80	0.390625	99.60938	22.2	7.94	5.5	1.44
10	20	0	100	23.1	0.57	0	-

Table D.4: Linearity test EC meter ECM_{WB} mixing standard sample with de-mineralized water

E

DIVERS

This Appendix describes the procedure to derive water depths at the measurement stations. We applied a device, location and temporal correction. All these corrections are relative to barometer Messica Downstream Station (Schlumberger P1312), since this is our main barometric measurement station.

Divers are used to derive water levels in the cross-section and waterdepths above construction crests. Therefore divers are installed as water pressure meters and as barometers, see tables E.1 and E.2 which gives respectively an overview of the applied divers and the locations where they have been installed and Fig. 2.6 for the locations of the divers. For every location, the cross-section bathymetry or construction dimensions together with the level of the water pressure device is measured with a water level instrument, see Appendix F.1 for cross-sections per location. Due to a shortage of divers not every location is equipped with a barometer. Therefore we transferred barometric pressures time series from the one to the other location, using a 'location correction'. To do so, we developed a measurement plan. Furthermore we discovered structural measurement errors between divers. We corrected for this with a so called 'device constant'.

Serie number device	Producer	Type	Owner	Remark
N01-25340 210	Schlumberger	TD-Diver=3	Wouter Beekman	Device didn't register pressures lower than 950 cm
.00-L7925 214	Schlumberger	Mini-Diver=14	TU Delft	
.00-L8009 214	Schlumberger	Mini-Diver=14	TU Delft	
.00-L8024 214	Schlumberger	Mini-Diver=14	TU Delft	
.00-P1312 214	Schlumberger	Mini-Diver=14	TU Delft	
N01-77479 210	Schlumberger	TD-Diver=3	Wouter Beekman	
N01-57308 210	Schlumberger	TD-Diver=3	Wouter Beekman	
.00-S2662 214	Schlumberger	Mini-Diver=14	TU Delft	
.00-L7899 214	Schlumberger	Mini-Diver=14	TU Delft	
unknown	Schlumberger	TD-Diver=3	Wouter Beekman	Broken

Table E.1: Metadata applied divers

E.1. DEVICE CONSTANT

The individual divers show (small) structural deviations between each other. We derived the deviation constant, the 'device constant', relative to our main barometer at Messica Downstream Station (P1312) and applied this device corrections to all time series. This device constant is derived from a 8-days during home journey. During this partly land, partly air journey, all divers recorded every 30 minutes at the same time the air pressure. Unfortunately, some divers stayed in Mozambique, so conclusions around these are based on shorter time series. Basic assumptions:

- Diver correction are time ánd altitude invariant; implying that the structural deviation or device constant is not time dependent nor elevation dependent (For some this can be argued, for example Revue_5).
- Due to randomness in measurements, average deviation represents device constant best.

Serienummer diver	Meetserie	Type Measurements	Date from	Date to	Time interval	Location	CrossSection	CrosssectionID	Altitude Garmin	Depth diver - refpoint
N01-57308 210	GodiDS_1	WaterPressure	12/08/2013 13:00	25/03/2014 15:00	01:00	Godi_10_1_ds_out	TRUE	Cross_Godi_ds_1	671.36	-1.668
N01-57308 210	GodiDS_2	WaterPressure	25/03/2014 16:00	07/04/2014 09:00	01:00	Godi_10_1_ds_out	TRUE	Cross_Godi_ds_1	671.36	-1.658
N01-57308 210	GodiDS_3	WaterPressure	07/04/2014 10:00	08/05/2014 16:00	01:00	Godi_10_1_ds_out	TRUE	Cross_Godi_ds_1	671.36	-1.658
N01-57308 210	GodiDS_4	WaterPressure	08/05/2014 17:00	24/05/2014 12:00	01:00	Godi_10_1_ds_out	TRUE	Cross_Godi_ds_1	671.36	-1.658
N01-57308 210	GodiDS_5	WaterPressure	24/05/2014 13:00	22/07/2014 10:00	01:00	Godi_10_1_ds_out	TRUE	Cross_Godi_ds_1	671.36	-1.658
N01-57308 210	GodiDS_6	Barometer	22/07/2014 11:00	23/07/2014 10:00	01:00		FALSE			
N01-25340 210	GodiDS_baro_1	Barometer	12/08/2013 13:00	25/03/2014 15:00	01:00	Godi_10_1_ds_out	FALSE		671.36	-1.058
N01-25340 210	GodiDS_baro_2	Barometer	25/03/2014 16:00	07/04/2014 09:00	01:00	Godi_10_1_ds_out	FALSE		671.36	-1.058
.00-L7925 214	GodiUS_1	WaterPressure	26/03/2014 17:00	08/05/2014 12:30	00:30	Godi_6	FALSE		805.7	-0.28
.00-L7925 214	GodiUS_2	WaterPressure	08/05/2014 13:00	07/06/2014 11:00	00:30	Godi_6	FALSE		805.7	-0.28
.00-L7925 214	GodiUS_3	WaterPressure	07/06/2014 11:30	21/07/2014 14:30	00:30	Godi_6	FALSE		805.7	-0.28
.00-L7925 214	GodiUS_4	WaterPressure	21/07/2014 15:00	30/07/2014 08:30	00:30		FALSE			
.00-L8009 214	GodiUS_baro_1	Barometer	08/05/2014 13:00	07/06/2014 11:00	00:30	Godi_6	FALSE		805.7	
.00-L8009 214	GodiUS_baro_2	Barometer	07/06/2014 11:30	21/07/2014 14:30	00:30	Godi_6	FALSE		805.7	
.00-L8009 214	GodiUS_baro_3	Barometer	21/07/2014 15:00	30/07/2014 08:30	00:30		FALSE			
.00-L8024 214	MessDS_1	WaterPressure	26/03/2014 11:00	07/04/2014 15:00	00:30	Messica_3_ds_out	FALSE		635.55	-0.736
.00-L8024 214	MessDS_2	WaterPressure	07/04/2014 15:30	21/04/2014 08:30	00:30	Messica_3_ds_out	FALSE		635.55	-0.696
.00-L8024 214	MessDS_3	WaterPressure	21/04/2014 09:00	05/06/2014 15:00	00:30	Messica_3_ds_out	FALSE		635.55	-1.04
.00-L8024 214	MessDS_4	WaterPressure	05/06/2014 15:30	23/07/2014 10:00	00:30	Messica_3_ds_out	FALSE		635.55	-1.04
.00-L8024 214	MessDS_5	Barometer	23/07/2014 10:30	30/07/2014 08:30	00:30		FALSE			
.00-P1312 214	MessDS_baro_1	Barometer	07/04/2014 17:00	21/04/2014 08:30	00:30	Messica_3_ds_out	FALSE		635.55	
.00-P1312 214	MessDS_baro_2	Barometer	21/04/2014 09:00	05/06/2014 14:30	00:30	Messica_3_ds_out	FALSE		635.55	
.00-P1312 214	MessDS_baro_3	Barometer	05/06/2014 15:00	23/07/2014 10:00	00:30	Messica_3_ds_out	FALSE		635.55	
.00-P1312 214	MessDS_baro_4	Barometer	23/07/2014 10:30	30/07/2014 08:30	00:30		FALSE			
.00-L8009 214	MessDS_baro_5	Barometer	07/04/2014 17:00	21/04/2014 08:30	00:30	Messica_3_ds_out	FALSE		635.55	
N01-77479 210	ChirDS_1	WaterPressure	12/08/2013 15:00	26/03/2014 12:00	01:00	Chir_7_ds_out	TRUE	Cross_Chir_ds_1	659.1	-0.681
N01-77479 210	ChirDS_2	WaterPressure	26/03/2014 13:00	07/04/2014 13:00	01:00	Chir_7_ds_out	TRUE	Cross_Chir_ds_1	659.1	-0.681
N01-77479 210	ChirDS_3	WaterPressure	07/04/2014 14:00	05/06/2014 12:00	01:00	Chir_7_ds_out	TRUE	Cross_Chir_ds_1	659.1	-0.681
N01-77479 210	ChirDS_4	WaterPressure	05/06/2014 13:00	22/07/2014 19:00	01:00	Chir_7_ds_out	TRUE	Cross_Chir_ds_2	659.1	-0.724
.00-L8009 214	ChirDS_baro_1	Barometer	25/03/2014 14:22	02/04/2014 12:37	00:05	Chir_7_ds_out	FALSE		659.1	
.00-L8009 214	ChirDS_baro_2	Barometer	02/04/2014 13:00	07/04/2014 13:30	00:30	Chir_7_ds_out	FALSE		659.1	
.00-S2662 214	MessUS_1	WaterPressure	26/03/2014 16:00	07/04/2014 12:00	00:30	Messica_1_us_in	TRUE	Cross_Mess_up_1	641.56	-1.346
.00-S2662 214	MessUS_2	WaterPressure	07/04/2014 12:30	05/06/2014 11:30	00:30	Messica_1_us_in	TRUE	Cross_Mess_up_1	641.56	-1.356
.00-S2662 214	MessUS_3	WaterPressure	05/06/2014 12:00	22/07/2014 09:00	00:30	Messica_1_us_in	TRUE	Cross_Mess_up_1	641.56	-1.356
.00-S2662 214	MessUS_4	Barometer	22/07/2014 09:30	23/07/2014 10:00	00:30		FALSE			
.00-S2662 214	MessUS_5	Barometer	23/07/2014 10:30	30/07/2014 08:30	00:30		FALSE			
.00-L8009 214	Revue_baro_1	Barometer	21/04/2014 14:00	06/05/2014 15:00	00:30	Revue_1	FALSE		641.8	
.00-L8009 214	Revue_baro_2	Barometer	06/05/2014 15:30	08/05/2014 12:30	00:30	Revue_1	FALSE		641.8	
.00-L7899 214	Revue_1	WaterPressure	27/03/2014 11:00	21/04/2014 12:30	00:30	Revue_1	TRUE	Cross_Revue_1	641.8	-0.858
.00-L7899 214	Revue_2	WaterPressure	21/04/2014 13:00	06/05/2014 15:00	00:30	Revue_1	TRUE	Cross_Revue_1	641.8	-0.858
.00-L7899 214	Revue_3	WaterPressure	06/05/2014 15:30	11/06/2014 12:30	00:30	Revue_1	TRUE	Cross_Revue_1	641.8	-0.858
.00-L7899 214	Revue_4	WaterPressure	11/06/2014 13:00	23/07/2014 10:00	00:30	Revue_1	TRUE	Cross_Revue_2	641.8	-1.424
.00-L7899 214	Revue_5	Barometer	23/07/2014 10:30	30/07/2014 08:30	00:30		FALSE			
.00-P1312 214	RuagaDS_1	WaterPressure	26/03/2014 14:30	07/04/2014 09:30	00:30	Ruaga_2	TRUE	Cross_Ruaga_1	650.69	
N01-25340 210	RuagaDS_2	WaterPressure	07/04/2014 11:00	05/06/2014 10:00	00:30	Ruaga_1_ds_out	TRUE	Cross_Ruaga_2	650.69	-0.795
N01-25340 210	RuagaDS_3	WaterPressure	05/06/2014 10:30	22/07/2014 10:00	00:30	Ruaga_1_ds_out	TRUE	Cross_Ruaga_2	644.2	-0.795
N01-25340 210	RuagaDS_4	Barometer	22/07/2014 10:30	23/07/2014 10:30	00:30		FALSE			

Table E.2: Divers and their specific measurement series. For more detail about applied device constants, see separate Excel Sheets. See database Measurements.accdb Table Diver_Metadata

Some small notes about Fig. E.1

- Diver Revue_5 (pink) shows in general a clear deviation ánd a time dependent device constant (Note measurement point Revue is not applied in this study). Observe its deviation at night from 22 to 23 July, which is disappeared after read out diver, but present again during night 24-25 July. We cannot draw any general conclusions about time dependency of this deviation with current information.
- RuagaDS_4 (green) shows the largest structural error. This diver acts as barometer from august 2013 to march 2014. Secondly, the diver appeared not to record any values lower than 950 Pa. This diver stayed in Mozambique.

Barometer Messica DS (Diver L8024) acts as reference diver. All deviations and locations constants are calculated relative to this diver. This diver is located at the most downstream location of our catchment, namely Messica DS, and was therefore considered to be the most important measurement station. We could not extend barometric pressure measurements, induced by Weemstra *et al.* [7], since the installed barometers were not functioning well:

- Baro Godi DS (series number unknown) has device constant of 12Pa and a unrealistic lower bound of 950Pa.
- Baro Chirodzo DS is broken between August 2013 and March 2014. The data on this diver is lost. Schlumberger Company was not able to recover the data from this diver.

Table E.3 gives the average deviation and standard deviation (STDEV) relative to barometer Messica downstreams. The average error is calculated by first subtracting both raw timeseries from each other and then taking the average and STDEV over the difference.

Divers L8009 and N01-25430 are corrected with the device constant and their barometric pressures are compared with diver P1312, the latter is the new permanent barometer at Messica downstream.

A new device constant for L8009 of 1.765 cm is found, see Table E.4. Since L8009 and P1312 have been measuring for about 2 weeks at the same spot at Messica downstream, they must have recorded the same barometric pressure, see Fig. E.4a. After these two weeks diver L8009 is subsequently located at four other

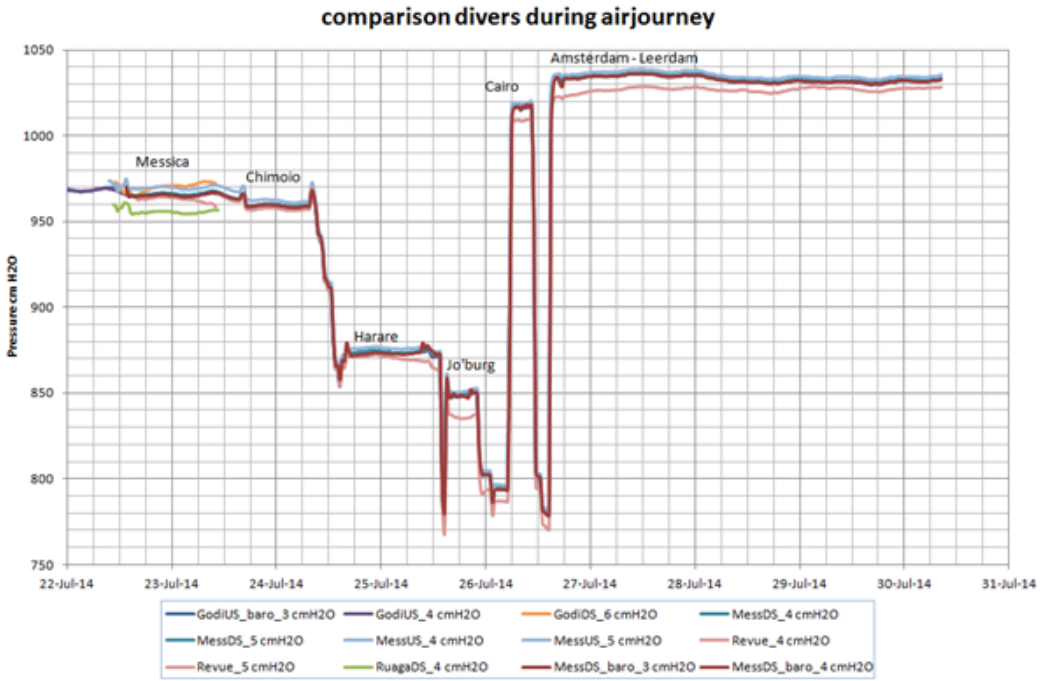

Figure E.1: Recorded barometric pressures from all 8 divers during a partly land – partly air journey: from Messica (Mozambique) to Chimoio (Mozambique) by land, from Chimoio to Harare (Zimbabwe) by land, from Harare to Johannesburg (South-Africa) by air, from Johannesburg to Cairo (Egypt) by air, from Cairo to Amsterdam (The Netherlands) by air, from Amsterdam to Leerdam (The Netherlands) by land

			Last location	Godi US	Godi DS	Godi IS diver	Mess DS	MessIS diver	Revue	Ruaga diver/ GodiDS Baro
Location	**Start**	**End**		**Baro L8009**	**Diver N01-57308**	**L7925**	**Diver L8024**	**S2662**	**Diver L7899**	**N01-25340**
			SerieNumber							
Messica	22/07/2014 18:00	23/07/2014 10:30	Avg [cm]	-0.1	-5.5	-0.2	-0.5	-4.4	2.8	10.2
			stdev	0.2	1.2	0.4	-	0.2	2.1	0.3
Whole journey	22/07/2014 18:00	30/07/2014 08:00	Avg [cm]	**-0.3**	**-5.5***	**-0.3**	**-0.8**	**-3**	**4.9**	**10.2***
			stdev	1.6	1.20*	1.7	1.7	1.8	3.2	0.3*

Table E.3: Correction relative to barometer Messica downstream (P1312). In bold the correction factors for every diver/ barometer. * divers stayed in Chimoio Mozambique

locations, after applying the new device constant to all L8009-series, we calculated the average pressure difference because of elevation (the location constant).

E.2. LOCATION CONSTANT

Since not every location is equipped with a barometer, we transferred barometric time series from the one location to the other. Therefore we corrected for the altitude effects, this is what we call the 'location constant'. In order to find the location constant caused by altitude, we used two barometers. First they measured together at MessicaDS the barometric pressure (L8009 and P1312). Since they measured exactly at the same spot, with the same frequency, on the same time stamp, they should measure exactly the same air pressure. We averaged the measured pressures during two weeks and derived a mutual device constant of 1.765cm. (see previous paragraph and Table E.4.). Now we subsequently installed barometer L8009 Chirodzo DS, Revue DS and Godi US. From there we were able to derive location constants for these locations. So after correction for location, we can derive the barometric pressures for these locations. Fig E.2 shows the location dependent deviation in barometric pressure for Revue DS, Godi US and Caritas (our residence just south of the catchment) between the several locations (after applying diver constants and location constants for Chirodzo DS, Godi DS and Messica DS). However, since we did not install barometer L8009 at all locations. Godi DS, Messica IS, Ruaga DS (and Chirodzo DS) are missing, we applied another trick for those stations. We measured at

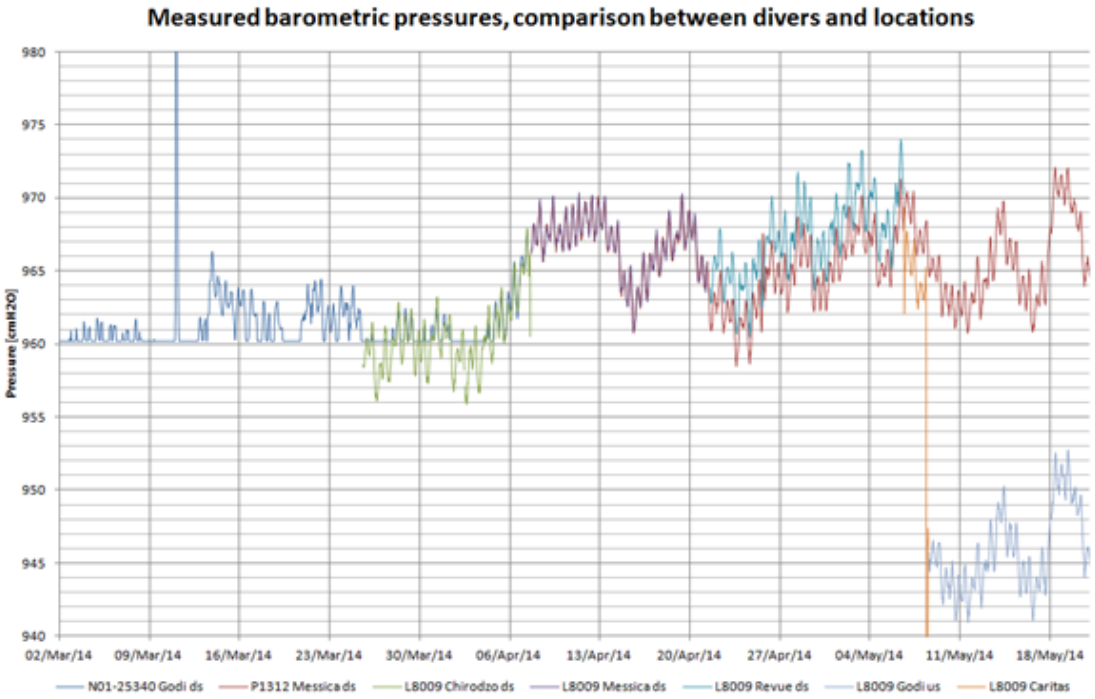

Figure E.2: Barometric pressure after correction with device constant

several moments the water levels and depths [1] relatively to the waterpressure diver. Since we know the waterdepth, the waterpressure at the location and the barometric pressure at other locations and we know that the waterpressure ± diver constant – barometric pressure ± location constant equals the waterdepth, we derived the location constant from these point observations. Note, we did not make use of elevation information, since the resolution from Aster2 [35] is too course and not accurate enough to derive point locations. Also elevations retrieved from handheld GPS Garmin serve as best estimates, rather than exact elevation values (see for example fig E.3 altitude information near confluence MessicaIS and RuagaDS and Table E.4).

E.3. BAROMETRIC PRESSURE SPACE INVARIANT AT DAILY TIMESCALE

We assume that the average daily barometric pressure is the same everywhere in our catchment (apart from the altitude effect), however on smaller higher frequencies (smaller timesteps) barometric pressures can vary between the several locations, leading to wrong waterdepths (and therefore discharges). We know that barometric pressures vary during the day, the pressure is minimal during night and maximal during day (depends on air temperature). Graph E.4a shows that there is a small randomness (noise) in measurements that is ±1 cmH2O, even when divers measures at exactly the same place. 4-hourly and 24-hourly averages filter out the highest noise frequencies, but since we assume functioning of both devices time invariant and we assume that weather influences on long term should average out, we should find one constant deviation; which is altitude induced. Input waterdepths are calculated on timestep base (so 30minutes time resolution), however, since we use daily averaged input values, we get rid of the noise as well. Remember that averaging the sum of is the sum of the averages, according to the linearity principle.

not that in order to filter randomness or noise or perturbations, in general this equation hold:

$$p(x,t) = \bar{p}(x,t) + p'(x,t) \tag{E.1}$$

for which in Eq. E.1 $p(x,t)$ is the pressure in kPa, $\bar{p}$ the average pressure, p' the perturbation. Note that this method strive to filter the relevant signal from the random noise. It depends on our question what we define as noise, is it the hourly variation, is it the randomness (between) devices, is it the daily variation, is it the weekly variation. For the location constant, every variation within the whole period is called noise. For

[1] See Table pH, EC, T in database Modelinput.accdb

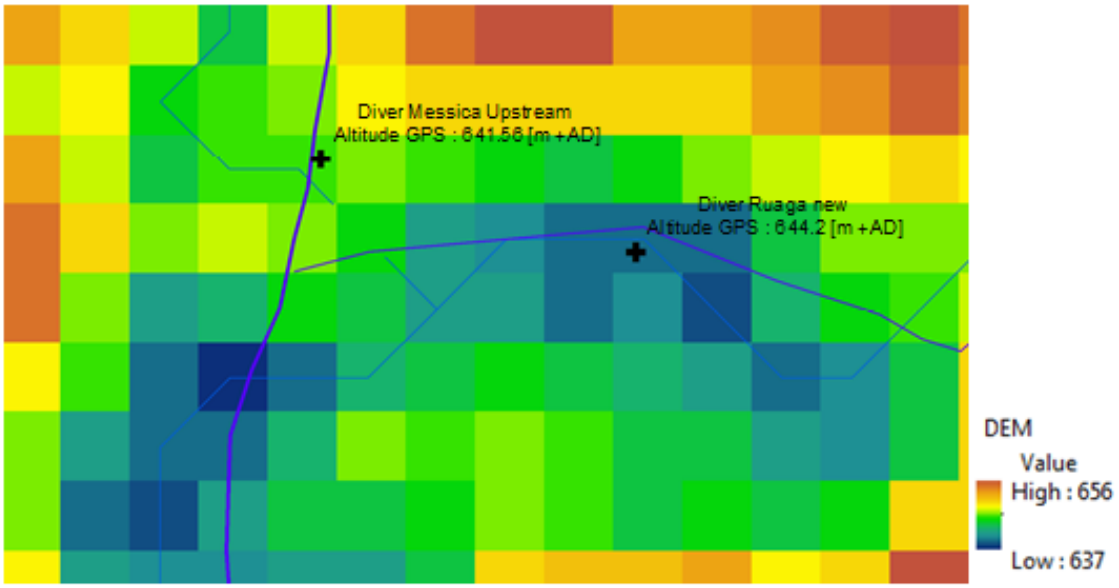

Figure E.3: Excerpt from Digital Elevation Map (DEM) [35] around confluence Ruaga and Messica. Dark blue: real stream locations, light blue: streams calculated with DEM

the daily

E.4. IRRIGATION CORRECTION

This daily averaged barometric assumption effects the correctness of the waterdepths at smaller timesteps (hourly base). Since we do not have the exact waterdepth variation during the day, we cannot apply Meyboom [48]'s method anymore, since we therefore have to know the 'exact' maximum values within the day.

Before calculating the 30 minute waterdepth variation, in order to calculate for irrigation and or riparian transpiration as explained [48] we have to check if the errors due to spatial shifts are not unacceptable.

Diver ID	**N01-25340**	**L8009**	**P1312**	**L8009**	**L8009**	**L8009**	**L8009**
Location	Godi ds	Chirodzo ds	Messica ds	Messica ds	Revue ds	Caritas	Godi us
start date	12/08/2013 13:00	25/03/2014 15:00	07/04/2014 17:00	07/04/2014 17:00	21/04/2014 14:00	06/05/2014 15:00	08/05/2014 13:00
end date	12/08/2013 13:30	07/04/2014 15:00	23/07/2014 10:00	21/04/2014 08:30	06/05/2014 14:30	08/05/2014 12:30	21/07/2014 14:30
Device correction constant for pressure [cm H2O] rel to P1312:	**10.2**	**1.765**	0	1.765	1.765	1.765	1.765
Elevation correction constant for pressure rel. to P1312 [cm H2O]	-	-	-	0	-2.409	3.365	19.416
Elevation correction for pressure rel. to N01-25430 [cm H2O]	-	0.165	-	-	-	-	-
Altitude DEM [m+AD]	650	647	622	622	603	660	826
altitude GPS [m+AD]		653	635	635	641	669	805
Average Altitude [m+AD]	650	650	628.5	628.5	622	664.5	815.5
Barometric gradient [cmH2O/m] based on DEM		0.055			0.127	0.089	0.095
correction [cmH2O/m] for GPS					-0.402	0.099	0.114
correction [cmH2O/m] for Avg altitude	-	-	-	-	0.371	0.093	0.104

Table E.4: Location and device correction

E.5. SMALL NOTES

Some small notes about pressures:

- note that kPa = mBar = cmH2O = 1 cm waterdepth
- decreasing barometric pressure due to increasing altitude is approximated with 12 kPa / 100m or 0.12 to 0.125 kPa/m

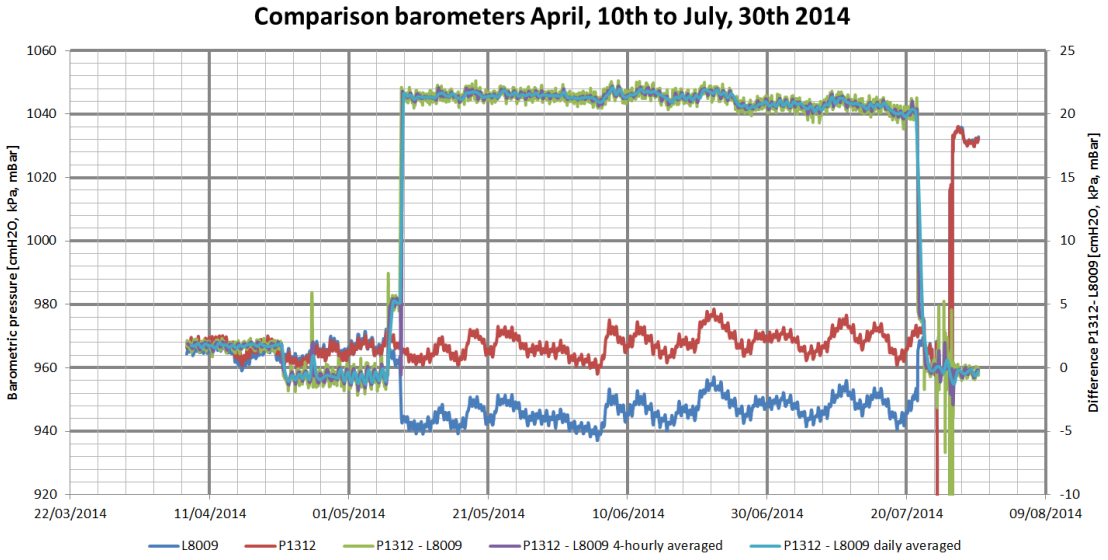

(a)

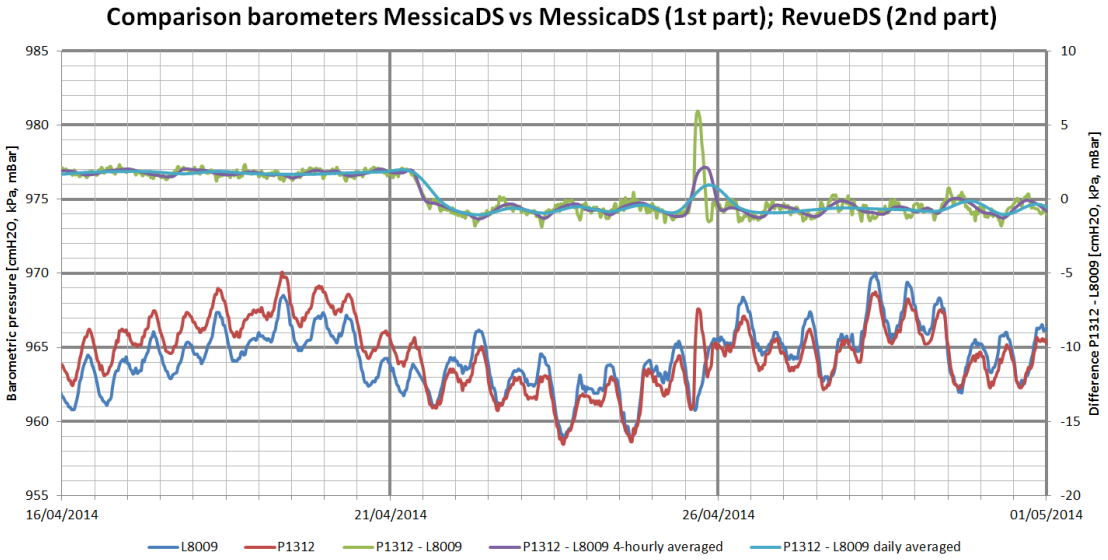

(b)

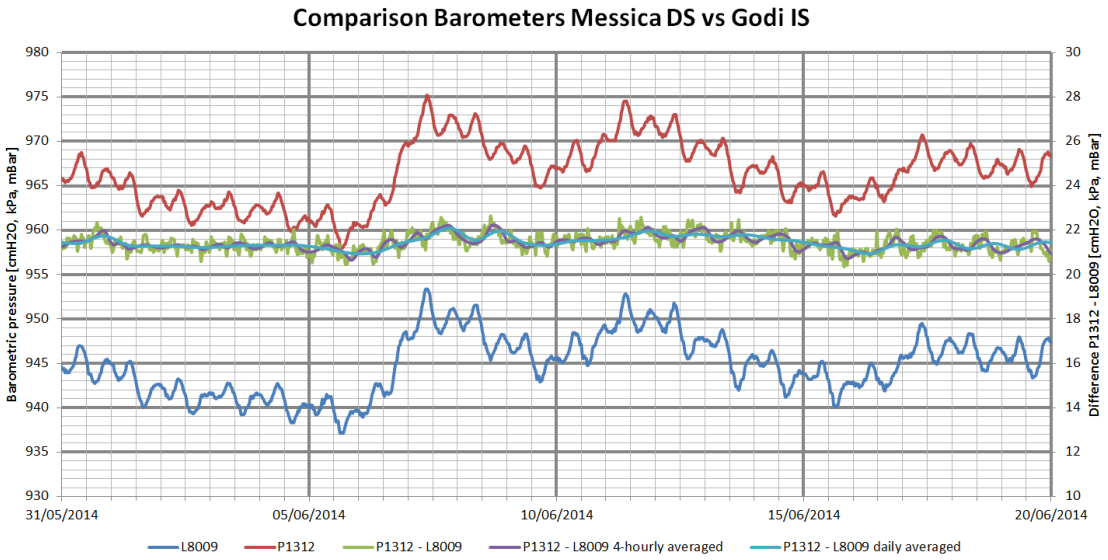

(c)

Figure E.4: Comparison barometers P1312 and L8009, device correction not applied. So difference is combined effect of device and location constant.
Subsequent periods: Messica Downstream (both), Revue DS, Godi US, Journey

F

(Flow) Measurement points

This chapter describes the measurement locations for the streamflow and water level measurements, isotope, pH and water temperature measurements.

At 7 locations measurement devices are installed; ChirDS, ChirIS, GodiDS, GodiIS, MessDS, MessIS and RuagaDS. During the fieldwork period also at other locations longitudinal routings are performed in order to achieve inside in the flow routing, irrigation influences and gaining stream flow.

Measurements are performed at the locations mapped in Fig. F.1.

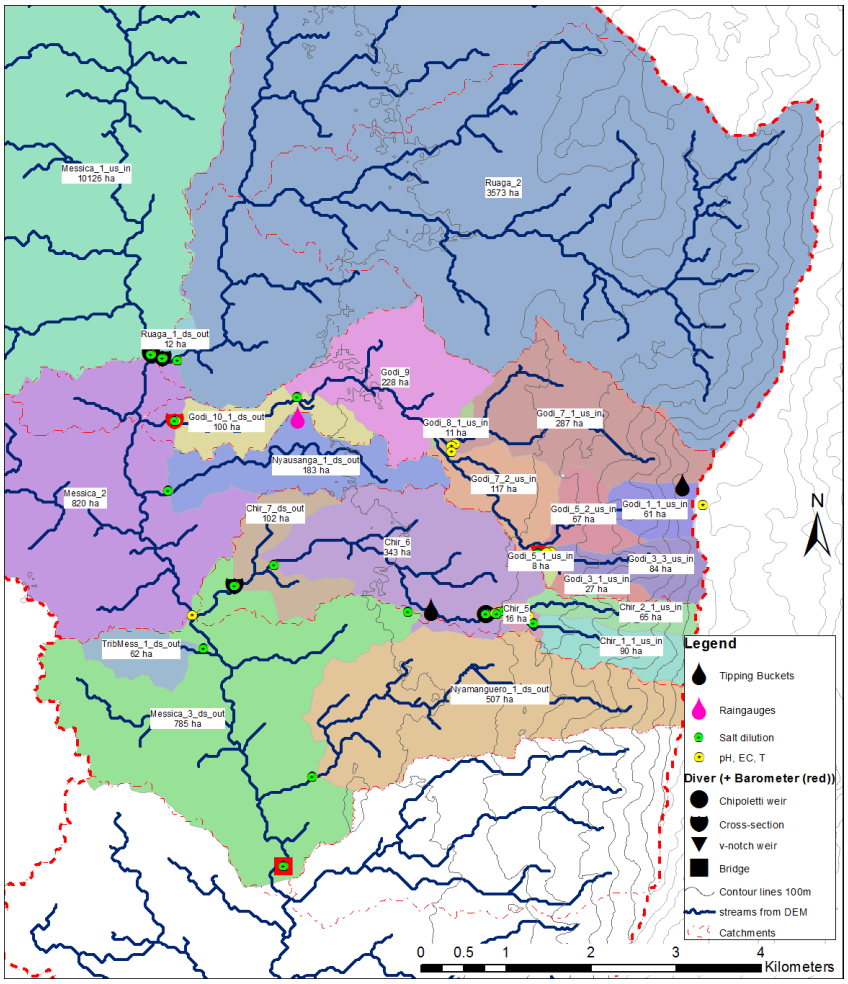

Figure F.1: Areas (sub-)subcatchments including measurement locations of Salt dilutions, pH, EC and Temperature

F.1. DERIVATION CROSS SECTION FROM MEASUREMENTS

The cross-section is measured with a water level instrument relative to a fixed reference point near the measurement location, for example a mark on a large rock or a tree trunk. Both the longitudinal profile and the cross-section are mapped together with the relative height of the diver. An $y-z$ cross-section table is made from the measurements. y is the distance relative to the left river bank and z the depth relative to the reference point. The accuracy of the measurements is 0.3cm (deviation from the water level instrument). For every 0.5cm we calculated (using linear interpolation) the Area and Perimeter with a VBA script in Microsoft Excel©(see hereafter). The calculation output is a lookup table, in which for every observed water depth (relative to the lowest point in the cross-section), the belonging Area, Perimeter (Conveyance and Hydraulic Radius) can be looked up.

```
sub CrossSection()
' calculates the cross-sectional area, perimeter and hydraulic radius until threshold value
' by definition the profile is left to right oriented, so seen from upstream to downstream

'declaring variables

Dim x1 As Single, x2 As Single
Dim y1 As Single, y2 As Single
Dim dx As Single, dy As Single
Set Mysheet = ActiveSheet

With Mysheet
   ULCrsClm = .Range("B11").Column
   ULCrsRw = .Range("B11").Row
   n = .Cells(Rows.Count, 2).End(xlUp).Row - ULCrsRw 'number of rows
   MinThres = .Range("B3").Value
   MaxThres = .Range("b4").Value
   Incr = .Range("b5").Value
   ultblcoordclm = 5
   ULTblCoordRw = 1

   'clear previous table
   .Cells(1, ultblcoordclm).Resize(.Cells(Rows.Count, ultblcoordclm).End(xlUp).Row, 4).
        ClearContents

   'table header
   With .Cells(ULTblCoordRw, ultblcoordclm)
      .Value = "h [m+AD]"
      .Offset(, 1).Value = "wet area [m2]"
      .Offset(, 2).Value = "wet perimeter [m]"
      .Offset(, 3).Value = "hydraulic radius [m]"
   End With

   For h = MinThres To MaxThres Step Incr
      WetArea = 0
      WetPerimeter = 0

      For i = ULCrsRw To ULCrsRw + n - 1

         'determine delta_x and delta_y
         x1 = .Cells(i, 3).Value
         x2 = .Cells(i + 1, 3).Value
         If x1 > x2 Then GoTo errorhandling
         y2 = .Cells(i + 1, 2).Value
         y1 = .Cells(i, 2).Value
         dx = x2 - x1
         dy = y2 - y1


         'if both values are larger, continue with next section
         If y1 >= h And y2 >= h Then GoTo 1


         'if both values are smaller than threshold value and if line is horizontal
         If y1 < h And y2 < h And y1 = y2 Then
            WetArea = WetArea + (h - WorksheetFunction.Max(y1, y2)) * dx
            WetPerimeter = WetPerimeter + dx 'horizontale line
            GoTo 1
         End If


         'if both values are smaller than threshold value, but line is not horizontal
         If y1 < h And y2 < h And y1 <> y2 Then
            WetArea = WetArea + Abs(0.5 * (dx / dy) * (y1 - y2) ^ 2) + (h - WorksheetFunction.Max(
                 y1, y2)) * dx
            WetPerimeter = WetPerimeter + (dx ^ 2 + dy ^ 2) ^ 0.5
            GoTo 1
         End If
```

```
         'if one of both values is smaller than threshold value
         If y1 < h Or y2 < h Then
            WetArea = WetArea + Abs(0.5 * (dx / dy) * (WorksheetFunction.Min(y1, y2) - h) ^ 2)
            WetPerimeter = WetPerimeter + (h - WorksheetFunction.Min(y1, y2)) * ((dx / dy) ^ 2 +
                1) ^ 0.5
            GoTo 1
         End If


      1    Next i

      'append table:
      With .Cells(ULTblCoordRw + 1 + (h - MinThres) / Incr, ultblcoordclm)
         .Value = h
         .Offset(, 1).Value = WetArea
         .Offset(, 2).Value = WetPerimeter
         If WetPerimeter <> 0 Then .Offset(, 3).Value = WetArea / WetPerimeter
      End With

      'set variables for new run
      WetArea = 0
      WetPerimeter = 0
   Next h

End With

Exit Sub

errorhandling:
MsgBox ("error in input values, x values must be sorted")

End Sub
```

F.2. MEASUREMENT STATIONS

F.2.1. CHIRODZO DOWNSTREAM STATION (CHIRDS)

Measurements at Chirodzo downstream are performed over a quite long period from December 2012 to July 2014. However, the measurements are less useful as might be expected based on the length of the time sequence.

- Dec 2012 to Jun 2013. measurements are performed at a location a little downstream between rocks. These obstructions cause backwatercurves. No cross-section information available. Weemstra *et al.* [7] derived a transfer function to match measured water levels from the old to the new location based on one month overlap (not published). The manual obtained waterdepths in this period are too low, due to sedimentation (source: interview Weemstra).
- June 2013 to June 5th 2014 measurements are performed in a known cross-section (Fig. F.5a). However, the diver has presumably been touched by local people. So measurements might be affected .
- In May 2014 the river dried up, and the diver measures barometric pressure variations. Therefore measurements from this observation to June 5th are excluded.
- from June 5th, 2014 to July 22th, 2014 measurements are performed at a third measurement location (see cross-section in Fig. F.4). However flow conditions are most likely not uniform but experience backwater influence. Therefore the quasi -static uniform flow assumption doesn't hold for this diver, and we did not include this period in the measurements

All in all, the waterdepths are not very reliable since the cross-section information is not very good. We did not derive a conveyance for this time sequence, but we did apply the Stevens method for the time series based on Fig. F.5a. This is an arbitrary choice. Because of the rather bad quality of the measurements, we used this location only for visual validation.

Figure F.2: Looking upstream at diver Chirodzo downstream

Figure F.3: Looking downstream at diver Chirodzo downstream

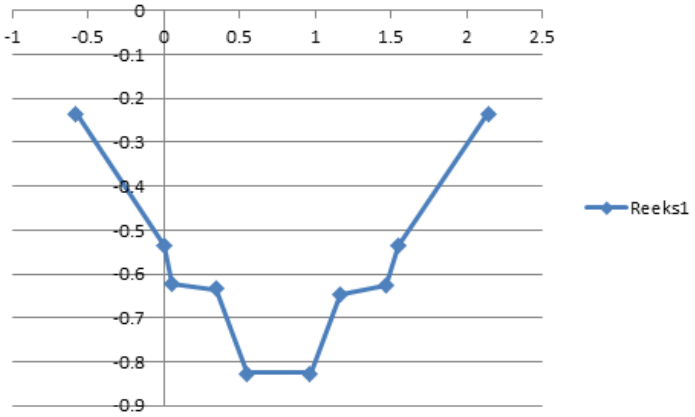

Figure F.4: Chirodzo Downstream cross-section between Jun 5th to Jul 22th 2014. However, quasi-static uniform flow assumption does not hold, we excluded this period.

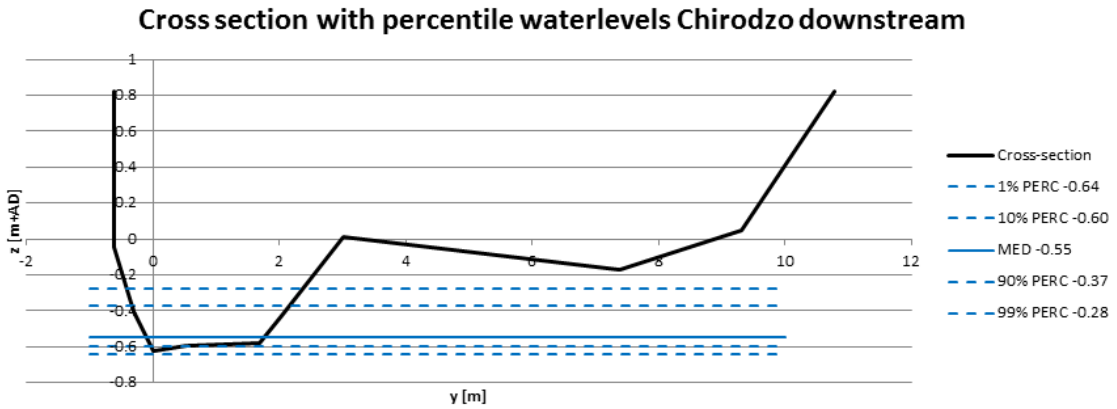

(a) Cross-section Chirodzo DS relative to reference point

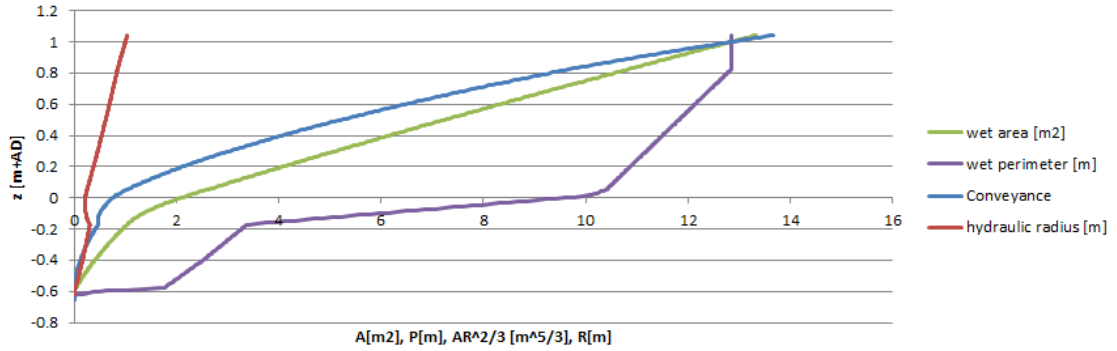

(b) Chirodzo DS: Area, Perimeter, Hydraulic Radius and Conveyance as function of the depth

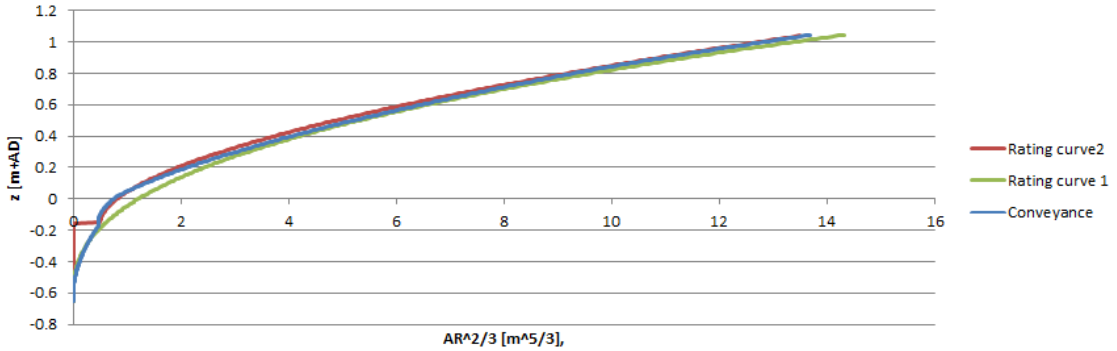

(c) Steven's method: $\tilde{a}(h-h_0)^b$ fitted on Conveyance $AR^{2/3}$; two rating curves used
RC1 with $\tilde{a}=4$, $b=2.5$ and $h_0=0.62$
RC2 with $\tilde{a}=9.5$, $b=1.8$ and $h_0=0.15$ with a horizontal shift of $+0.5m$

Figure F.5: Cross-sectional information of Chirodzo DS

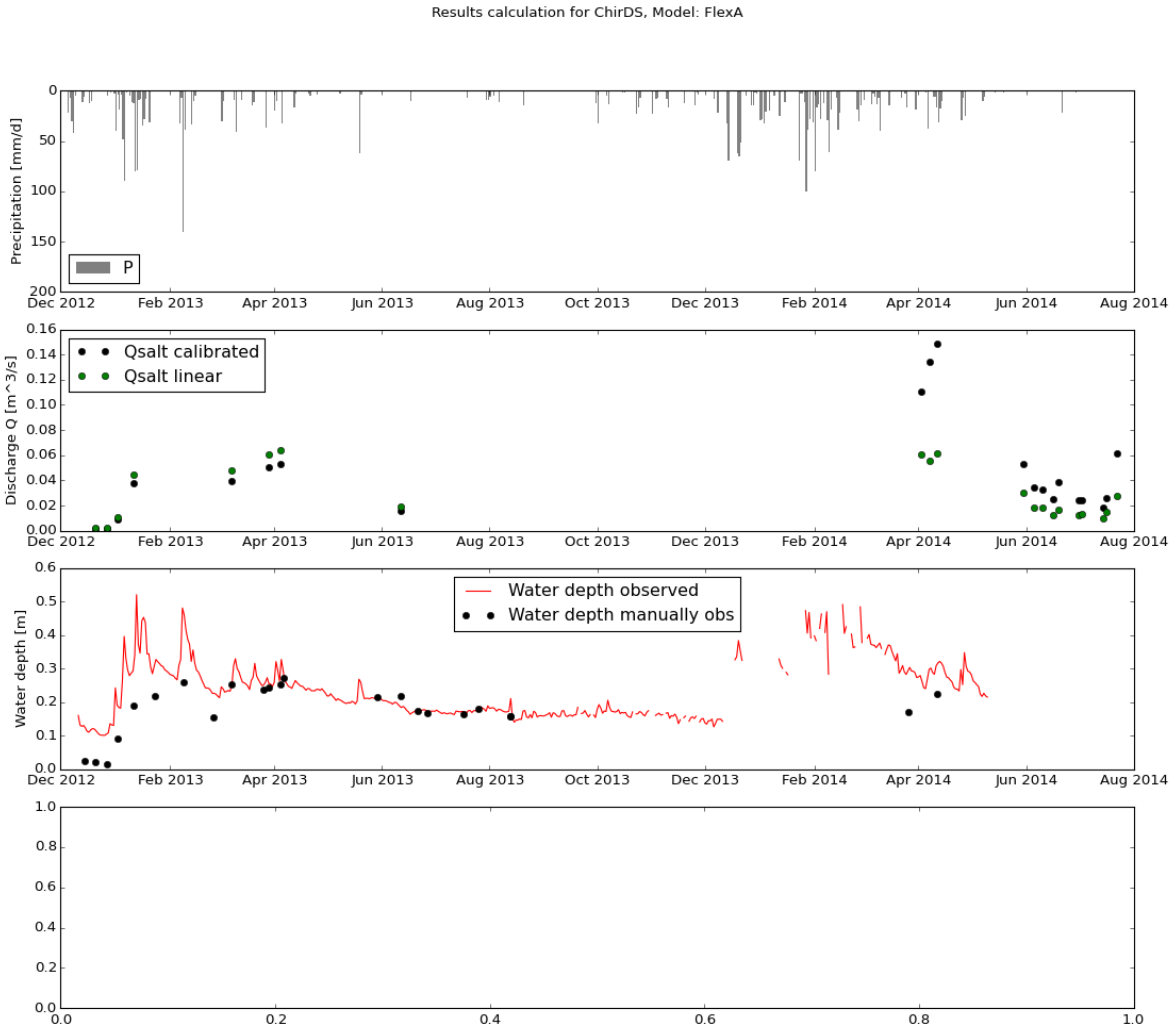

Figure F.6: Observed water depths (manual and divers) and discharges for Chirodzo Downstream Station

F.2.2. CHIRODZO INTERMEDIATE STATION (CHIRIS)

In the river Chirodzo are from July 2011 to August 2014 weekly discharge measurements conducted with a Chipoletti weir. Main goal was to investigate yearly discharge variations for the construction of irrigation canals. In this period, discharge measurements with multiple weirs have been performed in this area. We only used measurements from the weir in the main stream. The measurements took place every Friday morning at 9 am.

In general, the discharge observations are always performed by two personsn. They place the weir into the stream and use a large canvas to make the construction water tight. Unfortunately some leakage is unavoidable, estimates are about 10%. After a short re-stabilization period, the water depths relative to the weir are recorded. By means of Eq. F.1 the discharge Q in m^3/s can be calculated, where $h(t)$ is in situ obtained, the others are weir specific variables (Table F.1, Fig. F.7a).

For this location only discharges are applied, no waterdepths or conveyances.

$$Q(t) = 0.602 + 0.083 * b * \frac{2}{3} * \frac{\sqrt{2g}}{P} * h(t)^{5/2} \tag{F.1}$$

in m	Large (20-40 l/s)	Medium (10-20 l/s)	Small (5-10 l/s)
h	0.22	0.19	0.14
b	0.2	0.13	0.1
P	0.3	0.2	0.15
d	0.6	0.45	0.35
w	1	0.7	0.5
x	0.075	0.0626	0.05
y	0.3	0.25	0.02

Table F.1: Chipoletti weir constants. For ChirIS the large weir is applied.

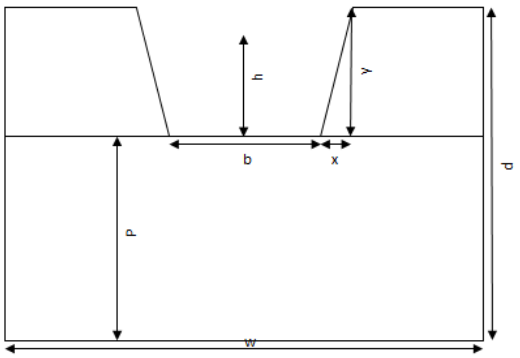

(a) Chipoleti weir; schematic representation

(b) Measurements as performed in the field

Figure F.7: Weekly performed discharge measurement with Chipoletti weir, Friday morning 9am

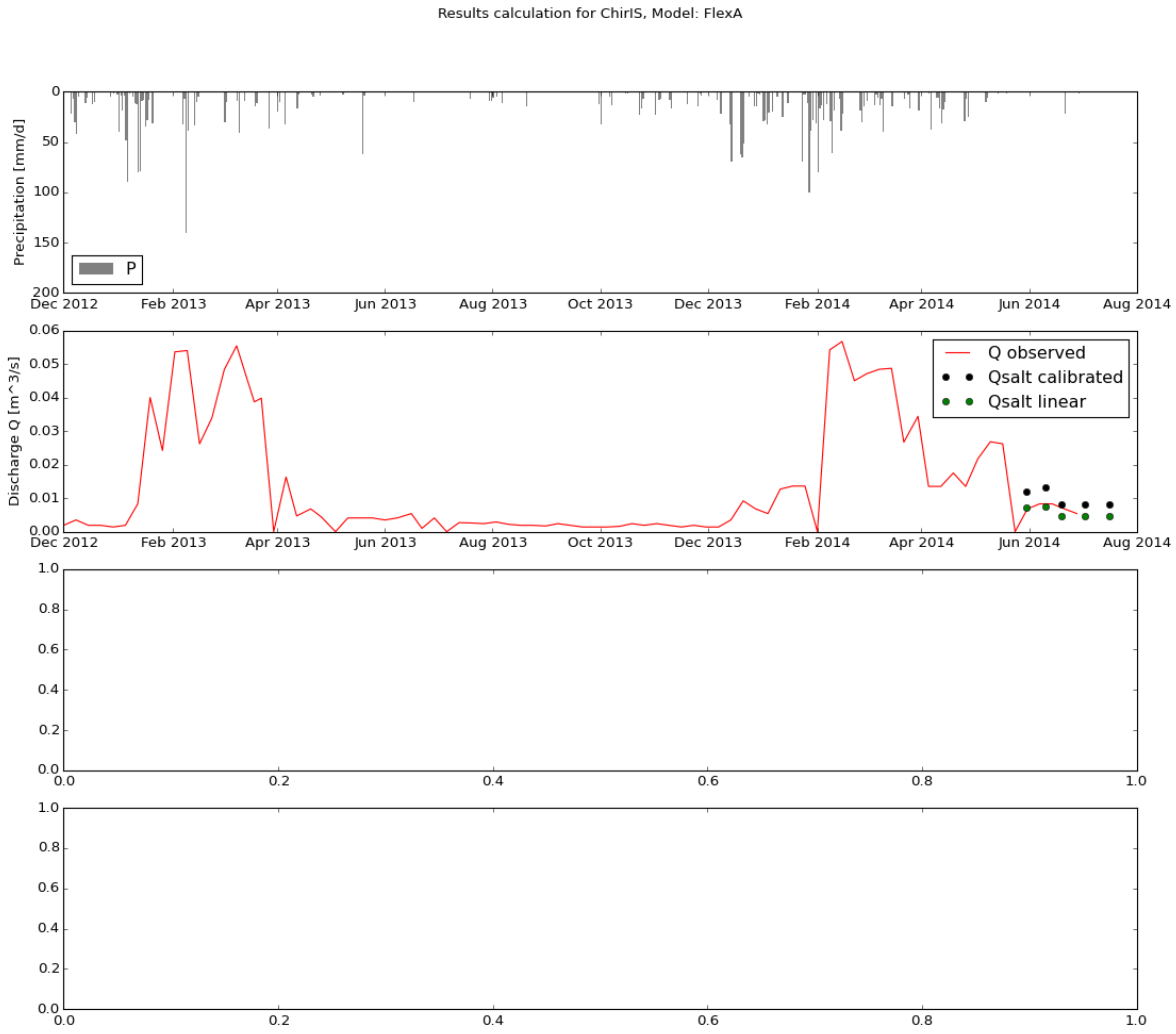

Figure F.8: Observed water depths (manual and divers) and discharges for Chirodzo Intermediate Station. Note the date axis are not equal.

F.2.3. GODI DOWNSTREAM STATION (GODIDS)

This measurement point is the main measurement station, since:

- Over year time series are available,
- known cross section,
- the river did not run dry,
- the diver is not replaced.

All other measurement locations lags on or more bullets. However, deriving the waterdepths relative to a reference level appeared rather challenging. Since:

- The diver's altitude changed several times.
- The local barometer has a large structural measurement error and an unrealistic lower measurement boundary of 950 kPa.
- The barometer have been flooded during high flows.
- Different barometers (from other measurement locations) are used to compensate for the large deviation and for the floodings.
- The structural barometer deviation for the other barometers is unknown.
- The bottom erosion rate is unknown.

Based on log files, personal notes (see inlay boxes) and some assumptions we have been able to reconstruct first the diver altitudes (see Table F.2). Then we assumed that the diver pile did not moved during the whole measurement period, except for the 4mm on March 7th, 2013 as found in the notes. Next, we assumed the cross-section bottom level to be constant at -1.75[m]+ref, so not undergoing any sedimentation nor erosion. According to Weemstra and Beekman (personal interviews), this assumption is rather arguable, since they observed bottom erosion. We agree upon this statement, but based on the following observations and arguments we do not correct for this on forehand, but will take it into account in the discussion of the results. For this reconstruction see Fig. F.9.

Furthermore, we determined the device constant (calibration deviation) (see App. E) of the diver and correct the obtained water pressures with this constant. Then we used the obtained water levels relative to the diver pile top to tune the combined device and altitude correction factor for the different barometers. These values are partly based on the analysis of App. E, see Table F.2. Note that these constants serves as indications, rather then absolute values. Since the time and spatial variant circumstances.

All in all, we have been able to successfully reconstruct the waterdepths relative to the bottom level compared to the manually obtained water levels relative to the diver pile top, see Fig. F.16.

Some notes concerning the measurement station:

- From the measurements we have an indication that the bottom lowered with 5cms between Februari 25th, 2013 and April 7th, 2014. This would imply that the waterdepths during the dry period in 2013 are even less, indicating even smaller discharges.
- Judging on a picture taken during the installation of the diver, we assume the diver to be placed in a mandug hole. This hole is most likely slowly silted, that is why most likely Weemstra elevated the diver above bottom on January 21th, 2013. Since we assume the diver to be placed in a hole, the water is not flowing in this hole, so the no-flow zone is larger. Which is in favor for our fixed bottom assumption of -1.75[m]+ref.

As explained earlier, the divers show mutual deviations (see also Appendix E). We derived these deviations and correct for this. These constants are based on the following sources and are iteratively determined together with the point observations.

	date	Altitude diver [m-ref]	Altitude top diver pile [m-ref]
Installed:	12-12-2012 0:00	-2.062	-0.832
Read out at (1):	22-1-2013 12:00	-1.803	-0.832
Read out at (2):	7-3-2013 12:00	-1.674	-0.828
Read out at (3):	21-6-2013 13:00	-1.677	-0.828
Read out at (4):	8-7-2013 18:00	-1.669	-0.828
Read out at (5):	12-8-2013 13:00	-1.668	-0.828
Read out at (6):	25-3-2014 15:00	-1.658	-0.828
Read out at (7):	7-4-2014 9:00	-1.658	-0.828
Read out at (8):	8-5-2014 16:00	-1.658	-0.828
Read out at (9):	24-5-2014 12:00	-1.658	-0.828
Deinstalled:	22-7-2014 10:00	-1.658	-0.828

Table F.2: Altitude diver relative to reference point

- The constant device deviations relative to barometer Messica downstream (P1312 Schlumberger) (see Appendix E) are respectively -5.5 cm, 10.2 cm and 1.765 cm for water pressure diver N01-57308 210 Schlumberger Godi downstream, barometer Godi downstream (N01-25430 210 Schlumberger) and barometer Godi downstream (L8009 Schlumberger). Note these diver constants are more a indication then an absolute value.
- The diverconstant for the barometers applied by Weemstra, we were able to derive it with the water-depth observations, comparing Weemstra's measurements we also find a large deviation constant between his barometers and our barometer N01-25430 210.

Barometer ID	Location barometer	Altitude barometer [m+AD]	Start date	Device constant [cm]	Elevation constant [cm]	Total pressure correction [cm]
N01-57308 210	Godi DS *	650	12-12-2012	-5.5		-5.5
(unknown)***	Messica IS **		12-12-2012	6.1		6.1
N01-25430 210	Godi DS **	650	12-08-2013	10.2		10.2
L8009	Chirodzo DS **	647	26-03-2014	1.765	2	3.765
P1312	Messica DS **	627	07-04-2014	0	-3.9	-3.9

Table F.3: Diver device constants (relative to P1312) and elevation constants as applied for Godi downstream. *) Water pressure; **) Barometer. Note the altitude concerns an approximation; ***) Weemstra applied two different barometers in this period. Comparing these series with N01-57308 210 we derived also a device constant between both divers, which supports our findings.

Aantekeningen gemaakt n.a.v. veranderingen of ter controle. Overige controle punten zijn terug te vinden in het overzicht van alle debietmetingen. Godi downstream:

- 22 jan Wl godi down 48.2 tov buis 11.30 uur.
- 22 jan DIV godi down onderste diver hangen we 25.9 cm hoger.
- 14 feb Wl godi down 49.2
- 15 feb Wl godi down 51.5 en tov van reference staat de peilbuis 25 cm lager (maar onnauwkeurig gemten zonder waterpas).
- 25 feb WL godi down 62.5 cm at 10.30 uur. Lenth top-bottom is 86 cm
- 27 feb WL godi down 63,0 cm 17.00 uur.
- 7 maart DIV: Godi down: open after smashing with hamer. Wl was toen 60.6 at 10.20 after it was 60.2 so level changed with 4 mm. daarna hebben we diver & barometer hoger gehangen.meetpunt-top buis was 82..0+14.2 nu is het 69.5 + 14.2 so differences is 12.5 cm. en dan nog die 4 mm evt.
- 7 maart Wl: godi down voor deze verandering is dus 60.6 at 10.20 uur.
- 4 april Godi do 65.1 tov pipe at 13.40
- 6 april godi down at 10.30 uur 59.2.
- 11 june wl Godi down at 11.15 uur 70.9

UIT OVERZICHT DEBIETMETINGEN; RATING CURVE:

Date	Time	River stage rel to pile top [cm]	h cor [cm] [92.90 - riverstage]	Discharge [l/s]
13-dec-12	-	88.50	4.40	2.1
20-dec-12	14:25	90.50	2.40	not measured
28-dec-12	9:20	90.50	2.40	0.3
01-jan-13	?	81.30	11.60	25.8
10-jan-13	11:09	66.80	26.10	65.6
22 jan-13	11:30	48.20	44.70	
14-feb-13	10:45	49.20	43.70	269.1
14-feb-13	11:15	49.20	43.70	234.9
15-feb-13	12:30	51.50	41.40	272.1
25-feb-13	10:30	62.50	30.40	97.0
27-feb-13	17:00	63.00	29.90	130.4
07-mrt-13	11:00	60.60	32.30	95.9
27-mrt-13	17:00	63.00	29.90	130.4
04-apr-13	13:40	65.10	27.80	71.1
06 april-13	10:30	59.20	33.70	
27-mei-13	13:00	not measured		31.2
11-jun-13	11:15	70.90	22.00	32.9

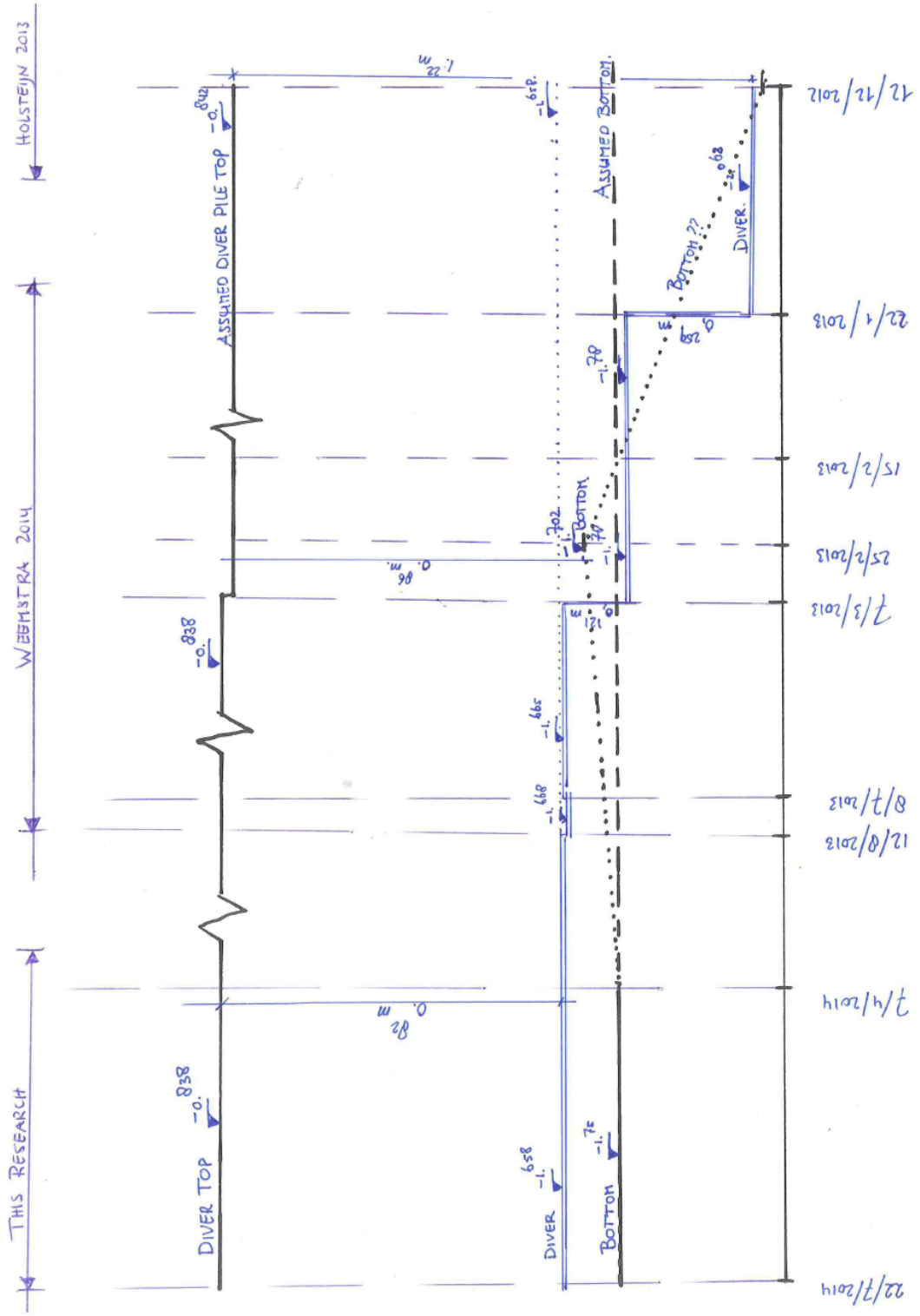

Figure F.9: Reconstructed diver, diver pile and bottom altitude. Note that the time axis is reversed. *The values in this drawing do not correspond with the values in the table, the values in the table are leading in that case*

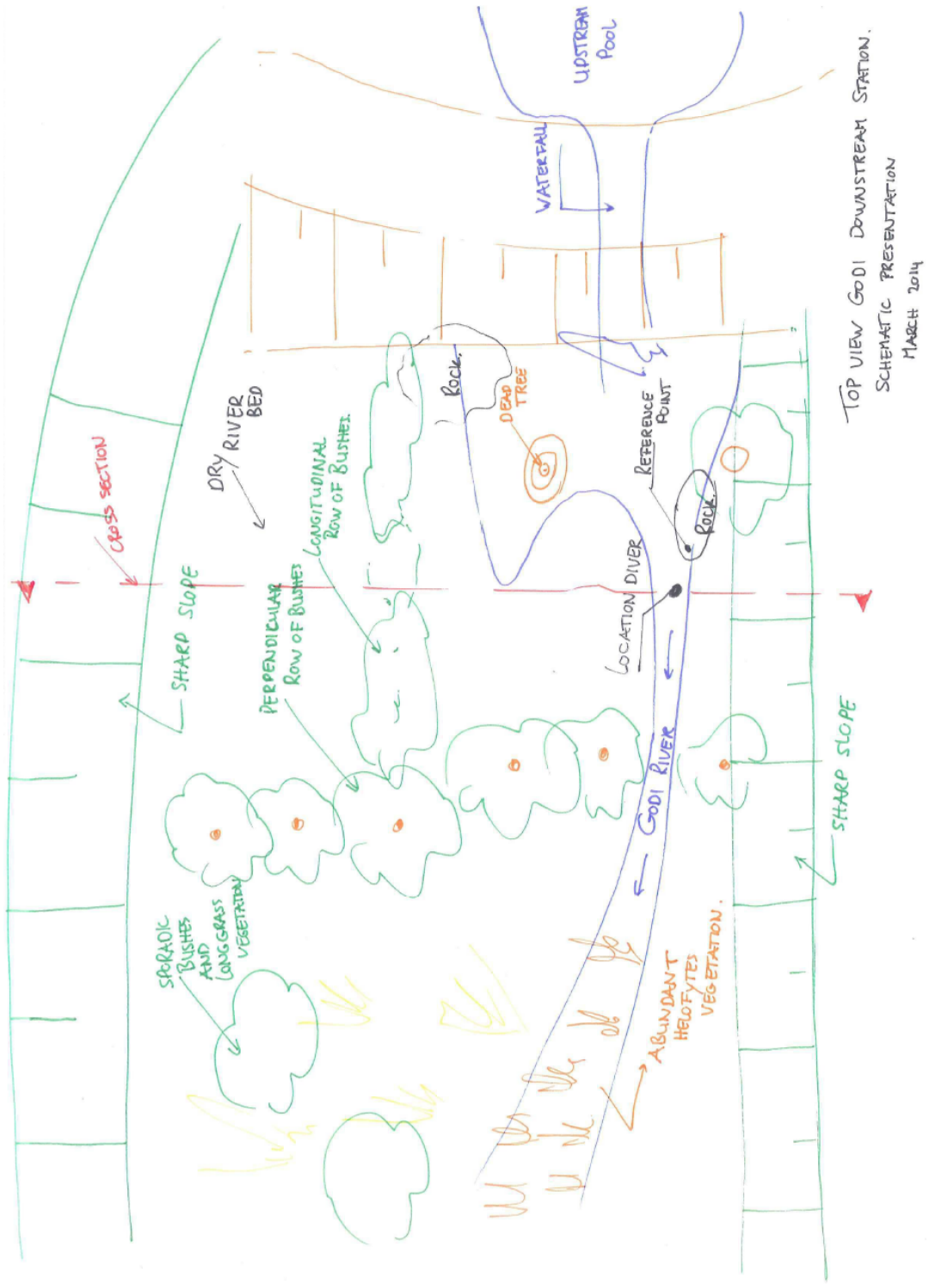

Figure F.10: Godi DS topview of the measurement location. Clearly visible the abundant bush and reed growth. They obstruct peak flows and give extra water level set up. This is not taken into account in the conveyance nor Steven's method.

HIGH FLOW CORRECTION

In the period August 10th, 2013 until March26th 2014 the barometer N01-25430 210 did not function well.

- The diver is located too low, so during peak flows the diver is flooded
- The diver shows a lower boundary of 950 mBar, since this lower boundary is often recorded, barometric pressures must have been lower.
- The diver structurally measures too low barometric pressures (about 10.2 cm relatively to barometer P1312)

Between medio december 2013 and march 2014 the barometric pressure appeared most of the time to be lower than 960.2 mBar (after correction). During the periods the barometer did record any pressures, the difference between the obtained waterpressure and the barometric pressures is about 60 cm, which is exactly the distance between both devices. This indicates that the barometer is flooded. A second barometer appeared to be broken and could not been recovered by the manufacturer anymore. We leave this period out of our calibration period and use the remaining values only for indicative purposes. The moments the barometer is overtoppped, give a first estimate for the frequency and length of peaks.

CROSS-SECTION

The cross-section is recorded on April 7th, 2014, see Fig. F.15a. We hold the cross-section as a fixed entity, while we have indication to expect sedimentation and erosion for at least a couple of centimeters between the dry February 25th, 2013 and April 7th, 2014.

We derived the Area an Perimeter as function of the depth relative to the bottom level. Note that this implicitly implies a non-obstructed free flow zone over the whole cross section, which is not true. There is dense vegetation situated in the flood plains (see Pictures F.10, F.12 and F.11) as well as in the cross-section itself (helofytes). Note also that during high flows the flood plains are flooded. This will increase resistance a give elevated water levels. Since this obstruction effect is not taken into account explicitly it will be compensated in the roughness and bottom slope constant and/ or will cause overestimation of the peak flows.

Figure F.11: Water fall right upstream of the diver location at Godi downstream (date 11-4-2014)

TUNING THE $\bar{a}$ PARAMETER

The conveyance is linear dependent on the discharge.

$$Q = \bar{a}(C - C_0)$$

We do have some discharge observations obtained with the salt dilution method, see App. D. Based on field observations we estimated the no-flow depth and calculated the associated conveyance value C_0. Then we tuned $\bar{a}$ to approximate the discharge measurements. For Godi DS we focused on the period 2012-2014,

Figure F.12: Looking to the diver location (near the person) and the river stretch (reeds) of Godi downstream from top of the waterfall. A line of mature shrubs is located perpendicular to the river stretch, just downstream of the diver.

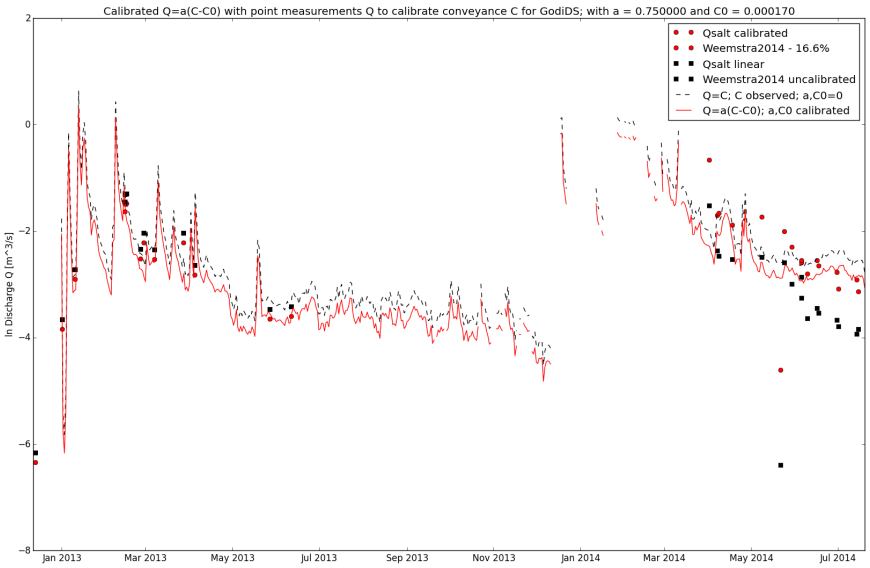

Figure F.13: Conveyance tuned to discharge measurements for Godi DS, $\bar{a} = 0.75$.

since Weemstra applied salt dilution method seems a little more reliable. We do however diminish his discharges with 16.6% due to the underestimation of the measurement timestep of 16,6%.

For GodiDS we found that $\bar{a} = 0.75$ and $C_0 = 0.00017$, see Fig. F.13. We used the python script called: Derive_roughness_Conveyance.py

Figure F.14: Godi downstream's river stretch just downstream of the diver

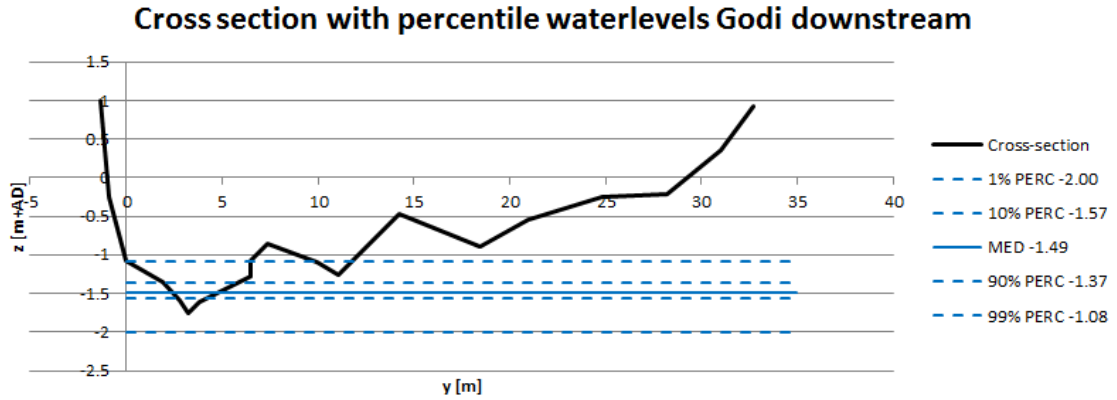

(a) Cross-section Godi DS relative to reference point

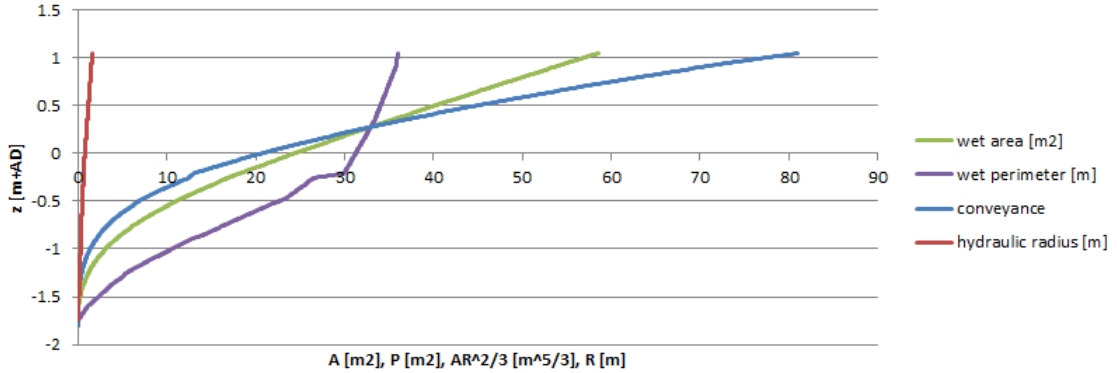

(b) Godi DS: Area, Perimeter, Hydraulic Radius and Conveyance as function of the depth

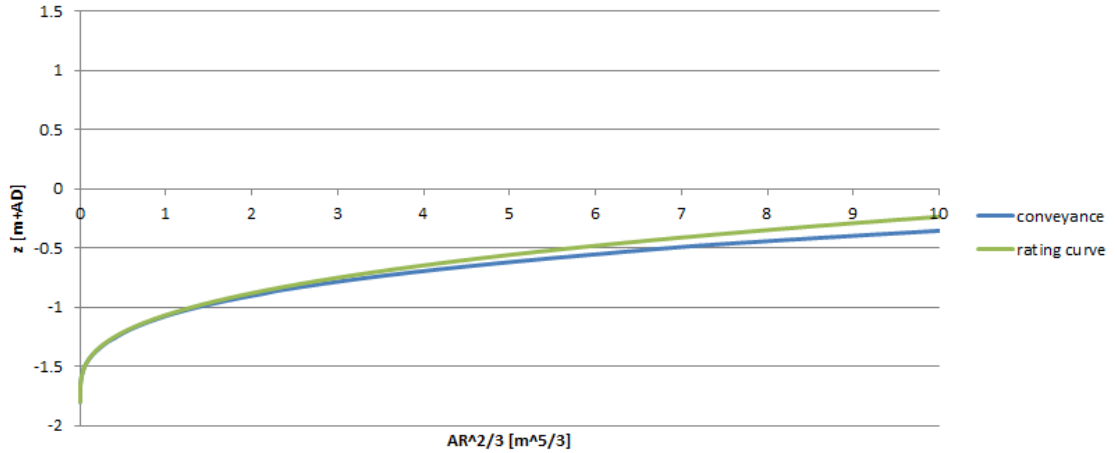

(c) Steven's method: $\tilde{a}(h-h_0)^b$ fitted on Conveyance $AR^{2/3}$, with $\tilde{a}=3.5$, $b=2.9$ and $h_0=1.75$

Figure F.15: Cross-sectional information of Godi DS

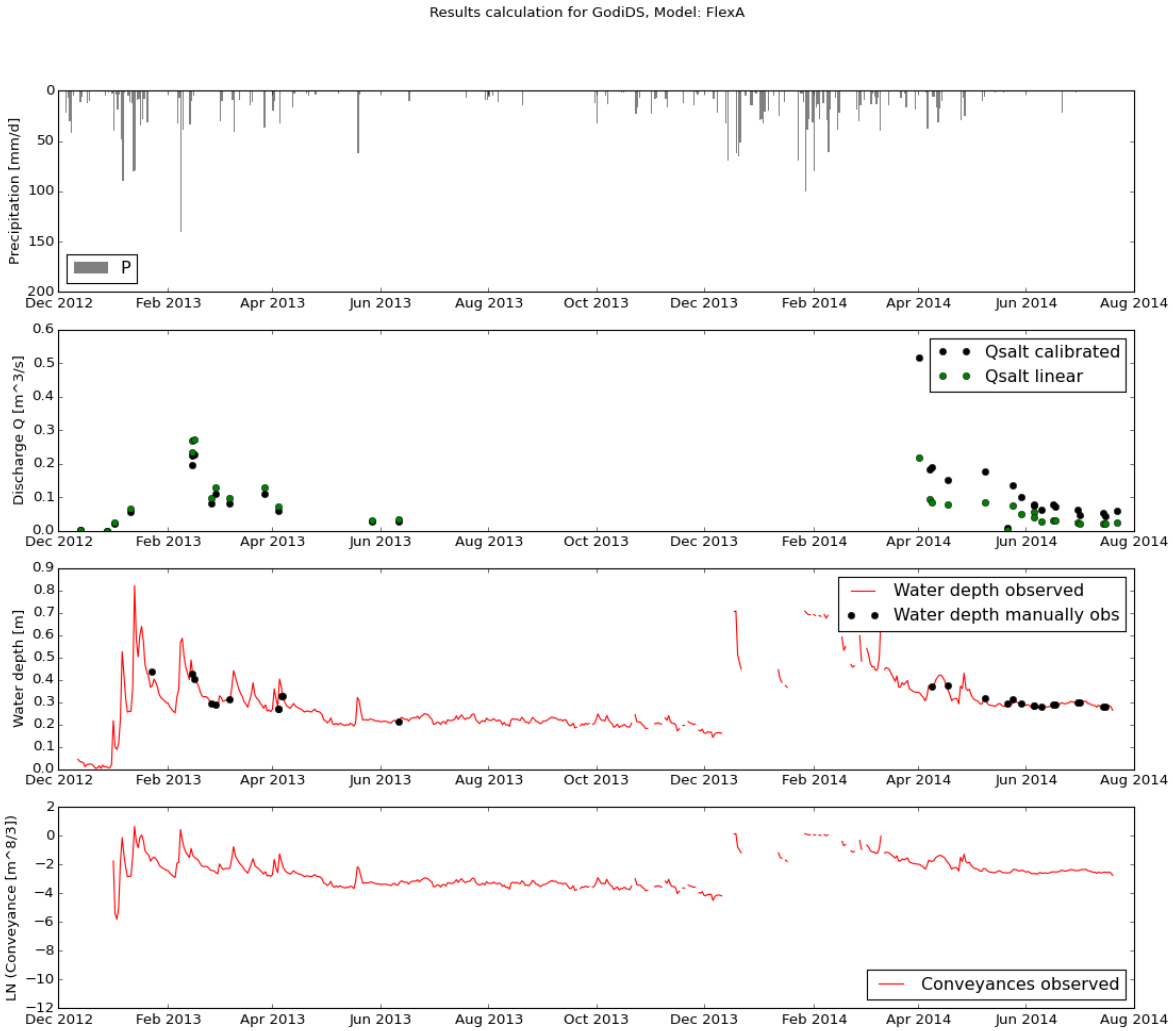

Figure F.16: Observed water depths (manual and divers) and discharges for Godi Downstream Station. Note the date axis are not equal.

F.2.4. GODI INTERMEDIATE STATION (GODIIS)

For discharge measurements at Godi upstream we manually construct a V-notch weir, since the very upstream headwaters are too steep and rocky to have a full developed equilibrium flow. The final construction is shown at Figs. F.17a and F.17b. Using a diver and barometer, we measured water levels relative to the v-notch. With the Kindsvater-Carter equation [51] (eq F.2) the 30min sampled discharges are calculated.

For the installation we used an iron crest, to approximate an official sharp crest best, with an angle of 90^o. Furthermore, we minimized leakage as much as possible by sealing the whole structure in plastic and minimize circumvention of the weir as good as possible. We estimate maximum 10% flow leakage (which passes the weir unmeasured).

Limits of application[1] for the Kindsvarter-Carter equation are:

a The ration h/p should be equal to or less than 1.2;

b The ration h/Bshould be equal to or less than 0.4;

c The head over the vertex of the notch h should not be less than 0.05m nor more than 0.60m;

d The heigth of the vertex of the notch above the bed of the approach channel (p) should not be less than 0.10m;

e the width of the rectangular approach channel should exceed 0.60m;

f the notch angle of a fully contracted weir may range between 25 and 100 degrees. Partially contracted weirs have a 90-degrees notch only;

g The tailwater level should remain below the vertex of the notch.

$$Q = 3.26 C_e \tan\left(\frac{\theta}{2}\right)(H+k)^{5/2} \tag{F.2}$$

Where Q is the discharge over the weir in $[m3/s]$, H the head over the weir in $[m]$, θ the angle of the V-notch $[^o]$, C_e the effective discharge coefficient $[-]$, and k the head correction $[m]$

$$C_e = 0.607165052 - 8.74466963E^{-4}\theta + 6.103933334E^{-6}\theta^2 \tag{F.3}$$

$$k = 0.3048\left[1.44902648E^{-2} - 3.3955535E^{-4}\theta + 3.29819003E^{-6}\theta^2 - 1.06215442E^{-6}\theta^3\right] \tag{F.4}$$

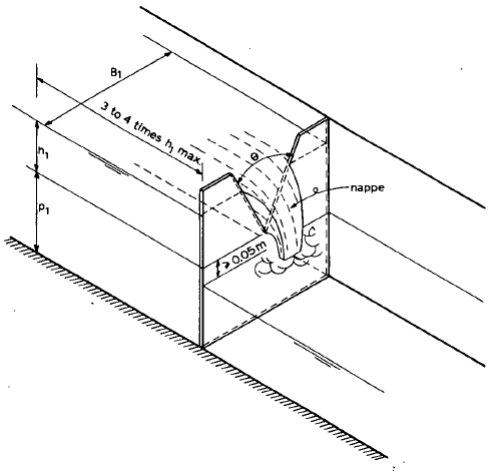

(a) V-notch weir; schematic representation

(b) Handmade 90^o V-notch weir

Figure F.17: Discharge measurements performed at Godi upstream

[1] source http://content.alterra.wur.nl/Internet/webdocs/ilri-publicaties/publicaties/Pub20/pub20-h5.0.pdf chapter 5.2.3

Partially	contracted	weir	Fully	contracted	weir
	h/p	≤ 1.2		h/p	≤ 0.4
	h/B	≤ 0.4		h/B	≤ 0.2
0.05m <	h	≤ 0.60m	0.05m <	h	≤ 0.38m
	p	≥ 0.10m		p	≥ 0.45m
	B	≥ 0.60m		B	≥ 0.90m

Table F.4: Classification and limits of application of V-notch sharp-crested (thin-plate) weirs

angle [°]	90	factor [-]	3.26
C_e [-]	0.577905	p [m]	0.432
k [m]	0.000885	B [m]	1.5
Q [l/s]	**H [m]**	**ratio H/p**	**ratio H/B**
1	0.04809	0.111319	0.03206
2	0.063738	0.147541	0.042492
3	0.075116	0.17388	0.050077
4	0.084385	0.195336	0.056257
5	0.092346	0.213764	0.061564
10	0.122134	0.282717	0.081423
15	0.143795	0.332858	0.095863
20	0.161439	0.373702	0.107626
25	0.176594	0.408783	0.117729
30	0.190021	0.439863	0.126681
35	0.202163	0.467969	0.134775
40	0.213303	0.493757	0.142202
45	0.223636	0.517675	0.14909
50	0.2333	0.540046	0.155533
55	0.2424	0.561112	0.1616
60	0.251017	0.581058	0.167345
65	0.259213	0.600029	0.172808
70	0.267038	0.618144	0.178025
75	0.274535	0.635498	0.183023
80	0.281738	0.65217	0.187825
85	0.288675	0.668229	0.19245
90	0.295371	0.68373	0.196914
95	0.301848	0.698723	0.201232
100	0.308124	0.71325	0.205416
105	0.314214	0.727346	0.209476
110	0.320132	0.741046	0.213421
115	0.325891	0.754377	0.217261
120	0.331501	0.767364	0.221001
125	0.336973	0.780031	0.224649
130	0.342316	0.792397	0.22821
135	0.347536	0.804481	0.231691
140	0.352642	0.8163	0.235094

Table F.5: Lookup table water level above crest [m] and discharge [l/s]. With constants in header row.

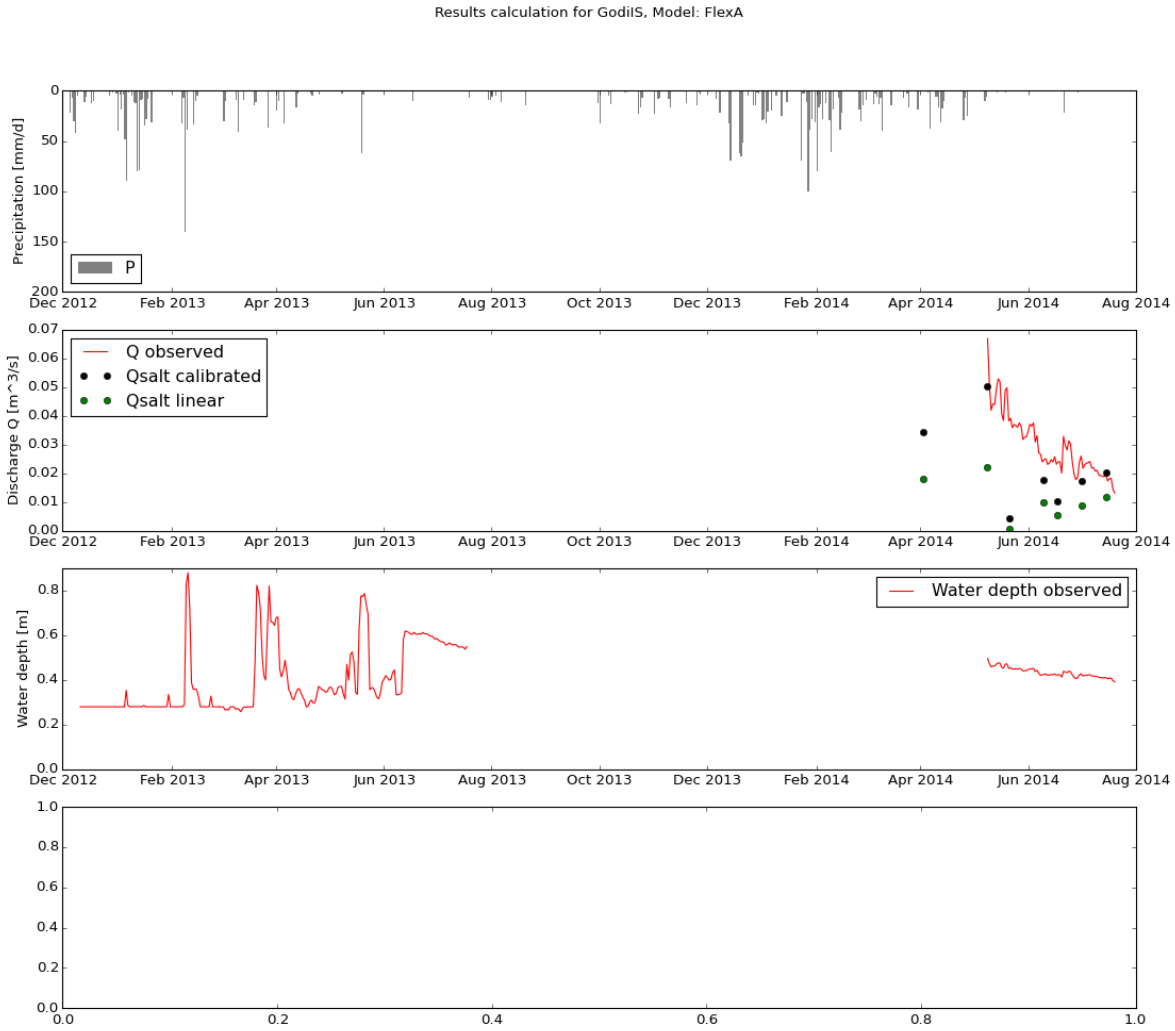

Figure F.18: Observed water depths (manual and divers) and discharges for Godi Intermediate Station. Note the date axis are not equal.

F.2.5. MESSICA DOWSTREAM STATION (MESSDS)

Messica Downstream Station (MessDS) acts as the very most downstream measurement station. At this location, a concrete bridge crosses the River Messica. Only during high flow periods, the bridge is flooded. The rest of the year the water flows through three gates, which acted together as a free-flow construction. Implying that the upstream water levels are not affected by the downstream ones. This gives us the ability to find a flow equation purely based on the upstream waterdepths above sill level. Therefore a barometric and waterpressure diver are installed a little upstream. Since the flow velocity in the upstream pool approaches zero, we assume a horizontal water level (see Figs. F.21 to F.24).

In this study, we conducted salt dilution measurements at this bridge. From a tree a little upstream we throw in a salt dilution sample and in the stream we measured the electronic conductivity change. Question whether the sample was well mixed. This assumption is often not harmed.

Earlier Weemstra *et al.* [7] performed measurements a little upstream from the bridge (Figs. F.19 and F.20). He also placed a waterpressure diver here. Because of the broader and wide character of the River Messica up here, besides the presence of crocodiles and snakes, we found the location less suitable and therefore decided to transfer the measurement location to the bridge. This was even extra motivated by the fact that the measurement location already was dismantled. Therefore we were not able to successfully continue measurements at the same location.

Figure F.19: Measurement statation MessDS as installed from date December 12th, 2012 to August 8th, 2013, in downstream direction

Figure F.20: Measurement location MessDS in upstream direction

	Gate 3	Gate 2	Gate 1
Width gate [m]	0.95	0.95	0.86
Height sill us gate [m-ref]	-1.04	-0.86	-0.79
Height sill ds gate [m-ref]	-1.24	-1.38	-1.02

Table F.6: Dimensions gates bridge Messica Downstream

Figure F.21: Free-flow (spillway) bridge Messica downstream

Figure F.22: Rapid downstream of bridge, just upstream of a waterfall (starting at the rocks downstream of the rapid)

Figure F.23: Gates upstream bridge, observe the water level curvation around the gates

Figure F.24: Opening bridge gates, observe the orientation angle of 27^o

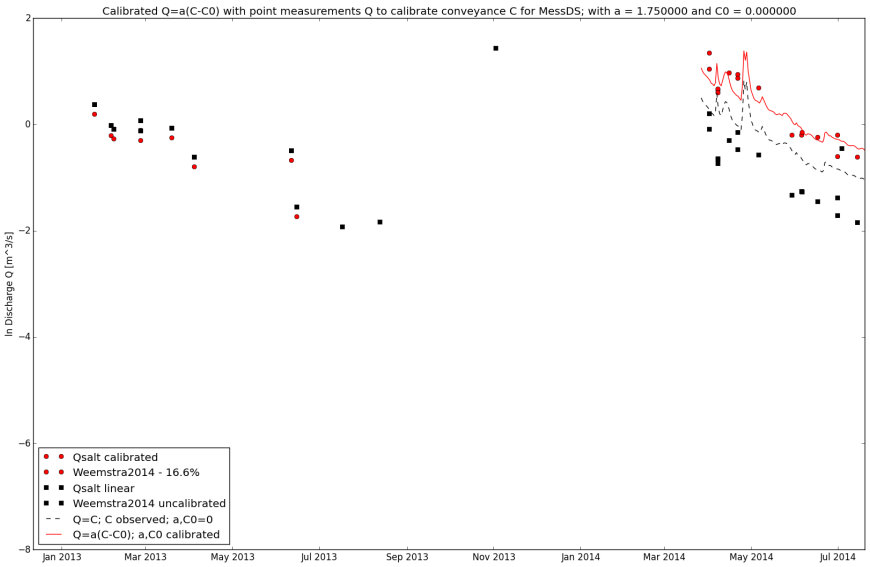

Figure F.25: Conveyance tuned to discharge measurements for Mess DS, $\bar{a} = 1.75$.

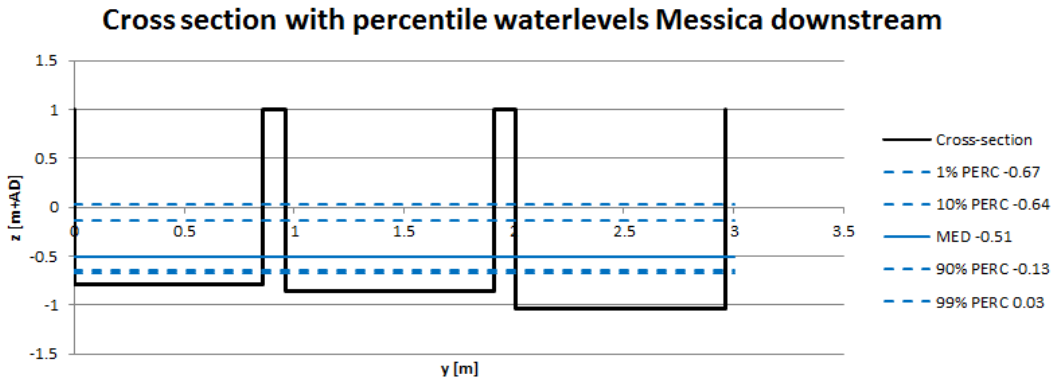

(a) Cross-section Messica DS relative to reference point

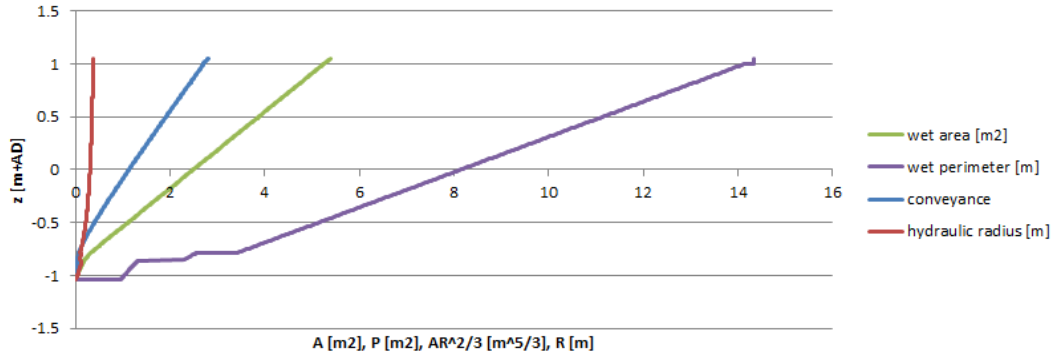

(b) Messica DS: Area, Perimeter, Hydraulic Radius and Conveyance as function of the depth

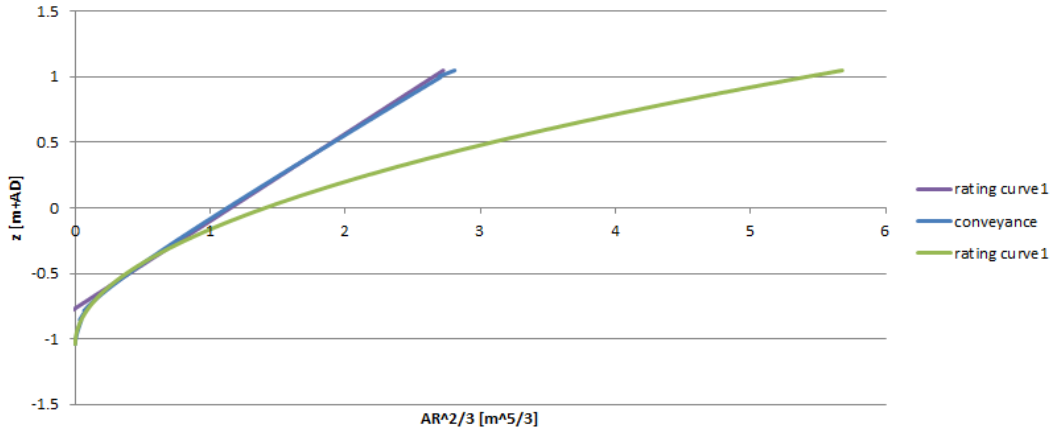

(c) Steven's method: $\tilde{a}(h-h_0)^b$ fitted on Conveyance $AR^{2/3}$; two rating curves used
RC1 with $\tilde{a}=1.3$, $b=2$ and $h_0=1.04$
RC2 with $\tilde{a}=1.5$, $b=1$ and $h_0=0.5$ with a horizontal shift of $+0.4m$

Figure F.26: Cross-sectional information of Messica DS

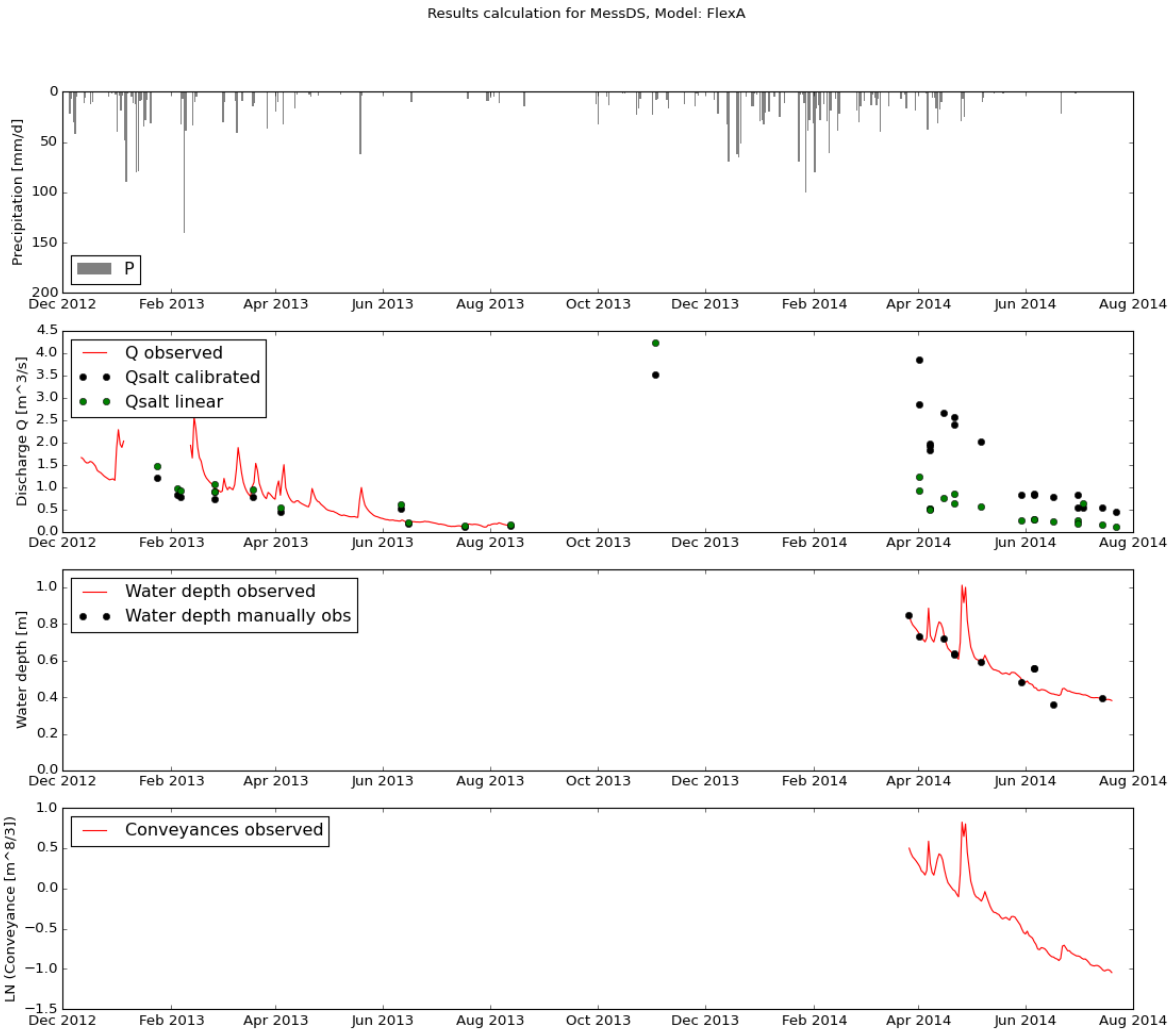

Figure F.27: Observed water depths (manual and divers) and discharges for Messica Downstream Station. Note the date axis are not equal.

F.2.6. MESSICA INTERMEDIATE STATION (MESSIS)

Messica Intermediate Station (MessIS) measures the upstream inflow of the River Messica. Earlier Holsteijn [10] and Weemstra *et al.* [7] performed already measurements at this point, all be it just downstream at a much wider cross-section. Therefore we were only able to use the salt dilution measurements, and their derived discharge relation[7], but we could not apply their waterdepth measurements in our conveyance method. Besides, the measurement station was already dismantled at the time we arrived, so it was impossible to continue their measurements.

The flow at the natural cattle-crossing is relative fast, which give extra turbulence and water level set-up around the reeds. It is arguable whether the uniform flow assumption holds at this location.

Due to the upstream pools, salt dilution measurement were hard to perform. Common problem is that salt dilution getting stuck in the pool.

A little downstream is the confluence of the headwater Ruaga, which we also measured. The confluence might give extra water level set-up and backwaters during peak flows. However, during low flow this does not occur.

Figure F.28: Diver located at a crossing, observe the strong currents and water level slope. David (at the right side) is standing next to the diver.

Figure F.29: Looking downstreams from the diver location at Messica upstream

Figure F.30: Looking upstreams from the diver location at Messica upstream

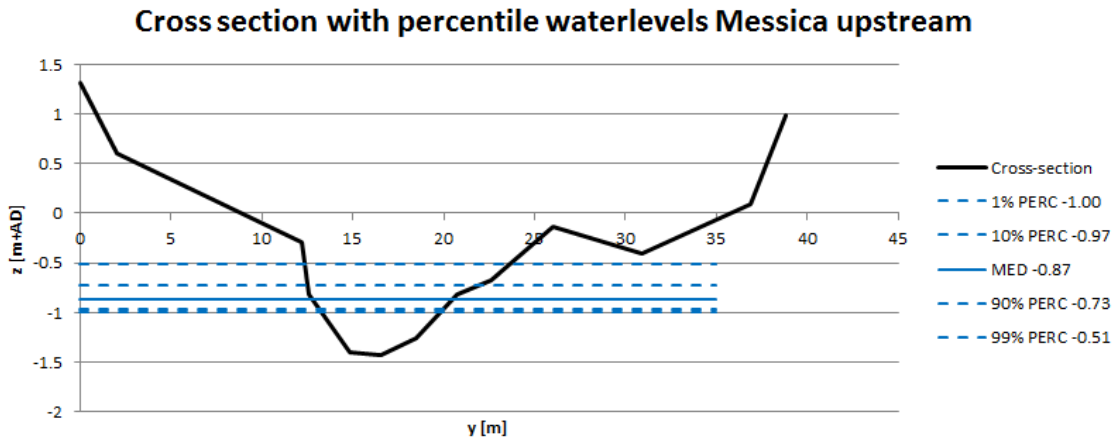

(a) Cross-section Messica IS relative to reference point

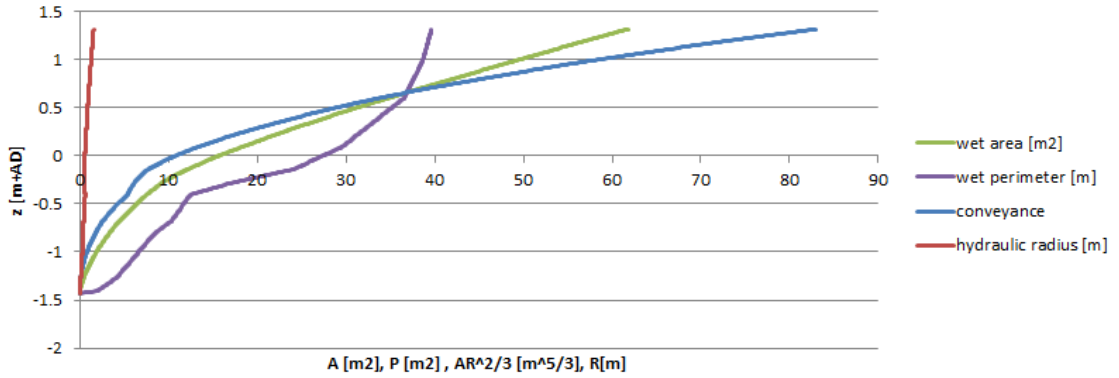

(b) Messica IS: Area, Perimeter, Hydraulic Radius and Conveyance as function of the depth

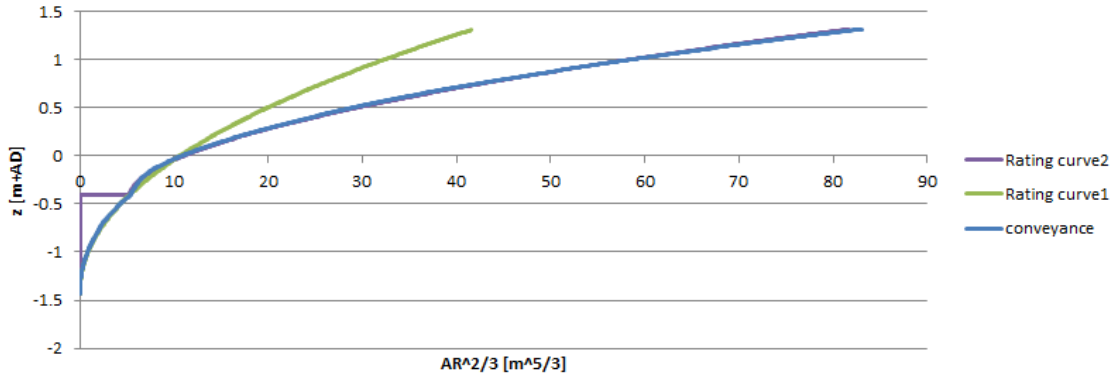

(c) Steven's method: $\tilde{a}(h-h_0)^b$ fitted on Conveyance $AR^{2/3}$; two rating curves used
RC1 with $\tilde{a}=3.2$, $b=4.1$ and $h_0=0.935$
RC2 with $\tilde{a}=28.5$, $b=1.8$ and $h_0=0.41$ with a horizontal shift of $+5.3m$

Figure F.31: Cross-sectional information of Messica IS

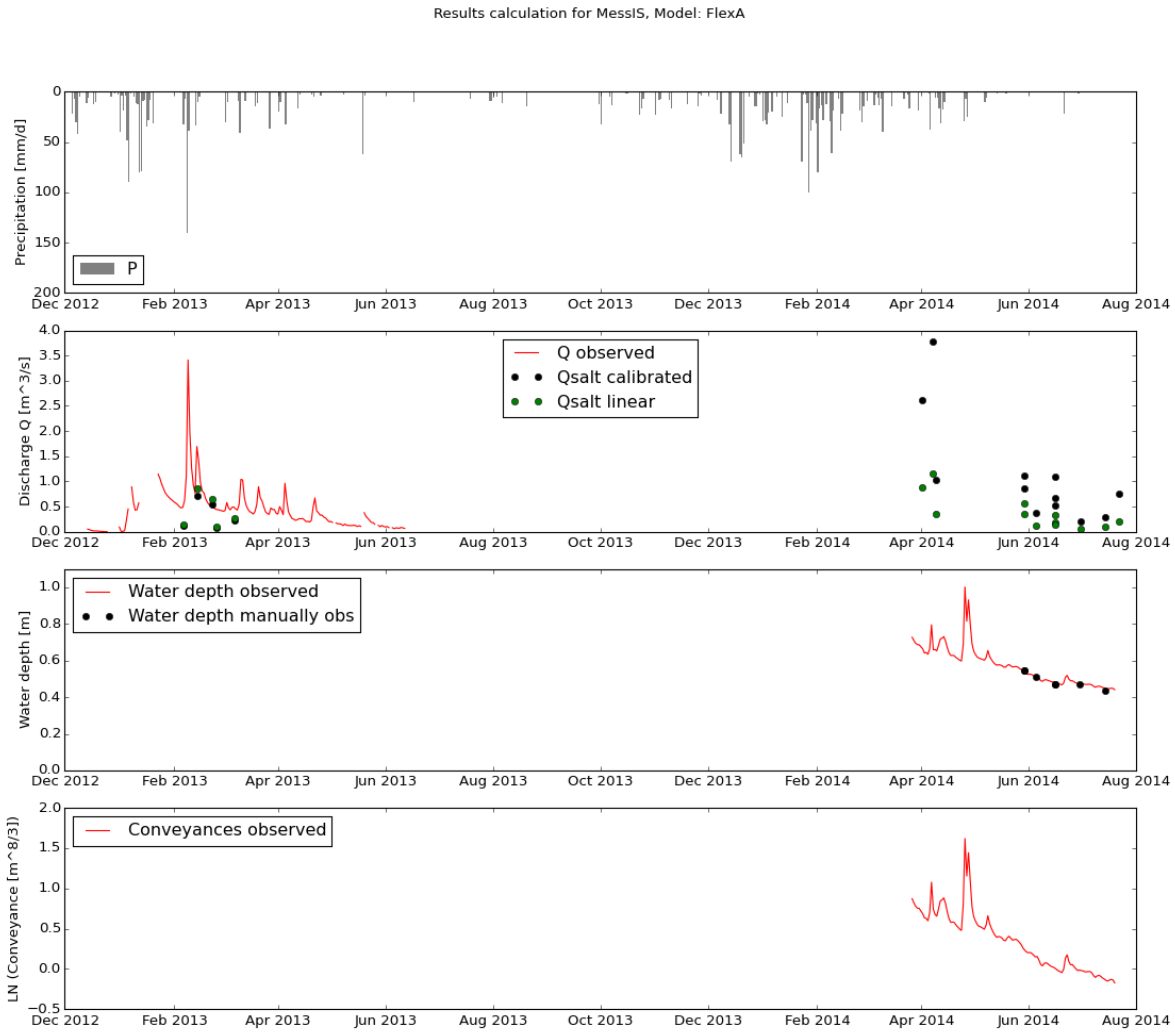

Figure F.32: Observed water depths (manual and divers) and discharges for Messica Intermediate Station. Note the date axis are not equal.

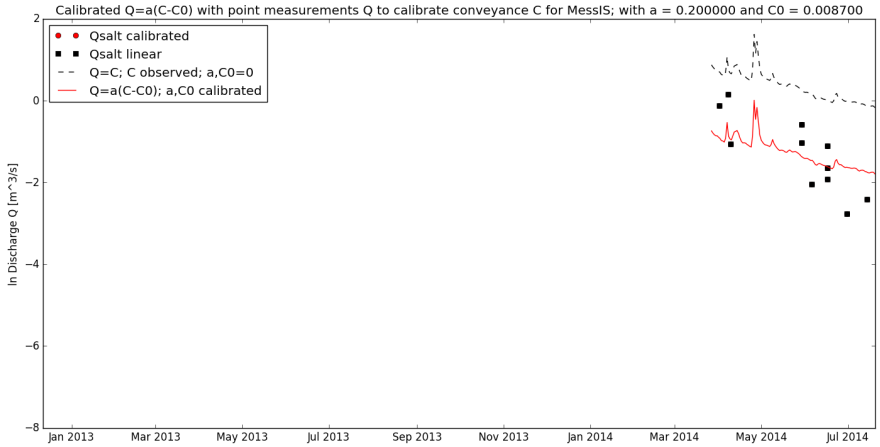

Figure F.33: Conveyance tuned to discharge measurements for MessIS, $\bar{a} = 0.2$.

F.2.7. RUAGA DOWNSTREAM STATION (RUAGADS)

For Ruaga Downstream Station(RuagaDS) measurements are performed at two different location. First we did some measurements upstream of a large rock, which behaves as a natural weir. However, the water level was strongly influenced by this rock and it was not possible to derive any $Q - h$ relation for it. So we moved a little downstream and placed the diver in a free-flowing stream full of reeds, see Figs. F.34 and F.38.

During our measurements we assume equilibrium flow, but during high flows we expect positive backwater curves due to the downstream conjunction with the River Messica.

Figure F.34: Measuring cross sections along and perpendicular to the river Ruaga

Figure F.35: Diver at Ruaga, placed at a crossing between the reeds

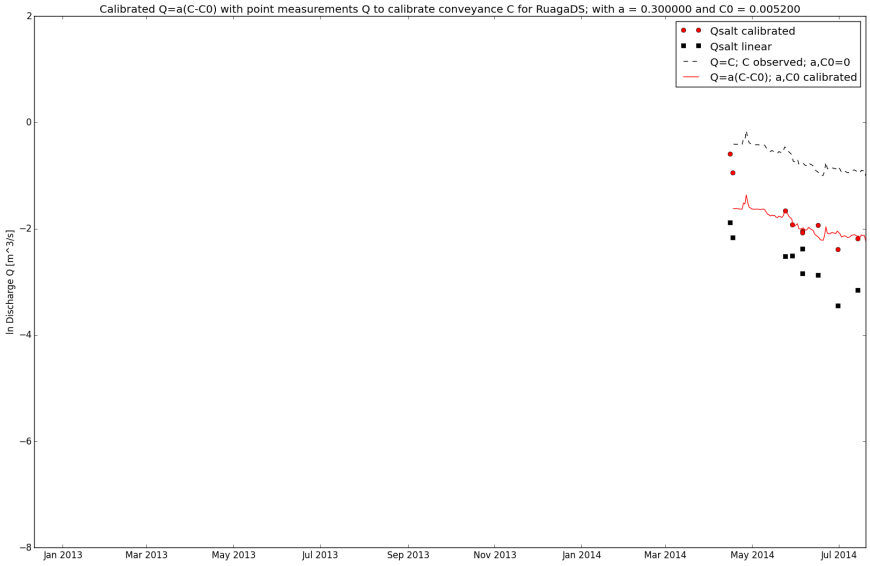

Figure F.36: Conveyance tuned to discharge measurements for Ruaga DS, $\bar{a} = 0.3$.

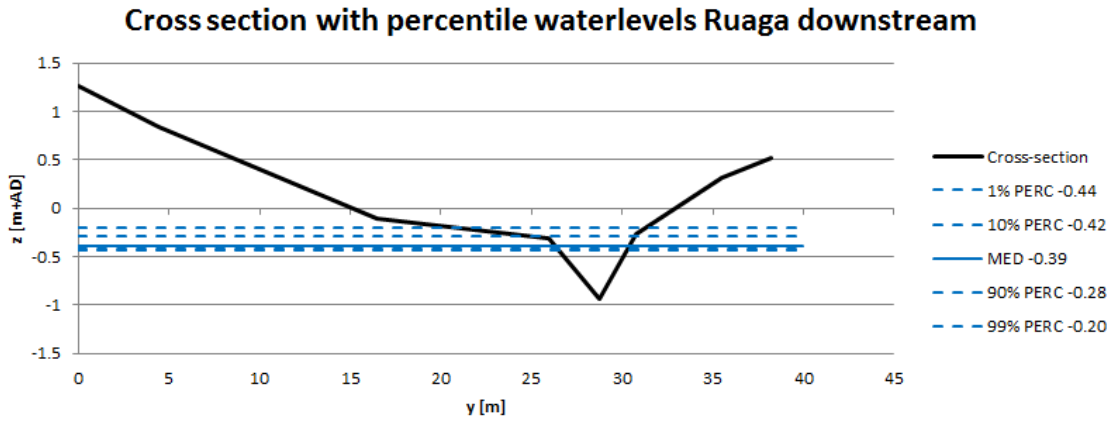

(a) Cross-section Ruaga DS relative to reference point

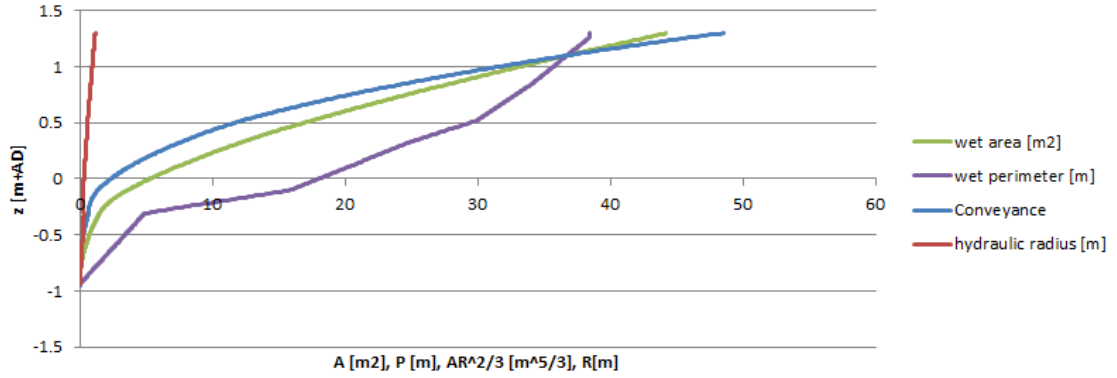

(b) Ruaga DS: Area, Perimeter, Hydraulic Radius and Conveyance as function of the depth

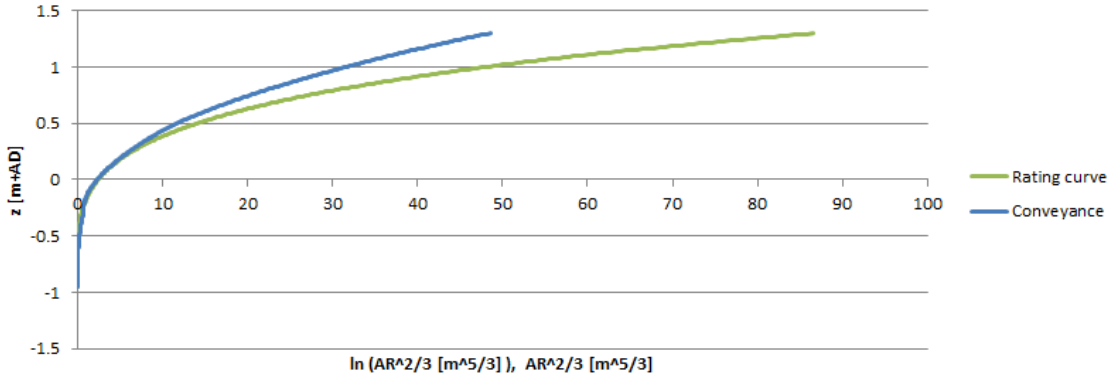

(c) Steven's method: $\tilde{a}(h-h_0)^b$ fitted on Conveyance $AR^{2/3}$. with $\tilde{a}=3.2$, $b=4.1$ and $h_0=0.935$

Figure F.37: Cross-sectional information of Ruaga DS

Figure F.38: Overview of the floodplains alongside the Ruaga near the diver location

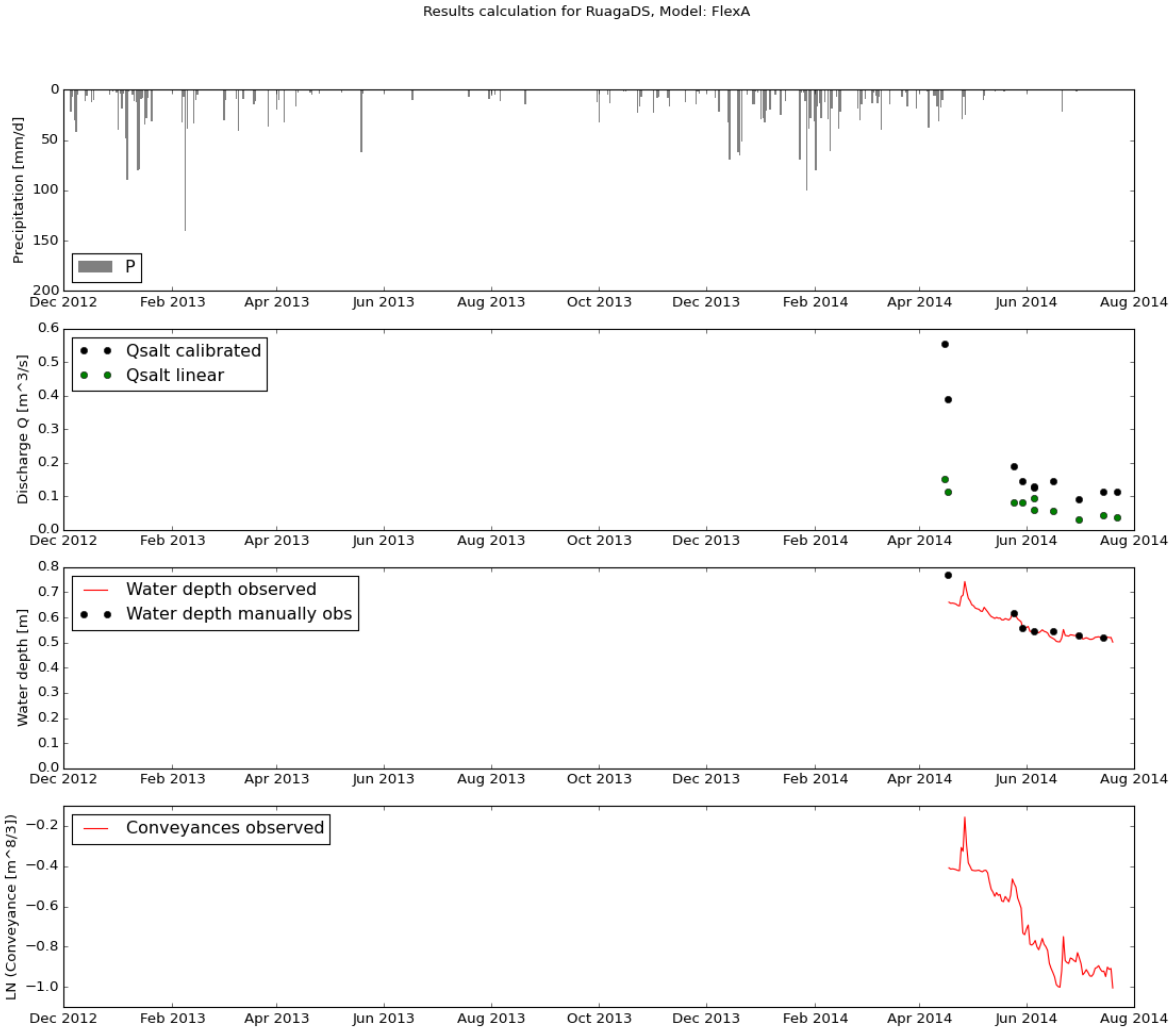

Figure F.39: Observed water depths (manual and divers) and discharges for Ruaga Downstream Station. Note the date axis are not equal.

F.3. OTHER MEASUREMENTPOINTS

Next to the previous described measurementpoints, measurements are performed along the river stretches. Near sources, conjunctions and confluences. Fig. I.1 gives overview of all measurement location along the streams.

At these locations the following measurements are performed:

- Salt dilutions measurements to obtain discharges, in case of conjunctions or confluences two of the three stretches are gauged, the third can then be derived.
- pH, EC and Temperature values obtained with a multimeter (See App. D). These values can serve as tracer.
- Water samples are taken for Isotope analyses. The latter are not taken further into account in this research, since the timespan is too short (approximately 4 months). Two years or more is highly preferred (interview Dr. M. Hrachowitz, TU Delft).

G

INFORMATION AVAILABLE IN DATABASES

1.) explain general set up databases. 2.) Give per database an overview of the available data.

G.1. MEASUREMENTS.ACCDB

The validated but unaltered data is stored in the database Measurements.accdb Microsoft Access database.

Barometers	Type
Id	Long integer
SerieID	Text
Date_time	Date/time
Druk_cm	Double precision
Temp_oC	Double precision

Table G.1: Overview table Barometers in Measurements.accdb

Chipoletti	Type
Id	Long integer
Datum	Date/time
p	Double precision
h	Double precision
Q	Double precision

Table G.2: Overview table Chipoletti in Measurements.accdb

CrossSections	Type
UID	Integer
CrossID	Text
h	Double precision
A_wet	Double precision
P_wet	Double precision
Conveyance	Double precision

Table G.3: Overview table CrossSections in Measurements.accdb

Diver_metadata	Type
Id	Long integer
Serienumber	Text
SerieID	Text
Type Measurements	Text
Altitude_GPS	Double precision
Date_from	Date/time
Date_to	Date/time
Time_interval	Text
Location	Text
CrossSection	Yes/No
CrossSectionID	Text
Alt_diver_(m-ref)	Double precision
Alt_top_us_wlvlstick_(m-ref)	Double precision
Altitude top ds wlvlstick (m-ref)	Double precision
Wlvl during readout (m-ref)	Double precision

Table G.4: Overview table Diver_metadata in Measurements.accdb

FAO_new_LocClim	Type
Id	Long integer
Date	Date/time
P	Double precision
Ep	Double precision
Tmin	Double precision
Tmean	Double precision
Tmax	Double precision

Table G.5: Overview table FAO_new_LocClim in Measurements.accdb

Isotopes	Type
SampleID	Text
Date	Date/time
Time	Date/time
Location	Text
DH_permil	Double precision
DH_STDEV_permil	Double precision
O18_permil	Double precision
O18_STDEV_permil	Double precision
Description	Text
Remarks sample quality	Text
Remarks general	Text

Table G.6: Overview table Isotopes in Measurements.accdb

Precipitation	Type
Id	Long integer
UID	Text
Datum	Date/time
Prec_Depth	Double precision
Comment	Text

Table G.7: Overview table Precipitation in Measurements.accdb

SaltDilutions	Type
Id	Long integer
UID	Text
time	Date/time
EC	Double precision
Remark	Text

Table G.8: Overview table SaltDilutions in Measurements.accdb

SoilMoisture	Type
Id	Long integer
UID	Text
Description	Text
Class	Text
Landuse	Text
Soil Moisture #1	Double precision
Soil Moisture #2	Double precision
Soil Moisture #3	Double precision
Soil Moisture AVG	Double precision
Date	Date/time
Time	Date/time
Remarks	Text

Table G.9: Overview table SoilMoisture in Measurements.accdb

Temperature	Type
Id	Long integer
Date time	Date/time
Temperature	Double precision

TippingBuckets	Type
Id	Long integer
UID	Text
Date time	Date/time
Prec_cum	Double precision

Table G.10: Overview table Temperature in Measurements.accdb

WaterPressure	Type
Id	Long integer
SerieID	Text
Date_time	Date/time
Druk_cm	Double precision
Temp_oC	Double precision

Table G.11: Overview table WaterPressure in Measurements.accdb

G.2. MODELINPUT.ACCDB

The validated and modelinput ready data (without resampling) is stored in the database ModelInput.accdb Microsoft Access database. This database is read out with the python script Toolbox.py. See App. M

Altitudes	Type
Id	Long integer
UID	Text
AREA	Double precision
AVG_catchment	Double precision

Table G.12: Overview table Altitudes in Modelinput.accdb

Waterlevels	Type
ID	Long integer
Date	Date/time
UID	Text
Wlvl us stick m-top	Double precision
Wlvl ds stick m-top	Double precision
Wlvl diver m-top	Double precision
Diver pile top m+ref	Double precision
W_lvl us stick m+ref	Double precision
W_lvl ds stick m+ref	Double precision
W_lvl_diver m+ref	Double precision
Reader	Text
ManualWaterlevels	Double precision

Table G.13: Overview table Waterlevels in Modelinput.accdb

Evaporation	Type
Id	Long integer
Datetime	Date/time
Hamon_+08_x115	Double precision
Hargreave	Double precision
Hamon	Double precision
FAO	Double precision

Table G.14: Overview table Evaporation in Modelinput.accdb

EC,PH,T,Q	Type
UID	Long integer
MeasID	Text
Title	Text
River	Text
Description location	Text
Location	Text
Date	Date/time
Operator	Text
Digitized_by	Text
Number_obs_errors	Double precision
Device	Text
starttime	Date/time
endtime_real	Date/time
Registrated_time_interval	Date/time
Timestep	Date/time
nTimesteps	Double precision
C_river_uS	Double precision
T_river_oC	Double precision
pH_river	Double precision
C_s_uS	Double precision
T_s_oC	Double precision
pH_s	Double precision
V_s_m3	Double precision
M_salt_guess_kg	Double precision
Q_river_guess_m3s	Double precision
Starttime_saltwave	Date/time
Endtime saltwave	Date/time
C_bckgrnd_50perc	Double precision
C_bckgrnd_5perc	Double precision
C_bckgrnd_95perc	Double precision
Wlvl_us_refpoint_m-top	Double precision
Wlvl_ds_refpoint_m-top	Double precision
Wlvl_diver_m-top	Double precision
Salt dilution measurement?	Yes/No
Q_m3s	Double precision
Device_cal_const_EC	Double precision
Device_cal_const_a	Double precision
Device_cal_const_b	Double precision
Device_cal_const_c	Double precision
Reliable result?	Yes/No
M_salt_calc_kg	Double precision
Corr_const_C_s	Double precision
Corr V_s	Double precision
Corr Mass Calc	Double precision
Corr Timestep	Double precision
Max_EC value measurement	Double precision
Ratio Max EC-Background_50perc	Double precision
Remarks	Text
Bucket discharge	Yes/No
Qlin_m3s	Double precision
Field1	Text

Table G.15: Overview table EC,pH,T,Q in Modelinput.accdb

Precipitation	Type
Id	Long integer
UID	Text
Datum	Date/time
Prec_Depth	Double precision
Comment	Text

Table G.16: Overview table Precipitation in Modelinput.accdb

Qseries	Type
Id	Double precision
UID	Text
date time	Date/time
Diver	Double precision
Baro	Double precision
Waterdepth	Double precision
conveyance	Double precision
Q	Double precision
Div2Wlvl	Double precision
Waterdepth_measured	Text
Q_Daniel_MessDS	Double precision

Table G.17: Overview table Qseries in Modelinput.accdb

StreamNetwork	Type
Id	Long integer
UID	Text
Feed_into_1	Text
Feed_into_2	Text
Length	Double precision

Table G.18: Overview table StreamNetworks in Modelinput.accdb

Subcatchment	Type
Id	Long integer
UID	Text
AREA	Double precision
Hillslope	Double precision
Terrace	Double precision
flat_wetland	Double precision
sloped_wetland	Double precision
LU Area	Double precision
LU Wetland	Double precision
LU Grass_Crop	Double precision
LU Forest	Double precision
Hill_800l	Double precision
Hill_800h	Double precision

Table G.19: Overview table Subcatchment in Modelinput.accdb

G.3. HRU.SHP

The landscape data, like altitude, slope, HAND etc are stored in a shape file, based on the resolution of the DEM rasters [35]. Every raster is converted to a single shape. This gives the user optimal flexibility to design own HRUs for every catchment. We used the class clsHRU (App. M) to read in this data. An GIS program can be used to alter the shape information.

Name	Type
POINTID	Integer
HAND20	Long
slop	Long
dist2str	Long
x	Long
y	Long
DEM	Long
FlowAcc	Long
GlobCover	Long
FlowLength	Long
Outlet	Text
UID	Text
Catchment	Text
HAND40	Long
HAND50	Long

Table G.20: Overview data in shape file HRU.shp

H

ESTIMATED DISCHARGE, BUDYKO CURVE

The Budyko curve [52] is an empirical relation to estimate yearly averaged discharge from a catchment based on long year precipitation and potential evaporation time series. However, its main assumption concerns the no storage change assumption. Since we encounter overyear groundwater storage effects, the budyko curve does not entirely hold for our situation. Furthermore, time series are rather short (September 2011 to August 2014), and potential evaporation is estimated. So all in all, the outcomes should be hold for a rough estimation of the discharge (coefficient).

The Budyko framework is based on the waterbalance Eq. H.1.

$$\bar{Q} + \bar{E_a} = \bar{P} \tag{H.1}$$

Dividing all terms by the precipitation P results into Eq. H.2.

$$\frac{\bar{Q}}{\bar{P}} + \frac{\bar{E_a}}{\bar{P}} = c + \frac{\bar{E_a}}{\bar{P}} = 1 \tag{H.2}$$

where c is the run-off coefficient.

$$\bar{E_a} = \bar{P}\left(1 - exp\left(-\frac{\bar{E_p}}{\bar{P}}\right)\right) \tag{H.3}$$

Test the average discharge from the catchment with Budyko's [52] empirical relation, see formula H.3 and figure H.1.

The actual evaporation can be estimated with formula H.3. Now applying formula H.2, we can calculate the run-off coefficient and, doing so, estimate the yearly average discharge. Assuming that the storage change is minor (which is basically not true).

Year	P_{David}* [mm/y]	E_{pot}** [mm/y]	E_{actual} [mm/y]	c [-]	Q_{est} [mm/y]
jul 2011 - jun 2012 ***	1027	1510	791	0.23	236
jul 2012 - jun 2013	1483	1529	954	0.36	529
jul 2013 - jun 2014	1853	1491	1024	0.45	829
jul 2012 - jun 2014	**1668**	**1510**	**993**	**0.40**	**674**
Weemstra *et al.* [7]	1224	1462	853	0.30	371
Chimoio					

Table H.1: Budyko estimated actual evaporation E_a, run-off coefficient c and discharge Q
* Precipitation depth measured at Davids location (altitude 878 m+AD)
** Potential evaporation constructed from FAO and Hamon
*** First precipitation measured from September 2011 onwards

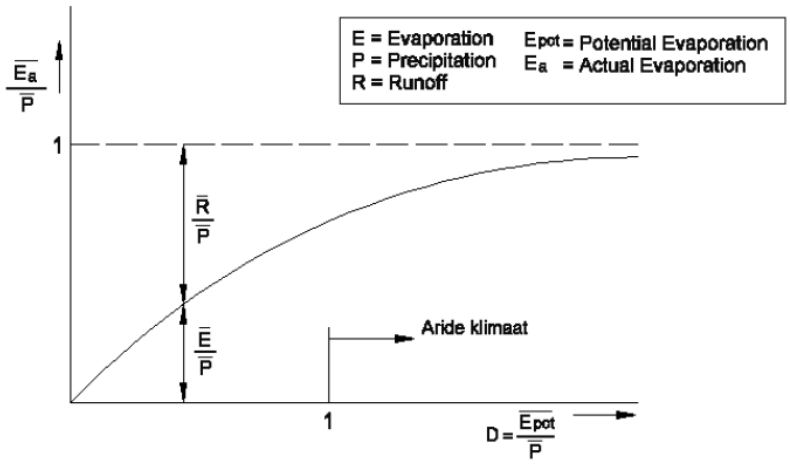

Figure H.1: Budyko's empirical relation between yearly averaged evaporation, precipitation and discharge

Table H.1 presents the yearly figures as well as the yearly averaged figures for the catchment combined with Chimoio weather station's long term evaporation observations (about 50 km westwards and 200 m lower).
A run-off coefficient of about 0.4 seems to be a quite large number. According to the Budyko curve, figure H.1 this region is close to an arid climate. This does not correspond with our perception based on field observations.
Without concerning the altitude effects, the average discharge for a (sub)catchment is about 1.85 mm/day. In case of Godi downstream (1000 ha) this results in a daily averaged discharge of $0.21 m^3/s$.
Weemstra *et al.* [7] estimated the yearly rainfall, potential evaporation, actual evaporation and discharge to be respectively 1224, 1462, 949 and 266 mm/year. Note that the FAO derived in Manica (30 km east of Messica) the following yearly rainfall statistics (see App. C.1): dry (713 mm/a), wet(1314 mm/a) and an average year (1014 mm/a). July 2011 to June 2012 can according to this figures be classified as a average year, where the years 2013 and 2014 belong to the (extreme) wet years. A real dry year is according to these statistics not observed in Messica catchment.

To conclude, the Budyko framework can be hold best as a rough estimation of the yearly runoff which is in the order of 20 to 40%. However, since overyearly storage is one of the area characteristics, the whole framework is not really applicable.

I

HRU'S AND (SUB-)CATCHMENTS

This Appendix gives some background information about the derivation of the (sub-)catchment's and about the HRUs (Hydrologic Response Units).

I.1. SUBCATCHMENTS

The subcatchments are based on the (main) measurement locations, e.g., Godi Downstream Station or Chirodzo Intermediate Station. These main stations are set as a pour point in an ArcGIS toolbox Hydrology, with this toolbox and a Digital Elevation Map [1] (DEM) the (sub-)catchment borders are determined. A more detailed description of the methodology can be found at this website [2].

A further catchment refinement is made based on measurements locations in the field. At these locations, samples, EC values and discharges are obtained. We coded all these points, and named the direct upstream catchment to the outlet name. These names, e.g.,Godi_10_1_ds_in, are based on the following principles and are shown in Fig. I.1:

- Name of the main stream (for example Godi)
- Conjunction / Bifurcation number (where measurements are performed) started upstream to downstream (1 to 10)
- Sub-number of branch, if continuous reach then no number, if connection between two or three branches then (1 to 4)
- Differentiation between downstream or upstream oriented of the point and inflow or outflow

Since, GIS analyses are performed on polygon base, and thus on the subcatchment base we have to aggregate upstream catchments to obtain the properties or inputs for the more downstream catchments. Therefore we summarized and/ or averaged the set of catchments for the more downstream ones. For example, Godi_10_1_ds_in is a ensemble of 'Godi'-named subcatchments in Fig. I.1. The results of this aggregations for FlexC and D are given in the tables hereafter.

I.2. HRUS

This appendix provides a support for the different Hydrological Response Units (HRU). The rainfall runoff model concepts Flex A to D have an increasing HRU complexity. While FlexA consists of a lumped approach of the catchment, FlexB, -C and -D distinguish multiple configurations of hydrological processes, which we link to landscape characteristics and landuse. Maps I.5 and I.6 show respectively the DEM and the slopes. Clearly observable the steep hill slopes from the Inselbergs, and the gently sloped surrounding areas.

[1] Aster2 Global Digital Elevation Map [35]
[2] http://www.readbag.com/lib-virginia-scholarslab-resources-class-foresthydro-foresthydroexercise checked at 12-10-2015

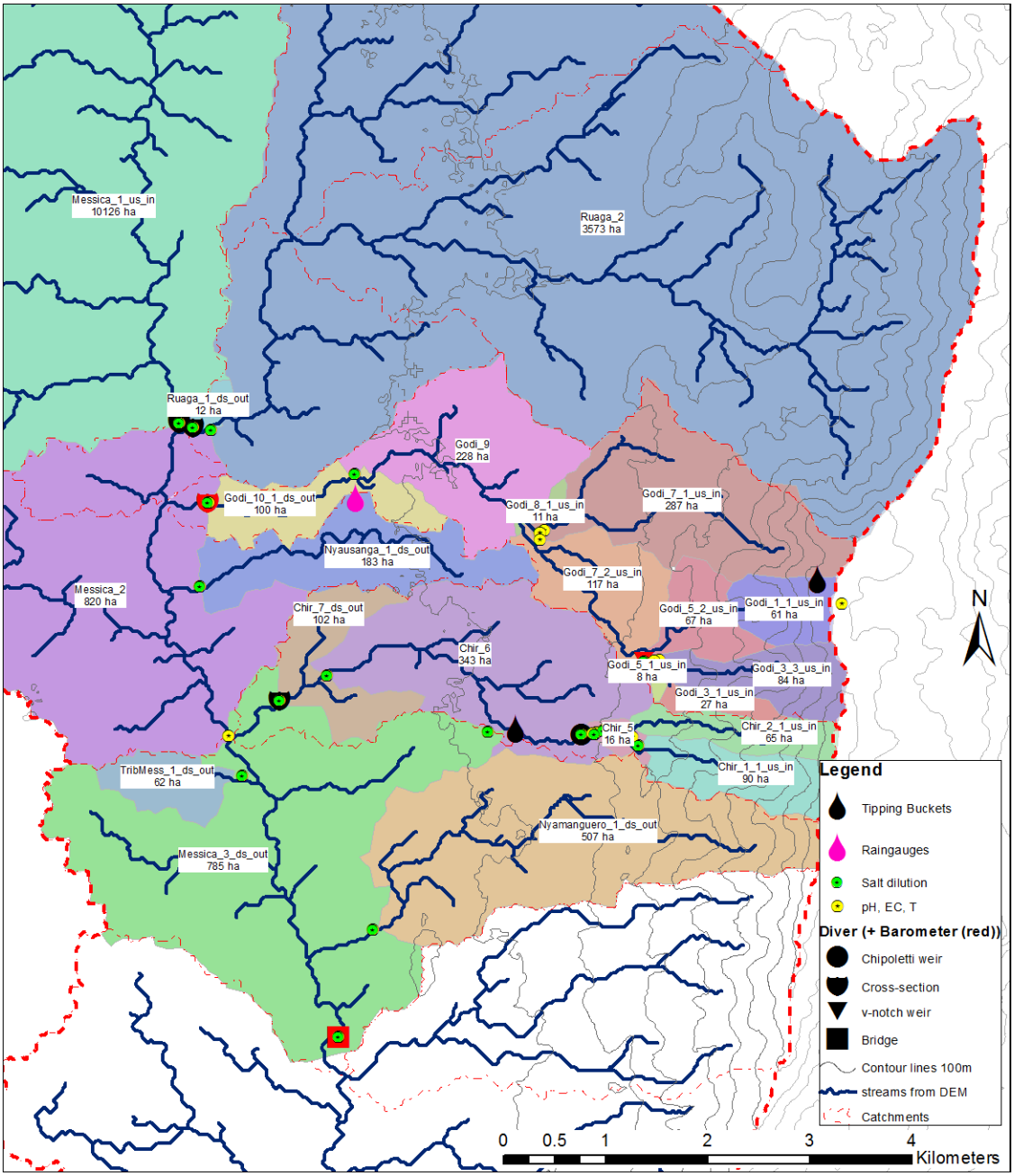

Figure I.1: Areas (sub-)subcatchments including measurement locations of Salt dilutions, pH, EC and Temperature

I.2.1. SET-UP INPUT FILES

Methodology to derive the HRUs. The input grids Globcover and DEM are clipped with Messica's watershed including a 3km additional buffer. This watershed is based on the DEM map. The buffer is meant to incorporate the east slope infiltration of the Inselberg.

From the DEM we derived the slope values. Furthermore we derived the Flow Direction, Flow Accumulation, Flow Length, Watersheds with the Arcmap Hydrology Toolbox ©. By means of a matlab script the HAND value and the flow distance from every individual cell to the nearest drainaged level is determined [25, 29].

The DEM raster file information is transfered to center points for every raster cell. We extract the values of all the separate grid points to this point shape file. After loading this file in a Pandas ©DataFrame in Python ©we can easily vary threshold values, e.g.,HAND and Slope, to assemble HRU units. See Appendix G for information in the HRU.shape file.

The stream threshold are set to FlowAccumulation >=20,40 and 50. This implies that a stream springs if more than 20, 40 or 50 grid cells (with an area of 30x30m2) contribute to that point.

I.2.2. DETERMINING THRESHOLDS

Threshold values for flow accumulation and HAND are very important. However, very difficult to derive. Reasons:

- All raster analyses are based on DEM map. This map is quite accurate, but on the smallest scale there are deviations between the observed deepest points (stream courses) and those derived from the DEM.
- Available Aster2 grid is an integer grid (so containing only integer values from elevations and no decimal numbers).

Since the stream courses cannot be derived very accurate from the DEM, it is hard to check whether the general contribution of wetland derived from the DEM is in line with our expectations. Furthermore, since the HAND values are also in one meter accurate, the degrees of freedom to tune the raster data to the HRU perception are very limited.

Certain information sources provide input for a further differentation of HRUs:

- Head Above Nearest Drainage Level [18, 29]
- Slopes (derived from DEM) [18, 29]
- Landuse information [20, 32]
- Mapped irrigation canals [9, 11]
- Own field observations [This research]

Gharari *et al.* [29] showed that differentiation between (sloped and flat) Wetlands, Hill slopes and Plateaus lead to a more sophisticated rainfall runoff description of the catchments. He distinguished between the three units based on threshold values for the HAND and the Slopes, see Table I.1. These values are also successfully applied in other studies in (very) different parts of the world.

	HAND < 5.9m	HAND > 5.9m
Slope < 12.9%	Flat Wetland	Plateau/ Terrace
Slope > 12.9%	Sloped Wetland	Hill slopes

Table I.1: Hydrological Response Units Wetland, Terrace/Plateau and Hill slopes with belonging threshold values for HAND and hill slope [29]. Warp catchment, Luxembourg, Europe

In this study we applied these values also and compared these to our own field observations, in order to check the validity of this assumption. The first calibration runs are based on these values. The final calculations, however, are performed on different thresholds.

I.2.3. COMPARE HRUS WITH OWN FIELD OBSERVATIONS

With HAND=5.9m, FlowAccumulation = 20 x 30*30m2 and hill slope = 12.9%, we compared the following things:

- Compare location wetlands with streams derived from DEM, mapped streams by [9, 11] and own field observations mapped with hand held GPS device.
- Compare location forests and grass lands with GlobCover
- Indicate irrigated fields based on mapped irrigated plots [This study] and mapped irrigation canals [9, 11].
- Give location surfacing Caprocks based on own observations.

Wetlands. Fig. I.2 show that the derived wetlands based on thresholds in Table I.1 overlaps wetlands and streams well. However, large parts are blue. It is not very likely that these areas are all wetlands

Saturated excess overland flow (SOF) are the dominant hydrological process for wetlands. Savenije [16] describes them as areas where slopes are modest, open water is near and hece, groundwater levels are close to surface, with a small soil moisture storage capacity. After rainfall events, the area will become saturated and hence saturated excess overland processes will occur.

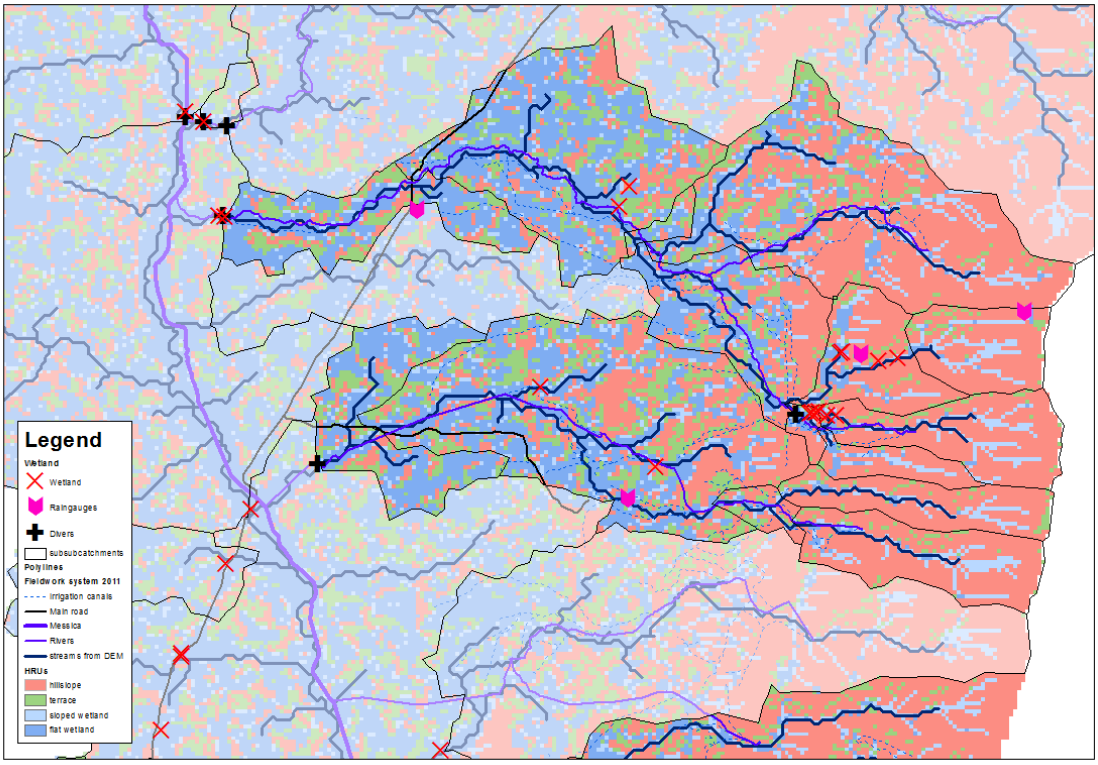

Figure I.2: Red crosses are indicated as wetland during field campaigns. Dark blue, angular streams are derived from DEM. Observe that both show overlap with the classified wetlands (blue areas). HRUs are based on intermediate results with HAND=5.9m, FlowAcc = 20 x 30*30m2 and hill slope = 12.9%.

Forests and shrub lands. Map I.3 shows the locations of non-wetlands. These locations turn brown in the dry season, and do not have enough soil moisture to successfully grow maize. Trees can survive. The groundwater therefore seems to be quite deep. Maybe the HAND threshold for separating wetlands from grasslands should be decreased.

Irrigation. The (funnel) irrigated plots have a few things in common, they are all located on sloped areas and have upstream water sources. Can we deduct in which landscape unit (HRU) these irrigated plots are located?

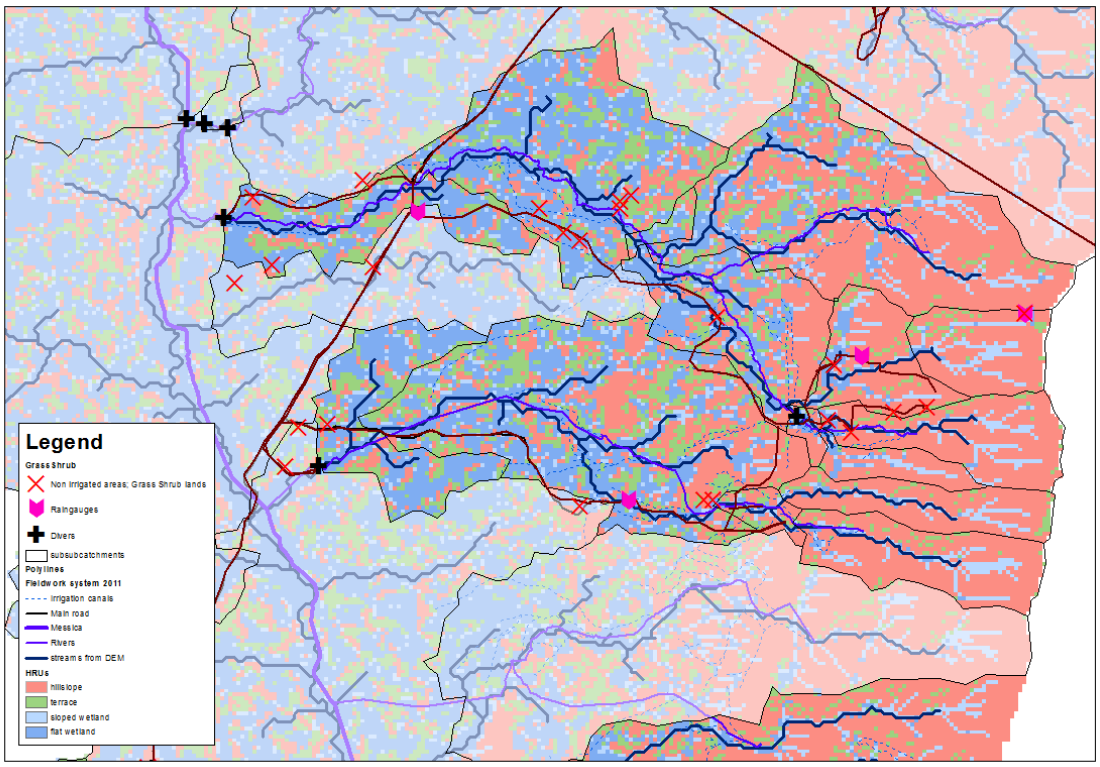

Figure I.3: Red crosses indicate locations of grasslands, shrub lands and rain fed maize. These locations tend to become too dry for agriculture in the rain season. These locations do not have an irrigation network (most because of avoidance of upstream sources and a sufficient gradient). HRUs are based on intermediate results with HAND=5.9m, FlowAcc = 20 x 30*30m2 and hill slope = 12.9%.

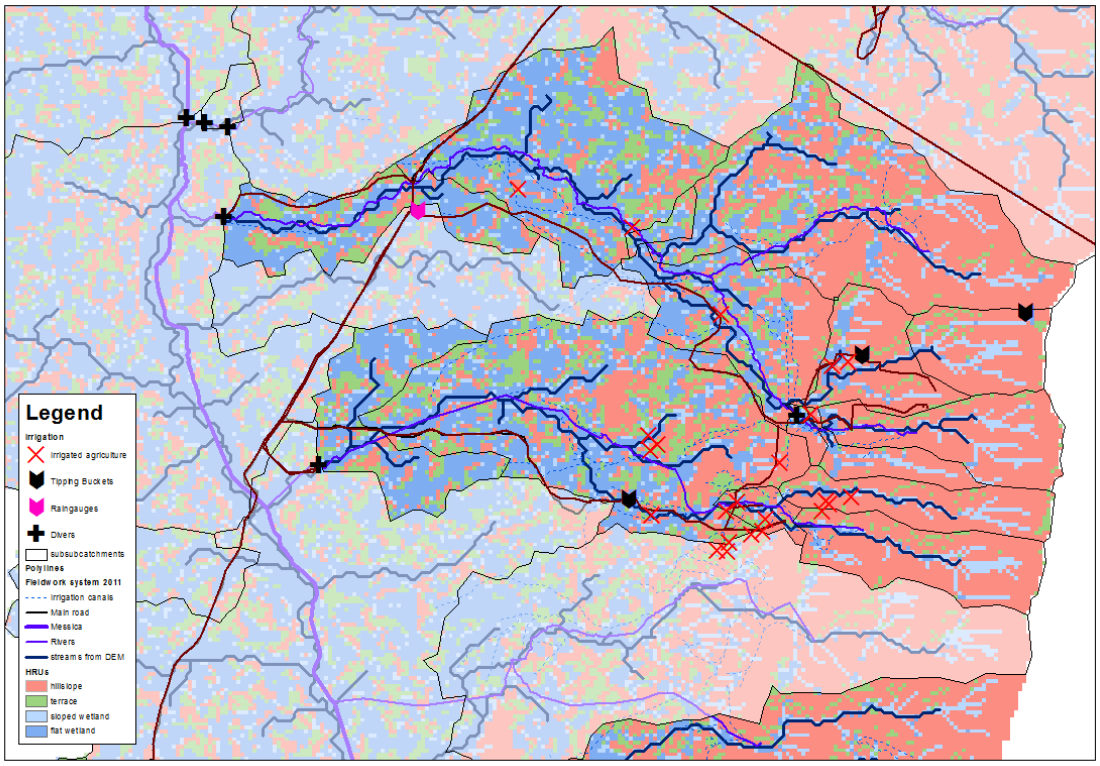

Figure I.4: Red crosses indicate locations of irrigated fields. From the irrigation network, we can obtain if there is an upstream source. HRUs are based on intermediate results with HAND=5.9m, FlowAcc = 20 x 30*30m2 and hill slope = 12.9%.

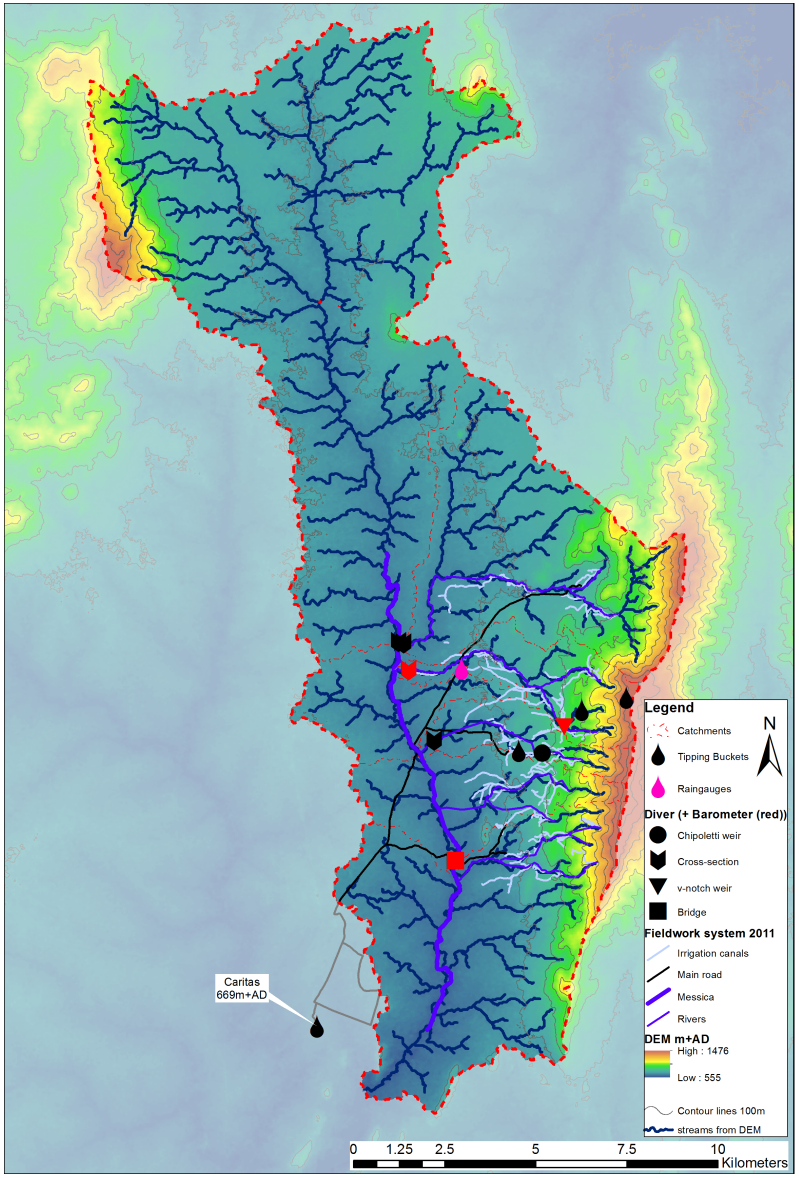

Figure I.5: DEM $30x30m^2$ [35], main catchments, and measurement locations for divers and precipitation, extra mapped raingauge at Caritas Centre in Messica

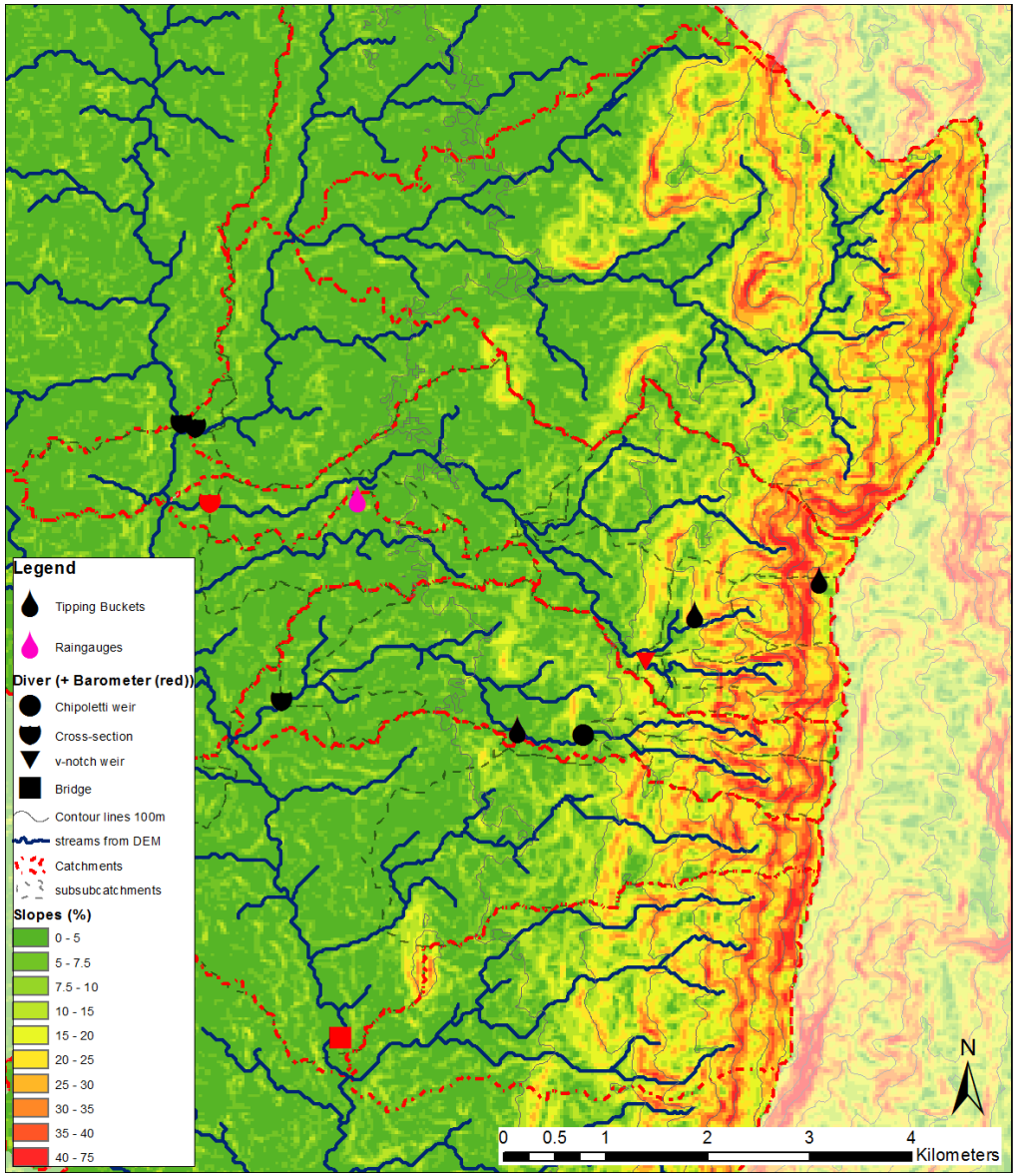

Figure I.6: Slopes derived from the DEM

UID [-]	Feed into (1) [-]	Feed into (2) [-]	Measurementpoint [-]	Total Area [ha]	[m+AD]	Wetland [ha]	[m+AD]	Grass/Crops [ha]	[m+AD]	Forests [ha]	[m+AD]
Chir_1_1_us_in	Chir_1_2_ds_out	Chir_1_3_ds_out		90.3659		15.7895		0		74.5764	
Chir_1_2_ds_out	Chir_3_2_us_in			90.3659		15.7895		0		74.5764	
Chir_1_3_ds_out				90.3659		15.7895		0		74.5764	
Chir_2_1_us_in	Chir_2_3_ds_out	Chir_2_2_ds_out		64.8529		10.0803		0		54.7726	
Chir_2_2_ds_out				64.8529		10.0803		0		54.7726	
Chir_2_3_ds_out	Chir_3_1_us_in			64.8529		10.0803		0		54.7726	
Chir_3_1_us_in	Chir_3_3_ds_out			64.8529		10.0803		0		54.7726	
Chir_3_2_us_in	Chir_3_3_ds_out			90.3659		15.7895		0		74.5764	
Chir_3_3_ds_out	Chir_4_1_us_in			155.2188		25.8698		0		129.349	
Chir_4_1_us_in	Chir_4_3_ds_out			155.2188		25.8698		0		129.349	
Chir_4_2_us_in	Chir_4_3_ds_out			0		0		0		0	
Chir_4_3_ds_out	Chir_5			155.2188		25.8698		0		129.349	
Chir_5	Chir_6		Chipoletti weir Chirodzo upstream	171.5435		30.2409		0		141.3026	
Chir_6	Chir_7_ds_out			514.3628		189.0279		93.6665		231.6685	
Chir_7_ds_out	Messica_3_ds_out		Diver Chirodzo downstream	616.0579		255.1297		129.2598		231.6685	
Godi_1_1_us_in	Godi_1_2_ds_out	Godi_1_3_ds_out		61.6415		12.0428		0		49.5986	
Godi_1_2_ds_out	Godi_2			61.6415		12.0428		0		49.5986	
Godi_1_3_ds_out				61.6415		12.0428		0		49.5986	
Godi_2	Godi_5_2_us_in			61.6415		12.0428		0		49.5986	
Godi_3_1_us_in	Godi_3_2_ds_out			27.4755		6.6905		0		20.785	
Godi_3_2_ds_out	Godi_5_1_us_in			111.4185		21.3203		0		90.0982	
Godi_3_3_us_in	Godi_3_2_ds_out			83.943		14.6298		0		69.3132	
Godi_3_4	Godi_3_2_ds_out			0		0		0		0	
Godi_3_5_us_in	Godi_3_2_ds_out			0		0		0		0	
Godi_4_1_us_in	Godi_4_2_ds_out			0		0		0		0	
Godi_4_2_ds_out	Godi_5_2_us_in			0		0		0		0	
Godi_5_1_us_in	Godi_5_3_ds_out			119.5363		24.3533		0		95.183	
Godi_5_2_us_in	Godi_5_3_ds_out			128.2785		28.0107		0		100.2677	
Godi_5_3_ds_out	Godi_6			247.8148		52.364		0		195.4507	
Godi_6	Godi_7_2_us_in		V-notch weir Godi upstream	247.8148		52.364		0		195.4507	
Godi_7_1_us_in	Godi_7_3_ds_out			287.6007		79.5719		0.9813		207.0475	
Godi_7_2_us_in	Godi_7_3_ds_out			364.4072		103.9252		0		260.482	
Godi_7_3_ds_out	Godi_8_1_us_in			652.008		183.4971		0.9813		467.5296	
Godi_8_1_us_in	Godi_8_3_ds_out	Godi_8_2_ds_out		662.8019		188.7603		0.9813		473.0604	
Godi_8_2_ds_out				662.8019		188.7603		0.9813		473.0604	
Godi_8_3_ds_out	Godi_9			662.8019		188.7603		0.9813		473.0604	
Godi_9	Godi_10_1_ds_out			891.2589		332.0254		48.885		510.3486	
Godi_10_1_ds_out	Messica_2		diver Godi downstream	991.7051		393.3993		83.8538		514.452	
Nyamanguero_1_ds_out	Messica_3_ds_out			506.8695		190.366		98.5728		217.9307	
Nyausanga_1_ds_out	Messica_2			183.4079		130.8655		44.7815		7.7609	
Ruaga_2	Ruaga_1_ds_out			3574.046		1912.491		92.3284		1569.2259	
Ruaga_1_ds_out	Messica_2		Diver Ruaga downstream	3586.356		1920.341		96.7887		1569.2259	
TribMess_1_ds_out	Messica_3_ds_out			61.8199		39.6075		22.2123		0	
Messica_1_us_in	Messica_2		Diver Messica upstream	10129.72		6208.572		554.684		3366.4628	
Messica_2	Messica_3_ds_out			15714.38		9203.759		1049.5999		5461.024	
Messica_3_ds_out			Diver Messica downstream	17684.23		10184.94		1579.217		5920.079	

Table I.2: FlexC's HRU classification for subcatchments, corresponding to Fig. I.7. Wetlands and Flatlands (i.e. Grass_Crops) are determined with HAND = 5.9m, Slope = 12.9% and FlowAccumulation = 20 x 30*30m2. The location of Forests are based on GlobCover [32] and overrule Flatlands. These numbers are *not* used in final calculations.

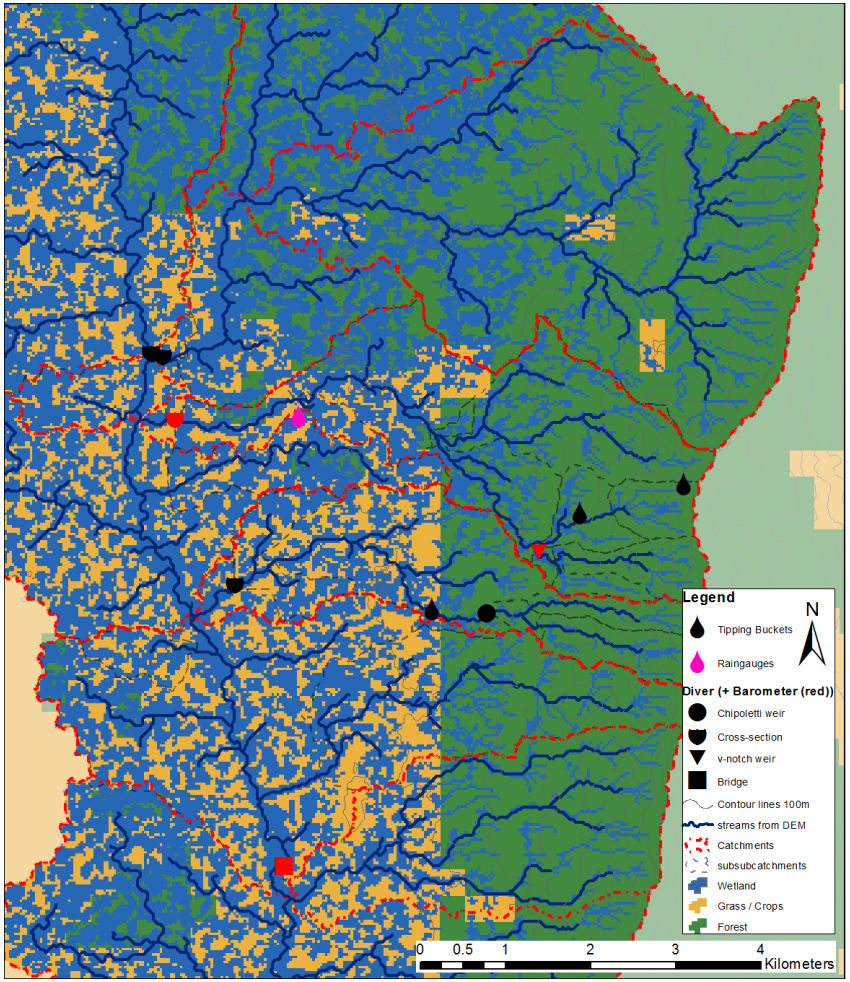

Figure I.7: Spatial distribution of HRU FlexC over subcatchments, related to Tbl. I.2. Wetlands and Flatlands (i.e. Grass_Crops) are determined with HAND = 5.9m, Slope = 12.9% and FlowAccumulation = 20 x 30*30m2. Forests are based on GlobCover [32] and overrule Flatlands. This classification is *not* used in the final calculations.

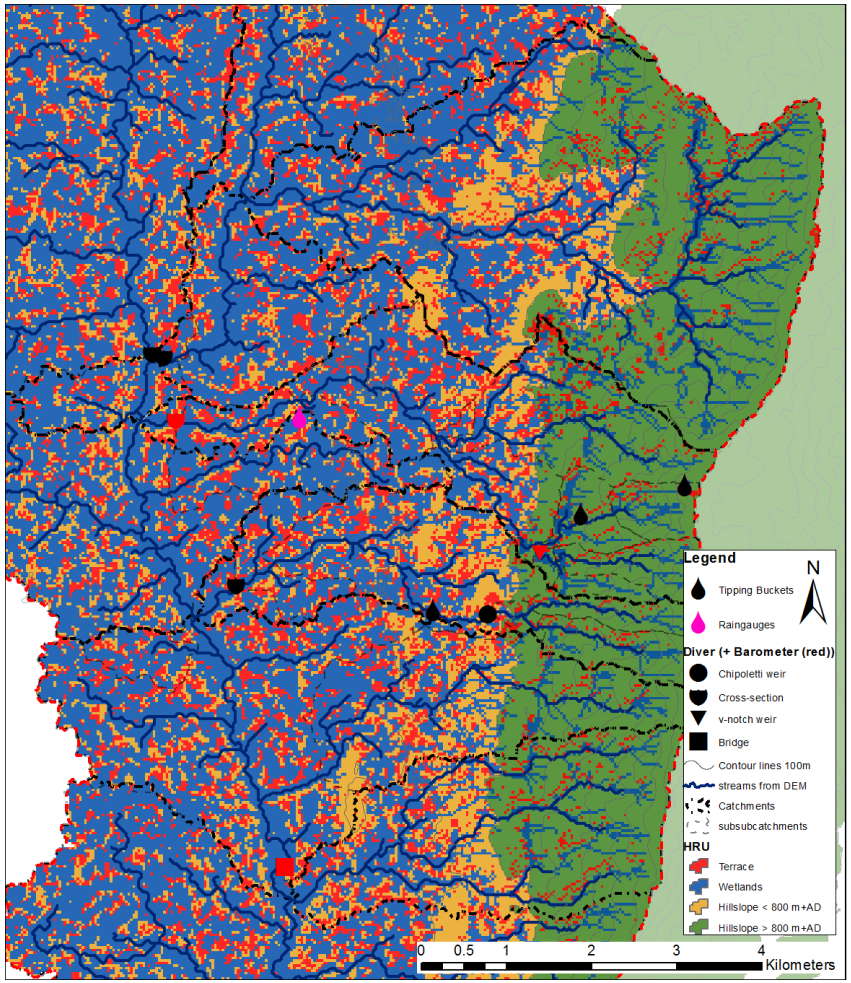

Figure I.8: Spatial distribution of HRU FlexD over subcatchments, related to Tbl. I.3. Wetlands, Terraces and Hillslopes are determined with HAND = 5.9m, Slope = 12.9% and FlowAccumulation = 20 x 30*30m2, see Tbl. I.1. Extra seperation is made for Hillslopes higher and lower than 800m+AD, since original forests remain untouched above this altitude. This classification is *not* used in the final calculations.

UID [-]	Feed into (1) [-]	Feed into (2) [-]	Measurementpoint [-]	Total Area [ha]	[m+AD]	Wetland [ha]	[m+AD]	Terrace [ha]	[m+AD]	$< 800m + AD$ [ha]	[m+AD]	$> 800m + AD$ [ha]	[m+AD]
Chir_1_1_us_in	Chir_1_2_ds_out	Chir_1_3_ds_out		90.3659		15.7895		5.0848		0		69.4916	
Chir_1_2_ds_out	Chir_3_2_us_in			90.3659		15.7895		5.0848		0		69.4916	
Chir_1_3_ds_out				90.3659		15.7895		5.0848		0		69.4916	
Chir_2_1_us_in	Chir_2_3_ds_out	Chir_2_2_ds_out		64.8529		10.0803		4.9063		0		49.8663	
Chir_2_2_ds_out				64.8529		10.0803		4.9063		0		49.8663	
Chir_2_3_ds_out	Chir_3_1_us_in			64.8529		10.0803		4.9063		0		49.8663	
Chir_3_1_us_in	Chir_3_3_ds_out			64.8529		10.0803		4.9063		0		49.8663	
Chir_3_2_us_in	Chir_3_3_ds_out			90.3659		15.7895		5.0848		0		69.4916	
Chir_3_3_ds_out	Chir_4_1_us_in			155.2188		25.8698		9.9911		0		119.3579	
Chir_4_1_us_in	Chir_4_3_ds_out			155.2188		25.8698		9.9911		0		119.3579	
Chir_4_2_us_in	Chir_4_3_ds_out			0		0		0		0		0	
Chir_4_3_ds_out	Chir_5			155.2188		25.8698		9.9911		0		119.3579	
Chir_5	Chir_6		Chipoletti weir Chirodzo upstream	171.5435		30.2409		13.2917		0.9813		127.0296	
Chir_6	Chir_7_ds_out			514.3628		189.0279		82.6941		100.8922		141.7486	
Chir_7_ds_out	Messica_3_ds_out		Diver Chirodzo downstream	616.0579		255.1297		103.4792		115.7004		141.7486	
Godi_1_1_us_in	Godi_1_2_ds_out	Godi_1_3_ds_out		61.6415		12.0428		4.4603		0		45.1383	
Godi_1_2_ds_out	Godi_2			61.6415		12.0428		4.4603		0		45.1383	
Godi_1_3_ds_out				61.6415		12.0428		4.4603		0		45.1383	
Godi_2	Godi_5_2_us_in			61.6415		12.0428		4.4603		0		45.1383	
Godi_3_1_us_in	Godi_3_2_ds_out			27.4755		6.6905		0.7136		0		20.0714	
Godi_3_2_ds_out	Godi_5_1_us_in			111.4185		21.3203		4.7279		0		85.3703	
Godi_3_3_us_in	Godi_3_2_ds_out			83.943		14.6298		4.0143		0		65.2989	
Godi_3_4	Godi_3_2_ds_out			0		0		0		0		0	
Godi_3_5_us_in	Godi_3_2_ds_out			0		0		0		0		0	
Godi_4_1_us_in	Godi_4_2_ds_out			0		0		0		0		0	
Godi_4_2_ds_out	Godi_5_2_us_in			0		0		0		0		0	
Godi_5_1_us_in	Godi_5_3_ds_out			119.5363		24.3533		5.0848		0		90.0982	
Godi_5_2_us_in	Godi_5_3_ds_out			128.2785		28.0107		10.2587		0		90.009	
Godi_5_3_ds_out	Godi_6			247.8148		52.364		15.3435		0		180.1073	
Godi_6	Godi_7_2_us_in		V-notch weir Godi upstream	247.8148		52.364		15.3435		0		180.1073	
Godi_7_1_us_in	Godi_7_3_ds_out			287.6007		79.5719		37.199		27.6539		144.96	
Godi_7_2_us_in	Godi_7_3_ds_out			364.4072		103.9252		33.7199		23.9073		203.3009	
Godi_7_3_ds_out	Godi_8_1_us_in			652.008		183.4971		70.9189		51.5612		348.2609	
Godi_8_1_us_in	Godi_8_3_ds_out	Godi_8_2_ds_out		662.8019		188.7603		74.2195		54.2374		348.2609	
Godi_8_2_ds_out				662.8019		188.7603		74.2195		54.2374		348.2609	
Godi_8_3_ds_out	Godi_9			662.8019		188.7603		74.2195		54.2374		348.2609	
Godi_9	Godi_10_1_ds_out			891.2589		332.0254		117.1277		96.6103		348.2609	
Godi_10_1_ds_out	Messica_2		diver Godi downstream	991.7051		393.3993		139.6077		113.9163		348.2609	
Nyamanguero_1_ds_out	Messica_3_ds_out			506.8695		190.366		69.4916		105.9769		141.035	
Nyausanga_1_ds_out	Messica_2			183.4079		130.8655		28.9028		26.0482		0	
Ruaga_2	Ruaga_1_ds_out			3574.046		1912.491		449.5991		483.9435		726.7628	
Ruaga_1_ds_out	Messica_2		Diver Ruaga downstream	3586.356		1920.341		453.435		484.9248		726.7628	
TribMess_1_ds_out	Messica_3_ds_out			61.8199		39.6075		13.1133		9.099		0	
Messica_1_us_in	Messica_2		Diver Messica upstream	10129.72		6208.572		1527.299		1724.8015		669.2248	
Messica_2	Messica_3_ds_out			15714.38		9203.759		2274.4008		2498.3083		1744.2484	
Messica_3_ds_out			Diver Messica downstream	17684.23		10184.94		2608.8347		2867.5327		2027.032	

Table I.3: FlexC's HRU classification for subcatchments, related to Fig. I.8. Wetlands, Terraces and Hillslopes are determined with HAND = 5.9m, Slope = 12.9% and FlowAccumulation = 20 x 30*30m2, see Tbl. I.1. Extra seperation is made for Hillslopes higher and lower than 800m+AD, since original forests remain untouched above this altitude. These numbers are *not* used in final calculations.

UID	Feed into (1)	Feed into (2)	Measurementpoint	Total Area		Wetland		Flatlands		Inselbergs	
[-]	[-]	[-]	[-]	[ha]	[m+AD]	[ha]	[m+AD]	[ha]	[m+AD]	[ha]	[m+AD]

Table I.4: FlexC's HRU classification for subcatchments, corresponding to Fig. **??**. Wetlands and Flatlands (i.e. Grass_Crops) are determined with HAND = 2m, Slope = 11% and FlowAccumulation = 50 x 30*30m2. These numbers *are* used in final calculations.

insert figure

caption: FlexC's HRU classification for subcatchments, corresponding to Tbl. I.4. Wetlands and Flatlands (i.e. Grass_Crops) are determined with HAND = 2m, Slope = 11% and FlowAccumulation = 50 x 30*30m2. These numbers *are* used in final calculations.

label: tbl:HRU FlexC final

J

LONGITUDINAL ROUTINGS RIVER MESSICA

We performed longitudinal routings around the River Messica, starting from Messica Intermediate Station up to Messica Downstream Station. At several dates we measured the inflow from upstream (MessIS) and from the large headwaters (RuagaDS, GodiDS, ChirDS and Nyuamanguere) furthermore we picked up several small streams, like Nyuasanga and another very small tributary to the River Messica. This longitudinal routings are meant to get insight in origin of water, the inflow from ungauged areas, but is also effected by infiltration to the 'deep' groundwater, a so called leakage term.

The measurements Q are calibrated according to App. D and are all performed with the same EC-meter. Some measurements are performed twice, since the operator did not trust the outcomes. In the tables below, we did not filter out these results, rather we averaged them.
A positive difference term means that water is 'disappeared'. Next to the obvious - measurements errors - water can infiltrated to the deeper groundwater. But also differences time of the day (the daily streamflow variation) is not taken into account just as high discharge wave velocities (i.e. we assume a constant flow during the routing, therefore we did not measure on or after rainy days).

The results are summarized in Tables J.1 to J.9. One might conclude from this tables that especially in the period april and may, the water balance is not closed and possibly water infiltrates to deeper groundwater sources. Unfortunately, hard evidence to support this analysis lacks. Though, Weemstra *et al.* [7] also hints to the infiltrating character of the River Messica.

We recommend future researchers to investigate this topic. It is very well possible that infiltration occurs, but the character and amounts of this infiltration is still unknown.

ID	Name	Date	Q in [m3/s]	Q out [m3/s]	Remark
11	MessDS	01/04/2014 11:23		3.85	#average
43	MessDS	01/04/2014 11:23		2.85	
12	RuagaDS	01/04/2014 13:00	1.47		
9	MessIS	01/04/2014 14:56	2.62		
10	GodiDS	01/04/2014 16:07	0.51		
15	ChirDS	02/04/2014 12:51	0.11		
	Difference			**1.37**	
	Total		**4.72**	**4.72**	

Table J.1: Longitudinal routing River Messica at 1/4/2014

ID	Name	Date	In m3/s	Out m3/s	Remark
19	GodiDS	07/04/2014 09:15	0.18		
20	RuagaDS	07/04/2014 10:15	1.61		#average
21	RuagaDS	07/04/2014 10:40	1.14		
22	MessIS	07/04/2014 11:30	3.77		
23	Nyausanga	07/04/2014 12:30	0.02		
24	ChirDS	07/04/2014 13:30	0.13		
25	Tributary Messica	07/04/2014 14:30	0.01		
16	MessDS	07/04/2014 16:12		1.92	#average
17	MessDS	07/04/2014 16:37		1.96	
44	MessDS	07/04/2014 16:37		1.81	
18	Nyamanguero	07/04/2014 17:08	0.13		
	Difference			**3.73**	
	Total		**5.63**	**5.63**	

Table J.2: Longitudinal routing River Messica at 7/4/2014

ID	Name	Date	In m3/s	Out m3/s	Remark
68	MessIS	29/05/2014 09:15	1.11		#average
69	MessIS	29/05/2014 09:45	0.85		
70	RuagaDS	29/05/2014 10:41	0.15		
71	GodiDS	29/05/2014 11:48	0.10		
72	Nyausanga	29/05/2014 13:13	0.01		
74	MessDS	29/05/2014 15:01		0.82	
75	Nyamanguero	29/05/2014 15:40	0.05		
73	ChirDS	29/05/2014 13:55	?		
	Difference			**0.47**	
	Total		**1.29**	**1.29**	

Table J.3: Longitudinal routing River Messica at 29/5/2014

ID	Name	Date	In m3/s	Out m3/s	Remark
85	GodiDS	05/06/2014 09:00	0.07		#average
86	GodiDS	05/06/2014 09:00	0.08		
87	RuagaDS	05/06/2014 10:24	0.13		#average
88	RuagaDS	05/06/2014 10:32	0.13		
89	MessIS	05/06/2014 12:00	0.37		
90	ChirDS	05/06/2014 12:40	0.03		
91	MessDS	05/06/2014 14:56		0.82	#average
92	MessDS	05/06/2014 15:45		0.86	
93	Nyamanguero	05/06/2014 16:30	0.05		
	Difference			**-0.18**	# average
	Total		**0.66**	**0.66**	

Table J.4: Longitudinal routing River Messica at 5/6/2014

ID	Name	Date	In m3/s	Out m3/s	Remark
42	MessIS	16/06/2014 08:53	0.67		#average
114	MessIS	16/06/2014 08:53	0.51		
115	MessIS	16/06/2014 09:30	1.09		
116	RuagaDS	16/06/2014 10:53	0.15		
117	GodiDS	16/06/2014 11:41	0.08		
118	Nyausanga	16/06/2014 12:57	0.01		
119	ChirDS	16/06/2014 13:31	0.03		
120	MessDS	16/06/2014 15:04		0.79	
121	Nyamanguero	16/06/2014 15:49	0.05		
	Difference			**0.28**	# average
	Total		**1.07**	**1.07**	

Table J.5: Longitudinal routing River Messica at 16/6/2014

ID	Name	Date	In m3/s	Out m3/s	Remark
142	MessIS	30/06/2014 09:19	0.21		
143	RuagaDS	30/06/2014 10:34	0.09		
144	GodiDS	30/06/2014 11:01	0.06		
145	Nyausanga	30/06/2014 11:43	0.01		
146	ChirDS	30/06/2014 12:35	0.02		
147	MessDS	30/06/2014 14:30		0.82	#average
148	MessDS	30/06/2014 14:46		0.55	
149	Nyamanguero	30/06/2014 15:16	0.06		
	Difference			**-0.23**	# average
	Total		**0.45**	**0.45**	

Table J.6: Longitudinal routing River Messica at 30/6/2014

ID	Name	Date	In m3/s	Out m3/s	Remark
169	MessIS	14/07/2014 08:48	0.30		
170	RuagaDS	14/07/2014 09:32	0.11		
171	GodiDS	14/07/2014 10:44	0.05		
172	Nyausanga	14/07/2014 11:28	0.01		
173	ChirDS	14/07/2014 12:06	0.02		
174	MessDS	14/07/2014 13:13		0.54	
175	Nyamanguero	14/07/2014 14:43	0.03		
	Difference			**-0.03**	
	Total		**0.51**	**0.51**	

Table J.7: Longitudinal routing River Messica at 14/7/2014

ID	Name	Date	In m3/s	Out m3/s	Remark
195	MessIS	22/07/2014 09:13	0.76		
196	RuagaDS	22/07/2014 09:50	0.11		
197	GodiDS	22/07/2014 10:39	0.06		
198	ChirDS	22/07/2014 12:15	0.06		
199	MessDS	22/07/2014 13:15		0.45	
	Difference			**0.53**	
	Total		**0.99**	**0.99**	

Table J.8: Longitudinal routing River Messica at 22/7/2014

ID	Name	Date	In m3/s	Out m3/s	Remark
26	GodiDS	08/04/2014 11:30	0.19		
27	RuagaDS	08/04/2014 15:00	1.06		
28	MessIS	09/04/2014 10:49	1.03		
38	ChirDS	11/04/2014 14:15	0.15		
29	MessDS	15/04/2014 12:15		2.65	
30	RuagaDS	15/04/2014 16:28	0.55		
31	RuagaDS	17/04/2014 12:49	0.39		
32	GodiDS	17/04/2014 14:42	0.15		
39	MessDS	21/04/2014 09:15		2.56	
40	MessDS	21/04/2014 09:46		2.40	
41	MessDS	06/05/2014 09:46		2.00	
54	GodiDS	08/05/2014 16:00	0.18		
65	GodiDS	21/05/2014 15:33	0.01		
66	GodiDS	24/05/2014 12:18	0.14		
67	RuagaDS	24/05/2014 13:45	0.19		
84	ChirDS	30/05/2014 15:03	0.05		
104	GodiDS	09/06/2014 13:58	0.06		
113	ChirDS	10/06/2014 12:28	0.03		
132	GodiDS	17/06/2014 17:22	0.07		
141	ChirDS	19/06/2014 13:42	0.04		
160	GodiDS	01/07/2014 15:32	0.05		
168	ChirDS	02/07/2014 12:32	0.02		
186	GodiDS	15/07/2014 14:16	0.04		
194	ChirDS	16/07/2014 12:40	0.03		

Table J.9: Remainder salt dilution discharge measurements at above measurement stations, but not connected to a particular longitudinal routing of the River Messica

K

FlexB and FlexD

K.1. FlexB

For FlexB two different HRUs are considered. Fig. K.1 suggests seperation between wetlands and the remainder area. It is also possible to separate between Inselbergs and the remainder area.

Another possibility is to include a more sophisticated model, for which a new element is introduced, Fig. K.2. This element accounts for deeper groundwater infiltration into the Kalahari Craton. Therefore geological information should be included into the HRU classification.

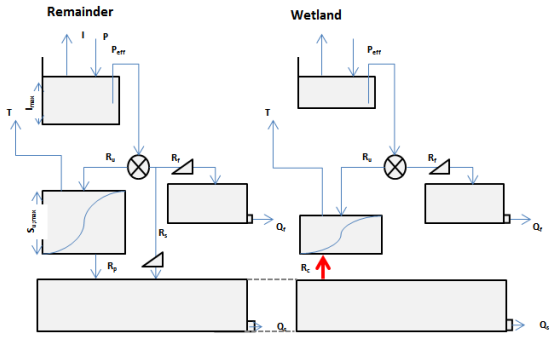

Figure K.1: Modelcode FlexB; Wetland separated

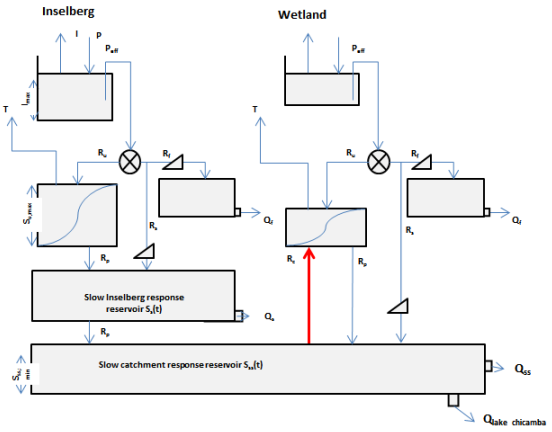

Figure K.2: Modelcode FlexB; Wetland separated

K.2. FlexD

FlexD also identify areas with a HAND < 5.9m as wetlands. The difference with FlexC however is the allocation of landuse classification. Whilst FlexC distinguishes landuse on the GlobCover map, FlexD states that all areas above 800m+AD are hill slopes and covered with original subtropical forests. Which is more or less true for this area, since the village chief of Chirodzo does not allow people to cut forests above these altitude nor making houses. [1]. We perceive that the groundwater storage of the Inselberg is predominantly recharged via cracks in the higher parts of the mountain. Furthermore, we suspect that due to the forests ánd the very steep hill slopes, the fast subsurface processes are faster than those from the lower parts in the catchments. The areas below 800m+AD are mostly cultivated, that is, the original forests made space for grass, crop and shrub lands. For this we differentiated between flat and sloped areas. From the DEM the slopes are calculated. Areas with slopes > 12.9% are considered as hill slopes (covered with grass/crops) the remainder as plateaus (covered with grass/crops). Note that plateaus do not have fast subsurface runoff, furthermore irrigation is

[1] However, from the east side of the Inselberg ridge, the villagers of Vanduzi are cutting forest on the edges and on the top of the mountain, creating rainfed maize land and large grasslands.

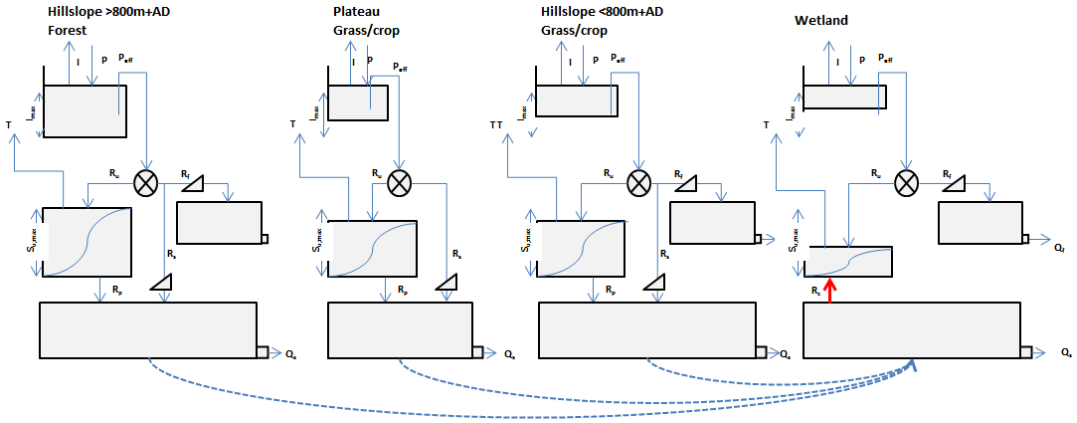

Figure K.3: Modelcode FlexD; Inselberg/ landuse based

not possible for the absence of gradients. All excess water percolates to the deep groundwater storage. Where sloped areas do have fast runoff processes and also irrigation takes place (so transpiration during dry periods should be higher than that of the plateaus).

FlexD and FlexC thus only differs in the relative forest contribution (predominantly in the lower areas) and in the smaller fast runoff contribution from the grass/croplands.

K.2.1. PARAMETER CONSTRAINTS

The hydrological response from the different HRU's are different. This can be taken into account in the parametrisation of the processes and bandwidths (Table 2.4). For example we know that the fast response processes from forests (on hill slopes) are faster than those of grass/crops and wetlands. The following parameter constraints are applied. All the parameter sets that do not fulfil these constraints are beforehand rejected.

$$\begin{cases} I_{max;forest} > I_{max;grass_crop} \\ I_{max;forest} > I_{max;wetland} \\ K_{f;forest} < K_{f;grass_crop} \\ K_{f;forest} < K_{f;wetland} \\ Su_{max;forest} > Su_{max;grass_crop} \\ Su_{max;forest} > Su_{max;wetland} \end{cases} \tag{K.1}$$

K.2.2. PROCESS CONSTRAINTS

Not applied yet.

K.3. PARAMETER BANDWIDTHS FLEXB, -D

Table K.1 present the parameter bandwidths for FlexB and FlexD.

		FlexB		FlexD			
		Wetland	Forests	Wetland	Plateau	$< 800m + AD$	$> 800m + AD$
I_{max}	Interception storage [mm]	1-5	2-3	2-3	2-3	2-3	3-5
$S_{u;max}$	Maximum rootzone capacity [mm]	50-100	200-500	50-100	150-300	150-300	300-500
B	Soil moisture distribution coefficient [-]	1-5	1-5	1-5	1-5	1-5	1-5
L_p	Transpiration coefficient [-]	0.5	0.5	0.5	0.5	0.5	0.5
F_c	Relative soil moisture at field capacity [-]	0	0	0	0	0	0
D	Divider fast - slow reservoir [-]	0-1	0-1	0-1	1	0-1	0-1
C	Maximum capillary rise rate [mm/day]	0-0.3	0	0-0.3	0	0	0
P_{per}	Maximum matrix percolation rate [mm/day]	0	0-0.5	0	0-0.5	0-0.5	0-0.5
K_f	Fast reservoir delay time [day]	0-10	0-10	0-10	0-10	0-10	0-10
K_s	Slow reservoir delay time [day]	500-700	500-700	500-700	500-700	500-700	500-700

Table K.1: **Check values for FlexB** Predefined parameter bandwidths for FlexB and FlexD

L

DISCRITIZATION FLEXMODELS

L.1. GENERAL MODEL CHOICES

The models are runned at daily timescale. To ensure a stable solution, a numerical time step of 0.5 day is used. This leads to a small numerical error in the unsaturated zone, ca 0.5 % of the total waterbalance. Smaller timesteps will reduce this error, but are also more expensive.

Precipitation measurements are available from September 2010 to July 2014, the period of interest starts December 2012 earliest. Evaporation measurements are derived from December 2012 to July 2014, in order to make the evaporation sequence from equal length, we applied the data from ...[date 1 to date 2]... to ... [date 3 - date 4].

In order to minimize model spin-up effects, we start calculations from ... [date] ... . Therefore we used the data [date1-date2] to pre-tend the forcing data.

Since the timeseries is shorter than the precipitations' one, the gaps are closed with comparable periods from other years. The over-yearly differences in evaporation are presumed to be negligible.

L.2. ANALYTICAL AND NUMERICAL DESCRIPTION OF FLEXA BENCHMARK MODEL

All the model codes are based on one basis model, see Fig. L.1. The analytical description (Tbl. L.1 and numerical implementation are described in this appendix. Generally, we used the following approach:

$$f(t) = I(t) - O(t) \tag{L.1}$$

$$\frac{dS}{dt} + O(S(t)) = I(t) \tag{L.2}$$

For which source terms (I in) are implicitly descritized and dissipative terms (O out) are explicitly descritized.

L.2.1. INTERCEPTION BUCKET

The storage change of the interception stock, Eq. **??**, is a result of three terms. The input consist of the precipitation $P(t) \forall P \in [0, \rightarrow)$ as function of time. This is an independent forcing. The outgoing fluxes are the interception $I(t)$ and the effective precipitation $P_e(t)$ which is the actual precipitation reduced by the interception, should obey interception equations given in Tbl. L.1.

Due to threshold behavior of $P_e(t)$ and $I(t)$, the function cannot be discretized implicitly effectively, since, depending on the outcome, the numerical scheme changes, therefore is cheaper to discretized the dissipative terms as 2 bounded fluxes.

$$I[i] = \max(0, \min(Si[i-1] + Pdt[i], \min(I_{\max}, E0dt[i]))) \tag{L.3}$$

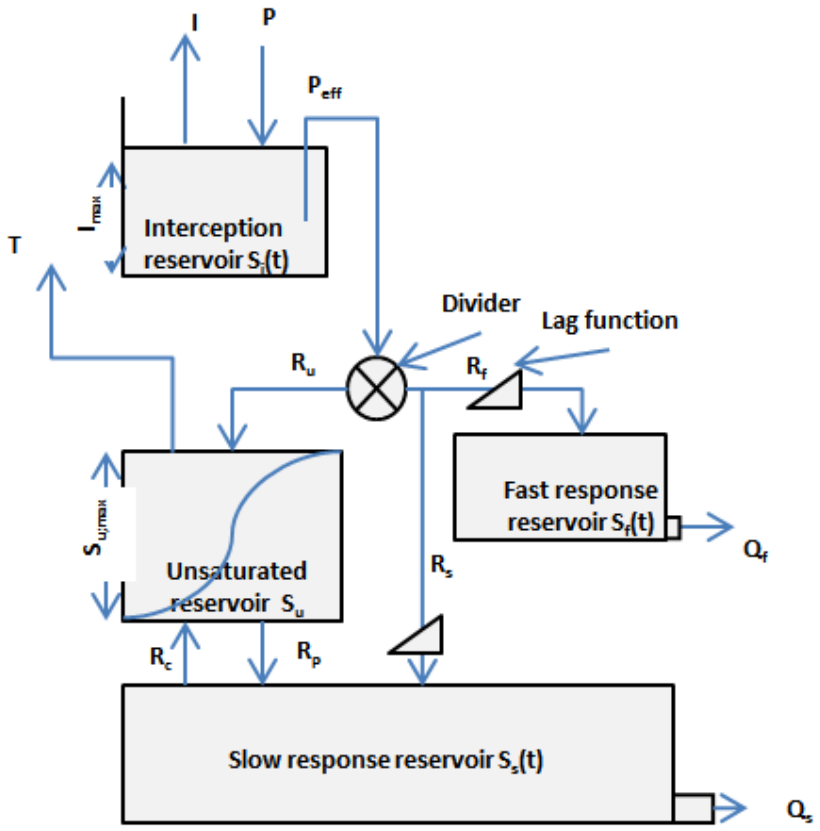

Figure L.1: Model code FlexA; lumped benchmark model

$$Eidt[i] = \max(0, \min(Si[i-1] + Pdt[i], I_{\max}, E0dt[i])) \tag{L.4}$$

L.2.2. UNSATURATED ZONE

For K_t and C_r, two things are important to realize. First, both functions are not first order smooth, implying that they have an inflection point in the domain of interest. Therefore, the solution cannot be given with one single function evaluation, nor for the analytical, nor for the discretized function. Therefore the calculations are iterative. The soil moisture is estimated based on the previous time step. After evaluating the functions, the outcomes are tested, and if necessary repeated with the new calculated soil moisture. The calculations are sensitive for the internal time step dt. The calculation crashes if after a few iterations no stable solution is reached.

$$K_t[i] = \begin{cases} \frac{Su[i]}{S_{u;\max} * L_p} & Su[i] < S_{u;\max} * L_p \\ 1 & Su[i] \geq S_{u;\max} * L_p \end{cases} \tag{L.5}$$

$$C_r[i] \begin{cases} \max\left(0, \min\left(1, 1 - \left(\frac{Su[i] - S_{u;\max} * Fc}{S_{u;\max} - S_{u;\max} * Fc}\right)^{\beta}\right)\right) & Su[i] \geq S_{u;\max} * F_c \\ 1 & Su[i] < S_{u;\max} * F_c \end{cases} \tag{L.6}$$

Both functions includes two domains, therefore 4 different discretizations (2*2) are possible. Depending on the soil moistures state of that particular time step. We narrowed it down to 2.

$$Su[i] = \begin{cases} Su[i] = \frac{Su[i-1] + C*dt + Crdt[i]*Pedt[i] - E0dt[i] + Eidt[i]}{1 + \frac{(C+Pper)dt}{Sumax}} & K_t[i] = 1 \\ Su[i] = \frac{Su[i-1] + C*dt + Crdt[i]*Pedt[i]}{1 + \frac{(C+Pper)dt}{Sumax} + \frac{E0dt[i] - Eidt[i]}{Sumax*Lp}} & 0 < K_t[i] < 1 \end{cases} \tag{L.7}$$

Reservoir	Water balance equation	Constitutive relations
Interception	$\frac{\Delta S_I}{\Delta t} = P - P_e - I$	$P_e = \begin{cases} 0 & S_I < I_{max} \\ (S_I - I_{max})/\Delta t & S_I = I_{max} \end{cases}$ $I = \begin{cases} E_p & E_p \Delta t < S_I \\ S_I/\Delta t & E_p \Delta t \geq S_I \end{cases}$
Unsaturated	$\frac{\Delta S_u}{\Delta t} = R_u - T - R_p + R_c$	$R_u = C_r P_e$ $T = K_T(E_p - I)$ $R_p = \left(\frac{S_u}{S_{u;max}}\right) P_{per}$ $R_c = \left(1 - \frac{S_u}{S_{u;max}}\right) C$ $C_r = \begin{cases} 1 - \left(\frac{S_u - S_{u;max}F_c}{S_{u;max} - S_{u;max}F_c}\right)^B & S_u \geq S_{u;max}F_c \\ 1 & S_u < S_{u;max}F_c \end{cases}$ $K_T = \begin{cases} \frac{S_u}{S_{u;max}L_p} & S_u < S_{u;max}L_p \\ 1 & S_u \geq S_{u;max}L_p \end{cases}$
Fast	$\frac{\Delta S_f}{\Delta t} = R_{f;lag} - Q_f$	$R_f = (1-D)(1-C_r)P_e$ $R_{f;lag} = R_f * N_{f;lag}$ $Q_f = S_f/K_f$
Slow	$\frac{\Delta S_s}{\Delta t} = R_{s;lag} - Q_s + R_p - R_c$	$R_s = D(1-C_r)P_e$ $R_{s;lag} = R_s * N_{s;lag}$ $Q_s = S_s/K_s$

Table L.1: Water balance equations and constitutive functions used in FlexA [19]. Meaning units also listed in Table 2.4
$*$ is the convolution parameter

L.2.3. FAST RESERVOIR

The preferential recharge to the fast reservoir is discretized as follows:

$$Rfdt[i] = (1-D) * (1 - Crdt[i]) * Pedt[i] \tag{L.8}$$

The inflow into the fast reservoir can be delayed with lag function(this is left out in the final calculations, and should be implemented). The lag function can be discretized using a convolution integral, where $K_{f;lag}$ is the impuls function and R_f the recharge.

$$R_{f;lag}(t) = \int_{t_0}^{t} K_{f;lag}(\tau) * R_{f;lag}(t-\tau) d\tau \tag{L.9}$$

We can apply a build in function of numpy library to calculate the convolution integral.

$$Rflagdt = \text{numpy.convolve(Rfdt,Nflag,'same')} \tag{L.10}$$

Observe that $R_{f;lag}(t)$ is a source term, where Q_f concerns a dissipative term.

$$\frac{dS_f(t)}{dt} = R_{f;lag}(t) - Q_f(t) = R_{f;lag}(t) - \frac{S_f(t)}{K_f} \tag{L.11}$$

Applying Implicit Euler to discretize Q_f, one end up with the following discretization. Being so, the storage S_f never can become negative. Note that discretizing a source term implicitly is unnecessary.

$$S[i] = \frac{S[i-1] + \text{Rflagdt}[i]}{1 + dt/K_f} \tag{L.12}$$

L.2.4. SLOW RESERVOIR

Similar to the fast reservoir we find:

$$Rsdt[i] = D * (1 - Crdt[i]) * Pedt[i] \tag{L.13}$$

$$Rslagdt = \text{numpy.convolve(Rsdt,Nslag, 'same')} \tag{L.14}$$

However, now we allowed the storage to become negative, since we left out the online connection with the unsaturated reservoir via capillary rise $Rcdt$.

$$Ss[i] = \frac{(Ss[i-1] + Rslagdt[i] + Rpdt[i] - Rcdt[i])}{(1 + dt/Ks)} \tag{L.15}$$

L.3. COMPILE FLEXB, -C, -D MODELS FROM FLEXA

The model concepts FlexB, C and D consist of multiple HRU units. Every HRU unit is identical to FlexA. The general assumption is that the subsequent HRUs are connected by through their slow reservoir.

In order to make the programmed model code more general, we apply linear superposition of the HRUs. This is allowed under certain conditions.

Note that the linear HRU assumption hold that

$$Q_{m;tot} = \sum_{i=1}^{N} a_i (Q_{f;i} + Q_{s;i}) \tag{L.16}$$

For which $Q_{m;i}$ is the total outflow of a the HRU. Q_f the fast outflow and Q_s the slow outflow. Furthermore must hold $\sum_{i=1}^{N} a_i = 1$ represents the relative area of the HRU.

For all the reservoirs apart from the slow reservoir, it is easy to observe that the Interception, Unsaturated Zone and Fast Reservoir represent separate processes belonging to the HRUs. Their subsequent contribution to the total flow is therefore the area multiplied with the outflow.

To make sure that it also holds for the slow response reservoir we restraint the process:

Firstly, the physic-numerical constraint ensures that the cumulative of the slow response reservoir outcome (Q_s) for the three HRUs is larger or equal than zero for every single time step ($\forall t$). Since otherwise the model would (physically speaking) introduce passive groundwater into the model, which is conceptually impossible, since we only take the active slow groundwater storage into account (that part that actually participate into the rainfall runoff process). This constraint read (Eq. L.17)

$$\sum_{HRU=1}^{3} Q_{s;HRU} \geq 0 \forall t \tag{L.17}$$

Secondly, the K_s values for all three units are equal, this is in line with progressions in earlier studies to combine the slow reservoir of the different HRUs to one single unit.

Thirdly, the initial storage in the groundwater reservoirs is important. We derived a methodology to simulate the groundwater storage as if there is an infinite amount of average years in front. Based on the rainfall amount assumptions, the initial values are changed for other catchments, see App. L.3.2.

L.3.1. LINEAR SUPERPOSITION FLEXA CLOSED MASS BALANCE FOR SLOW RESPONSE RESERVOIR

The mass balance for the slow response reservoirs is closed. Therefore, we can linear superpose the FlexA model.

The general equation for the slow reservoir reads:

$$\frac{\mathrm{d}S}{\mathrm{d}t} = R(t) - Q(t) \tag{L.18}$$

For which S [mm] represent the storage in the slow reservoir, R [mm/day] the recharge to the reservoir (source term) and Q [mm/day] the discharge from the reservoir (sink term).

If we assume the term S first order continuous we may write:

$$S^{t+\mathrm{d}t} = S^t + R * \mathrm{d}t - Q * \mathrm{d}t \tag{L.19}$$

Since Q is a sink term, we write this term implicitly to avoid numerical errors. Under the linear reservoir assumption we substitute $Q = S/K_s$.

$$S^{t+\mathrm{d}t} = S^t + R * \mathrm{d}t - \frac{S^{t+\mathrm{d}t}}{K_s} * \mathrm{d}t \tag{L.20}$$

If we have multiple HRU units feeding into one slow reservoir we have to account for the relative contribution for every recharge term. Mind that the recharge is defined as $R = R_{per} + R_s - R_c$ (Percolation + preferential recharge - capillary rise). We cannot calculate storage in terms of [mm] if we decouple the reservoirs. Therefore, we prove mass balance in m3. So S and R are now expressed in m3.

$$S_{Tot}^{t+\mathrm{d}t} = \sum_{i=1}^{N} \left(S_i^t + R_i \mathrm{d}t - \frac{S_i^{t+\mathrm{d}t}}{K_s} * \mathrm{d}t \right) \tag{L.21}$$

With

$$S_{Tot}^t = \sum_{i=1}^{N} S_i^t \tag{L.22}$$

hence,

$$S_{Tot}^{t+\mathrm{d}t} = S_{Tot}^t - \frac{S_{Tot}^{t+\mathrm{d}t}}{K_s} * \mathrm{d}t + \sum_{i=1}^{N} R_i \mathrm{d}t \tag{L.23}$$

$$(1 + \frac{\mathrm{d}t}{k}) S_{Tot}^{t+\mathrm{d}t} = S_{Tot}^t + \sum_{i=1}^{N} R_i \mathrm{d}t \tag{L.24}$$

Substitute $1 + \frac{\mathrm{d}t}{K_s} = \tilde{K_s}$ and use Eq. L.22 we find the general rule

$$S_{Tot}^{t+\mathrm{d}t} = \sum_{i=1}^{N} S_i^{t+\mathrm{d}t} = \sum_{i=1}^{N} \frac{S_i^t + R_i \mathrm{d}t}{\tilde{K_s}} \tag{L.25}$$

The outflow is still described with

$$Q_i^{t+\mathrm{d}t} = \frac{S_i^{t+\mathrm{d}t}}{K_s} \tag{L.26}$$

So after adding the relative area (A) contribution term a ($a = \sum_{i=1}^{N} \left(a_i = \frac{A_{\mathrm{HRU};i}}{A_{Total}} \right) \equiv 1$) into our slow reservoir we can apply linear superposition as proposed by Eq. L.16.

Check:

$$Q_{s;Tot} = \sum_{i=1}^{N} a_i Q_{s;i} = \sum_{i=1}^{N} a_i \frac{S_{s;i}^{t+\mathrm{d}t}}{K_s} \tag{L.27}$$

Note that we removed the mutual connection between the seperate HRUs, i.e. they are evaluated independently. Hence, one Slow Reservoir might become negative (e.g. Wetlands) where others stay positive. To avoid incorrect total storage, we apply the constraint Eq. L.17.

L.3.2. INITIAL STORAGE SLOW RESERVOIR S_{s0}

The initial slow groundwater stage is calculated based on a couple of assumptions:

- The average yearly precipitation is represented by year sept 2012- sept 2013.
- Having an infinite sequence of average yearly precipitation volumes should result in storage change $\Delta S_s = 0$.
- Assuming that due to the end of the dry season, the discharge is purely baseflow from the slow response reservoir and not from the fast response reservoir anymore.
- Given the fact that November 2010 to November 2011 and the assumption that Q at 1 November is purely caused by Q_s, the $Q_{s;0} = Q_{s;n}$ for $n = 1, 2, \ldots$ years

- Recharge Slow Response Reservoir: $R = R_s + R_p - R_c$, where R_s is recharge via preferential flow [mm], R_p via matrix percolation [mm], R_c capillary rise [mm]
- $E_a = E_i + E_T = (1-a)P_{year}$ with a the recharge coefficient to preferential flow paths (both fast and slow)
- $P_{year} - E_a = R_s + R_f = R = P_e = a * P_{year}$
- $P_{year} \approx 1400[mm]$ is HRU dependent for the precipitation correction, see Tables L.2 and L.3.
- The recharge to the slow reservoir $R \approx P_e * D = a * P_{year} * D$ where $D \in [0,1]$ is the divider between slow (D=0) and fast (D=1) reservoir.
- R_{year} is added instantaneous (impuls function) to reservoir at February 1st
- $Q = \frac{Aq}{8640}$ [m3/s]; q [mm/day]; A [ha]
- linear reservoir $q = \frac{S}{K}$
- linear reservoir $q(s) = q_0 \exp(-t/K)$
- time delta between November 1st (start 'baseflow year') and February 1st (instantaneous yearly precipitation amount) = 90 days

We describe the groundwater fluctuation with a simplified convolution integral. Where R is the recharge in [mm] and $\exp(\tau/K_s)$ the linear response of the reservoir.

$$q_s(t) = \int_{-\infty}^{\infty} (R(t-\tau)\exp(\frac{\tau}{K_s})\mathrm{d}\tau) \tag{L.28}$$

Eq. L.29 describes the evolution of q_s starting from November 1st and adding instantaneous yearly precipitation amount at February 1st. Where q_0 is the outflow at t=0. Note that the equation takes multiple reservoirs into account, where $\sum_{n=1}^{N}(a_n) = 1$ the relative area of n reservoirs.

$$q_s(t) = \sum_{n=1}^{N} a_n (q_0 \exp(\frac{-t}{K_s}) + \frac{R_n D_n}{K_s} \exp(\frac{-(t-90)}{K_s})) \tag{L.29}$$

To do so, we first have to calculate the S_{s_0} at November 1st. We know that at every November 1st, the discharge $q_s = q_0 = \frac{S_{s0}}{K_s}$; $t = 365$ for only the slow reservoir, so a=1 (1 reservoir).
So Eq. L.29 becomes:

$$\frac{S_{s0}}{K_s} = \frac{S_{s0}}{K_s} \exp(\frac{-t}{K_s}) + \frac{RD}{K_s} \exp(\frac{-(t-90)}{K_s} \tag{L.30}$$

Because of the harmonic character of Eq. L.30 this can be simplified to

$$\frac{S_{s0}}{K_s}(1 - \exp(\frac{-t}{K_s})) = \frac{R*D}{K_s} \exp(\frac{-(t-90)}{K_s} \tag{L.31}$$

from Eq. L.31 we can calculate S_{s0} at November 1st.

$$S_{s0} = \frac{R*D\exp(\frac{-(t-90)}{K_s})}{1-\exp(\frac{-t}{K_s})} \tag{L.32}$$

Now we can calculate the Storage $S_{s0} = q_s(t) * K_s$ at 1 September where $t = 305$ and q_s is calculated with Eq. L.29.

$$S_s(t=305) = \frac{S_{s0}}{K_s} \exp(\frac{-t}{K_s}) + \frac{RD}{K_s} \exp(\frac{-(t-90)}{K_s}) \tag{L.33}$$

AVERAGE PRECIPITATION

Since this methodology is sensitive for divider D (not to name the difficulty for HRU altitude corrected precipitation and multiple HRU). Therefore, we calibrated the recharge with the model.

First we calculated 10 000 Monte Carlo samples with FlexA and FlexC. Then we determined from the model evaluations with the highest 2% of LogNS Conveyance values the total average recharge of the slow reservoir from November 1st, 2010 to November 1st, 2011. Next to this, we derived the HRU specific precipitation amount within the same time interval. Then we calibrated the factor a in the formula $\bar{R} = aP_{Year} * D \rightarrow a = \frac{\bar{R}}{P_{Year}D}$.

This result for FlexC in Table L.2. This is initial condition is hold as a best assumption. Another alternative is to calculate the initial storage for every single model evaluation, however, to limit the computational effort we make this assumption.

HRU	Name	Precipitation [mm/year]	a [-]	Ss0 [mm]
HRU1	Gently flatland Grass Crop	1408 (was 1100)	0.15	165
HRU2	Inselberg Forest	1865 was (1400)	0.15	210
HRU3	Wetland	1415 was(1200)	-0.075	-90

Table L.2: Calibrated constants to determine the HRU specific Ss0 for FlexC

Applying the same technique for FlexA we find

HRU	Name	Precipitation [mm/year]	a [-]	Ss0 [mm]
HRU1	lumped model	1575 was 1000	0.087 was 0.2 plus divider	135

Table L.3: Calibrated constants to determine the Ss0 for FlexA

L.4. ALTITUDE CORRECTED PRECIPITATION

The precipitation is altitude corrected, according to Eq.C.3. First the average altitude for the catchment is derived. Then the total precipitation volume is calculated. Next, this total precipitation volume is divided over the HRUs. This is an arbitrary choice, since we correct the total precipitation depth based on the catchment's average altitude instead on the HRU's average altitude. We chose to do so, in order to ensure that the total precipitation volume for FlexA and FlexC is equal. Otherwise, models would not be comparable.

M

SCRIPTS

M.1. GENERAL

In this study we programmed the FlexTopo model concept from scratch, see Fig. M.1. The gray box contains the user-interface. *Model.ini* is an initialization file and contains calculation specific information. Like paths to databases and output folders, Parameters for measurement points, parameters and/or bandwidths for FlexTopo models and internal calculation timesteps. *RunModel.py* is a simple script from which the model can be runned.

The python model itself (blue box) consist of three layers. The upper layer contains one class *clsMP*, where MP stands for Measurement Point. From this layer all relevant information for this measuremement point and catchment is loaded. Also plots can be made and statistics for the final results are made at this layer.

The second layer consist of different types of FlexModels, like *clsFlexA*. They all have exactly the same functions (and names and variables). So they are interchangeable with each other. In this class model parameter sets with monte carlo are made. Parameter and process constraints are tested. Process charts are made. This layer also steers the calculations of the different HRUs.

The third layer contains the different conceptual rainfall runoff models. We generalized all the HRUs to one single Lumped Conceptual Model class (*clsLCM*). With parameters we turn processes on and off. At this level internal iterations, balance checks and result aggregation is performed. Also log files concerning the calculations are performed at this level.

In the red box the different data sources are presented. The *ModelInput.accdb* is a Microsoft Access database and contains all validated model input. However, aggregation of data is done outside of the database. This gives optimal flexibility.

The *HRU.shp* is a shape file based on the resolution of the Digital Elevation Map [35]. Every single raster is converted into a grid at the same location. See appendix G for further description.

We generalize often used function in two python scripts. *Toolbox.py* contain all functions to read and write to databases. But also scripts for data analysis and evaporation calculations (like Hargreaves and Hamon).

clsHRU reads the shape file and with optimized algorithms queries can be done. The result is model specific HRU compilations.

Finally, the predefined output is given in the green box. At several levels outputs are created. Like box plots, pareto fronts, measurements charts, model calculation charts with bandwidths, parameter sets with objective scores and locations stored.

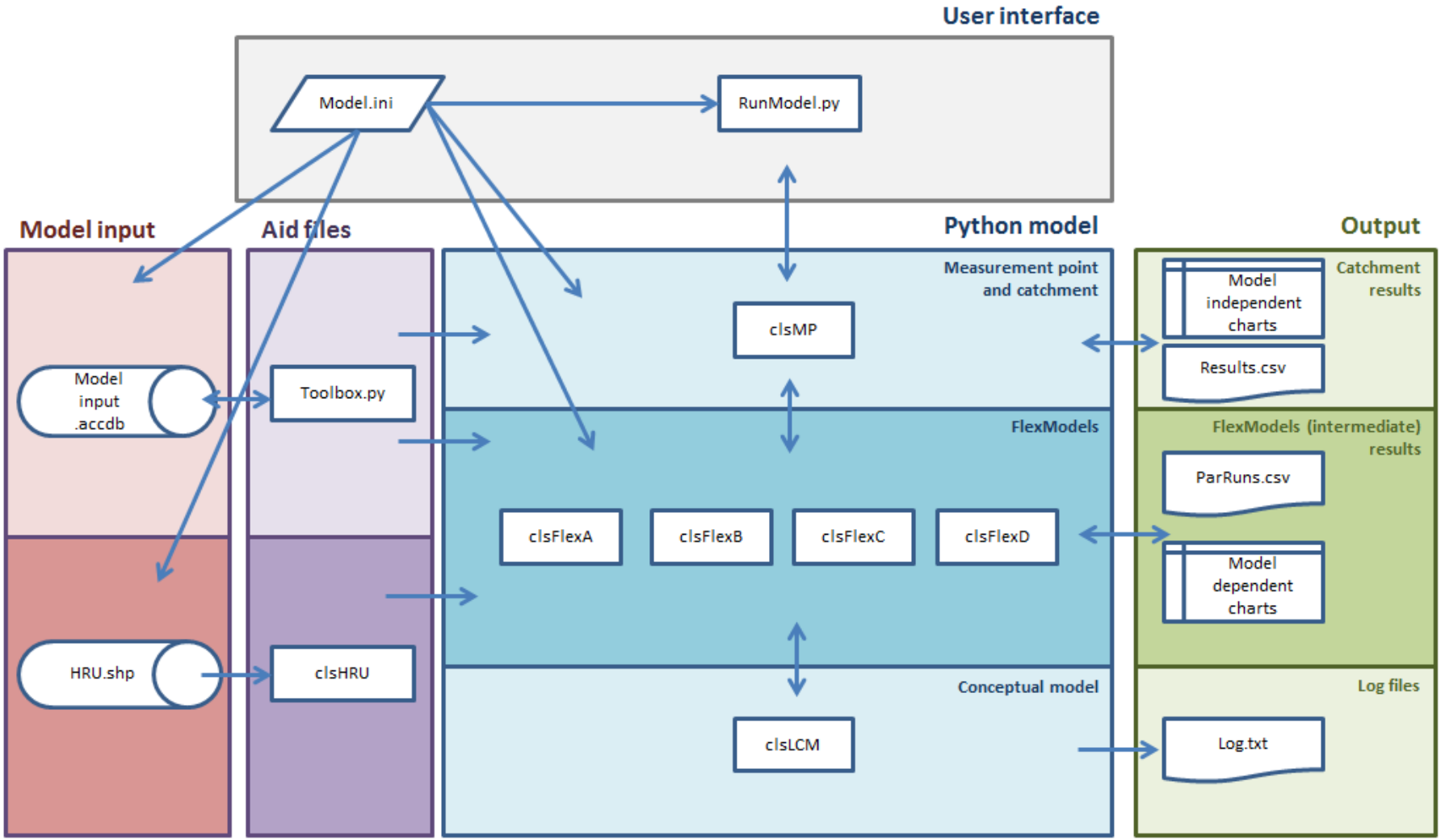

Figure M.1: Flow chart of FlexTopo models.

M.2. SOFTWARE

The model is based on the following software and packages:

- Spyder 2.3.7 Win 7, 32bit
- jdcal 1.0
- pyodbc 3.7
- configparser 3.5.0b2
- Microsoft Access Databases 2010, 32bit[1]
- ESRI ArcMap 10.1[2]

M.3. MODEL.INI

```
[results]
Results_MaxRunsTable = 250
Path_ParRR_Load = D:\Thesis\FlexC\GodiDS_calc1/
Path_Results_Load = D:\Thesis\FlexC\GodiDS_calc1/
Path_Results_Save = D:\Thesis\FlexC\GodiDS_calc1/

[figures]
Path_figs = D:\Thesis\FlexC\GodiDS_calc1/
plot_start_date = 1-9-2010
plot_end_date = 20-7-2014

[mdb]
dbInput = D:/Thesis/Database/Modelinput.accdb
dbMeas = D:/Thesis/Database/Measurements.accdb
path_HRUpoints = D:/Thesis/Database/HRU_points.dbf

[period]
Startdate = '1-9-2010'
Enddate = '20-7-2014'

[constraints]
StartDryMonthNbr = 4
EndDryMonthNbr = 11
Startdate_constraints = 1-9-2011
Enddate_constraints = 20-7-2014
Ea_wetdry_constraint = True
RunoffConstraint = True
RunoffCoef_min = 0.1
RunoffCoef_max = 0.9
ConstraintsFlexB = True
ConstraintsFlexC = True
ConstraintsFlexD = True

[forcing]
# Not used values indicate as -1
StartdateForcing = '1-9-2010'
EnddateForcing = '21-7-2014'
UID_P = 'David'
UID_E = 'Hamon_+08_x115'
nExtensions = 0
nYears = 2
nDays = 365
```

[1] This can be replaced with another open source database structure
[2] This can be replaced with another open source GIS program

```
AltitudeCorrection = False
Altitude = 878

[general]
Scale2mm = True
ScaleQ2mm = False
OCM_RC_Type = LinearRatingCurve
#OCM_RC_Type = LinearRatingCurve or RatingCurve

[FlexA]

[FlexB]

[FlexC]
# Not used values indicate as -1
HRU1_Name = Grass_Crop FlexC
HRU1_dt = 0.5
HRU1_Imax = -1
HRU1_Imax_min = 2.
HRU1_Imax_max = 3.
HRU1_Fc = 0
HRU1_Fc_min = 0
HRU1_Fc_max = 0
HRU1_B = -1
HRU1_B_min = 1.
HRU1_B_max = 5.
HRU1_Sumax = -1
HRU1_Sumax_min = 150
HRU1_Sumax_max = 300
HRU1_Lp = 0.5
HRU1_Lp_min = 0.5
HRU1_Lp_max = 0.5
HRU1_Pper = -1
HRU1_Pper_min = 0
HRU1_Pper_max = 0.5
HRU1_C = 0
HRU1_C_min = 0
HRU1_C_max = 0
HRU1_D = -1
HRU1_D_min = 0.
HRU1_D_max = 1.
HRU1_Nflag = 1
HRU1_Nflag_min = 1
HRU1_Nflag_max = 1
HRU1_Kf = -1
HRU1_Kf_min = 0.
HRU1_Kf_max = 10.
HRU1_Nslag = 1
HRU1_Nslag_min = 1
HRU1_Nslag_max = 1
HRU1_Ks = -1
HRU1_Ks_min = 300
HRU1_Ks_max = 700
HRU1_Si0 =  0
HRU1_Su0 = 0.144
HRU1_Sf0 =  0
HRU1_Ss0 = 0.167

HRU2_Name = Forest FlexC
HRU2_dt = 0.5
etc. etc.
```

```
HRU3_Name = Wetland FlexC
HRU3_dt = 0.1
etc.etc.


[FlexD]


[GodiDS]
UID_O = 'GodiDS_D'
UID_Loc = 'Godi_10_1_ds_out'
Calibration_startdate = 12-12-2012
Calibration_enddate = 1-11-2013
Calibration2_startdate = 1-4-2014
Calibration2_enddate = 20-7-2014
OCM_Bottomslope = 0.01
OCM_a = 1
OCM_a_min = 0
OCM_a_max = 6
OCM_a_C = 0.75
OCM_a_C_min = 0
OCM_a_C_max = 6
OCM_a_Stevens = 3.5
OCM_b_Stevens = 2.9
OCM_bottomoffset = True
OCM_z0 = -1.75
OCM_d0 = 0.03
OCM_d0_min = 0
OCM_d0_max = 0.2
OCM_c0 = 0.00017
OCM_c0_min = 0
OCM_c0_max = -1
Ks = 175
plot_bandwidths = FALSE
Baro_avg = 940
Baro_bandwidth = 20
Bandwidth_startdate = 1-8-2013
Bandwidth_enddate = 25-3-2014
Load_Obs_Qsalt = True
Load_Obs_Qsaltlin = True
Load_Obs_Qsaltcal = True
Load_Obs_C = True
Load_Obs_WDepth = True
Load_Manual_Obs_Wdepth = True
OCM_bottomoffset_manual_obs_Wdepth = True
Load_Obs_Q = False
Load_Obs_pH = true
Load_Obs_Isotopes = True
Load_Obs_EC = True
Load_Obs_Temp = True
Save_Results_qspec = False
Save_Results_Q = True
Save_Results_C = True
Save_Results_WDepth = True

[MessDS]
etc. etc.
```

M.4. RUNMODEL.PY

```
#Import libraries and classes
import clsMP as mp
import pandas as pd
#import Toolbox as tb
#from termcolor import colored
import matplotlib.pyplot as plt
plt.ioff() #suppress automatic show of plots

#Declarate variables
path = r'c:\Daniel\GoogleDrive\Thesis\FlexC\Godi\Calc8/'
Name = "GodiDS"
Model_ini = path + "Model.ini"
ModelCode='FlexC'
FileName = "ParRuns.csv"
nMC = 10000


#Start calculation
River = mp.MP(Name,Model_ini=Model_ini)

River.RR(ModelCode=ModelCode,PrecAltCor='HRUwise')

#generate table with OCM parameters
River.OCMParGen(nMC)
River.ParOutcomesgen(nMC)

#Save and load table with OCM parameters
#River.OCMParSave()
#River.OCMParLoad()


River.RR.LoadForcings(HRUmethod="GIS",handname="HAND50",handvalue=2,slope=11)
River.RR.ParRRgen(nMC)
River.RR.ParRRconstraints(nMC)

River.Results_init_tables()


#Start Loop
for i in River.RR.ParRR.RunID.tolist():
   print "run: ", i

   try:
      River.RR.Calc(i)
   except ValueError as err:
      print err
      #print colored(err, 'red')
      continue

   River.RR.ProcessConstraints(i,Name='all')

   River.RR.Outcome()

   River.OCMmodel(i)

   River.Objectives(i)

   River.Calculation_keep(i)
```

```
    River.ParRunsSave(filename=FileName)
    River.Results_save()



#Postprocessing

#Load results
River.RR.ParRRload(FileName)
River.ParRunsLoad(FileName)
River.OCMParLoad(FileName)
River.ParOutcomesload(FileName)


#Define 'best' calculation
#Cum =  LogNS_C + NS_C > 1-percentile value
x = pd.DataFrame(zip(River.ParRuns.LogNS_C,River.ParRuns.NS_C,River.ParRuns.
    LogNS_C+River.ParRuns.NS_C),index=River.ParRuns.RunID, columns=['LogNS_C','
    NS_C','Cum'])
X = x[x.LogNS_C >= x.LogNS_C.quantile(q=0.99)] #1% best calculations
Best = X[X.LogNS_C == X.LogNS_C.max()].index[0]

#Plot 'best' calculations
River.RR.Calc(int(Best))
River.RR.Outcome()
River.OCMmodel(int(Best))
River.RR.pltFluxes(save=True)
River.RR.pltStorages(save=True)

#Plot final results.
River.pltParameters(ModelCode=ModelCode, Objective='LogNS_C')
River.pltPareto(ModelCode=ModelCode)
River.pltConversionParameters()
River.pltBoxPlotObjectives(ModelCode = ModelCode, SaveFigs=True, filename="
    Boxplot Objectives.png")

#Plot Final hydrographs with modeloutcomes and bandwidths
River.Results_load_all()
River.pltCalculation(save=True,n=int(Best),filename="Best Calculation, nr %i
    LogNS_C = %f.png" % (Best,round(X.ix[int(Best), 'LogNS_C'],2)))
River.pltBandWidths(save=True)
```

M.5. clsHRU

```
#import packages
import pandas as pd
import pysal as ps
import numpy as np
import operator as op #for example ge >=, le <=, eq ==

class HRU():
"""This class module imports a shapefile with centerpoints at every grid cell
    within the area of interest.
The point shapes contains information of several datasources, e.g.,DEM from
    Aster2 and GlobCover.
Every point represents an area of 30x30m2.

For information about shapefile see self.__info__
```

```
With this module fast sensitivity analysis can be performed.

Not implemented, but possible: calculate per HRU
- the average distance to stream,
- the routing distance through the stream,
- the eucledian distance between points,
- the volume in the catchment, the ...
- an infiltration zone from the other side of the
mountain within a certain radius and a certain infiltration inclination from
    the outlet point
"""

def __init__(self,file=r'\6.Thesis\3.HTB\HRU\9.HRU_POINTS\HRU_points.dbf'):
""" initialisation of class file"""

self.filename = file
#open file:
dbf = ps.open(self.filename)
#d = {col: dbf.by_col(col) for col in dbf.header}
self.HRU = pd.DataFrame({col: dbf.by_col(col) for col in dbf.header}) #pretty
    slow routine

# sqlCatchment filter query
self.sql_catchment = {
'Chir_1_1_us_in'       : "UID == 'Chir_1_1_us_in' ",
'Chir_2_1_us_in'       : "UID == 'Chir_2_1_us_in' ",
'Chir_5'               : "UID == 'Chir_1_1_us_in' or UID == 'Chir_2_1_us_in' or
    UID == 'Chir_5'",
'Chir_6'               : "UID == 'Chir_1_1_us_in' or UID == 'Chir_2_1_us_in' or
    UID == 'Chir_5' or UID == 'Chir_6'",
'Chir_7_ds_out'        : "UID == 'Chir_1_1_us_in' or UID == 'Chir_2_1_us_in' or
    UID == 'Chir_5' or UID == 'Chir_6' or UID== 'Chir_7_ds_out'",
#'Godi_1_1_us_in'       : ,
#'Godi_3_1_us_in'       : ,
#'Godi_3_3_us_in'       : ,
#'Godi_5_1_us_in'       : ,
#'Godi_5_2_us_in'       : ,
'Godi_6'               : "UID == 'Godi_1_1_us_in' or UID =='Godi_5_2_us_in' or
   UID =='Godi_5_1_us_in' or UID =='Godi_3_3_us_in' or UID == 'Godi_3_1_us_in'
    ",
#'Godi_7_1_us_in'       : ,
#'Godi_7_2_us_in'       : ,
#'Godi_8_1_us_in'       : ,
#'Godi_9'               : ,
'Godi_10_1_ds_out'     : "UID == 'Godi_10_1_ds_out' or UID == 'Godi_9' or UID
   == 'Godi_7_1_us_in' or UID == 'Godi_8_1_us_in' or UID == 'Godi_7_2_us_in'
   or UID == 'Godi_1_1_us_in' or UID =='Godi_5_2_us_in' or UID ==
   Godi_5_1_us_in' or UID =='Godi_3_3_us_in' or UID == 'Godi_3_1_us_in' ",
'Messica_1_us_in'      : "UID == 'Messica_1_us_in'",
#'Messica_2'            : ,
'Messica_3_ds_out'     : "UID != '' and UID != 'Revue_1'", #everything apart
   from this two catchments
'Nyamanguero_1_ds_out' : "UID == 'Nyamanguero_1_ds_out'",
'Nyausanga_1_ds_out'   : "UID == 'Nyausanga_1_ds_out'",
'Revue_1'              : "UID == 'Revue_1'",
'Ruaga_1_ds_out'       : "UID == 'Ruaga_1_ds_out' and UID == 'Ruaga_2'",
}


#"""Shape file contains the following information"""
self.__info__ = {
```

```
'POINTID'    : "Unique ID of this point",
'Catchment'  : "Unique code of Catchment",
'DEM'        : "DEM value in [m+AD] from Aster2 raster",
'FlowAcc'    : "Total number of draining cells to this specific raster cell",
'FlowLength' : "Total flow length [m] from this point to the very outlet of the
    catchment",
'GlobCover'  : "GlobCover grid value from GlobCover FAO",
'HAND20'     : "Calculated HAND value [m] = DEM this point - DEM nearest
   drainage cell",
'Outlet'     : "Unique ID catchment if this point is the catchment outlet",
'UID'        : "Unique ID from this catchment",
'dist2str'   : "Calculated distance [m] from this point to nearest drainage
   point",
'slop'       : "Slope [degrees] calculated from the DEM",
'x'          : "y-coordinate HRU point",
'y'          : "y-coordinate HRU point"
}


def dffilterstatement(df, col, operator, value):
""" build a filter statement for pandas dataframe:
df: dataframe
col: column name
Operator with packages operator, typically operator.ge >=, operator.le <=,
   operator.eq ==
value: value to compare with"""
return operator(df[col],value)


def dffilteror(self,*b):
"""Filter dataframe with multiple or-statements from dffilterstatement() """
self.HRU[np.logical_or(*b)]


def dffilterand(self,*b):
""" filters dataframe on multiple and-statements dffilterstatement()"""
self.HRU[np.logical_and(*b)]


def dffilterCatchment(self,UID):
""" filter HRU for catchment
"""
self.HRU.query(self.sql_catchment[UID])


def FlexA(self,UID):
""" returns values for HRU FlexA, is dffiltercatchment(UID) """
self.FlexA_Area = self.HRU.query(self.sql_catchment[UID])


print " "
print "FlexA"
print "Total: " , len(self.FlexA_Area)


def FlexB(self,UID,hand=5.9):
""" Returns values for HRU FlexB """

self.FlexB_Wetland   = self.HRU.query("(%s) and HAND20<=%f" % (self.
   sql_catchment[UID], hand))
```

```
self.FlexB_Remainder = self.HRU.query("(%s) and HAND20> %f" % (self.
    sql_catchment[UID], hand))

print " "
print "FlexB"
print "Wetland: " , len(self.FlexB_Wetland)
print "Remainder: " , len(self.FlexB_Remainder)


def FlexC(self,UID, hand=5.9):
""" Returns values for HRU FlexC
Wetland   : HAND20 <= hand
Forest    : HAND20 >  hand and GlobCover* = [40, 50, 60, 90, 100]
GrassCrop : HAND20 >  hand and GlobCover* = [14, 30, 120, 130]

* based on GlobCover map from FAO
"""
self.FlexC_Wetland   = self.HRU.query("(%s) and HAND20<=%f" % (self.
    sql_catchment[UID],hand))
self.FlexC_Forest    = self.HRU.query("(%s) and HAND20> %f and (GlobCover == 40
     or GlobCover == 50 or GlobCover == 60 or GlobCover == 90 or GlobCover ==
    100 ) " % (self.sql_catchment[UID],hand))
self.FlexC_GrassCrop = self.HRU.query("(%s) and HAND20> %f and (GlobCover == 14
     or GlobCover == 30 or GlobCover == 120 or GlobCover == 130 )" % (self.
    sql_catchment[UID],hand))

print " "
print "FlexC"
print "Wetland: " , len(self.FlexC_Wetland)
print "Forest: " , len(self.FlexC_Forest)
print "Grass Crop: " , len(self.FlexC_GrassCrop)


def FlexD(self,UID, hand=5.9, slop=12.9, hillhigh = 800):
""" Returns values for HRU FlexD
Wetland   : HAND20 <= hand
Plateau   : HAND20 >  hand and slope < slop
Hill_high : HAND20 >  hand and slope >= slop and DEM >= 800
Hill_low  : HAND20 >  hand and slope >= slop and DEM < 800
"""
self.FlexD_Wetland  = self.HRU.query("(%s) and HAND20<=%f" % (self.
    sql_catchment[UID],hand))
self.FlexD_Plateau  = self.HRU.query("(%s) and HAND20> %f and slop<=%f" % (self
    .sql_catchment[UID],hand,slop))
self.FlexD_Hillhigh = self.HRU.query("(%s) and HAND20> %f and slop> %f and DEM
    >=%f" % (self.sql_catchment[UID],hand,slop,hillhigh))
self.FlexD_Hilllow  = self.HRU.query("(%s) and HAND20> %f and slop> %f and DEM<
     %f" % (self.sql_catchment[UID],hand,slop,hillhigh))

print ""
print "FlexD"
print "Wetland: " , len(self.FlexD_Wetland)
print "Plateau: " , len(self.FlexD_Plateau)
print "Hill high: " , len(self.FlexD_Hillhigh)
print "Hill low: " , len(self.FlexD_Hilllow)
```

M.6. REMAINDER MODEL

The remainder of the model code is not reported here. If interested, be welcome to contact the author.

M.7. IMPROVEMENTS

Several improvements are already mentioned. In order to:

- Improve speed (1), one should calculate on multiple GPU cores.
- Improve speed (2), cythonize several scripts
- Improve speed (3), make tailor made models (so not working with classes, but strait forward)
- Improve calibration (1), implement calibration routines like AMALGAM [46] or MOSCEM-UA[45].
- Improve calibratoin (2), implement GLUE to calculate weighed model outcomes (a different method than using percentiles).
- Implement HRU classification directly from source data.
- Read in spatial deviated data directly from source grids.

N

CALIBRATION GODI DS

N.1. INTRODUCTION

Calibrating on Godi downstream station.

General settings:

- 10,000 runs
- consider best 1% runs, where best is NS Conveyance + LnNS Conveyance.
- calculation timestep $\Delta t = 0.1$ days, which give more stable outcomes for the wetlands.

- Remember that during peak flows the water levels will have a extra setup due to vegetation and obstruction, so the fact that we do not really calculate the very peaks might be explained with this.

- Remember that the flow depth might be less in dry season 2013, implying less outflow, implying more storage in the system and therefore more outflow in 2013-2014.

parameters NSLN_c and LogNS_C are linear related. So using both objectives does not provide any additional information.

N.2. FLEXA

N.2.1. GODIDS CALC0

This run gives a pretty good first result of for our models. A Ks value between 400 and 600 days seems to approximate the slow baseflow pretty good, the sudden dip in around december 2013 is not explained by the models. It is not clear what happened in at that moment.

In general the base flow in the dry season of 2013 is nicely approximated by the models, the dry season of 2014 is less good approximated, although the recession curve in 2014 is maybe more likely than the flat observed conveyance, possibly we have here positive backwatercurves.

However, the peaks waterdepts and conveyances are underestimated and the discharges Q are broadly overestimated. Apparently the Output Conversion Model is perfectly closing the conveyance- or water balance with the roughness and bottom slope term $\bar{a}$. Therefore we will fixate this parameter. To do so, we derived $\bar{a}$ from the conveyance method as described in Chapter 2.4.

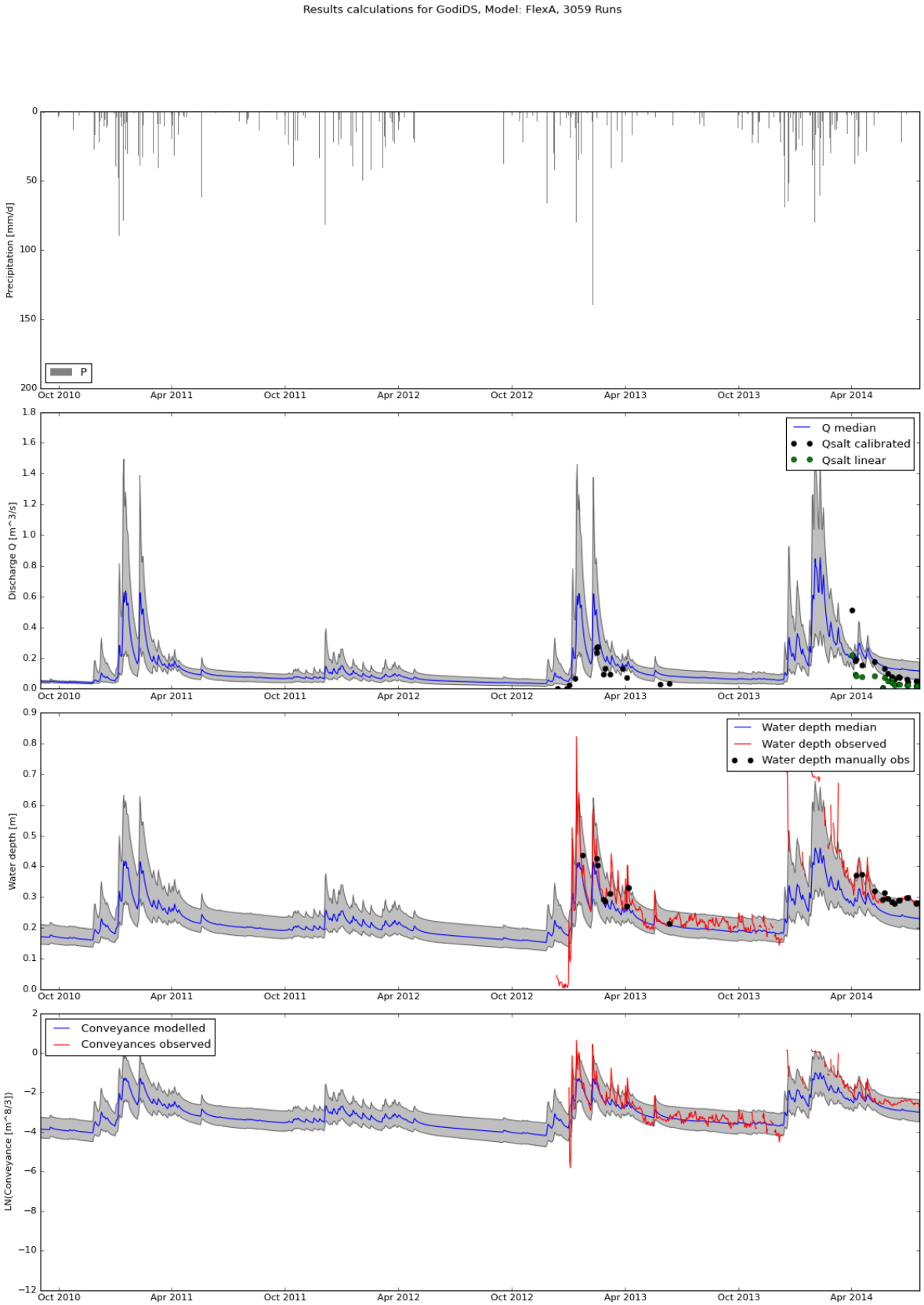
Results calculations for GodiDS, Model: FlexA, 3059 Runs
Precipitation [mm/d]
P
Discharge Q [m^3/s]
Q median
Qsalt calibrated
Qsalt linear
Water depth [m]
Water depth median
Water depth observed
Water depth manually obs
LN(Conveyance [m^8/3])
Conveyance modelled
Conveyances observed
Oct 2010
Apr 2011
Oct 2011
Apr 2012
Oct 2012
Apr 2013
Oct 2013
Apr 2014

Figure N.1

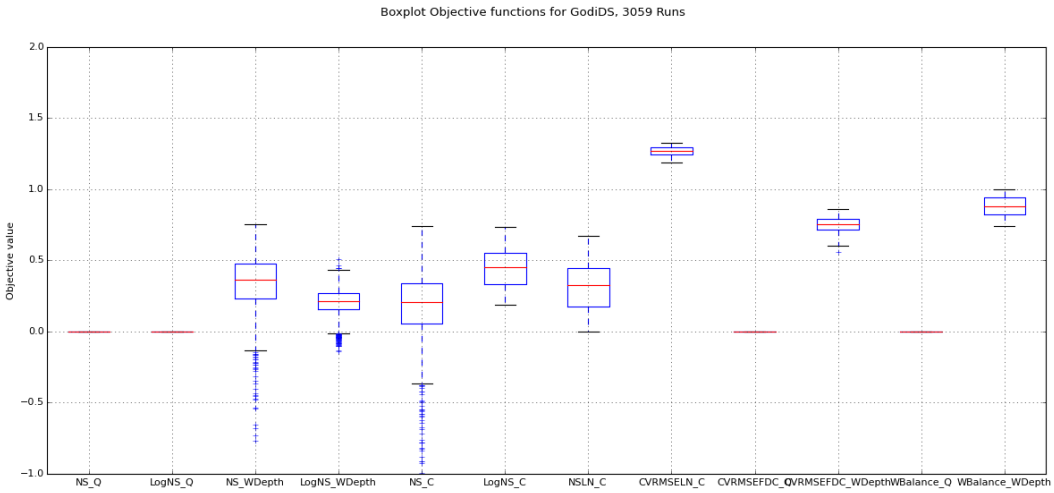

Figure N.2

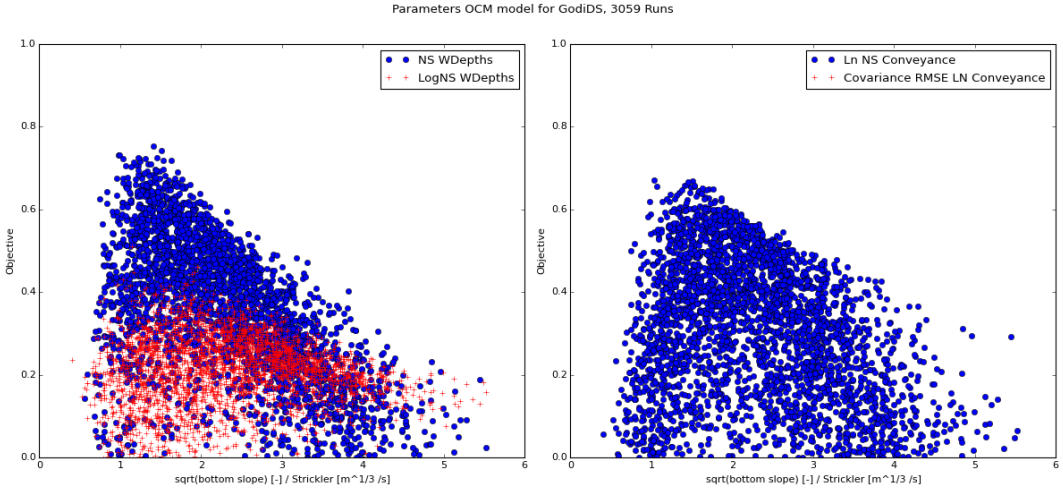

Figure N.3

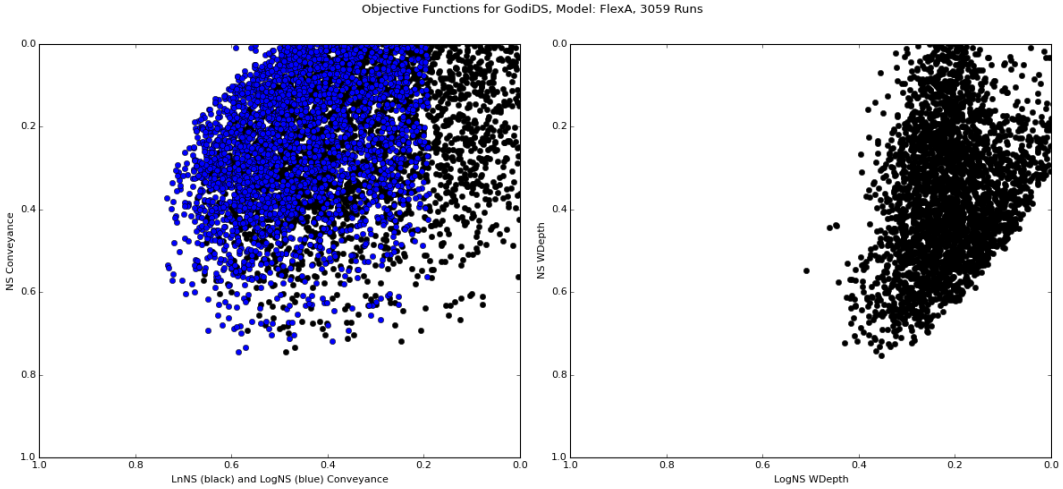

Figure N.4

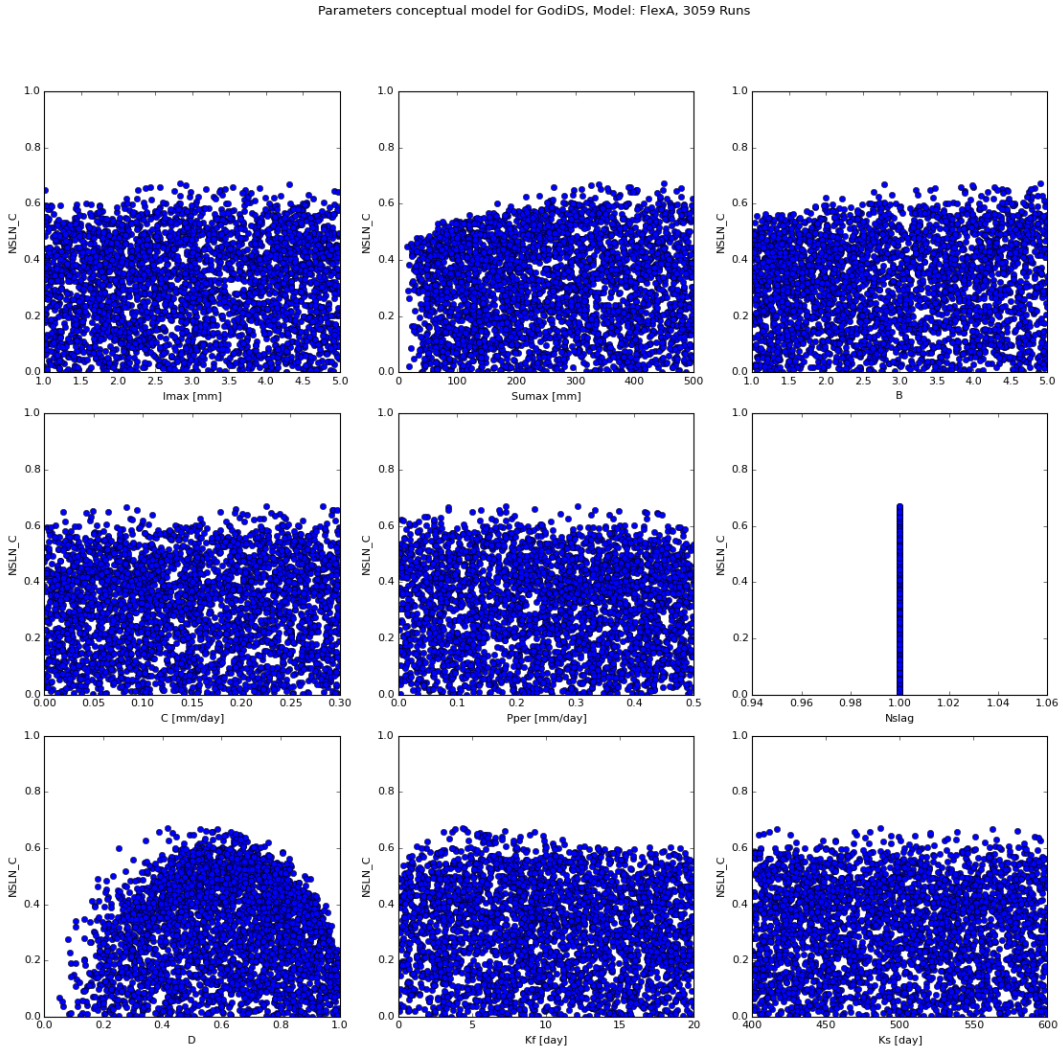
Parameters conceptual model for GodiDS, Model: FlexA, 3059 Runs
NSLN_C
Imax [mm]
Sumax [mm]
B
C [mm/day]
Pper [mm/day]
Nslag
D
Kf [day]
Ks [day]

Figure N.5

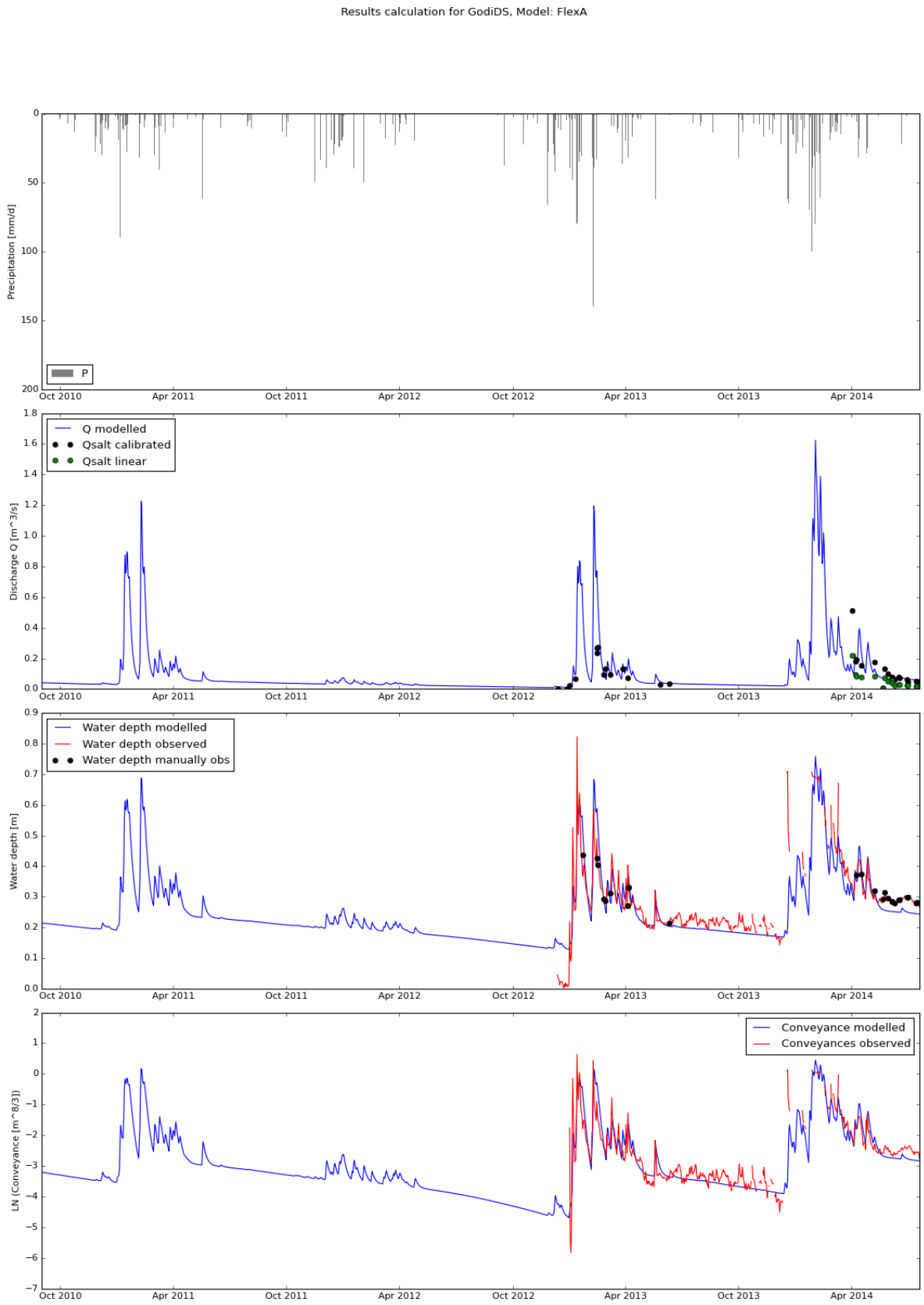

Figure N.6: On of the best calculations, Nr 9416 with LnNS_C = 0.67

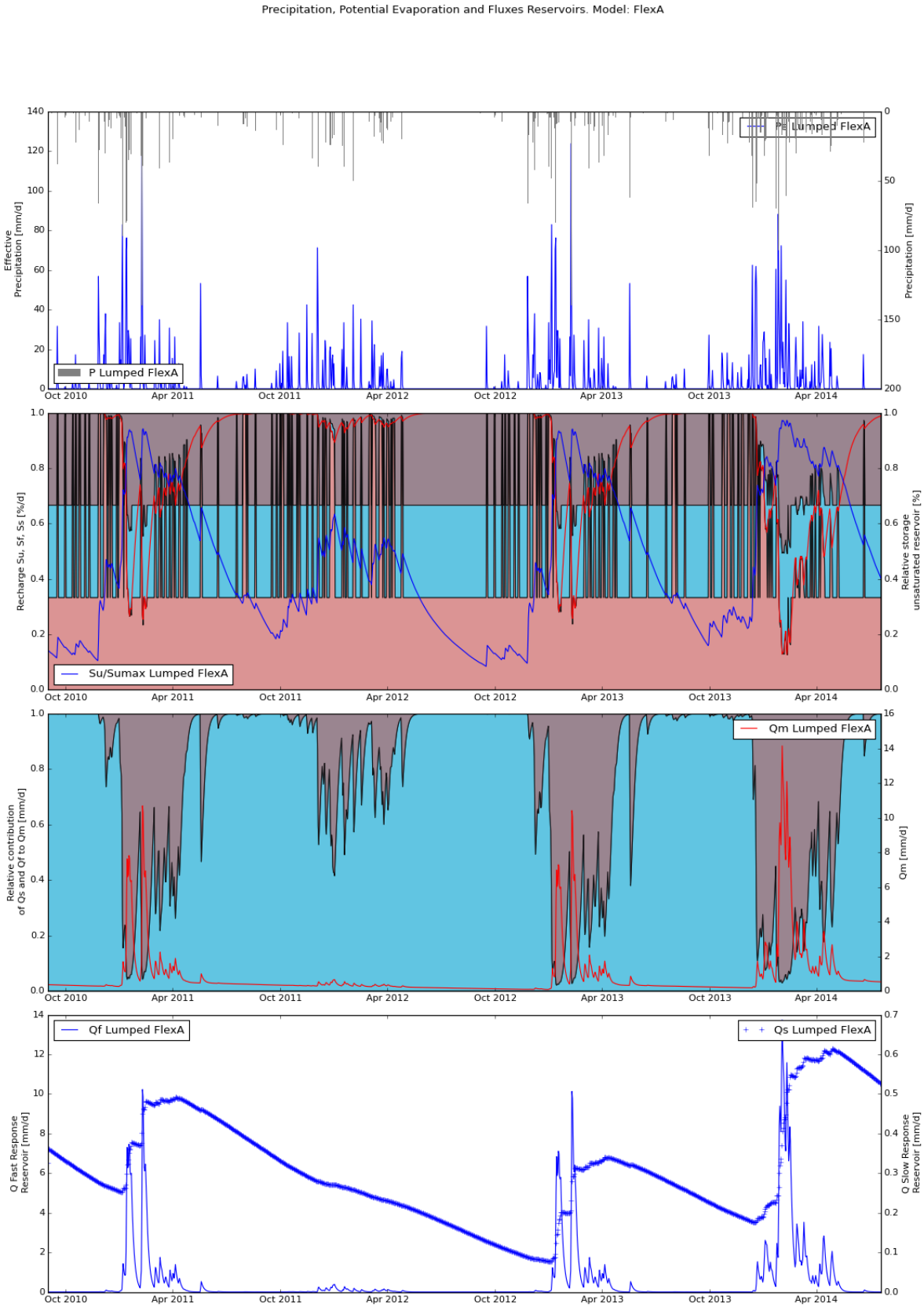
Precipitation, Potential Evaporation and Fluxes Reservoirs. Model: FlexA
Effective Precipitation [mm/d]
Precipitation [mm/d]
Pe Lumped FlexA
P Lumped FlexA
Recharge Su, Sf, Ss [%/d]
Relative storage unsaturated reservoir [%]
Su/Sumax Lumped FlexA
Relative contribution of Qs and Qf to Qm [mm/d]
Qm [mm/d]
Qm Lumped FlexA
Q Fast Response Reservoir [mm/d]
Q Slow Response Reservoir [mm/d]
Qf Lumped FlexA
Qs Lumped FlexA
Oct 2010
Apr 2011
Oct 2011
Apr 2012
Oct 2012
Apr 2013
Oct 2013
Apr 2014

Figure N.7

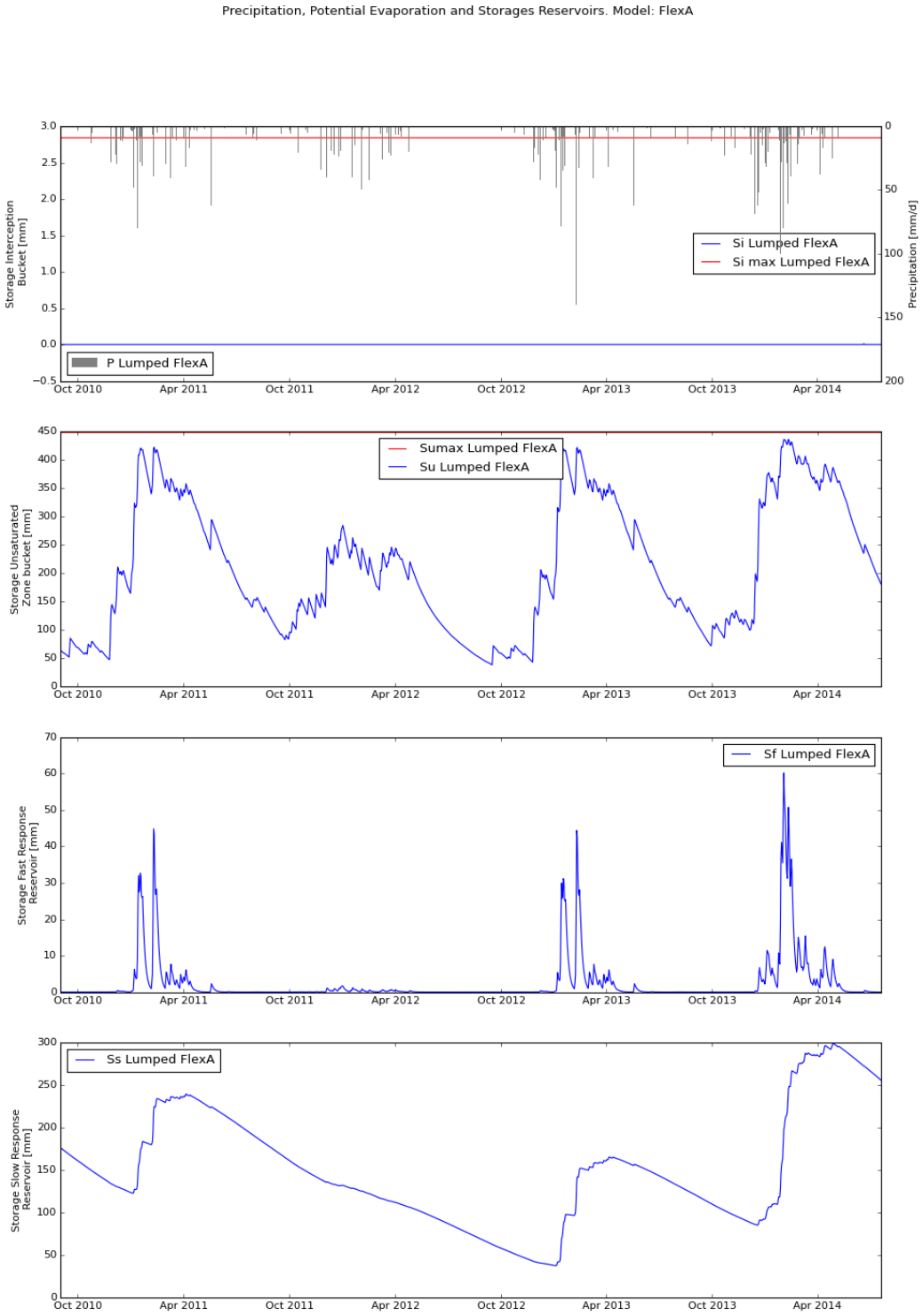
Precipitation, Potential Evaporation and Storages Reservoirs. Model: FlexA
Storage Interception Bucket [mm]
Precipitation [mm/d]
Si Lumped FlexA
Si max Lumped FlexA
P Lumped FlexA
Storage Unsaturated Zone bucket [mm]
Sumax Lumped FlexA
Su Lumped FlexA
Storage Fast Response Reservoir [mm]
Sf Lumped FlexA
Storage Slow Response Reservoir [mm]
Ss Lumped FlexA
Oct 2010
Apr 2011
Oct 2011
Apr 2012
Oct 2012
Apr 2013
Oct 2013
Apr 2014

Figure N.8

N.2.2. GODIDS CALC1

Applied settings Godi DS - Calc 0

Adjustments. Adjust $\bar{a} = 0.75$ based on the deriving roughness and bottom slope coefficient from the conveyance method.

Observe that the observed values are nicely within the 10th and 90th percentile values of all model outcomes, Fig. N.9. This is an improvement compared to the previous calculation GodiDS_Calc0. Although the results look less impressive, the model outflow Q and the salti dilution measurements are more in line with each other (which is of course a result of our $\bar{a}$ choice). For the conveyances both the peaks and the dry weather recession are a little overestimated. From the boxplot Fig. N.12 we observe that the overall objective outcomes are pretty low. The boxplot also explains the skewness of the Pareto fronts in Fig. N.10.

The plots in Figs. N.13, N.14 and N.15 of one of the best calculations with a LnNS = 0.59, shows us that the storage in the slow reservoir increases during the wet seasons of 2012-2013 and 2013- 2014, which is line with our expectations based on both the increased discharges measured (or elevated water levels) and based on the amount of rainfall compared to 2011-2012, for which the system just emptied. The peaks in the wet season are mainly caused by the fast components according to this model schematisation. This is plausible, but there might be a little to less groundwater depletion. In majority of the models show a slow -fast flow divider of around 0.4, which implies that more water goes to the fast process than the slow one.

The Conveyance graph might be a little to spiky. On the one hand, the spikiness is good, since this can be explained by the fast processes, on the other hand, the highest conveyances are maybe caused by the increased flow resistance, and not by peak flows only.

Improvements for the next calculation. Since the Sumax and the β parameters show clear optima at the upper boundary, we stretch these parameter spaces to observe the effect.

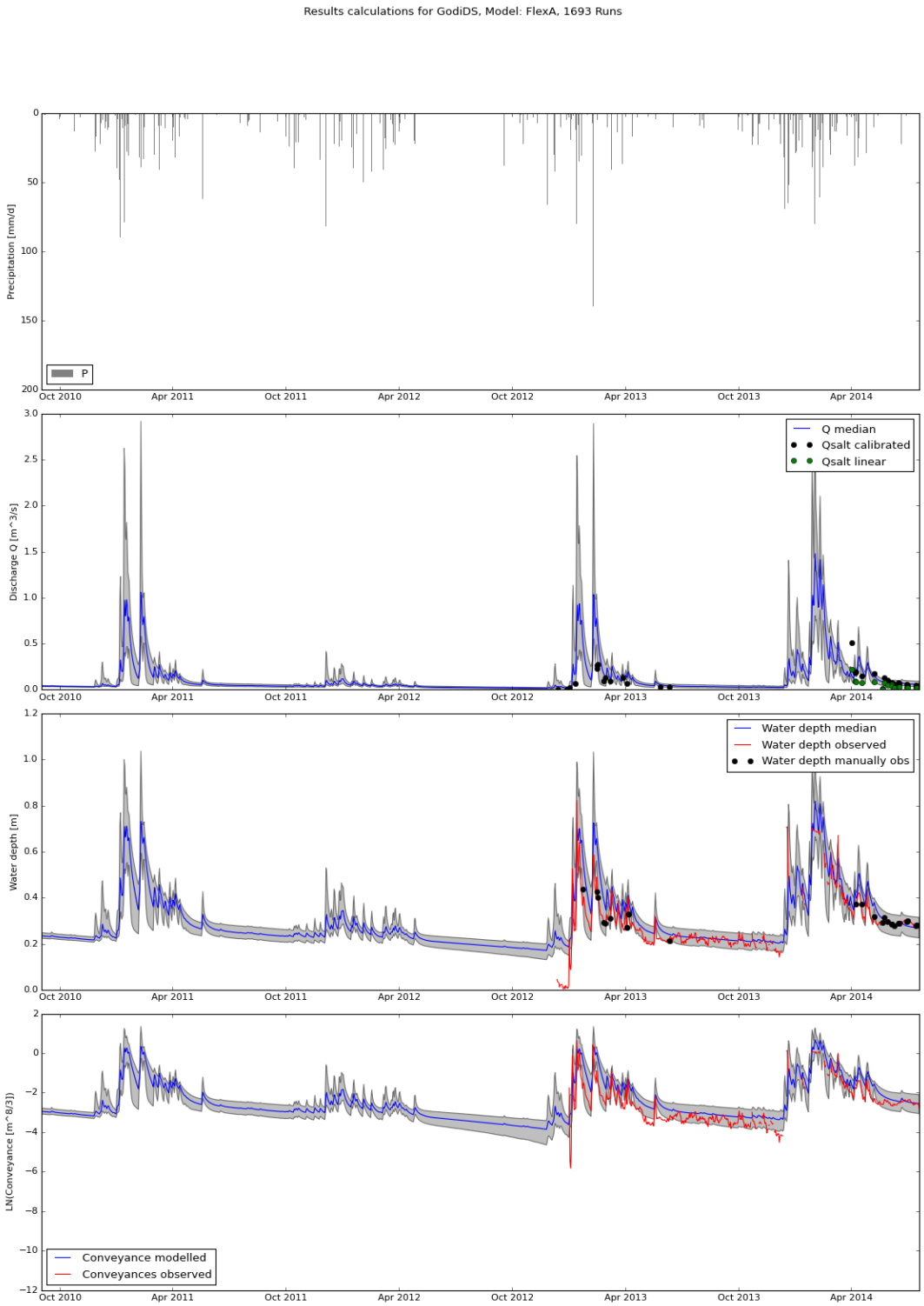

Figure N.9: GodiDS Calc1, bandwidth around observations

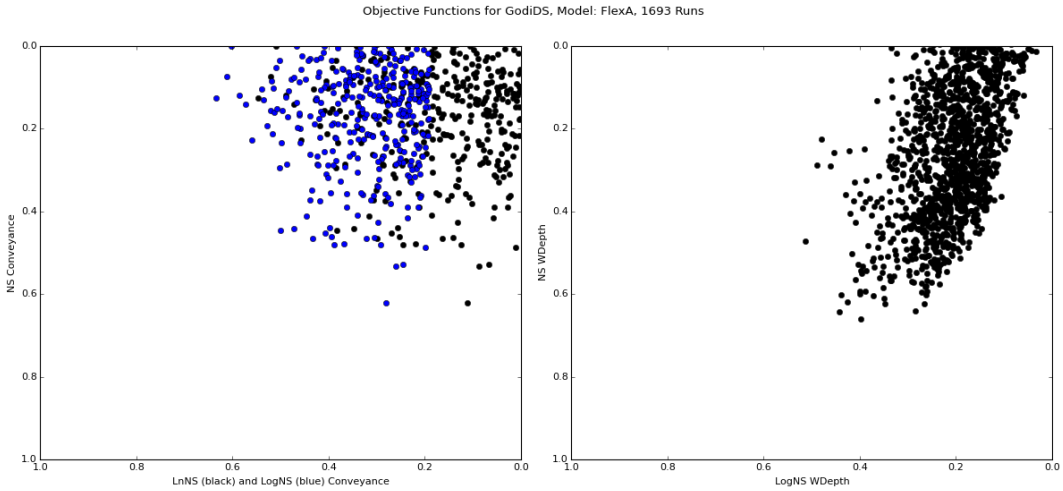

Figure N.10

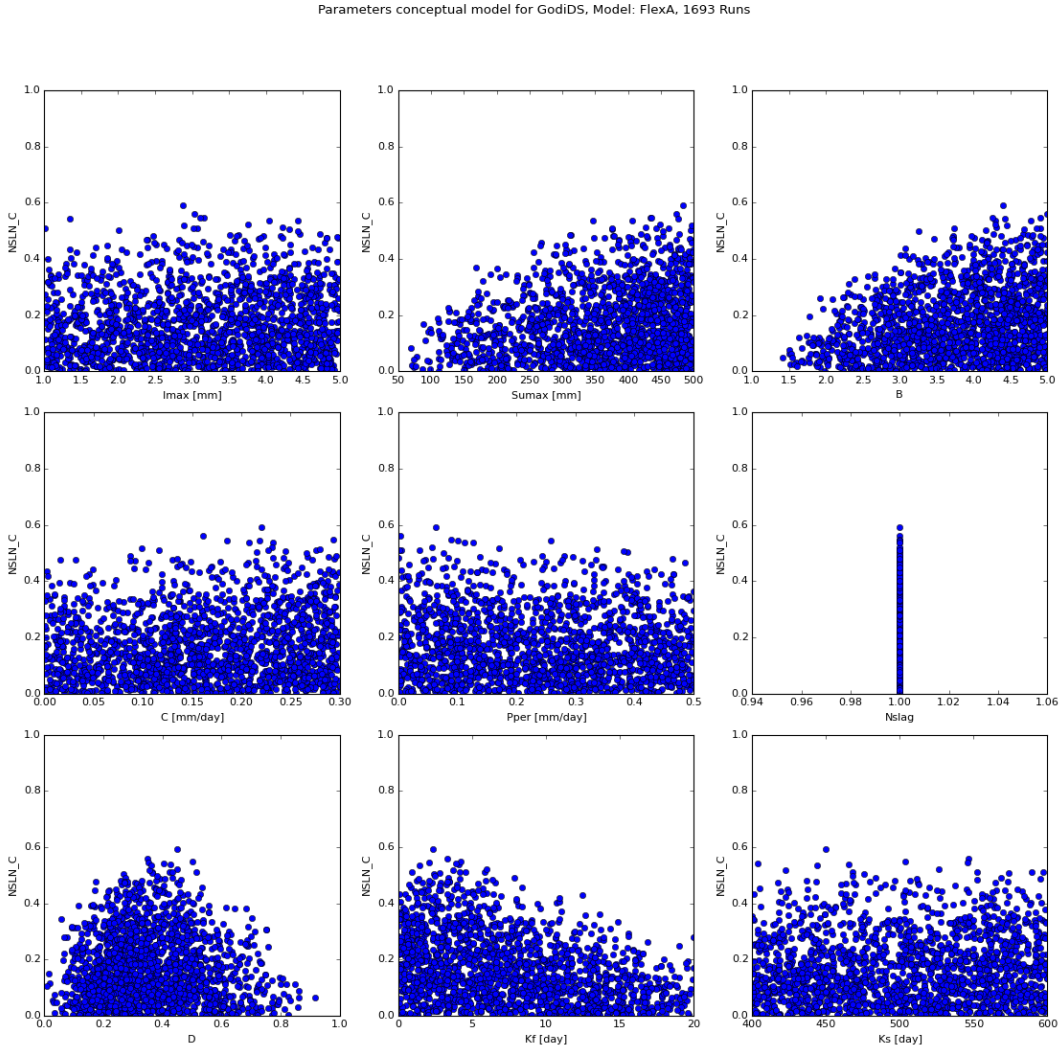

Figure N.11: Parameter plot belonging to Calc1 Godi DS

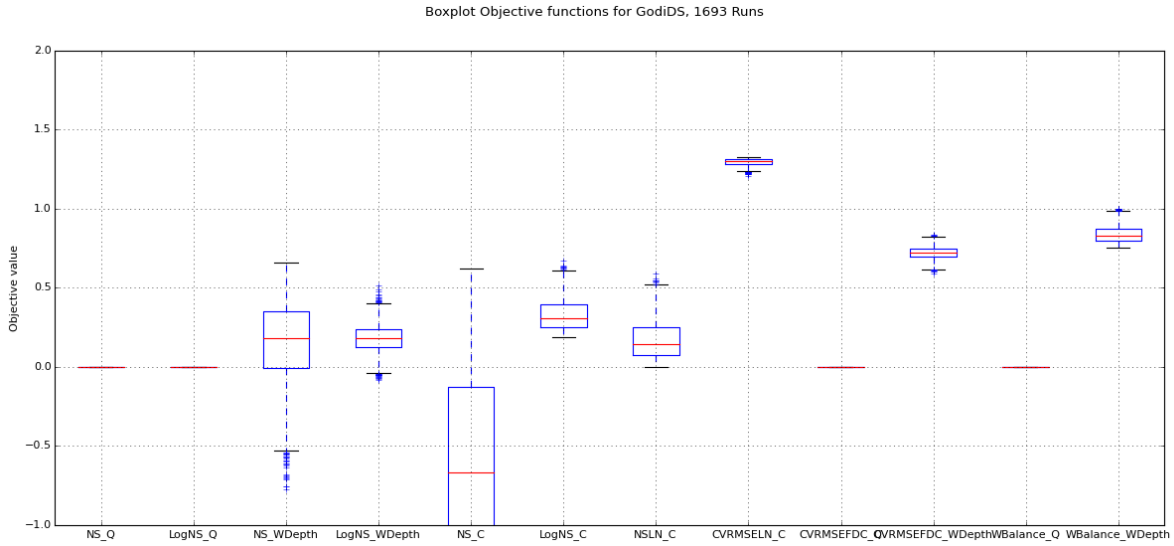

Figure N.12: Boxplot Objective functions Godi DS Calc1

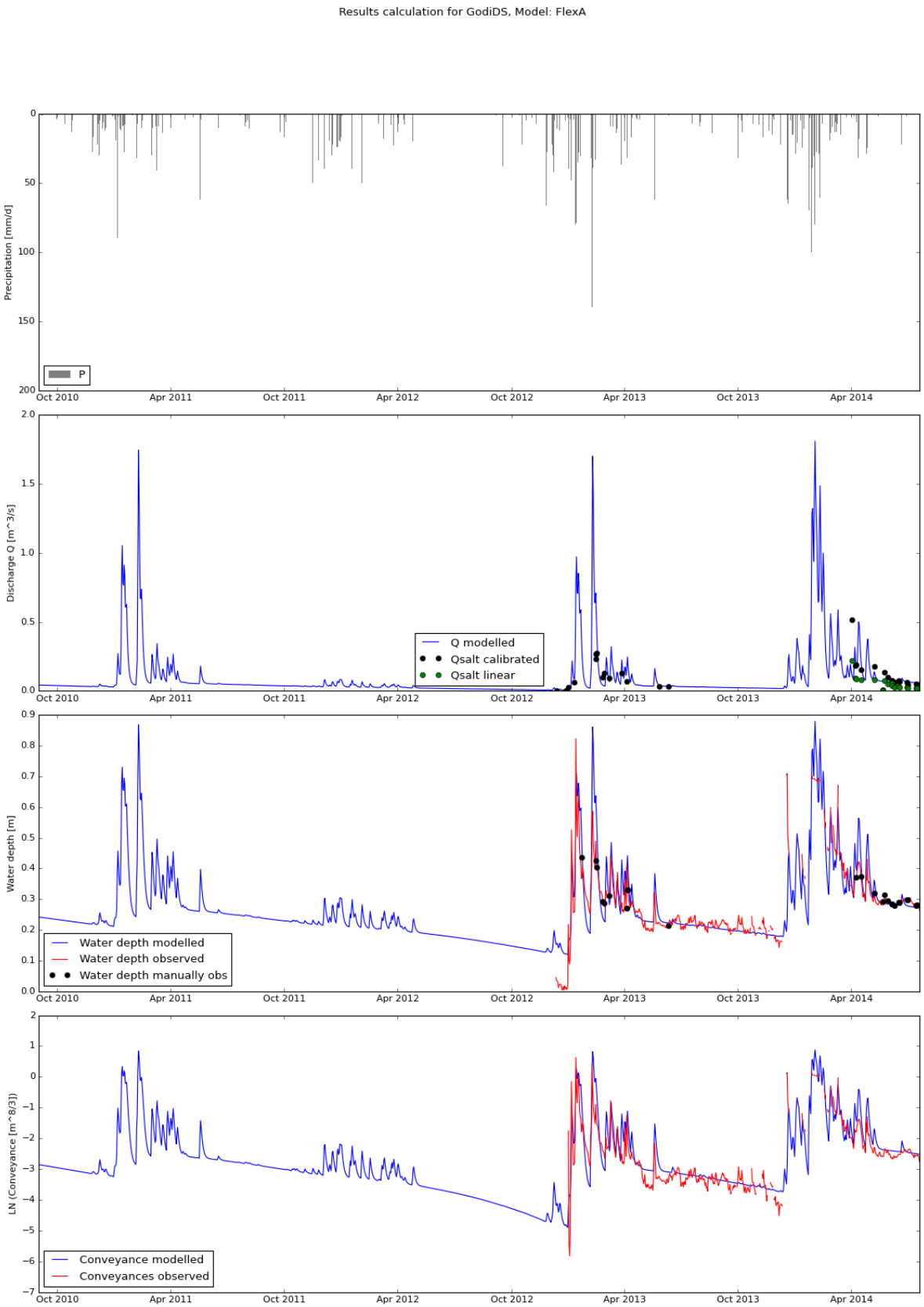

Figure N.13: One of the best calculations nr 1544 with LnNS Conveyance = 0.59

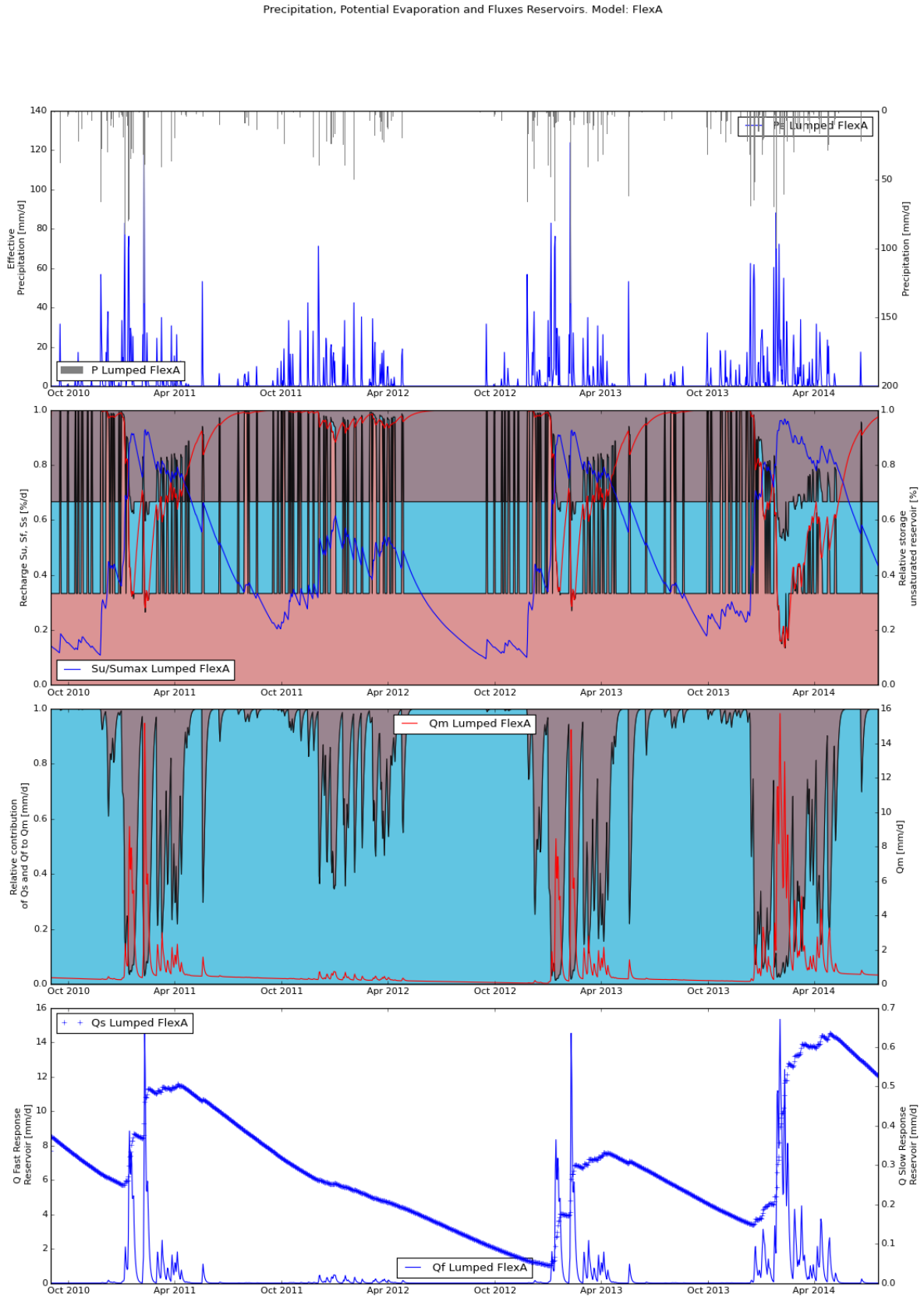
Precipitation, Potential Evaporation and Fluxes Reservoirs. Model: FlexA
Effective Precipitation [mm/d]
Precipitation [mm/d]
P Lumped FlexA
Pe Lumped FlexA
Recharge Su, Sf, Ss [%/d]
Relative storage unsaturated reservoir [%]
Su/Sumax Lumped FlexA
Relative contribution of Qs and Qf to Qm [mm/d]
Qm [mm/d]
Qm Lumped FlexA
Q Fast Response Reservoir [mm/d]
Q Slow Response Reservoir [mm/d]
Qs Lumped FlexA
Qf Lumped FlexA
Oct 2010
Apr 2011
Oct 2011
Apr 2012
Oct 2012
Apr 2013
Oct 2013
Apr 2014

Figure N.14

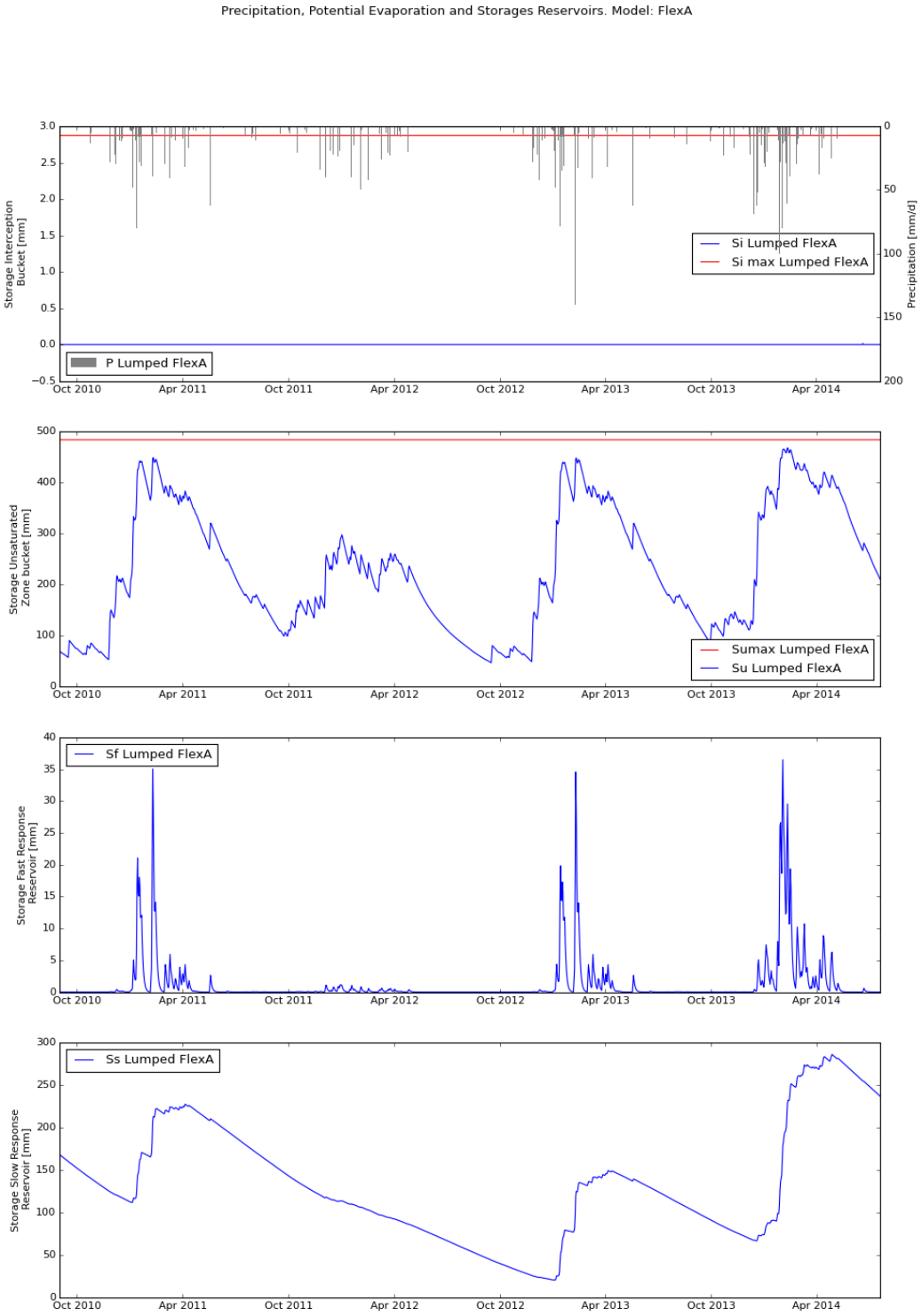
Precipitation, Potential Evaporation and Storages Reservoirs. Model: FlexA
Storage Interception Bucket [mm]
Precipitation [mm/d]
Si Lumped FlexA
Si max Lumped FlexA
P Lumped FlexA
Storage Unsaturated Zone bucket [mm]
Sumax Lumped FlexA
Su Lumped FlexA
Storage Fast Response Reservoir [mm]
Sf Lumped FlexA
Storage Slow Response Reservoir [mm]
Ss Lumped FlexA
Oct 2010
Apr 2011
Oct 2011
Apr 2012
Oct 2012
Apr 2013
Oct 2013
Apr 2014

Figure N.15

N.2.3. GODIDS CALC2

Same settings as GodiDS Calc1, but Sumax $\in [10, 1000] mm$ and $\beta \in [1, 10]$.

The extended parameter samples of Sumax and β do lead to a better overall performance in the boxplots Fig. N.19 and pareto fronts Fig. N.17. Since the risk of over compensation by other parameters is increased, we will restrict the Sumax and β values, but leave the original samples a little larger.

Sumax $\in [10, 600]$ and $\beta \in [1, 6]$.

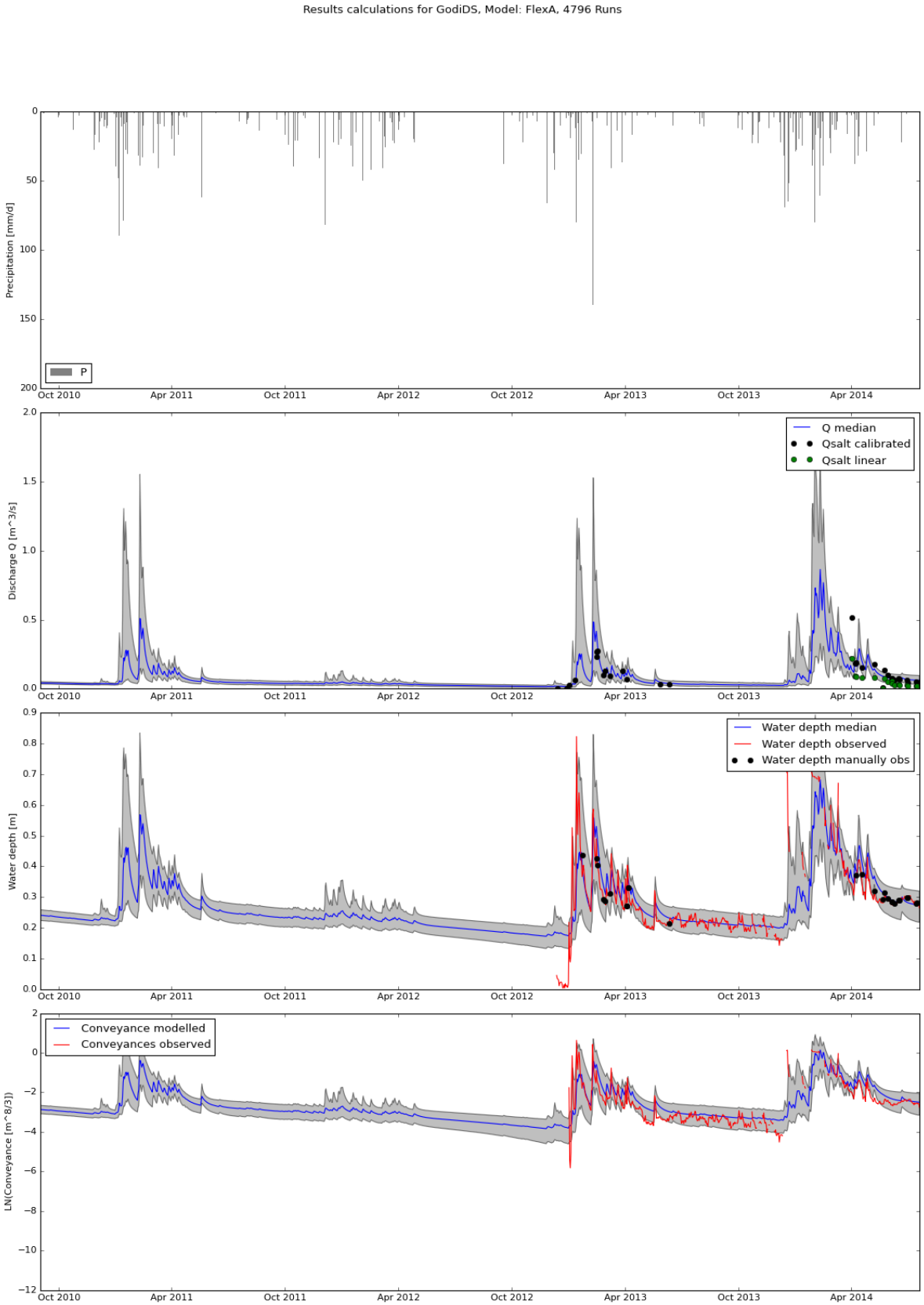
Results calculations for GodiDS, Model: FlexA, 4796 Runs
Precipitation [mm/d]
P
Discharge Q [m^3/s]
Q median
Qsalt calibrated
Qsalt linear
Water depth [m]
Water depth median
Water depth observed
Water depth manually obs
LN(Conveyance [m^8/3])
Conveyance modelled
Conveyances observed
Oct 2010
Apr 2011
Oct 2011
Apr 2012
Oct 2012
Apr 2013
Oct 2013
Apr 2014

Figure N.16

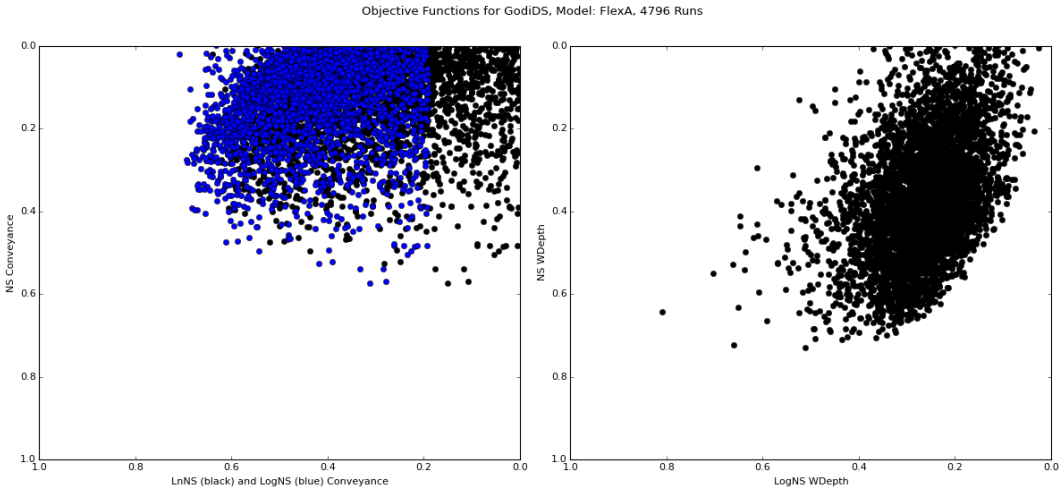

Figure N.17

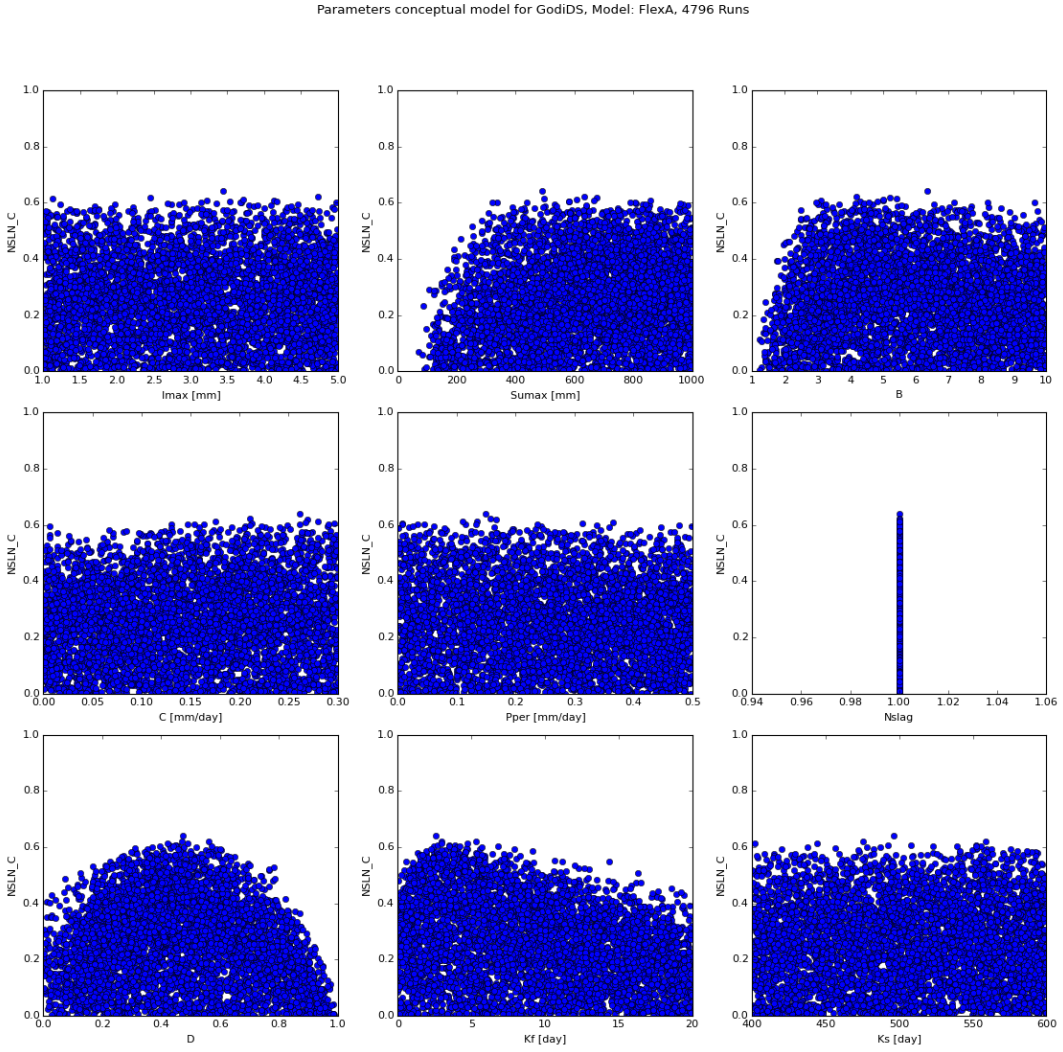

Figure N.18

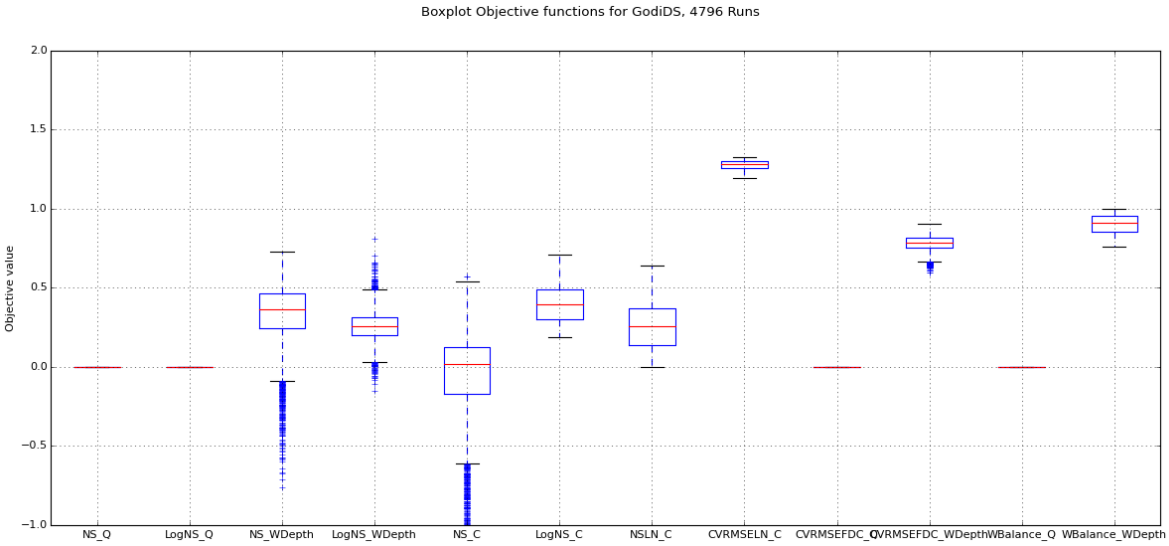
Boxplot Objective functions for GodiDS, 4796 Runs
Objective value
NS_Q
LogNS_Q
NS_WDepth
LogNS_WDepth
NS_C
LogNS_C
NSLN_C
CVRMSELN_C
CVRMSEFDC_Q
CVRMSEFDC_WDepth
WBalance_Q
WBalance_WDepth

Figure N.19

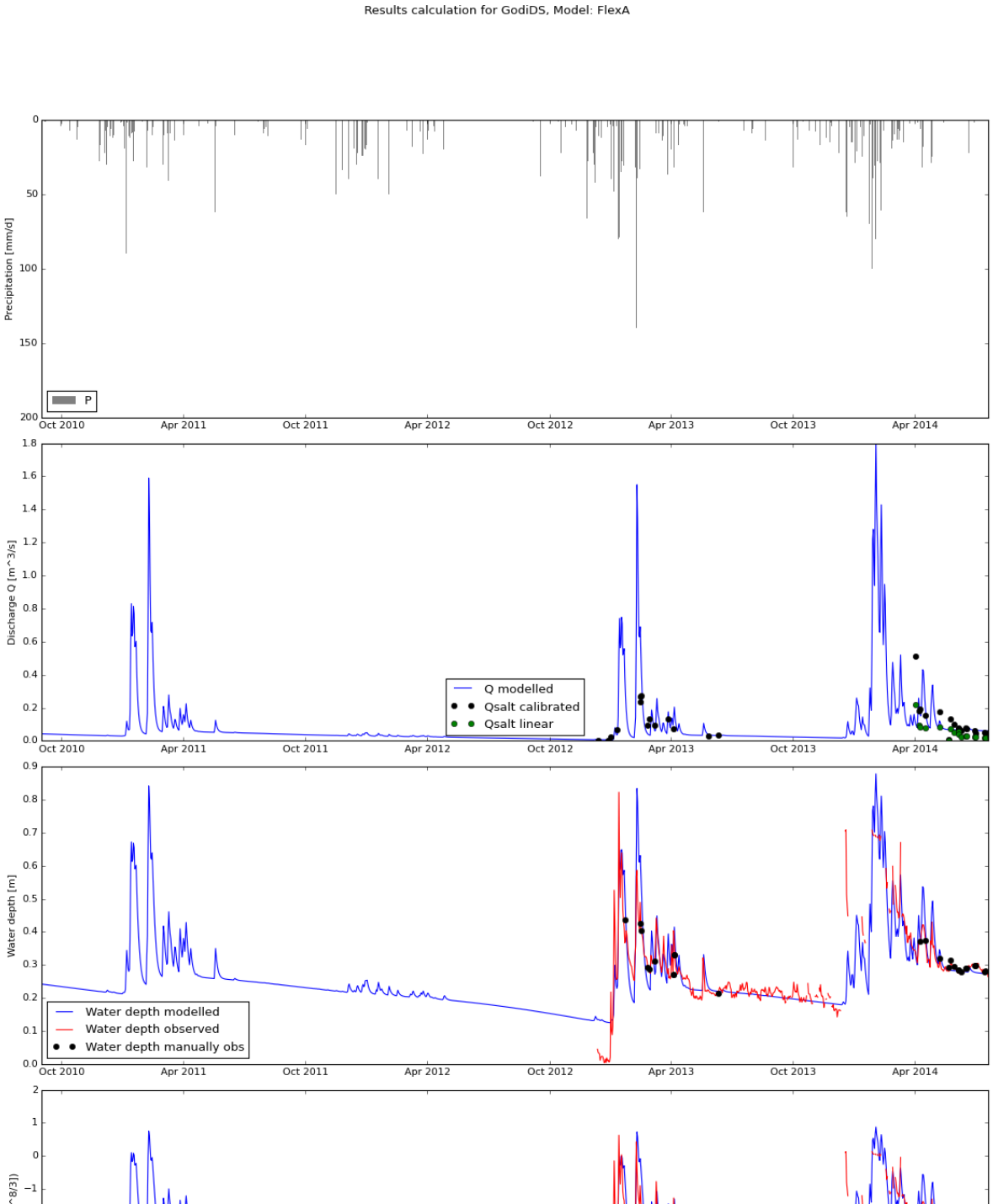
Results calculation for GodiDS, Model: FlexA
Precipitation [mm/d]
P
Discharge Q [m^3/s]
Q modelled
Qsalt calibrated
Qsalt linear
Water depth [m]
Water depth modelled
Water depth observed
Water depth manually obs
Oct 2010
Apr 2011
Oct 2011
Apr 2012
Oct 2012
Apr 2013
Oct 2013
Apr 2014

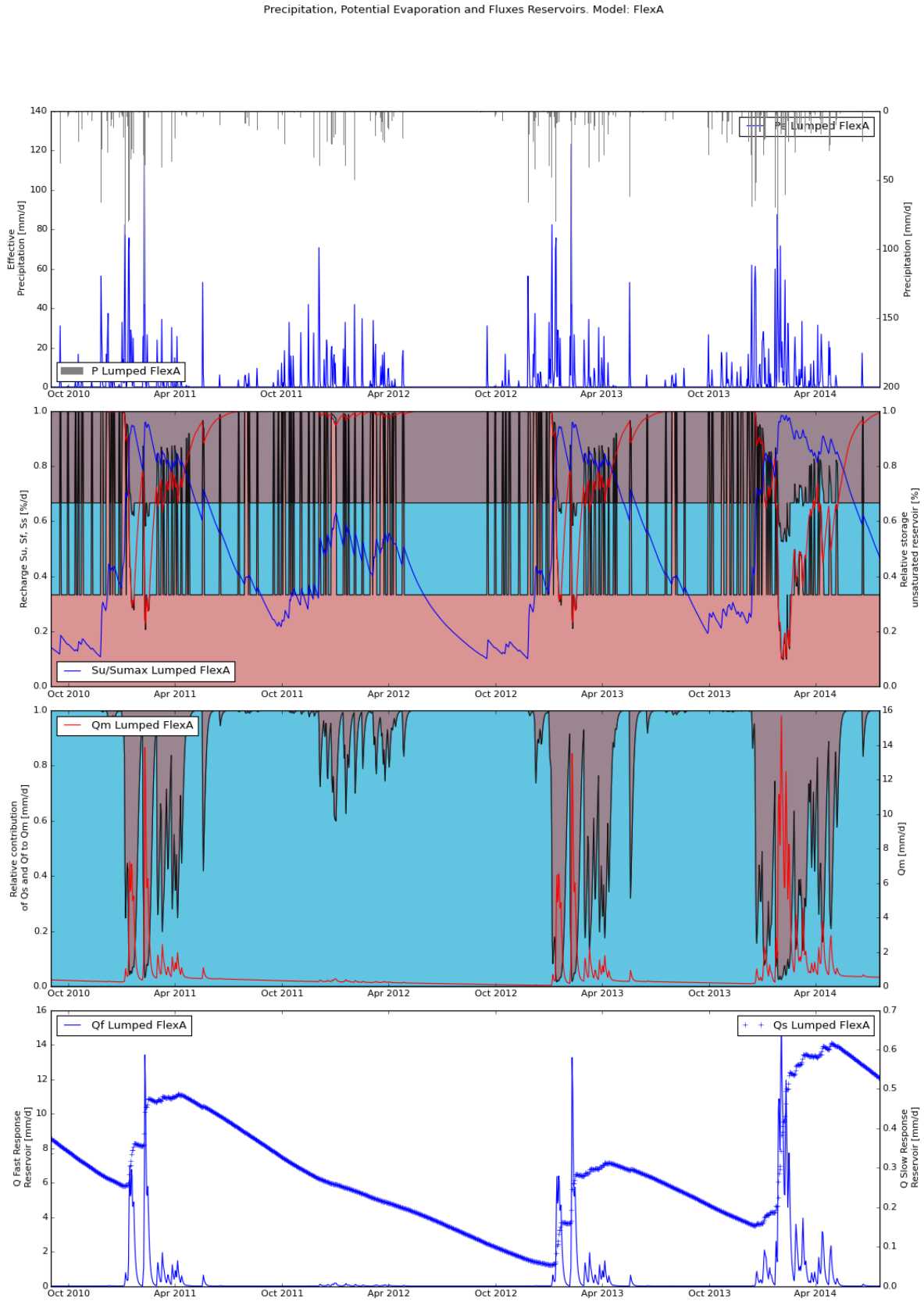
Precipitation, Potential Evaporation and Fluxes Reservoirs. Model: FlexA
Effective Precipitation [mm/d]
Precipitation [mm/d]
P Lumped FlexA
Pe Lumped FlexA
Recharge Su, Sf, Ss [%/d]
Relative storage unsaturated reservoir [%]
Su/Sumax Lumped FlexA
Relative contribution of Qs and Qf to Qm [mm/d]
Qm [mm/d]
Qm Lumped FlexA
Q Fast Response Reservoir [mm/d]
Q Slow Response Reservoir [mm/d]
Qf Lumped FlexA
Qs Lumped FlexA
Oct 2010
Apr 2011
Oct 2011
Apr 2012
Oct 2012
Apr 2013
Oct 2013
Apr 2014

Figure N.21

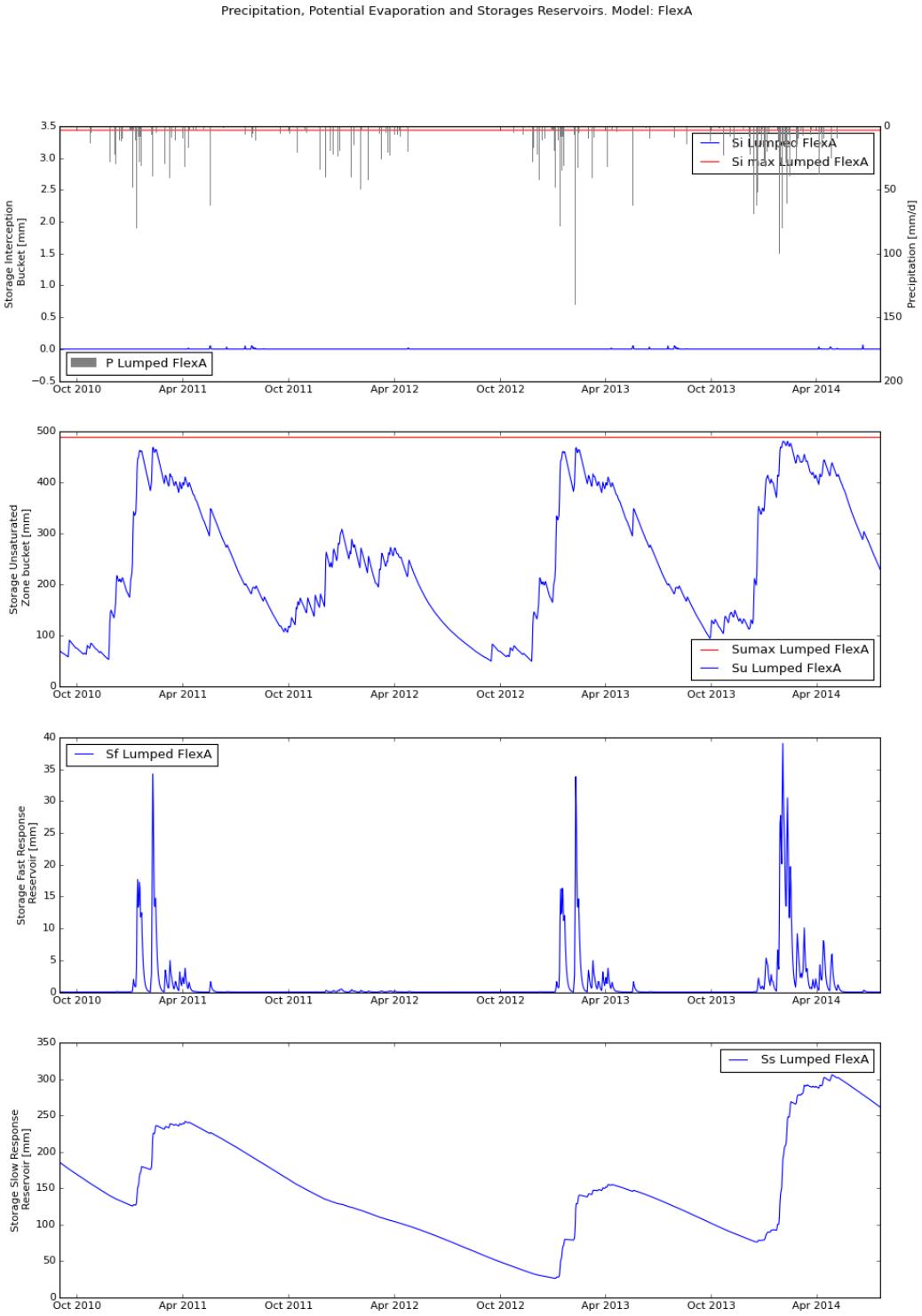
Precipitation, Potential Evaporation and Storages Reservoirs. Model: FlexA
Storage Interception Bucket [mm]
Precipitation [mm/d]
Si Lumped FlexA
Si max Lumped FlexA
P Lumped FlexA
Storage Unsaturated Zone bucket [mm]
Sumax Lumped FlexA
Su Lumped FlexA
Storage Fast Response Reservoir [mm]
Sf Lumped FlexA
Storage Slow Response Reservoir [mm]
Ss Lumped FlexA
Oct 2010
Apr 2011
Oct 2011
Apr 2012
Oct 2012
Apr 2013
Oct 2013
Apr 2014

Figure N.22

N.2.4. GODIDS CALC3

Settings are similar to GodiDS Calc1 and GodiDS Calc2. We changed the parameters Sumax $\in [10,600]$ and $\beta \in [1,6]$.

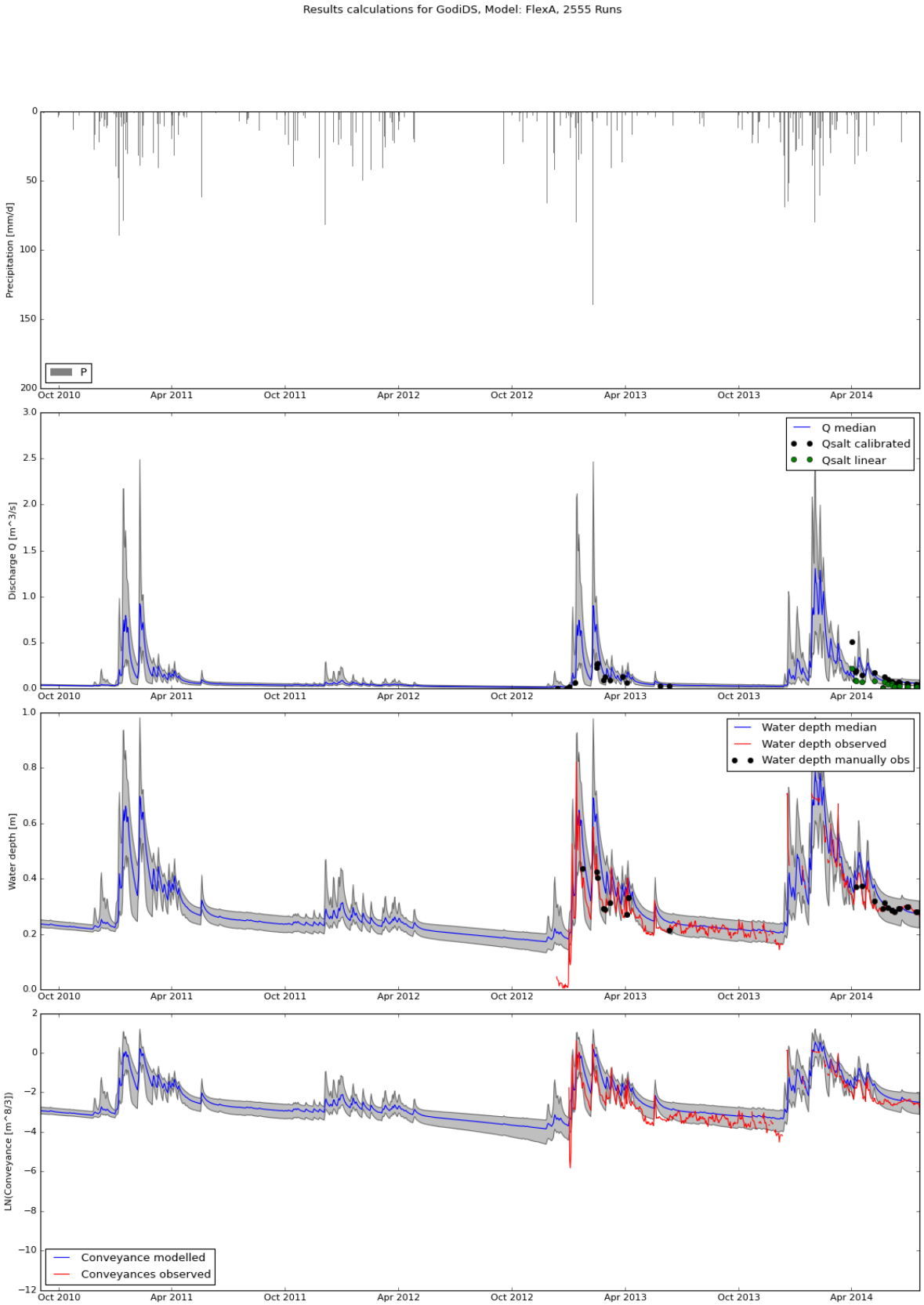
Results calculations for GodiDS, Model: FlexA, 2555 Runs
Precipitation [mm/d]
P
Discharge Q [m^3/s]
Q median
Qsalt calibrated
Qsalt linear
Water depth [m]
Water depth median
Water depth observed
Water depth manually obs
LN(Conveyance [m^8/3])
Conveyance modelled
Conveyances observed
Oct 2010
Apr 2011
Oct 2011
Apr 2012
Oct 2012
Apr 2013
Oct 2013
Apr 2014

Figure N.23

N.2.5. GODIDS CALC4

Settings are similar to GodiDS Calc0. Now we fixate the roughness and bottom slope parameter $\bar{a}$ based on plot N.3. If we consider the lnNS Conveyance objective function in the right graph, we see a clear optimum around $\bar{a} = 1.5$. If we consider the 1% modelruns with the highest NSLN_C coefficients, and we take the mean of $\bar{a}$, we find also a value of $1.50044 \approx 1.5$.

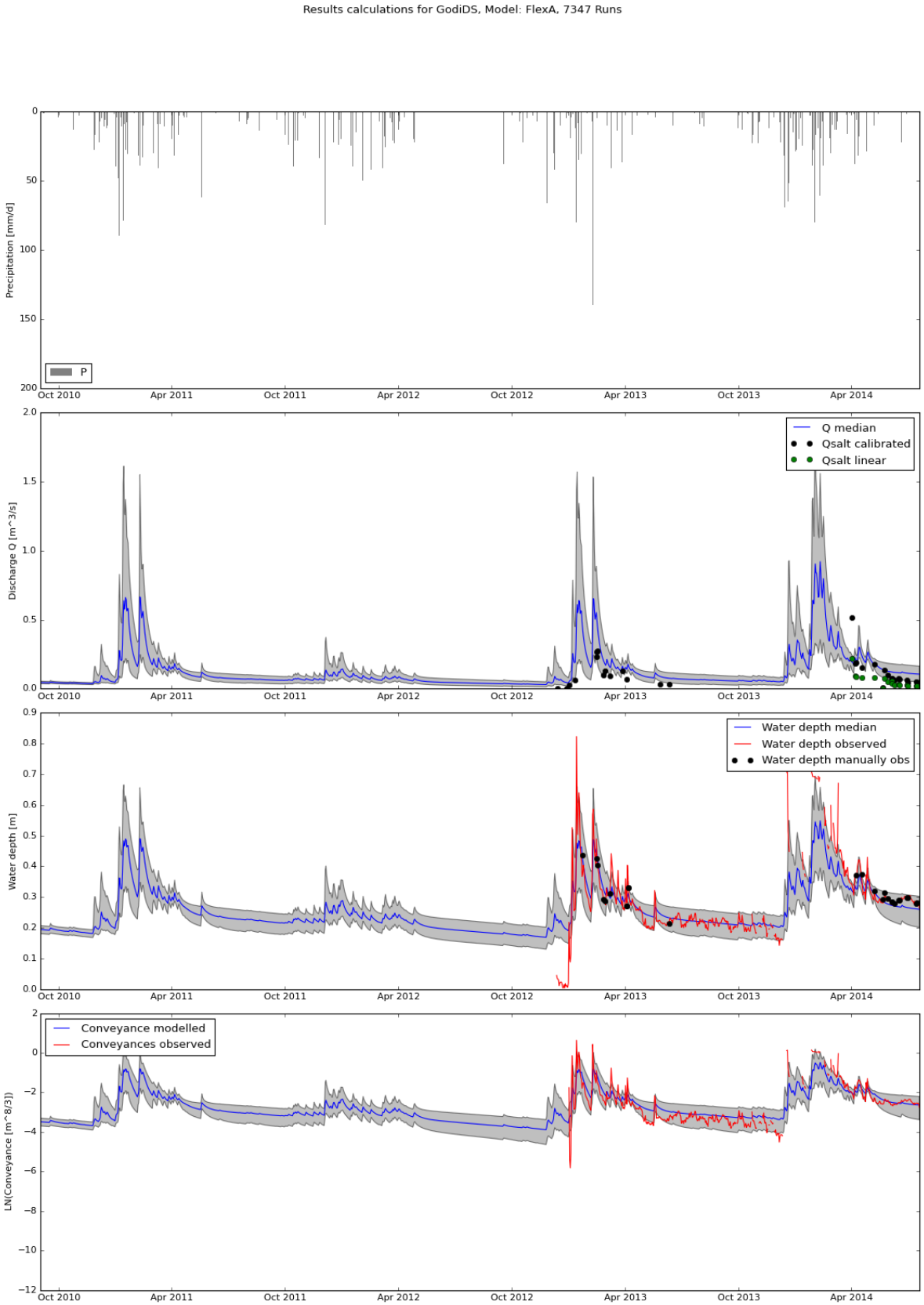
Results calculations for GodiDS, Model: FlexA, 7347 Runs
Precipitation [mm/d]
P
Discharge Q [m^3/s]
Q median
Qsalt calibrated
Qsalt linear
Water depth [m]
Water depth median
Water depth observed
Water depth manually obs
LN(Conveyance [m^8/3])
Conveyance modelled
Conveyances observed
Oct 2010
Apr 2011
Oct 2011
Apr 2012
Oct 2012
Apr 2013
Oct 2013
Apr 2014

Figure N.24

N.2.6. GODIDS CALC5

Settings are similar to GodiDS Calc3.

applied signatures:

- Based on the Budyko framework, we expect a runoff coefficient $c \in [0.2, 0.4]$. We applied this information in a signature and reject all runs which have a runoff coefficient $c \notin [0.2, 0.6]$
- The relative actual evaporation in the wet season must be higher than during the dry season, because of the higher moisture contents everywhere.

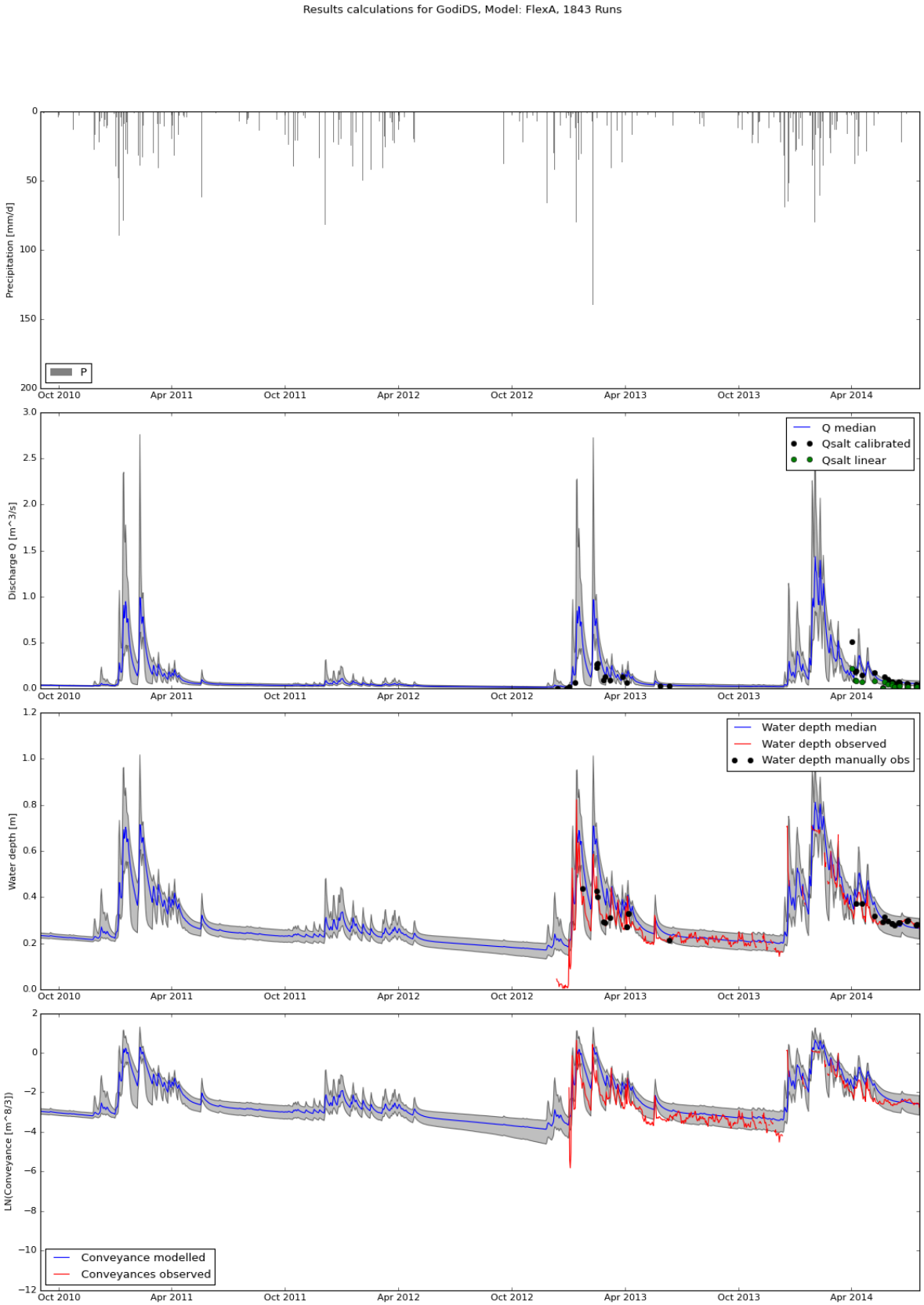
Results calculations for GodiDS, Model: FlexA, 1843 Runs
Precipitation [mm/d]
P
Discharge Q [m^3/s]
Q median
Qsalt calibrated
Qsalt linear
Water depth [m]
Water depth median
Water depth observed
Water depth manually obs
LN(Conveyance [m^8/3])
Conveyance modelled
Conveyances observed
Oct 2010
Apr 2011
Oct 2011
Apr 2012
Oct 2012
Apr 2013
Oct 2013
Apr 2014

Figure N.25

N.2.7. GODIDS CALC6

Settings are similar to GodiDS Calc4.

applied signatures:

- Based on the Budyko framework, we expect a runoff coefficient $c \in [0.2, 0.4]$. We applied this information in a signature and reject all runs which have a runoff coefficient $c \notin [0.2, 0.6]$
- The relative actual evaporation in the wet season must be higher than during the dry season, because of the higher moisture contents everywhere.

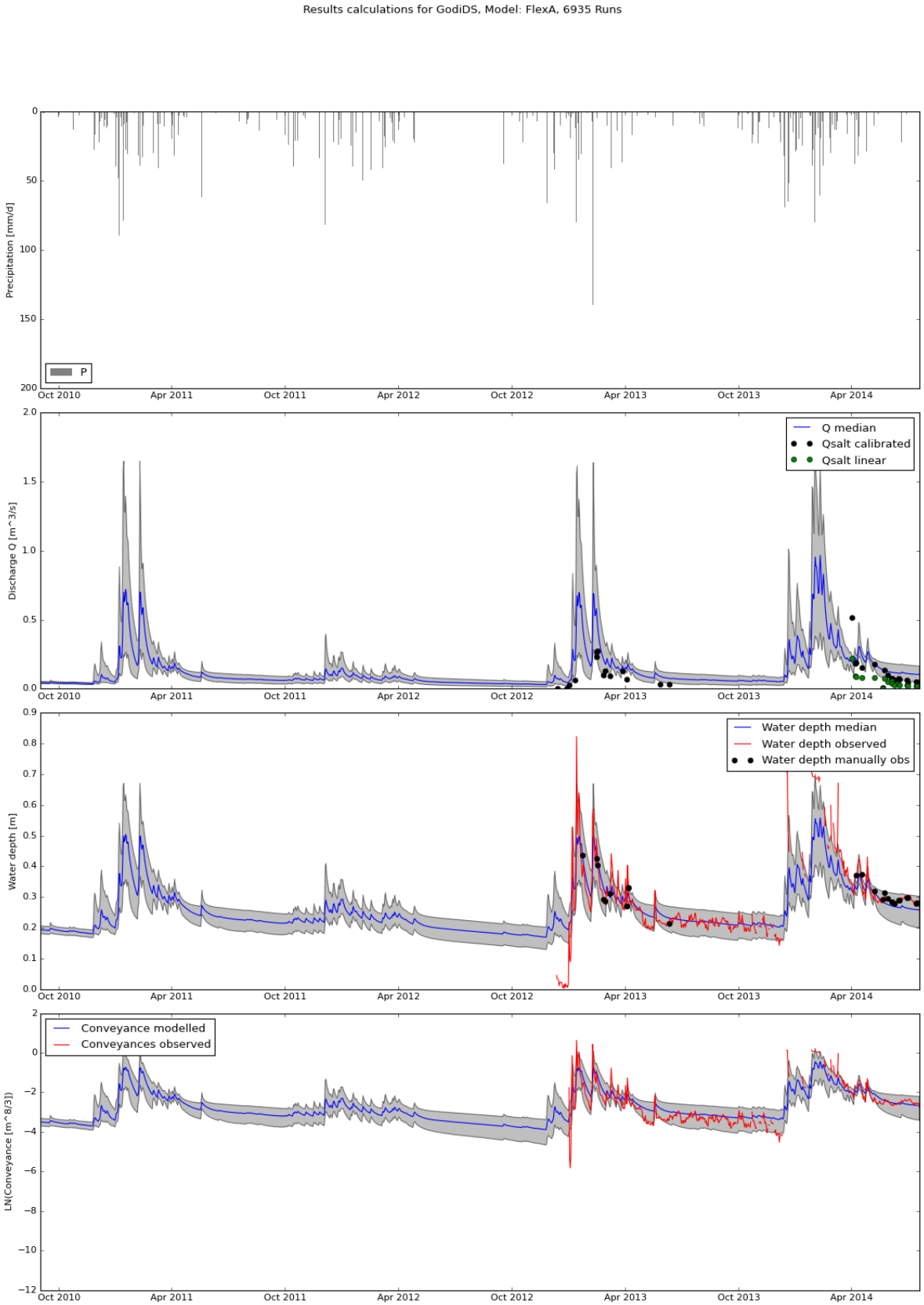
Results calculations for GodiDS, Model: FlexA, 6935 Runs
Precipitation [mm/d]
P
Discharge Q [m^3/s]
Q median
Qsalt calibrated
Qsalt linear
Water depth [m]
Water depth median
Water depth observed
Water depth manually obs
LN(Conveyance [m^8/3])
Conveyance modelled
Conveyances observed
Oct 2010
Apr 2011
Oct 2011
Apr 2012
Oct 2012
Apr 2013
Oct 2013
Apr 2014

Figure N.26

N.2.8. GODIDS CALC7

Settings are similar to GodiDS Calc4.

precipitation corrected model HRUwise roughness coefficient $\bar{a} = 1.5$

N.2.9. GODIDS CALC8

Settings are similar to GodiDS Calc4.

precipitation HRUwise
roughness coefficient $\bar{a} = 0.75$ runs 10000

N.2.10. GODIDS CALC9

Settings are similar to GodiDS Calc4.

precipitation HRUwise
roughness coefficient $\bar{a} = 0.75$
40000 runs
objective functions NS_Conveyence, LogNS_Conveyance >= 0

N.2.11. GODIDS CALC10

Settings are similar to GodiDS Calc8.

Different initial state of slow groundwater response reservoir. initial states are calculated in front, leading to better results.

N.2.12. GODIDS CALC11

Final Calculation

- Settings are similar to GodiDS Calc9.
- 10000 runs
- Area from HRUpoints, to make sure that the precipitation amount for both the models are equal.
- objective function LogNS_conveyance
- roughness coefficient $\bar{a} = 0.75$.
- Precipitation HRU wise
- Ss0 first estimated, based on 200 * D mm groundwater depletion. Then corrected with a calculation, by extracting the total Slow Reservoir recharge over November 2010 to November 2011.

N.3. FLEXB

N.3.1. GODIDS CALC0

describe initial parameters Most of them are equal to FlexA

N.3.2. GODIDS CALC1

Similar to GodiDS Calc0. But applied signatures:

- Based on the Budyko framework, we expect a runoff coefficient $c \in [0.2, 0.4]$. We applied this information in a signature and reject all runs which have a runoff coefficient $c \notin [0.2, 0.6]$
- The relative actual evaporation in the wet season must be higher than during the dry season, because of the higher moisture contents everywhere.
- additional constraints FlexB

N.3.3. GODIDS CALC2

Similar to GodiDS Calc0 60000 runs HRUmethod = Database with hand = 5.9 and FlowAcc = 15

N.3.4. GODIDS CALC3

HRU method = GIS with hand = 5.9 and FlowAcc = 20 benchmark to make comparison between Calc2 and Calc4. 60000 runs

applied signatures

N.3.5. GODIDS CALC4

HRU method = GIS with hand = 3.1 and FlowAcc = 20 60000 runs

applied signatures.

Result is smaller contribution of wetlands.

N.4. FLEXC

We forced that Recharge slow reservoir for the forest is higher than recharge slow reservoir of the grass/crop areas, since we believe that the first contribute more to the recharge.

N.4.1. GODIDS CALC0

In general the baseflow recession seems too large, indicating a too small K_s value.

Note that the conveyance of the baseflow in 2013 is over predicted. This implies that there is more base flow modeled than measured.

The peaks are too steep, implying to much discharge during events. Especially the peaks at the end of the dry season of 2012 are odd, since we es and to much weight to the fast processes, which is purely caused by the wetlands, see Fig. N.36. We expect the wetland response to be smaller. Maybe too much area is defined as wetland, where large parts are better to be considered as flatland.

The contribution of the wetlands is ca 40%, the forested hills about 52% and the grasslands around 8%. We believe that the percentage of wetlands is overrated in disadvantage of grasslands.

From Table N.1 we observe that the 1% calculations with highest LogNS conveyance values have very low K_f values for the wetlands. Which is in line with our expectations based on perception and on the conveyance time series, see Chapters 2.4 and 2.5.

RunID	1519	2105	3938	4488	4855	5365	5469	6379	6568	7997	8007	8152	8720	10126	10225
Imax_Grass	2.66	2.62	2.16	2.93	2.16	2.20	2.68	2.39	2.30	2.25	2.89	2.36	2.11	2.27	2.76
B_Grass	3.61	3.62	3.85	2.52	2.88	2.57	2.28	2.62	2.86	3.51	1.98	3.66	3.87	1.60	4.80
Sumax_Grass	202.01	225.83	245.44	284.18	226.84	291.54	281.47	189.50	245.19	225.43	266.90	280.64	236.73	246.43	279.84
Pper_Grass	0.17	0.06	0.09	0.34	0.07	0.21	0.15	0.29	0.27	0.21	0.47	0.04	0.45	0.14	0.32
D_Grass	0.12	0.76	0.11	0.69	0.11	0.37	0.95	0.03	0.24	0.13	0.27	0.01	0.51	0.32	0.82
Kf_Grass	3.07	5.64	9.12	0.49	8.95	1.27	7.90	3.53	0.73	9.77	8.83	3.96	9.65	2.91	4.61
Imax_Forest	3.08	4.46	4.20	4.25	4.42	4.83	3.99	3.04	4.10	4.15	3.12	3.79	3.30	4.74	3.76
B_Forest	4.75	4.94	2.99	3.86	3.90	4.73	4.25	4.20	4.57	4.20	4.77	2.72	4.22	4.16	4.86
Sumax_Forest	416.62	454.23	489.55	407.97	464.61	466.40	375.22	419.66	467.92	498.57	499.94	426.85	400.26	367.81	419.23
Pper_Forest	0.16	0.47	0.16	0.19	0.27	0.07	0.46	0.28	0.17	0.10	0.46	0.24	0.04	0.40	0.27
D_Forest	0.57	0.50	0.70	0.59	0.56	0.68	0.30	0.62	0.66	0.56	0.54	0.48	0.45	0.45	0.77
Kf_Forest	3.05	6.00	6.06	6.71	3.37	9.60	6.85	8.48	5.99	4.41	2.10	4.21	1.61	5.68	5.02
Imax_Wetland	2.89	2.97	2.67	2.02	2.36	2.27	2.96	2.97	2.15	2.31	2.89	2.80	2.68	2.32	2.43
B_Wetland	2.81	2.54	4.93	3.55	4.93	2.83	4.74	4.22	3.57	4.35	4.77	4.88	4.24	3.90	3.70
Sumax_Wetland	93.58	96.49	85.11	97.36	93.03	70.54	75.03	89.98	68.82	77.45	97.89	90.13	87.42	85.81	70.08
C_Wetland	0.36	0.47	0.21	0.41	0.31	0.41	0.41	0.42	0.03	0.25	0.42	0.21	0.17	0.38	0.50
Kf_Wetland	0.15	0.59	0.76	0.24	0.08	0.46	0.06	0.71	0.13	0.31	0.06	0.00	0.42	0.01	0.20
Ks_all	518.89	482.55	577.99	474.92	404.06	557.32	472.66	450.87	452.39	510.68	529.45	501.06	531.78	581.18	584.55
LogNS_C	0.39	0.40	0.40	0.43	0.48	0.41	0.42	0.40	0.39	0.43	0.49	0.42	0.39	0.40	0.40

RunID	11044	12070	12956	12971	13644	13940	14204	15393	16355	16716	17235	18221	18223	18746	18904	18961
Imax_Grass	2.30	2.93	2.49	2.23	2.51	2.77	2.64	2.83	2.04	2.52	2.54	2.74	2.36	2.36	2.77	2.69
B_Grass	1.57	1.01	3.70	1.64	3.29	4.77	2.19	1.10	1.78	2.81	3.61	1.54	4.34	3.95	2.79	3.28
Sumax_Grass	225.90	275.03	216.38	219.28	200.37	252.89	293.03	253.84	270.23	279.62	238.44	218.62	274.59	255.95	264.72	246.66
Pper_Grass	0.03	0.30	0.17	0.38	0.15	0.36	0.21	0.34	0.38	0.20	0.35	0.34	0.44	0.12	0.20	0.25
D_Grass	0.33	0.79	0.40	0.32	0.55	0.05	0.78	0.03	0.52	0.01	0.16	0.28	0.95	0.50	0.46	0.53
Kf_Grass	6.54	9.86	2.45	0.93	6.50	8.09	1.76	4.04	2.46	4.75	5.20	5.66	4.44	7.29	3.08	4.60
Imax_Forest	4.26	4.46	4.54	3.14	4.53	3.23	3.42	4.65	3.77	3.17	3.22	4.50	3.68	3.49	3.13	4.49
B_Forest	3.43	4.55	3.34	3.84	3.89	3.97	4.78	4.18	4.54	3.20	4.69	4.07	4.43	4.36	4.97	4.89
Sumax_Forest	482.71	458.33	392.74	379.95	487.15	440.32	447.76	456.55	468.72	496.20	446.74	388.99	460.67	406.01	490.37	382.00
Pper_Forest	0.33	0.08	0.11	0.05	0.14	0.49	0.08	0.05	0.41	0.46	0.34	0.46	0.14	0.40	0.17	0.17
D_Forest	0.75	0.83	0.44	0.68	0.61	0.63	0.49	0.84	0.61	0.71	0.70	0.54	0.47	0.59	0.76	0.64
Kf_Forest	7.03	2.80	4.51	4.58	7.40	5.25	3.85	7.08	1.78	6.74	7.49	1.88	1.70	5.48	0.33	5.78
Imax_Wetland	2.99	2.01	2.86	2.18	2.31	2.73	2.80	2.76	2.24	2.29	2.59	2.39	2.23	2.95	2.82	2.81
B_Wetland	4.32	4.63	3.28	4.42	3.56	4.15	2.84	3.93	4.82	4.38	4.94	3.47	4.04	3.82	4.61	3.63
Sumax_Wetland	74.00	98.29	77.17	82.49	72.27	83.33	95.52	74.28	67.99	78.56	77.89	87.54	99.22	93.56	94.59	90.41
C_Wetland	0.37	0.47	0.20	0.48	0.19	0.47	0.47	0.40	0.40	0.22	0.35	0.49	0.02	0.46	0.39	0.45
Kf_Wetland	0.15	0.33	0.03	0.19	0.38	0.74	0.14	0.45	0.06	0.05	0.01	0.14	0.02	0.07	0.33	0.48
Ks_all	539.52	579.06	478.82	594.36	459.95	511.33	477.58	516.75	540.09	428.28	548.78	413.35	510.02	420.97	459.25	471.20
LogNS_C	0.41	0.40	0.39	0.43	0.40	0.41	0.43	0.41	0.40	0.39	0.50	0.40	0.40	0.49	0.42	0.45

Table N.1: 1% best calculations, having the highest LogNS Conveyances values. Only the non-fixated parameters are given in this overview

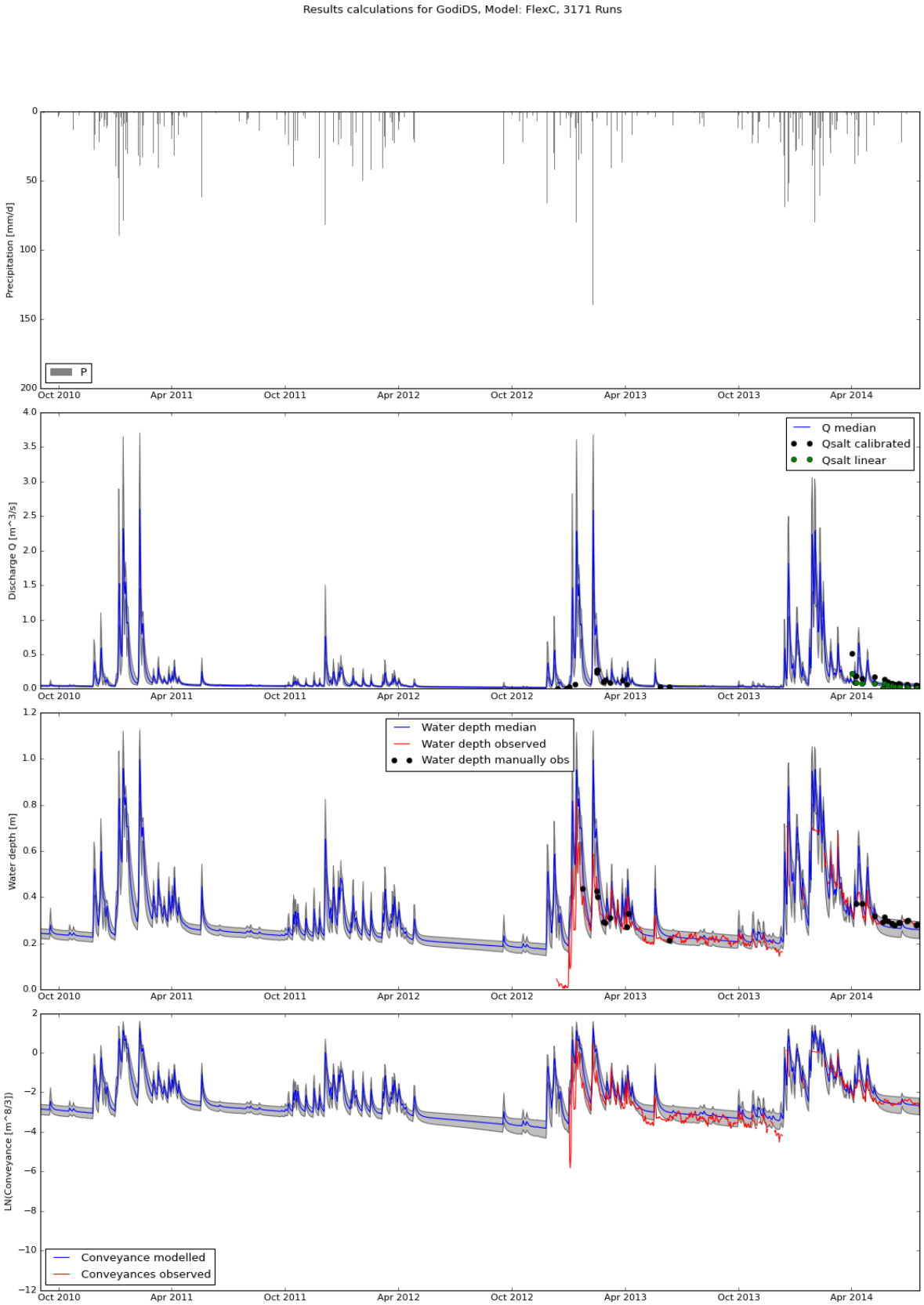
Results calculations for GodiDS, Model: FlexC, 3171 Runs
Precipitation [mm/d]
P
Discharge Q [m^3/s]
Q median
Qsalt calibrated
Qsalt linear
Water depth [m]
Water depth median
Water depth observed
Water depth manually obs
LN(Conveyance [m^8/3])
Conveyance modelled
Conveyances observed
Oct 2010
Apr 2011
Oct 2011
Apr 2012
Oct 2012
Apr 2013
Oct 2013
Apr 2014

Figure N.27

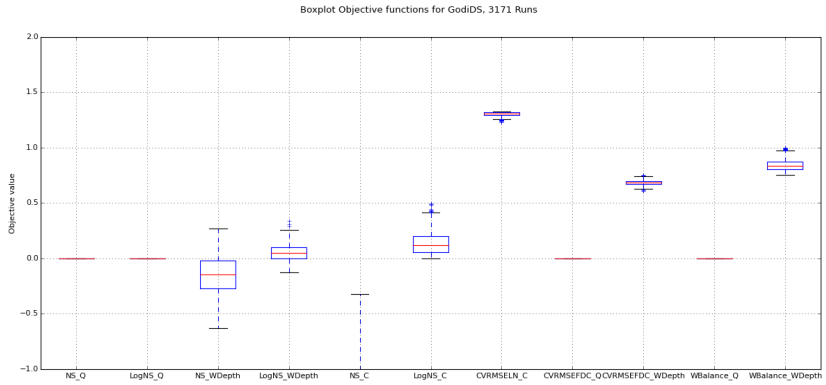

Figure N.28

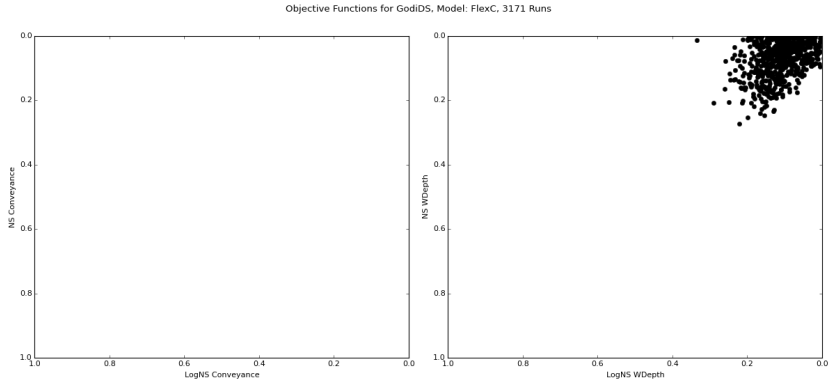

Figure N.29

N.4.2. GODIDS CALC2

Further restrictions for calibration parameters based on insights from GodiDS_FlexC_ Calc0. Since the recession curve is suspected too low, we enlarge the parameter space $K_s \in [400, 800]$. Furthermore we switch the areas of wetlands and Grasslands, since we believe that that is more plausible.

We refine the calibration bandwidth for $K_{f;wetland} \in [0, 1]$ since we believe that the riparian areas will response within a day.

We enlarge for the grasslands the $K_{f;grasscrop} \in [0, 40]$ where we believe that this area will slowly empty.

The original wetland's area contribution is ca 40%, the forested hills about 52% and for grasslands around 8%. Since, we believe that the percentage of wetlands is overrated in disadvantage of grasslands, we changed the areas of the wetlands with the grasslands.

From Fig. N.40 we observe exactly the expected behavior, some tuning with areas, K_s values and percolation and capillary fluxes will do the job. Is this explainable?

N.4.3. GODIDS CALC4

Model concept FlexC calculated for Godi DS.

- 10000 MC samples
- $0.1 < runoff < 0.9$
- Recharge constraint $R_{s;forest} > R_{s;grasscrop}$ removed
- Wetland: HAND <= 2 based on FlowAccumulation 50
- Flatland / Grass Crop HAND > 2 and Slope < 11

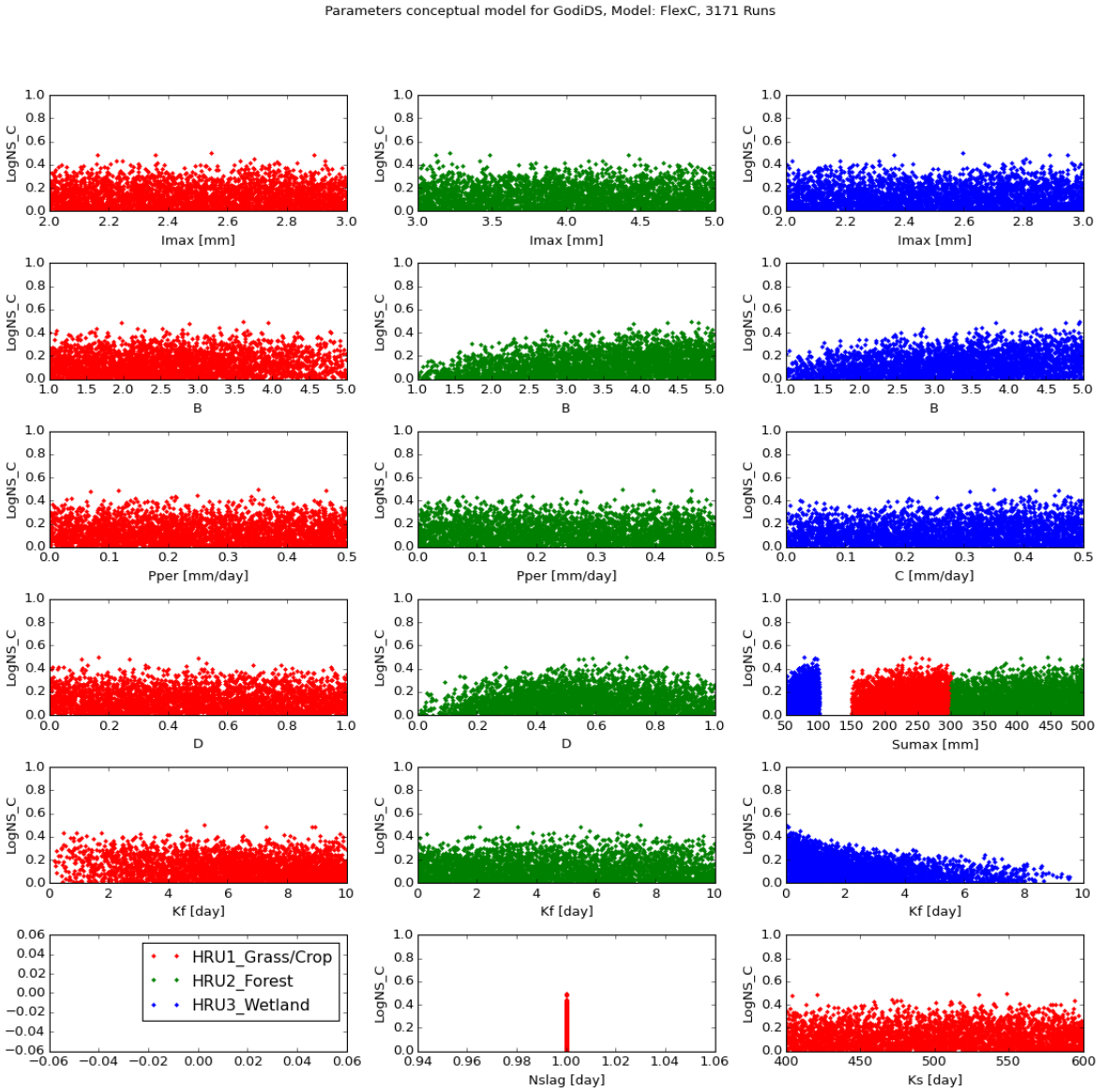

Figure N.30

- Hill / Forest HAND > 2 and Slope >= 11

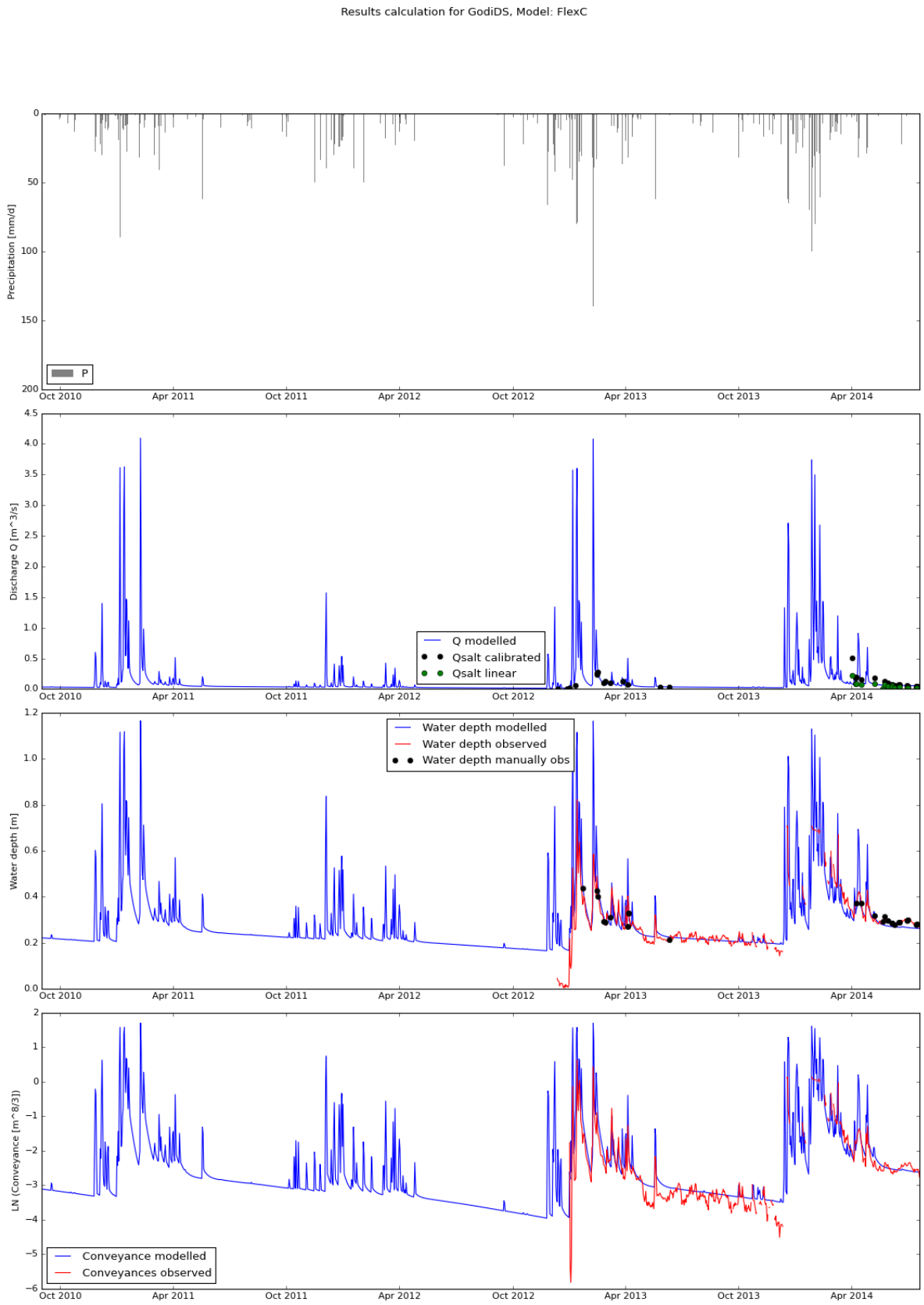

Figure N.31: On of the best calculations nr 17235, with LogNS Conveyance = 0.50

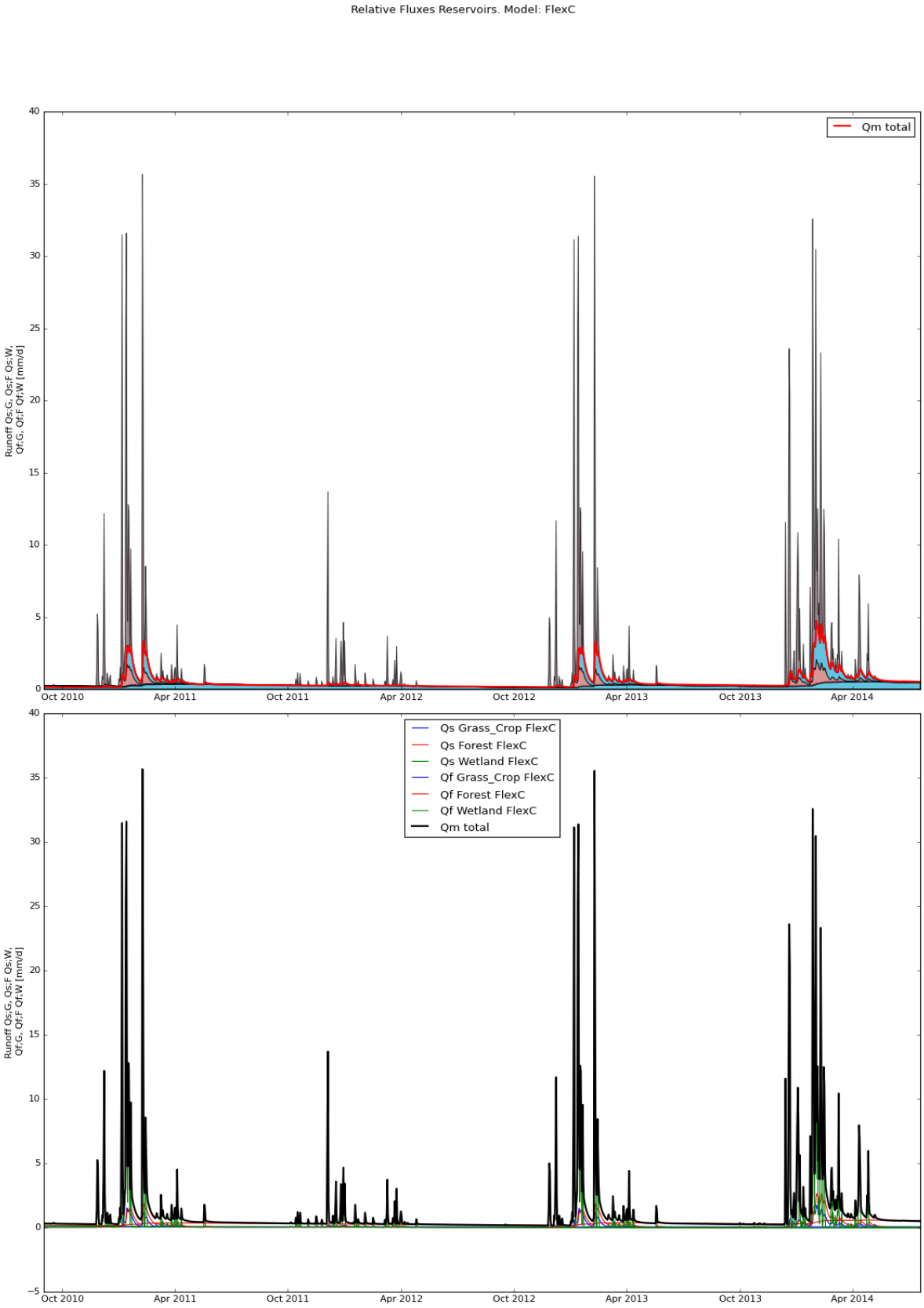
Relative Fluxes Reservoirs. Model: FlexC
Qm total
Runoff Qs;G, Qs;F Qs;W, Qf;G, Qf;F Qf;W [mm/d]
Oct 2010
Apr 2011
Oct 2011
Apr 2012
Oct 2012
Apr 2013
Oct 2013
Apr 2014
Qs Grass_Crop FlexC
Qs Forest FlexC
Qs Wetland FlexC
Qf Grass_Crop FlexC
Qf Forest FlexC
Qf Wetland FlexC
Qm total

Figure N.32

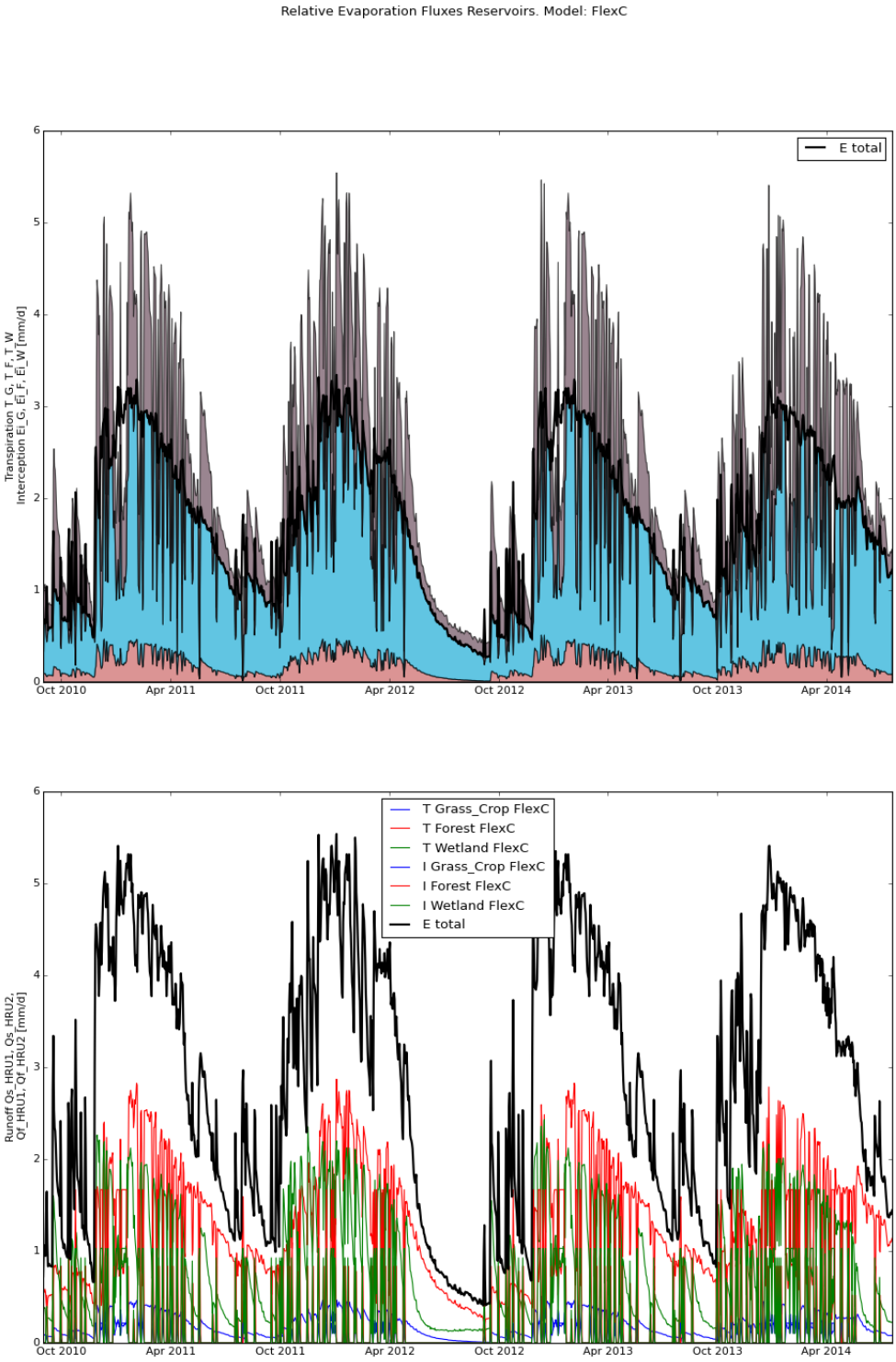
Relative Evaporation Fluxes Reservoirs. Model: FlexC
E total
Transpiration T_G, T_F, T_W
Interception Ei_G, Ei_F, Ei_W [mm/d]
Oct 2010
Apr 2011
Oct 2011
Apr 2012
Oct 2012
Apr 2013
Oct 2013
Apr 2014
T Grass_Crop FlexC
T Forest FlexC
T Wetland FlexC
I Grass_Crop FlexC
I Forest FlexC
I Wetland FlexC
E total
Runoff Qs_HRU1, Qs_HRU2,
Qf_HRU1, Qf_HRU2 [mm/d]

Figure N.33

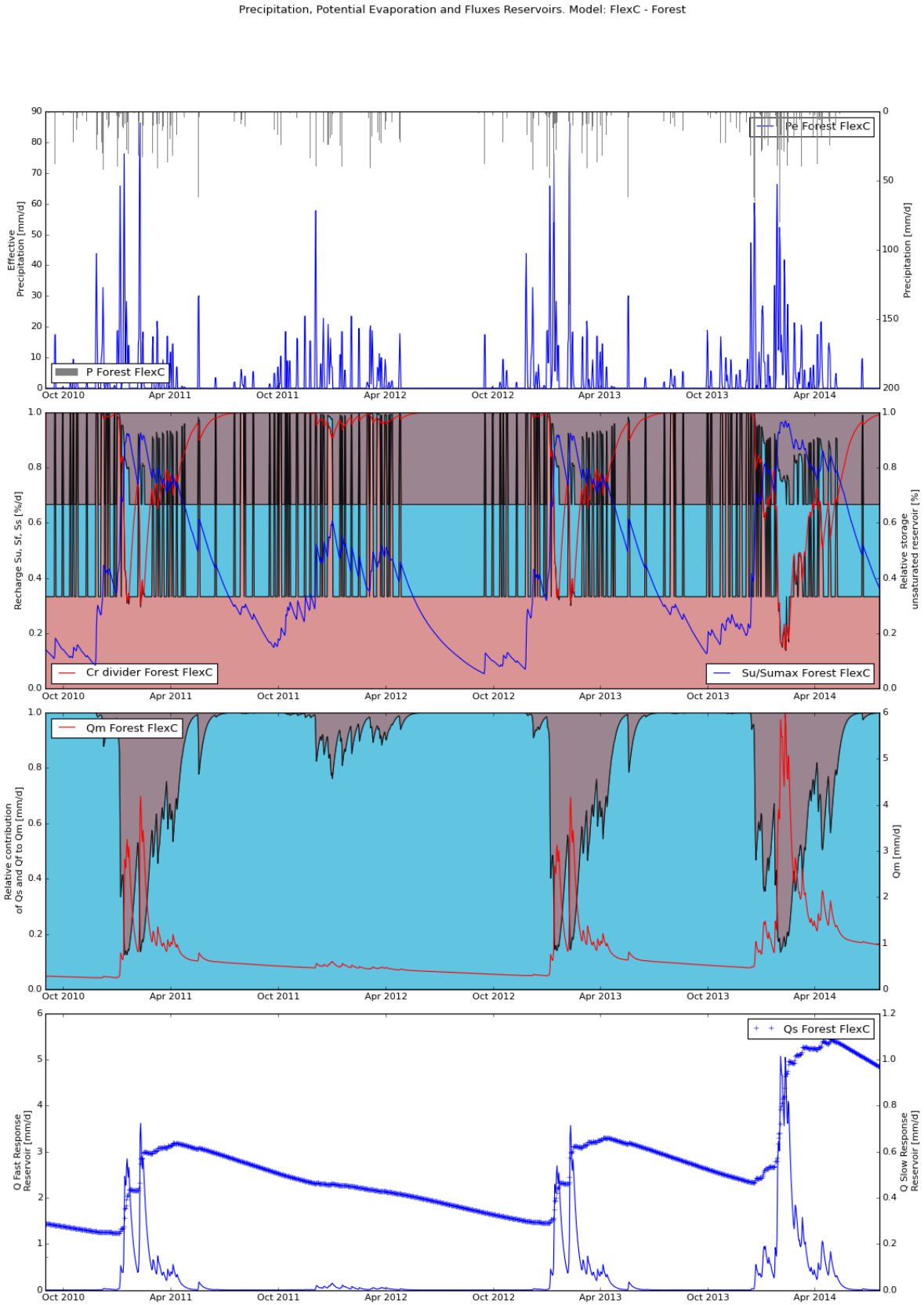
Precipitation, Potential Evaporation and Fluxes Reservoirs. Model: FlexC - Forest
Effective Precipitation [mm/d]
Precipitation [mm/d]
Pe Forest FlexC
P Forest FlexC
Recharge Su, Sf, Ss [%/d]
Relative storage unsaturated reservoir [%]
Cr divider Forest FlexC
Su/Sumax Forest FlexC
Relative contribution of Qs and Qf to Qm [mm/d]
Qm [mm/d]
Qm Forest FlexC
Q Fast Response Reservoir [mm/d]
Q Slow Response Reservoir [mm/d]
Qs Forest FlexC
Oct 2010
Apr 2011
Oct 2011
Apr 2012
Oct 2012
Apr 2013
Oct 2013
Apr 2014

Figure N.34

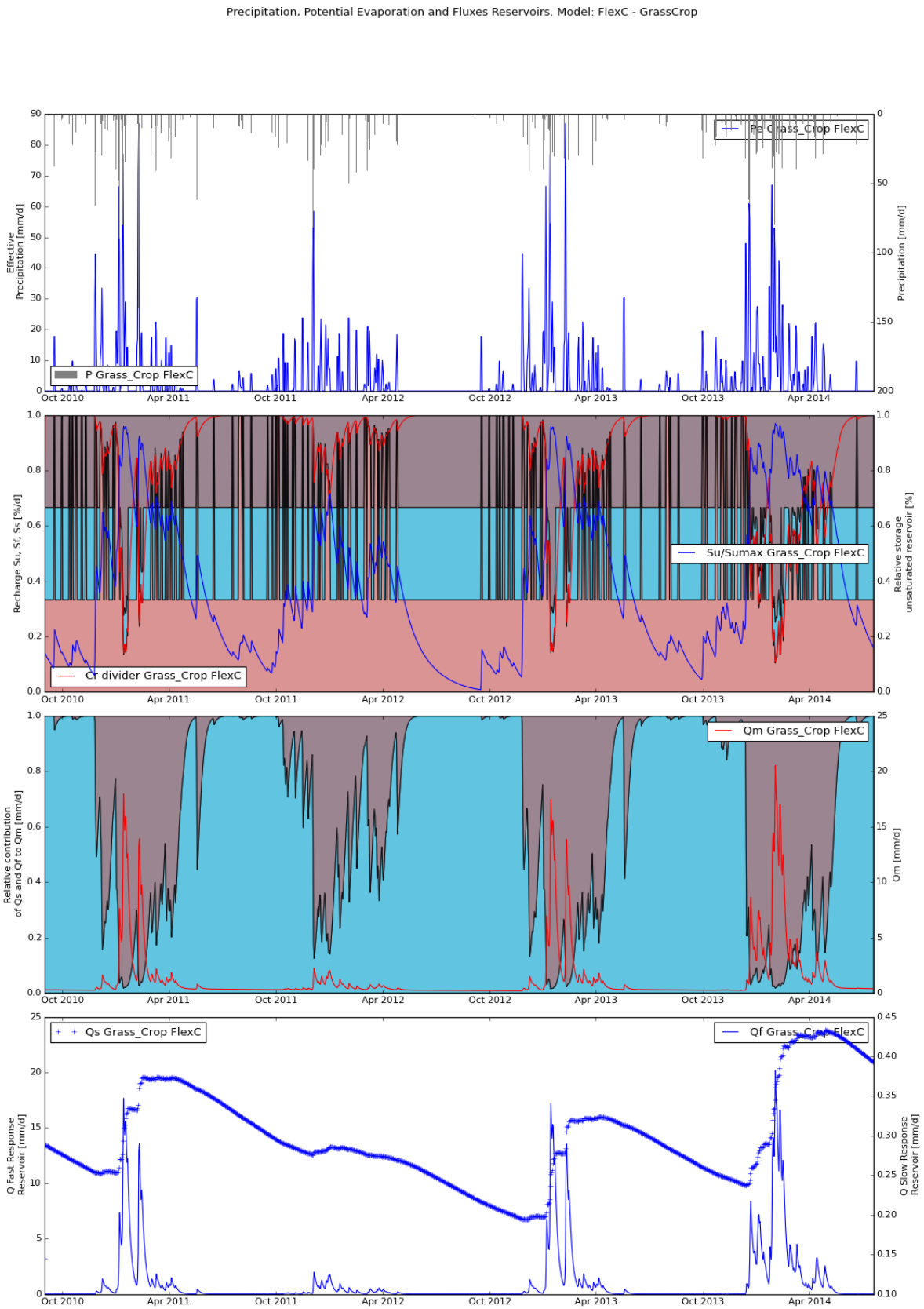
Precipitation, Potential Evaporation and Fluxes Reservoirs. Model: FlexC - GrassCrop
Effective Precipitation [mm/d]
Precipitation [mm/d]
Pe Grass_Crop FlexC
P Grass_Crop FlexC
Recharge Su, Sf, Ss [%/d]
Relative storage unsaturated reservoir [%]
Su/Sumax Grass_Crop FlexC
Cr divider Grass_Crop FlexC
Relative contribution of Qs and Qf to Qm [mm/d]
Qm [mm/d]
Qm Grass_Crop FlexC
Q Fast Response Reservoir [mm/d]
Q Slow Response Reservoir [mm/d]
Qs Grass_Crop FlexC
Qf Grass_Crop FlexC
Oct 2010
Apr 2011
Oct 2011
Apr 2012
Oct 2012
Apr 2013
Oct 2013
Apr 2014

Figure N.35

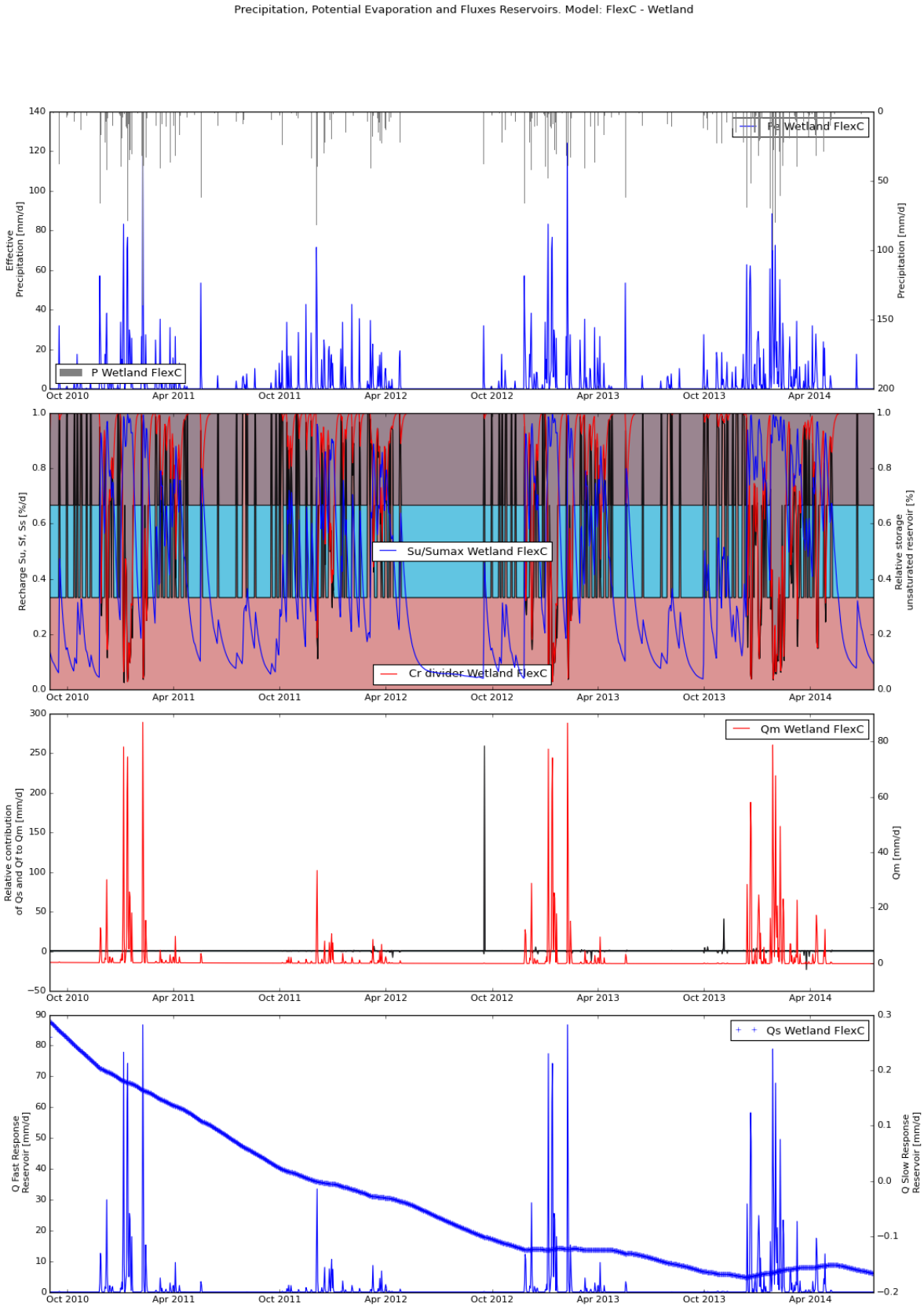
Precipitation, Potential Evaporation and Fluxes Reservoirs. Model: FlexC - Wetland
Effective Precipitation [mm/d]
Precipitation [mm/d]
P Wetland FlexC
Ps Wetland FlexC
Recharge Su, Sf, Ss [%/d]
Relative storage unsaturated reservoir [%]
Su/Sumax Wetland FlexC
Cr divider Wetland FlexC
Relative contribution of Qs and Qf to Qm [mm/d]
Qm [mm/d]
Qm Wetland FlexC
Q Fast Response Reservoir [mm/d]
Q Slow Response Reservoir [mm/d]
Qs Wetland FlexC
Oct 2010
Apr 2011
Oct 2011
Apr 2012
Oct 2012
Apr 2013
Oct 2013
Apr 2014

Figure N.36

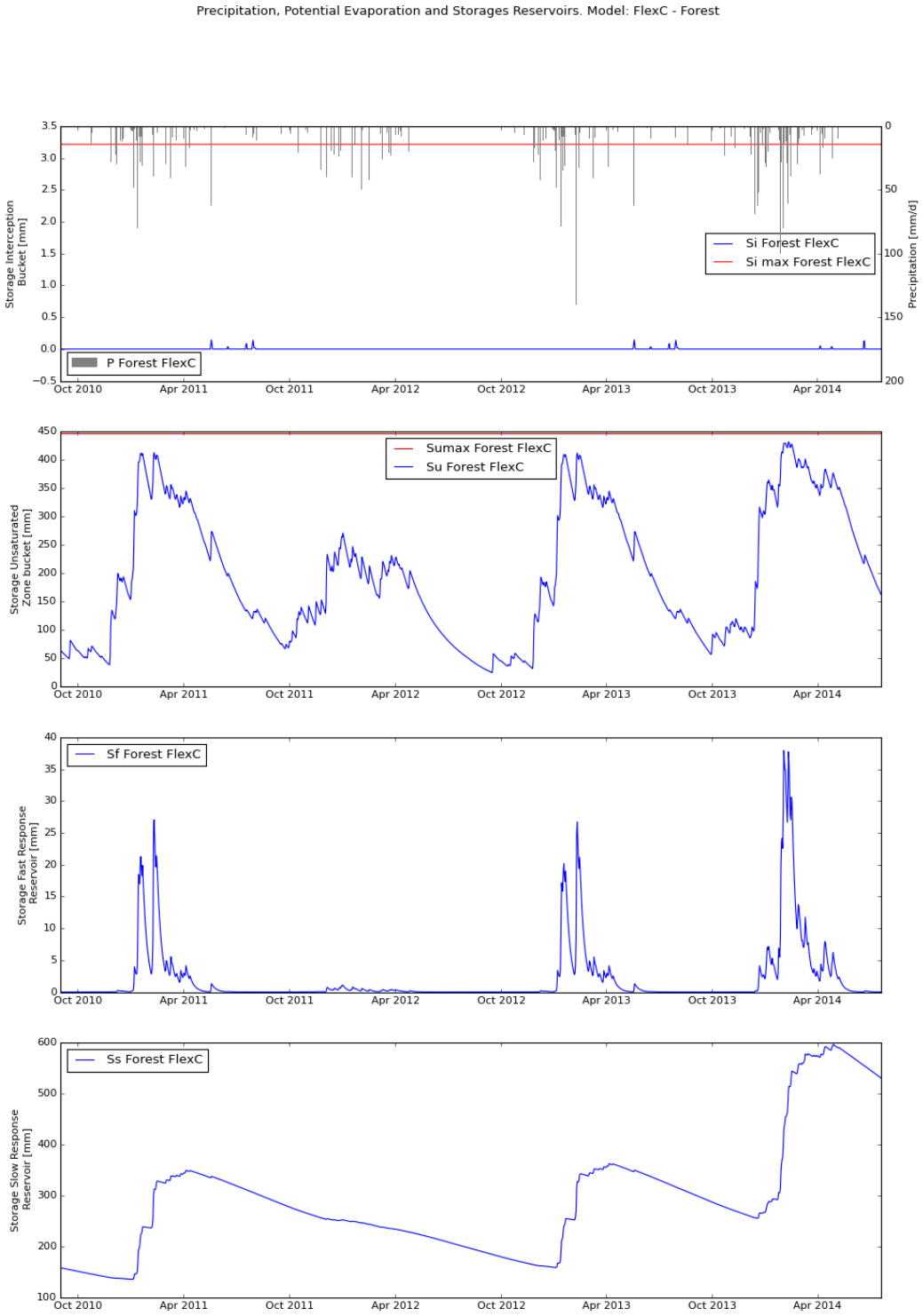
Precipitation, Potential Evaporation and Storages Reservoirs. Model: FlexC - Forest
Storage Interception Bucket [mm]
Precipitation [mm/d]
Si Forest FlexC
Si max Forest FlexC
P Forest FlexC
Storage Unsaturated Zone bucket [mm]
Sumax Forest FlexC
Su Forest FlexC
Storage Fast Response Reservoir [mm]
Sf Forest FlexC
Storage Slow Response Reservoir [mm]
Ss Forest FlexC
Oct 2010
Apr 2011
Oct 2011
Apr 2012
Oct 2012
Apr 2013
Oct 2013
Apr 2014

Figure N.37

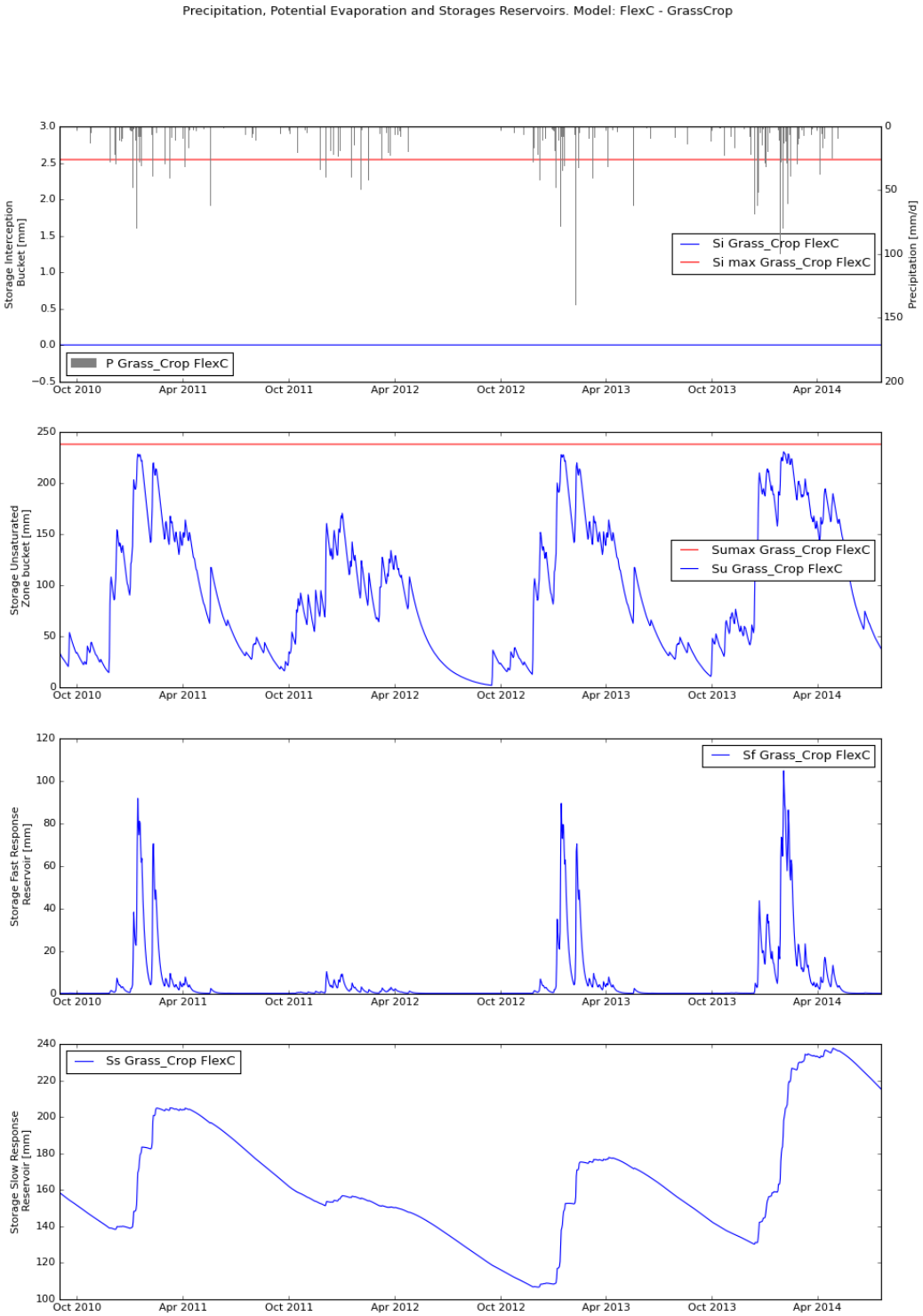
Precipitation, Potential Evaporation and Storages Reservoirs. Model: FlexC - GrassCrop
Storage Interception Bucket [mm]
Precipitation [mm/d]
Si Grass_Crop FlexC
Si max Grass_Crop FlexC
P Grass_Crop FlexC
Storage Unsaturated Zone bucket [mm]
Sumax Grass_Crop FlexC
Su Grass_Crop FlexC
Storage Fast Response Reservoir [mm]
Sf Grass_Crop FlexC
Storage Slow Response Reservoir [mm]
Ss Grass_Crop FlexC
Oct 2010
Apr 2011
Oct 2011
Apr 2012
Oct 2012
Apr 2013
Oct 2013
Apr 2014

Figure N.38

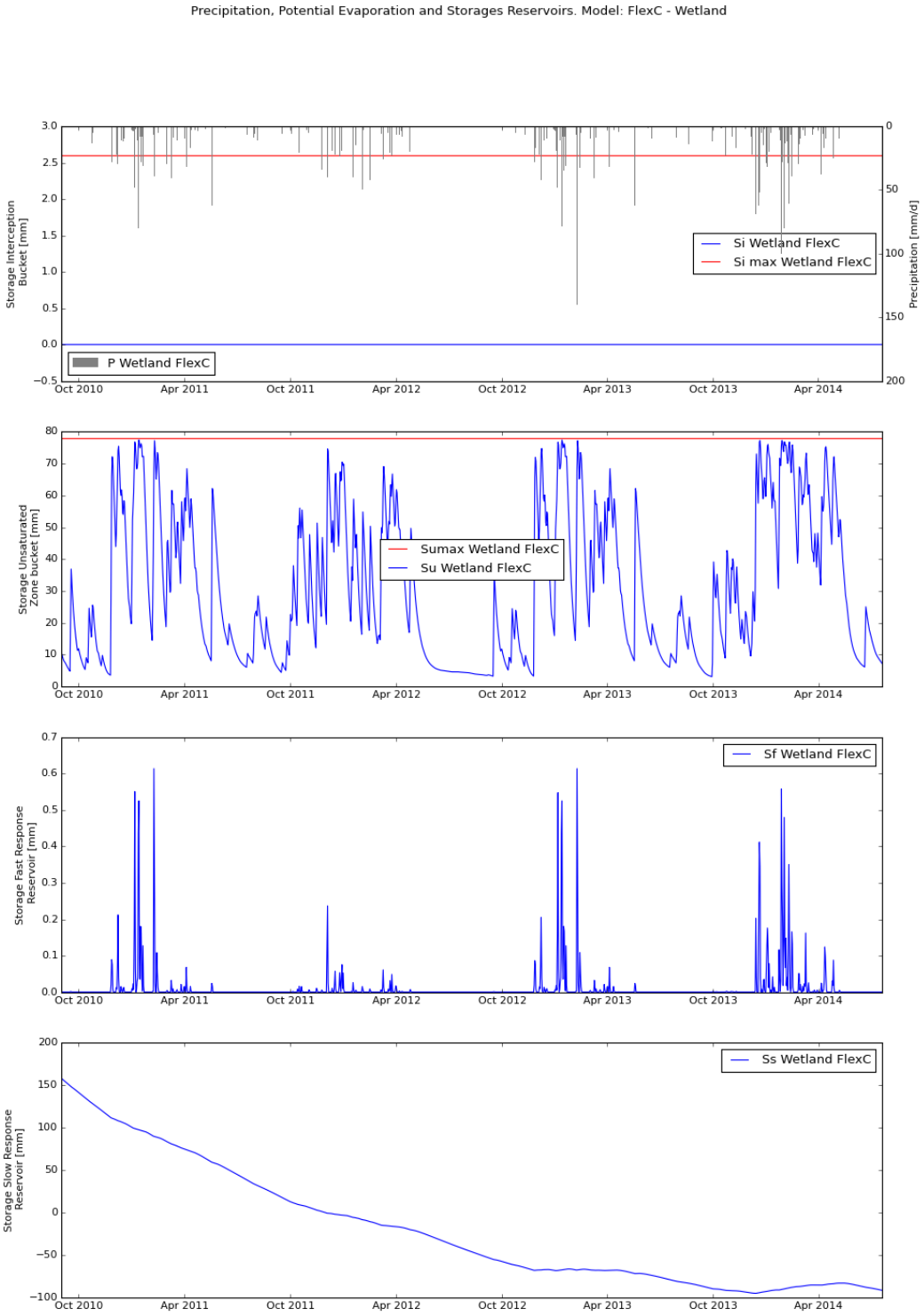
Precipitation, Potential Evaporation and Storages Reservoirs. Model: FlexC - Wetland
Storage Interception Bucket [mm]
Precipitation [mm/d]
Si Wetland FlexC
Si max Wetland FlexC
P Wetland FlexC
Storage Unsaturated Zone bucket [mm]
Sumax Wetland FlexC
Su Wetland FlexC
Storage Fast Response Reservoir [mm]
Sf Wetland FlexC
Storage Slow Response Reservoir [mm]
Ss Wetland FlexC
Oct 2010
Apr 2011
Oct 2011
Apr 2012
Oct 2012
Apr 2013
Oct 2013
Apr 2014

Figure N.39

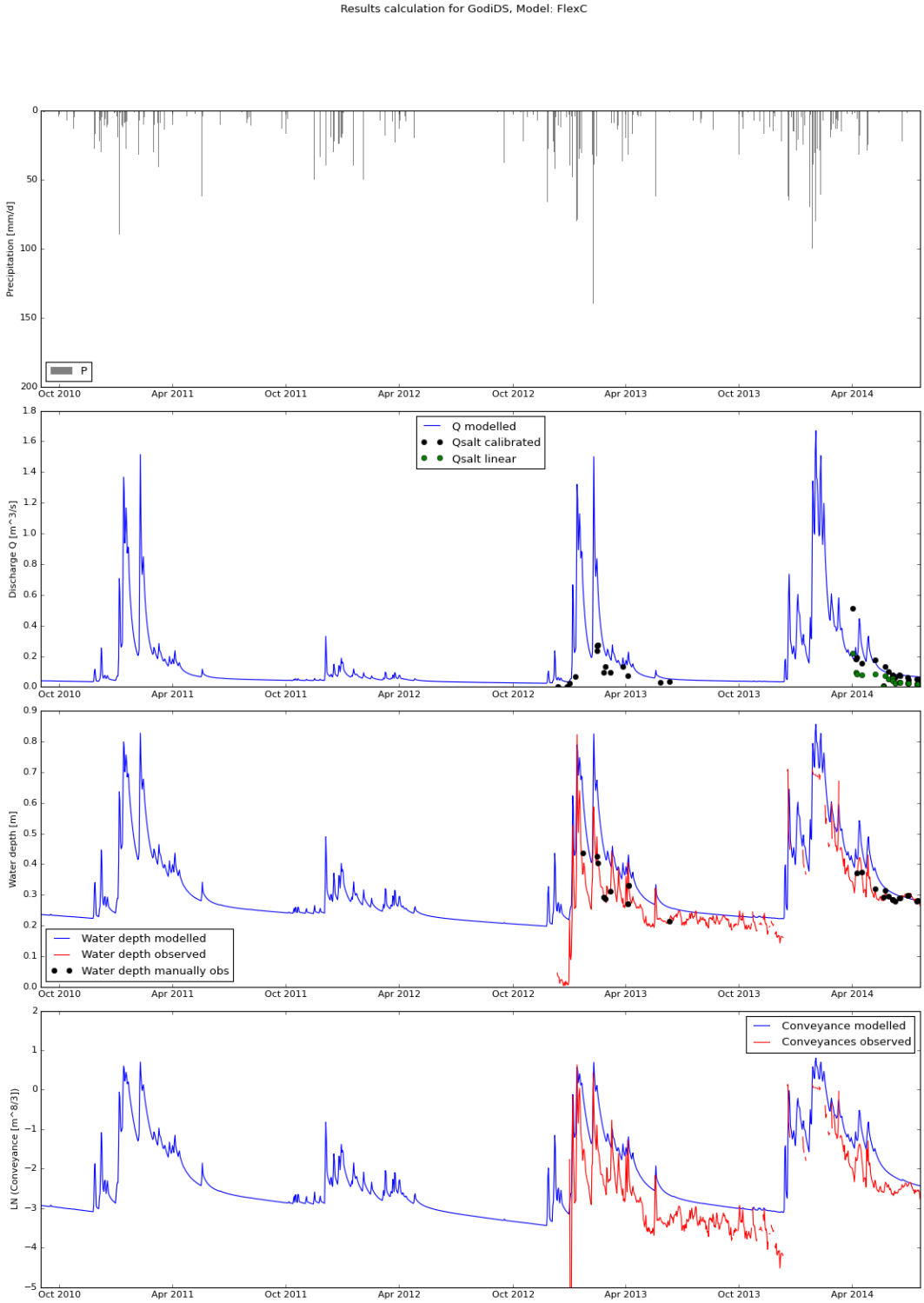

Figure N.40: However is LogNS_C= 0.01, the dynamics of the graphs are very good and in line with our expectations

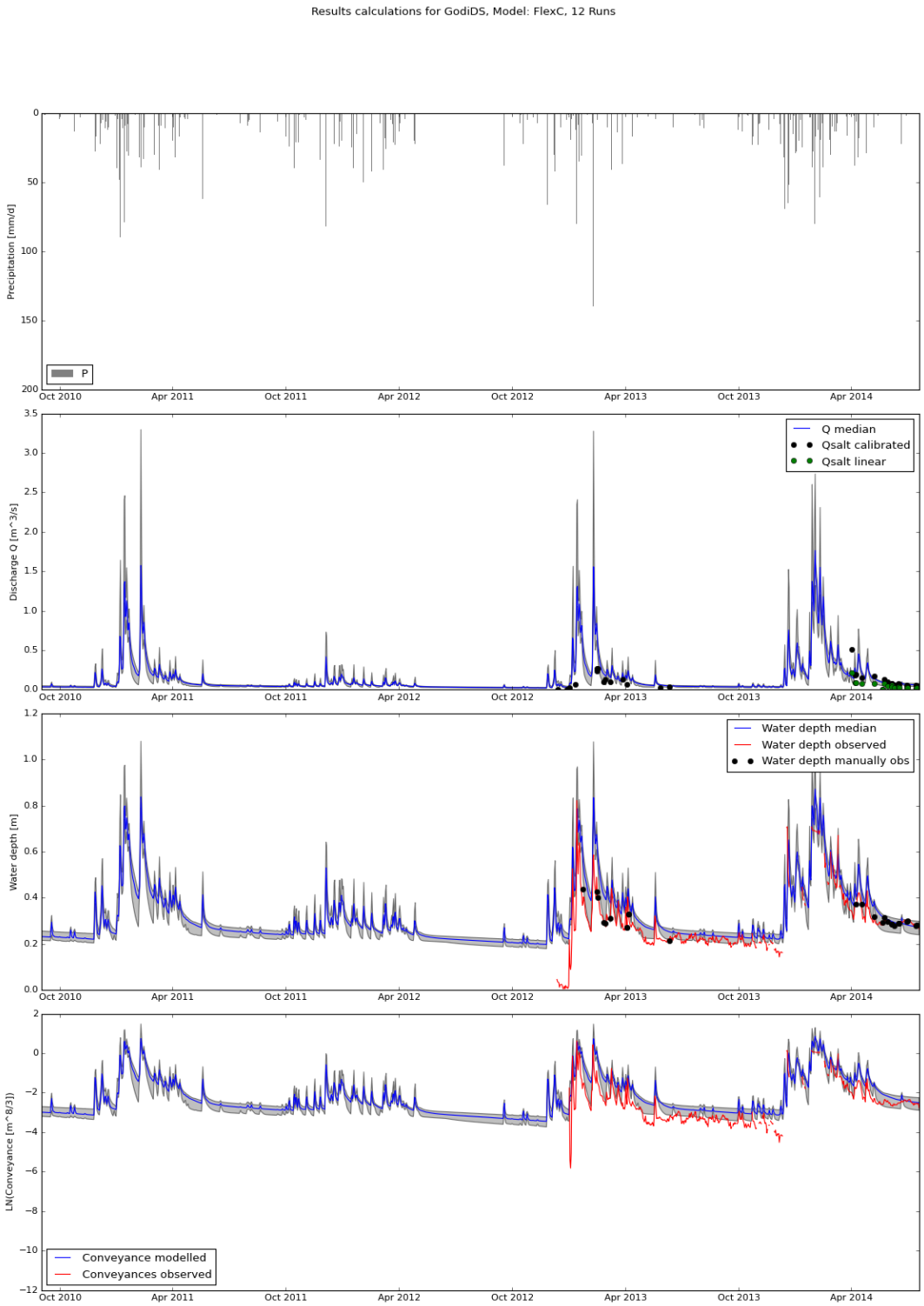

Figure N.41: Bandwidths of small ensemble of plots.

Table N.2: Add caption

RunID	3	4	16	21	30	36	39	52	56	73	91	97
Imax_Grass	2.62	2.52	2.30	2.66	2.30	2.21	2.94	2.11	2.59	2.16	2.56	2.12
B_Grass	4.98	3.13	3.11	4.41	4.21	1.55	1.74	3.48	1.12	2.32	2.14	3.08
Sumax_Grass	273.26	247.43	292.00	281.53	267.11	273.25	278.81	241.30	290.45	184.79	248.49	233.76
Pper_Grass	0.42	0.25	0.43	0.22	0.35	0.34	0.04	0.49	0.44	0.33	0.18	0.21
D_Grass	0.73	0.23	0.36	0.74	0.34	0.01	0.33	0.63	0.19	0.12	0.09	0.75
Kf_Grass	29.02	15.79	23.80	33.46	24.37	0.58	25.39	2.47	1.90	12.43	22.48	5.26
Imax_Forest	4.92	4.09	3.20	4.92	4.06	3.75	4.51	4.07	4.53	3.93	3.00	4.78
B_Forest	4.31	4.45	4.71	3.81	4.57	2.51	3.85	4.90	3.60	4.36	4.26	2.73
Sumax_Forest	447.44	336.73	307.81	337.17	317.33	457.76	491.87	368.50	318.71	440.91	412.01	303.19
Pper_Forest	0.04	0.34	0.22	0.11	0.43	0.25	0.21	0.07	0.24	0.39	0.22	0.11
D_Forest	0.47	0.79	0.30	0.07	0.29	0.41	0.14	0.24	0.22	0.69	0.50	0.07
Kf_Forest	4.08	1.99	5.42	9.32	4.68	5.37	2.38	6.60	1.80	8.73	2.20	6.02
Imax_Wetland	2.83	2.61	2.02	2.26	2.92	2.16	2.85	2.08	2.67	2.82	2.16	2.33
B_Wetland	2.02	2.34	4.55	2.05	1.13	1.71	1.08	1.09	3.83	4.80	3.67	1.42
Sumax_Wetland	84.23	58.27	94.23	56.68	91.88	62.77	63.39	75.00	65.51	75.00	54.07	76.88
C_Wetland	0.43	0.67	0.22	0.52	0.87	0.91	0.80	0.31	0.78	0.55	0.18	0.96
Kf_Wetland	0.64	0.43	0.31	0.71	0.89	0.31	0.57	0.23	0.91	0.56	0.47	0.90
Ks_all	739.66	722.96	493.00	580.37	609.11	462.97	560.81	417.18	707.44	659.18	565.94	746.20
LogNS_C	0.08	0.00	0.01	0.01	0.04	0.16	0.08	0.06	0.06	0.04	0.01	0.01

Table N.3: All calculation with LogNS Conveyances >0 out of 100 runs. Observe the parameters for Run 16. For all calculations

N.4.4. GODIDS CALC5

Model concept FlexC calculated for Godi DS. Goal of this calculation.

- 2000 MC samples
- $0.1 < runoff < 0.9$
- recharge constraint removed
- Wetland: HAND <= 2 based on FlowAccumulation 20
- Flatland / Grass Crop HAND > 2 and Slope < 11
- Hill / Forest HAND > 2 and Slope >= 11

In general the bandwidth around the calculations is too spiky. And the high flows are overpredicted.

The overall baseflow regression is good, since the median of the K_s values approximates also $K_s = 500$ [days], we fixated this parameter.

Remarkable is the fact that the soil moisture reservoir for the forest is less empty after two years than that of the Grasscrop. It reaches the discharge as found two years earlier, but then, there is groundwater accumulation in a average year, what we not expect. So there must be another process at work here. Maybe a slower process.

The GrassCrop HRU shows a more reliable behavior in the groundwater reservoir, though we expect this one just to be empty after one year.

Why does the GrassCrop slow reservoir show a yearly storage pattern, whereas the forest does not. This is not according to our assumptions. So apparently the recharge at the mountains(forest) is higher than for the flatland (grass). Is this reality?

From the parameter plot we observe that the GrassCrop divider passes more water to the slow reservoir than to fast one. Whereas the Forest divider shows a more equal division between the slow and fast reservoir. Since we do calculate the divider on forehand.

So test the slow reservoir initial storage formula and the linearity assumption.

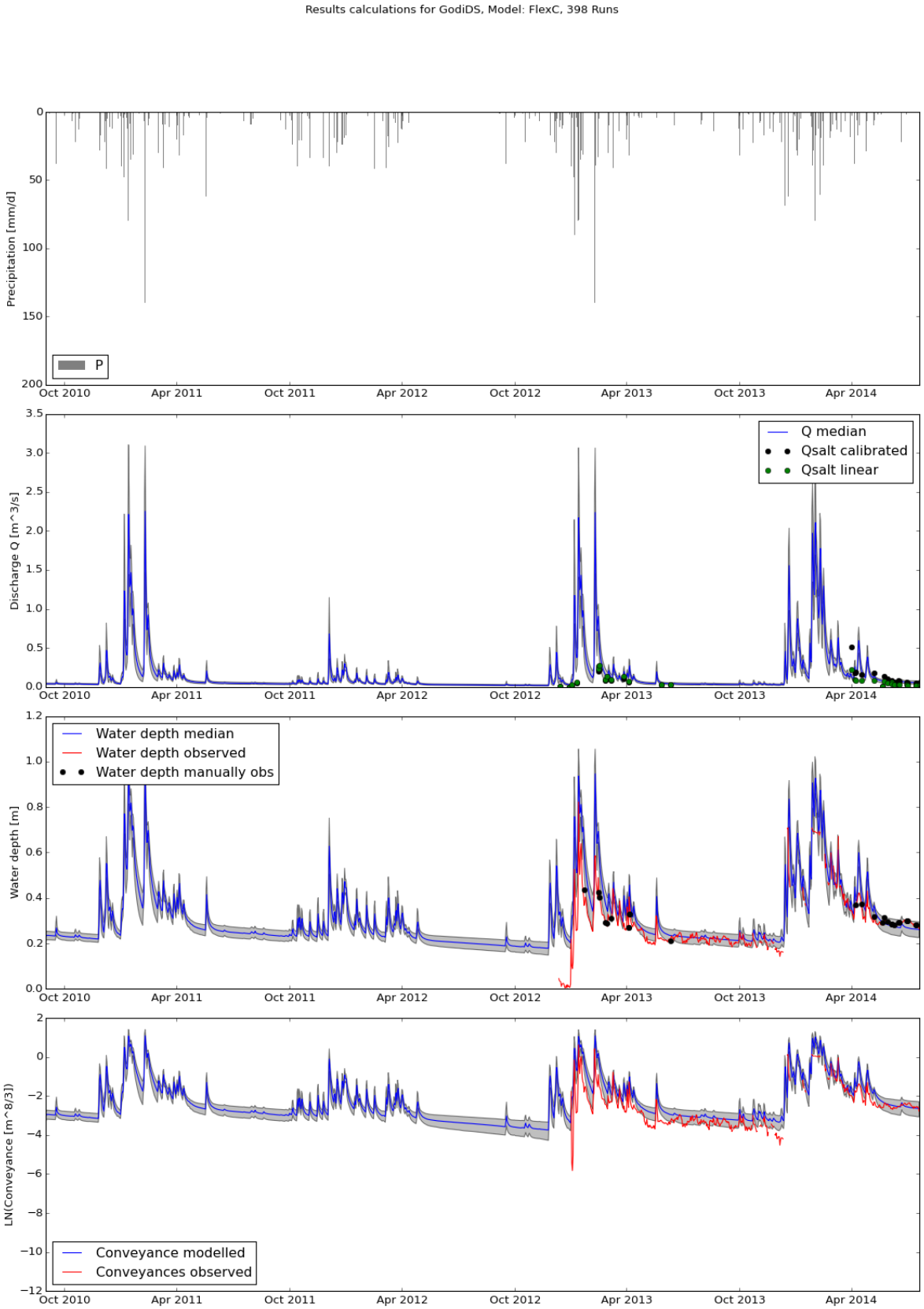
Results calculations for GodiDS, Model: FlexC, 398 Runs
Precipitation [mm/d]
P
Discharge Q [m^3/s]
Q median
Qsalt calibrated
Qsalt linear
Water depth [m]
Water depth median
Water depth observed
Water depth manually obs
LN(Conveyance [m^8/3])
Conveyance modelled
Conveyances observed
Oct 2010
Apr 2011
Oct 2011
Apr 2012
Oct 2012
Apr 2013
Oct 2013
Apr 2014

Figure N.42

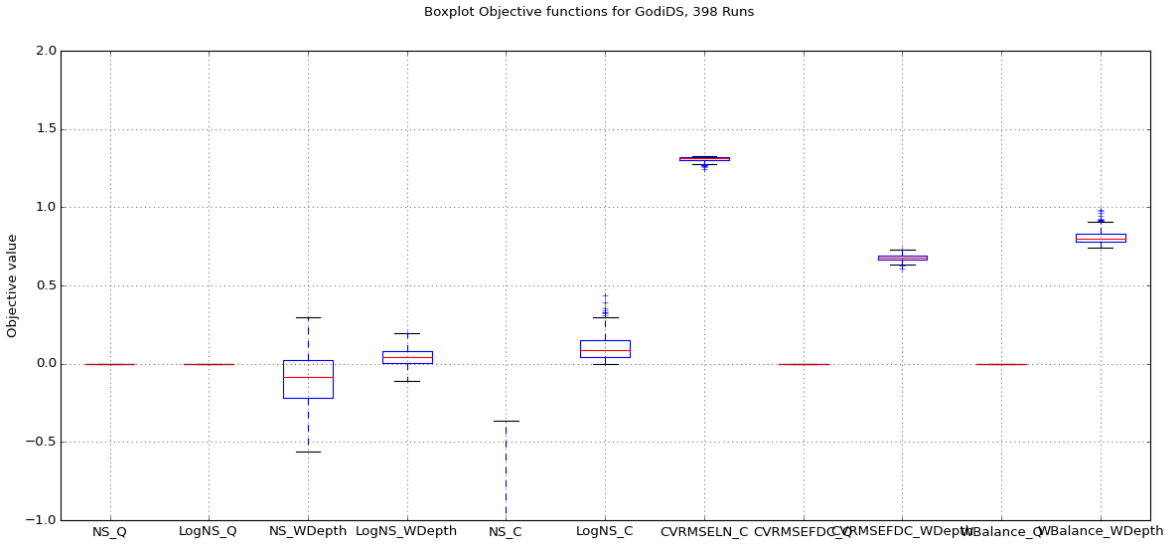
Boxplot Objective functions for GodiDS, 398 Runs
Objective value
2.0
1.5
1.0
0.5
0.0
−0.5
−1.0
NS_Q
LogNS_Q
NS_WDepth
LogNS_WDepth
NS_C
LogNS_C
CVRMSELN_C
CVRMSEFDC_C
CVRMSEFDC_WDepth
WBalance_Q
WBalance_WDepth

Figure N.43

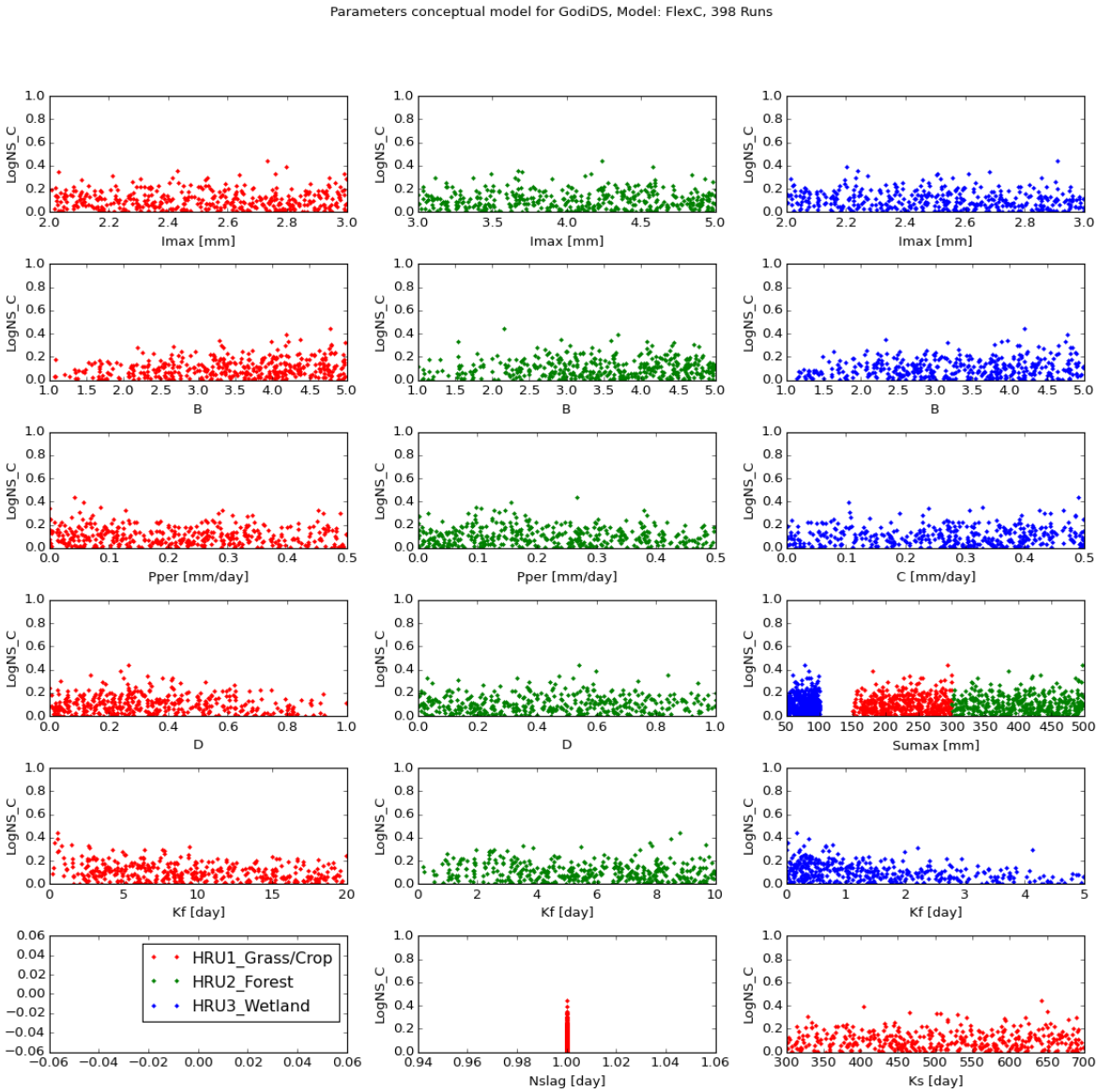
Parameters conceptual model for GodiDS, Model: FlexC, 398 Runs
LogNS_C
Imax [mm]
B
Pper [mm/day]
C [mm/day]
D
Sumax [mm]
Kf [day]
Nslag [day]
Ks [day]
HRU1_Grass/Crop
HRU2_Forest
HRU3_Wetland

Figure N.44

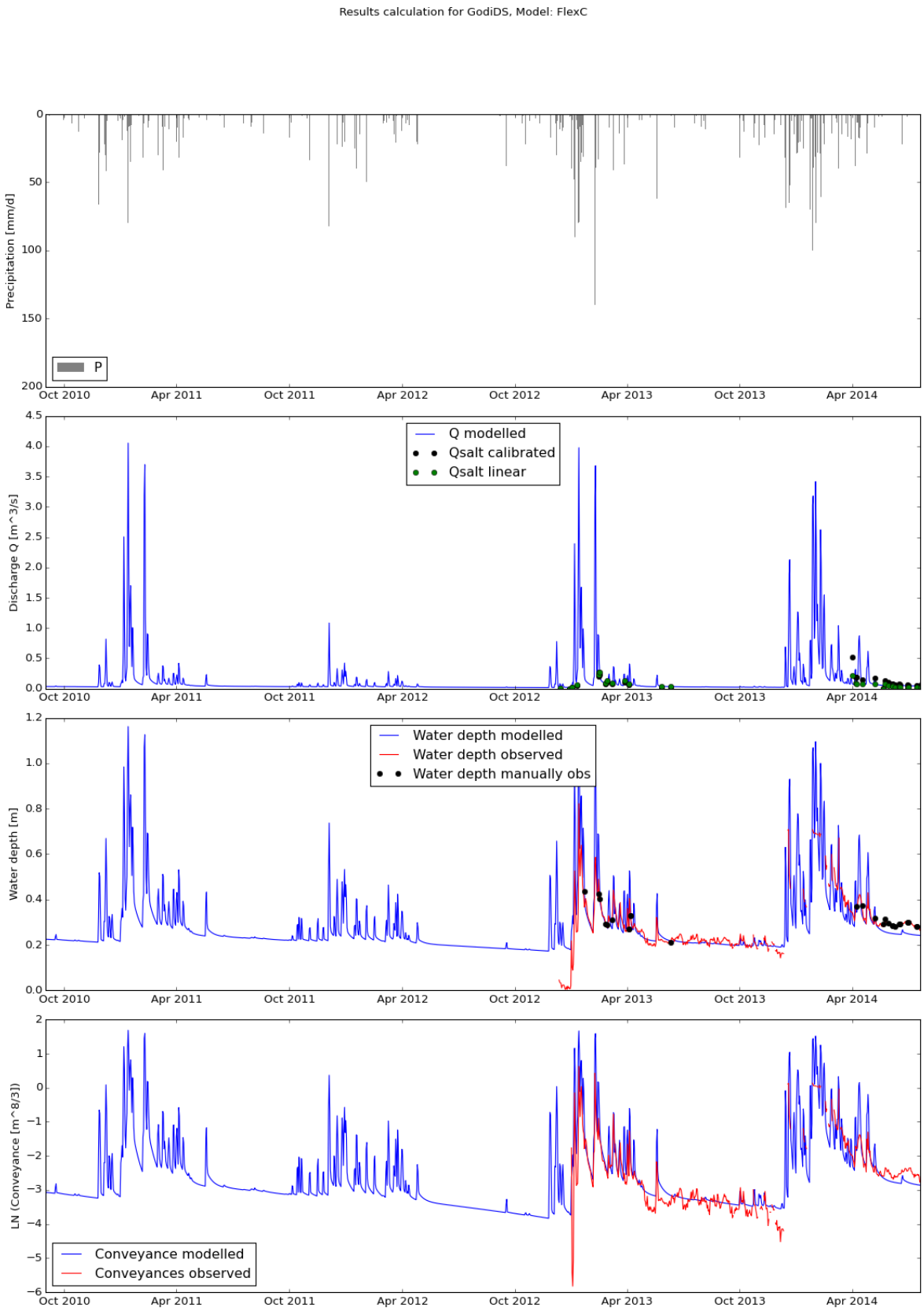

Figure N.45: One of the best calculations with LogNS Conveyance = 0.44

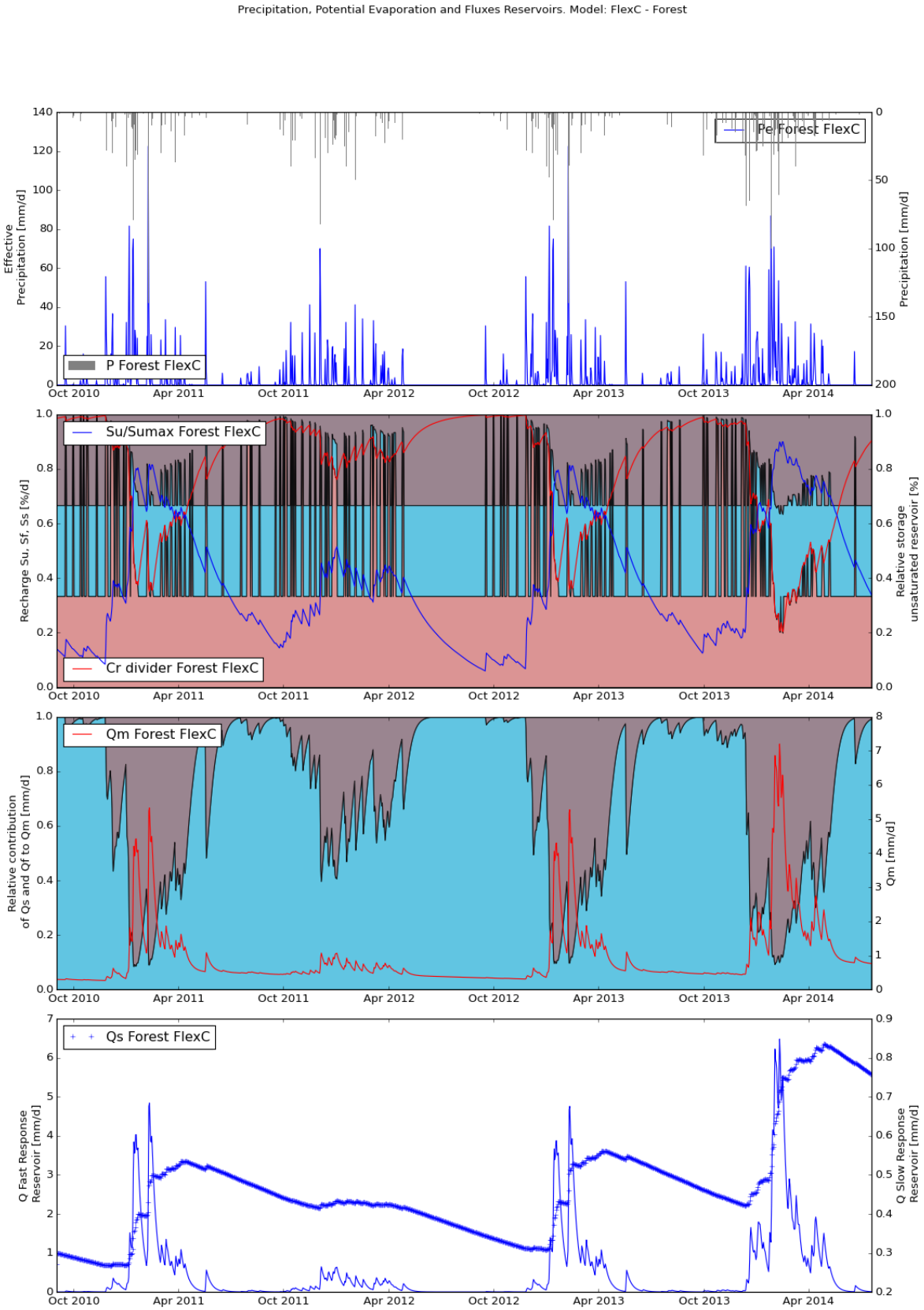
Precipitation, Potential Evaporation and Fluxes Reservoirs. Model: FlexC - Forest
Pe Forest FlexC
P Forest FlexC
Effective Precipitation [mm/d]
Precipitation [mm/d]
Su/Sumax Forest FlexC
Cr divider Forest FlexC
Recharge Su, Sf, Ss [%/d]
Relative storage unsaturated reservoir [%]
Qm Forest FlexC
Relative contribution of Qs and Qf to Qm [mm/d]
Qm [mm/d]
Qs Forest FlexC
Q Fast Response Reservoir [mm/d]
Q Slow Response Reservoir [mm/d]
Oct 2010
Apr 2011
Oct 2011
Apr 2012
Oct 2012
Apr 2013
Oct 2013
Apr 2014

Figure N.46

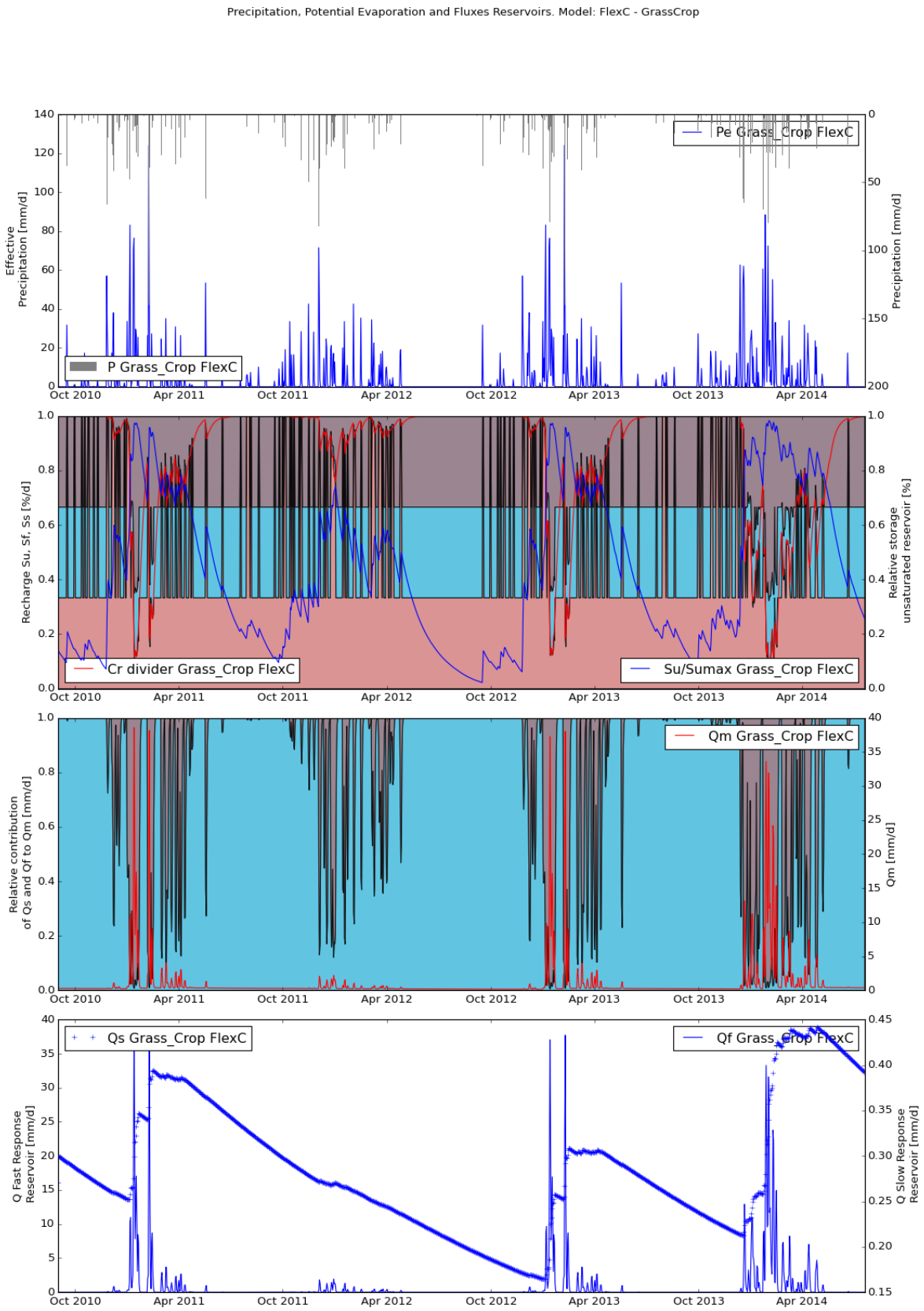
Precipitation, Potential Evaporation and Fluxes Reservoirs. Model: FlexC - GrassCrop
Effective Precipitation [mm/d]
Precipitation [mm/d]
Pe Grass_Crop FlexC
P Grass_Crop FlexC
Recharge Su, Sf, Ss [%/d]
Relative storage unsaturated reservoir [%]
Cr divider Grass_Crop FlexC
Su/Sumax Grass_Crop FlexC
Relative contribution of Qs and Qf to Qm [mm/d]
Qm [mm/d]
Qm Grass_Crop FlexC
Q Fast Response Reservoir [mm/d]
Q Slow Response Reservoir [mm/d]
Qs Grass_Crop FlexC
Qf Grass_Crop FlexC
Oct 2010
Apr 2011
Oct 2011
Apr 2012
Oct 2012
Apr 2013
Oct 2013
Apr 2014

Figure N.47

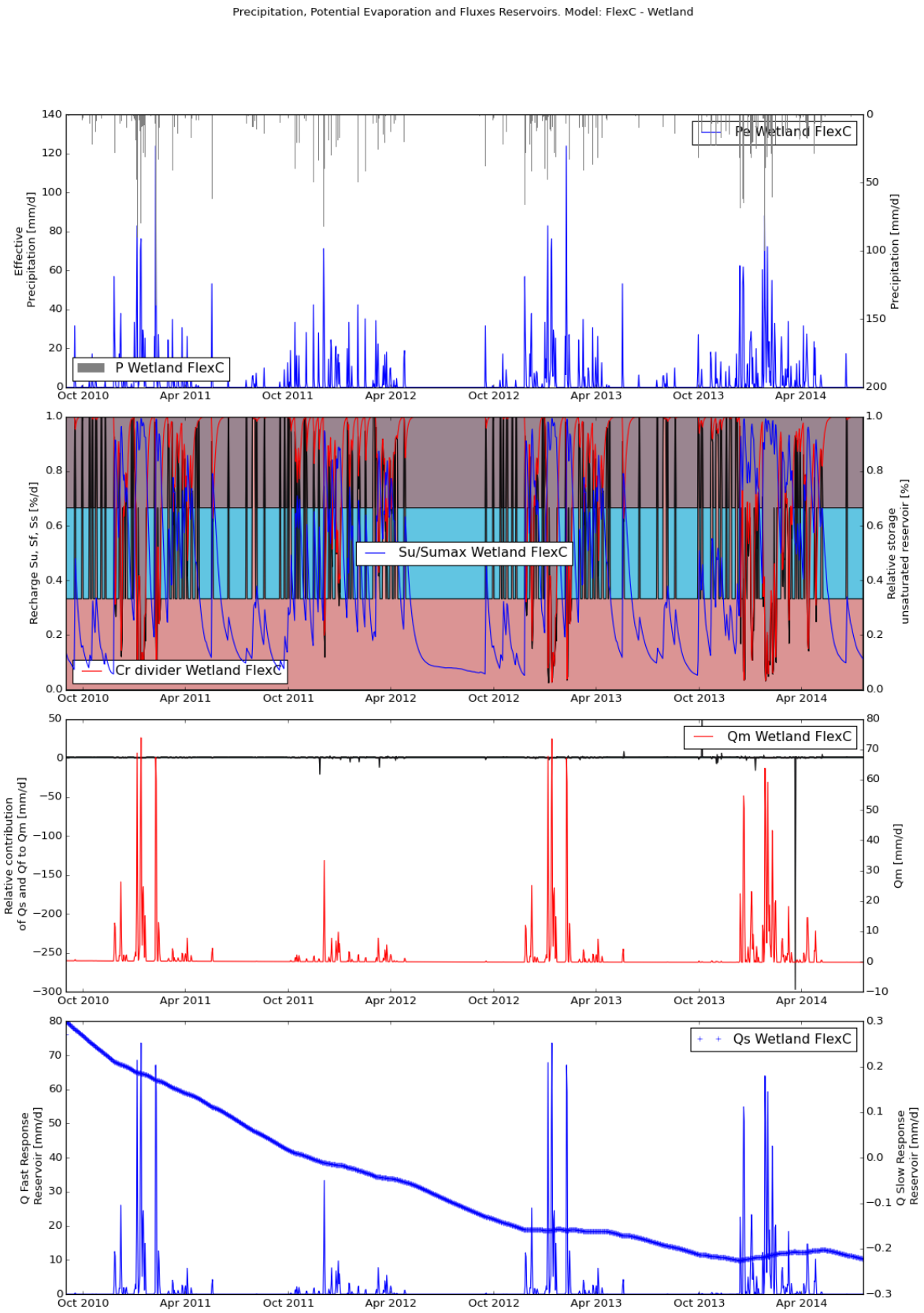
Precipitation, Potential Evaporation and Fluxes Reservoirs. Model: FlexC - Wetland
Effective Precipitation [mm/d]
Precipitation [mm/d]
Pe Wetland FlexC
P Wetland FlexC
Recharge Su, Sf, Ss [%/d]
Relative storage unsaturated reservoir [%]
Su/Sumax Wetland FlexC
Cr divider Wetland FlexC
Relative contribution of Qs and Qf to Qm [mm/d]
Qm [mm/d]
Qm Wetland FlexC
Q Fast Response Reservoir [mm/d]
Q Slow Response Reservoir [mm/d]
Qs Wetland FlexC
Oct 2010
Apr 2011
Oct 2011
Apr 2012
Oct 2012
Apr 2013
Oct 2013
Apr 2014

Figure N.48

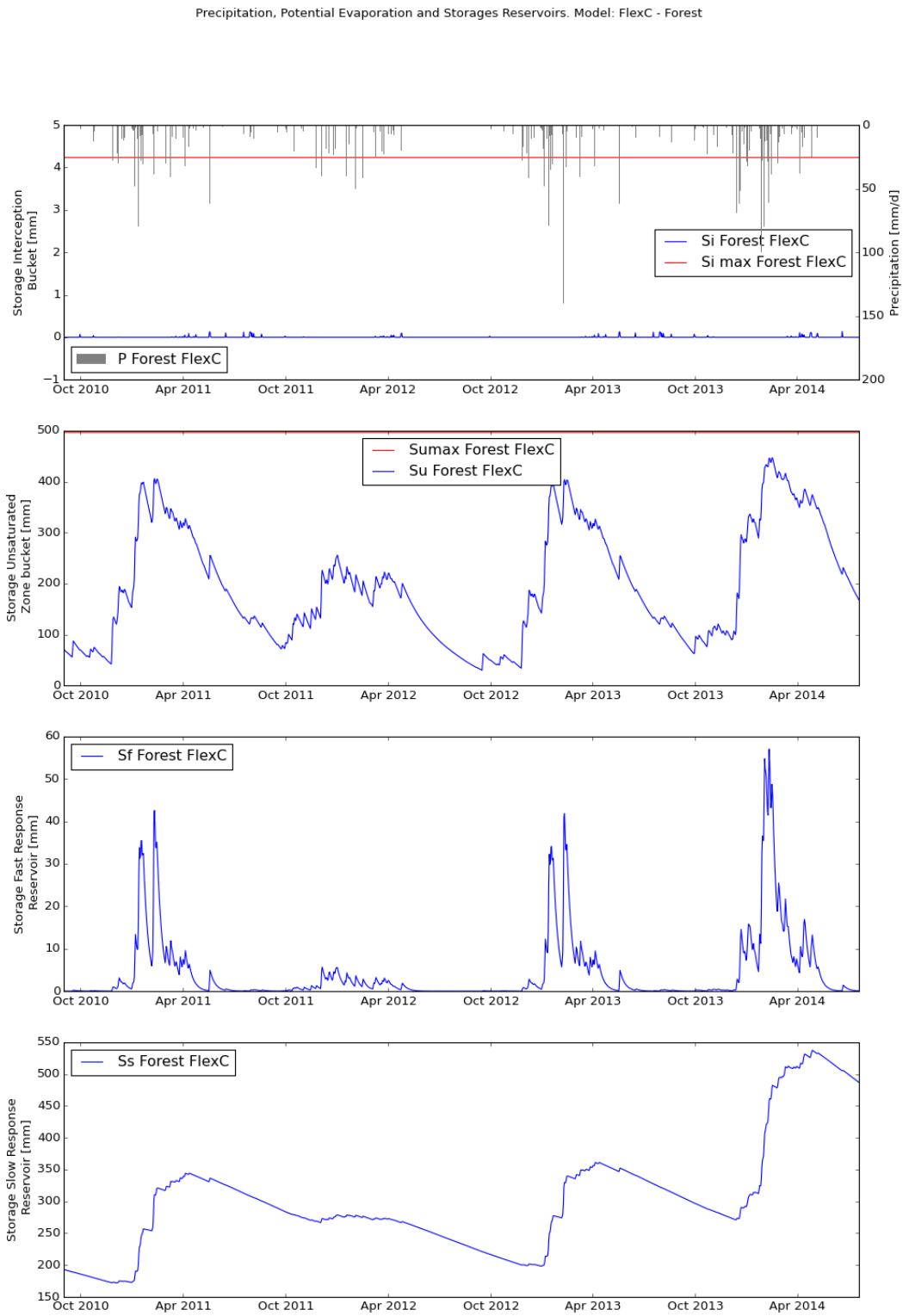
Precipitation, Potential Evaporation and Storages Reservoirs. Model: FlexC - Forest
Storage Interception Bucket [mm]
Precipitation [mm/d]
Si Forest FlexC
Si max Forest FlexC
P Forest FlexC
Storage Unsaturated Zone bucket [mm]
Sumax Forest FlexC
Su Forest FlexC
Storage Fast Response Reservoir [mm]
Sf Forest FlexC
Storage Slow Response Reservoir [mm]
Ss Forest FlexC
Oct 2010
Apr 2011
Oct 2011
Apr 2012
Oct 2012
Apr 2013
Oct 2013
Apr 2014

Figure N.49

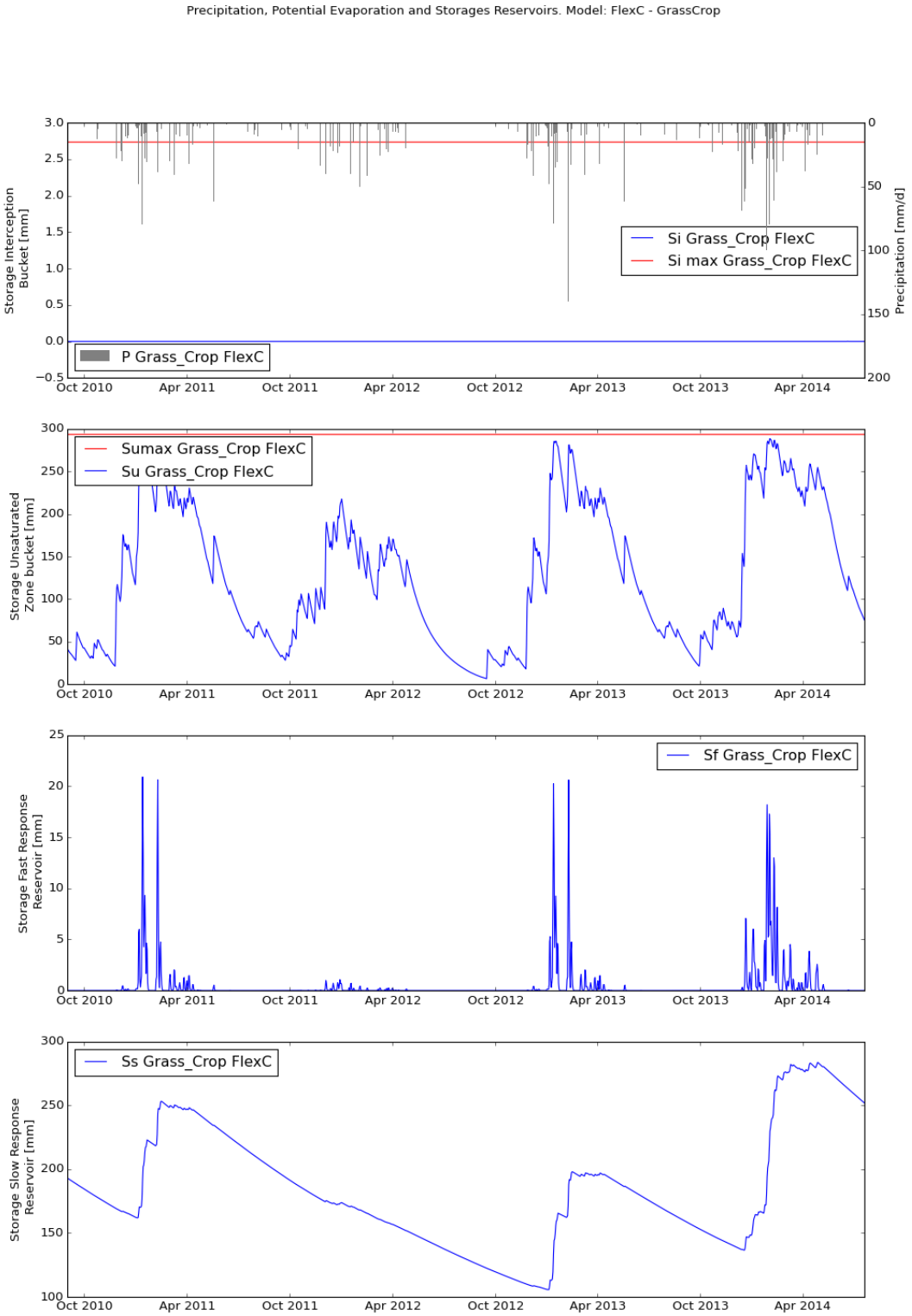
Precipitation, Potential Evaporation and Storages Reservoirs. Model: FlexC - GrassCrop
Storage Interception Bucket [mm]
Precipitation [mm/d]
Si Grass_Crop FlexC
Si max Grass_Crop FlexC
P Grass_Crop FlexC
Storage Unsaturated Zone bucket [mm]
Sumax Grass_Crop FlexC
Su Grass_Crop FlexC
Storage Fast Response Reservoir [mm]
Sf Grass_Crop FlexC
Storage Slow Response Reservoir [mm]
Ss Grass_Crop FlexC
Oct 2010
Apr 2011
Oct 2011
Apr 2012
Oct 2012
Apr 2013
Oct 2013
Apr 2014

Figure N.50

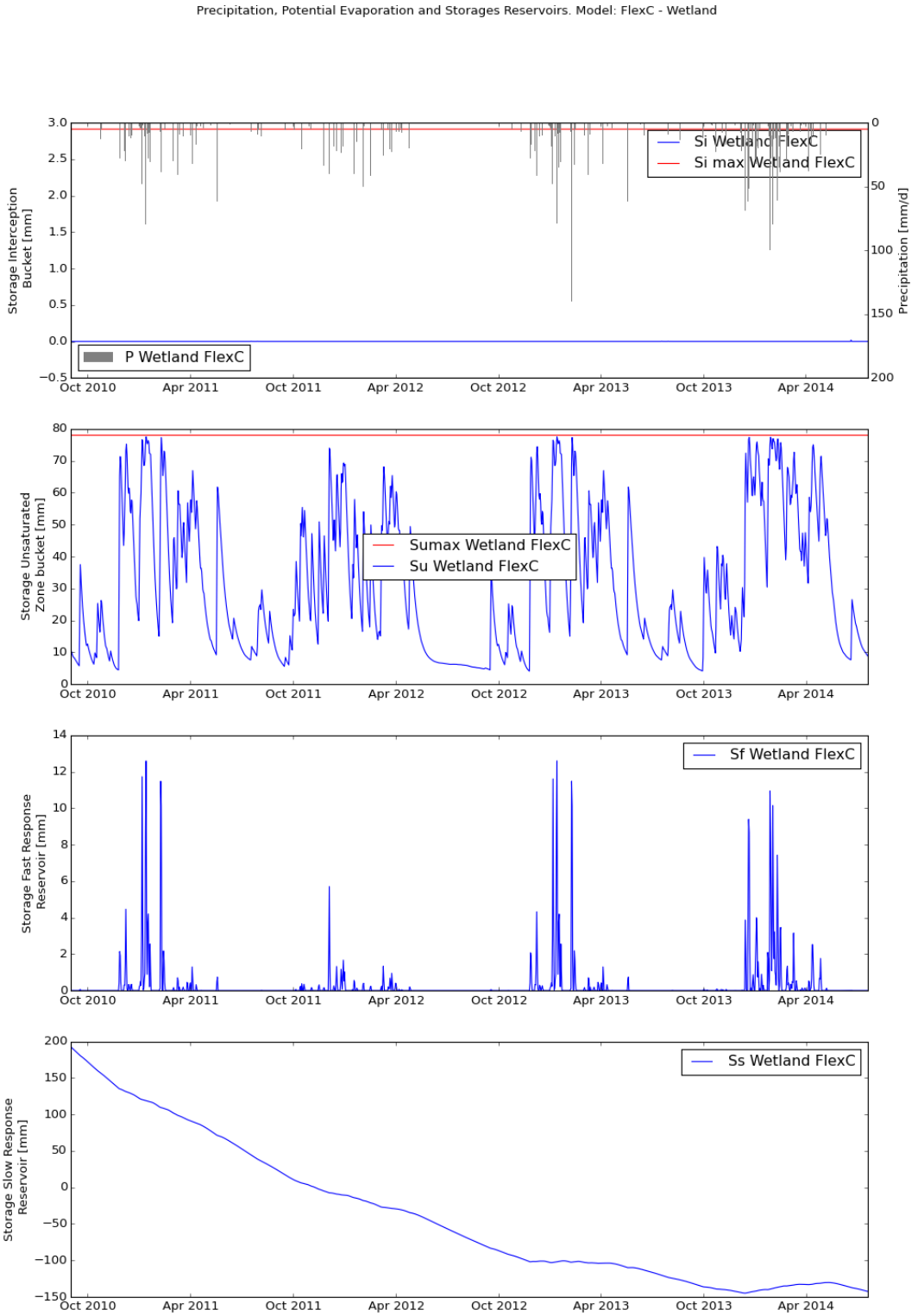
Precipitation, Potential Evaporation and Storages Reservoirs. Model: FlexC - Wetland
Storage Interception Bucket [mm]
Precipitation [mm/d]
Si Wetland FlexC
Si max Wetland FlexC
P Wetland FlexC
Storage Unsaturated Zone bucket [mm]
Sumax Wetland FlexC
Su Wetland FlexC
Storage Fast Response Reservoir [mm]
Sf Wetland FlexC
Storage Slow Response Reservoir [mm]
Ss Wetland FlexC
Oct 2010
Apr 2011
Oct 2011
Apr 2012
Oct 2012
Apr 2013
Oct 2013
Apr 2014

Figure N.51

N.4.5. GODIDS CALC6

Based on GodiDS Calc4. Model concept FlexC calculated for Godi DS.

- 10000 MC samples
- $0.1 < runoff < 0.9$
- recharge constraint removed
- Wetland: HAND <= 2 based on FlowAccumulation 50
- Flatland / Grass Crop HAND > 2 and Slope < 11
- Hill / Forest HAND > 2 and Slope >= 11
- Ks = 500 fixed

N.4.6. GODIDS CALC7

Re-run Calc6 with 10000 runs.

Re-run this calculation with 10000 runs, so we have a better parameter plots

N.4.7. GODIDS CALC8

Precipitation altitude effect HRU wise. Based on GodiDS Calc4.

Model concept FlexC calculated for Godi DS.

- 10000 MC samples
- $0.1 < runoff < 0.9$
- Recharge constraint $R_{s;forest} > R_{s;grasscrop}$ removed
- Wetland: HAND <= 2 based on FlowAccumulation 50
- Flatland / Grass Crop HAND > 2 and Slope < 11
- Hill / Forest HAND > 2 and Slope >= 11

Initial storage slow groundwater reservoir calculated based on first year november 2010 to november 2011.

N.4.8. GODIDS CALC9

Precipitation altitude effect HRU wise. Based on GodiDS Calc4.

Model concept FlexC calculated for Godi DS.

Objective functions. NS_Conveyance >= 0, LogNS_Conveyance >=0

- 40000 MC samples
- $0.1 < runoff < 0.9$
- Recharge constraint $R_{s;forest} > R_{s;grasscrop}$ removed
- Wetland: HAND <= 2 based on FlowAccumulation 50
- Flatland / Grass Crop HAND > 2 and Slope < 11
- Hill / Forest HAND > 2 and Slope >= 11

fixed assumption recharge slow reservoir 0.2*1000 mm * D based on grass_crop. == wrong

N.4.9. GODIDS CALC10

Precipitation altitude effect HRU wise. Based on GodiDS Calc4.

Model concept FlexC calculated for Godi DS.

- 10000 MC samples
- $0.1 < runoff < 0.9$
- Recharge constraint $R_{s;forest} > R_{s;grasscrop}$ removed
- Wetland: HAND <= 2 based on FlowAccumulation 50
- Flatland / Grass Crop HAND > 2 and Slope < 11
- Hill / Forest HAND > 2 and Slope >= 11

- iterations necessary for estimation initial condition. - determine slow reservoir recharge. based on 25 best model runs - rerun

N.4.10. GODIDS CALC12

Final calculation. GodiDS Calc11 is re-runned and called GodiDS Calc12.

Precipitation altitude effect HRU wise. Based on GodiDS Calc4.

Model concept FlexC calculated for Godi DS.

Objective functions. LogNS_Conveyance >=0

- 10000 MC samples
- $0.1 < runoff < 0.9$
- Recharge constraint $R_{s;forest} > R_{s;grasscrop}$ removed
- Wetland: HAND <= 2 based on FlowAccumulation 50
- Flatland / Grass Crop HAND > 2 and Slope < 11
- Hill / Forest HAND > 2 and Slope >= 11

fixed assumption recharge slow reservoir 0.2*1000 mm * D based on grass_crop. == wrong initial states groundwater reservoirs. Forest 300 mm * D Grass_crop 200 mm * D Wetland -100 mm

then calculate first year and extract the total recharge to the slow reservoir. From this the new recharge is calculated. For wetland the recharge (which is actually an extraction) is multiplied by 2, in order to have a more stable estimate.